

**BRITTLE FRACTURE MECHANISMS OF GLASS-FIBER
REINFORCED POLYMER INSULATORS**

Qiong Qiu

B.E., Beijing Polytechnic University, Beijing, China, 1982
M.S., Institute of Aeronautical Materials, Beijing, China, 1985

A dissertation submitted to the faculty of the
Oregon Graduate Institute of Science & Technology
in partial fulfillment of the requirements
for the degree Doctor of Philosophy
in
Materials Science and Engineering

October, 1995

The dissertation "Brittle Fracture Mechanisms of Glass-Fiber Reinforced Polymer Insulators" by Qiong Qiu has been examined and approved by the following Examination Committee:

Maciej S. Kumosa, Thesis Advisor
Associate Professor

David G. Atteridge
Professor

Jack H. Devletian
Professor

Wesley M. Jarrell
Professor

Dedicated to my beloved father

ACKNOWLEDGEMENT

I would like to acknowledge Bonneville Power Administration, Electrical Power Research Institute, Western Area Power Administration, and GlasForms, Inc. for sponsoring this project.

I wish to express my sincere appreciation to Dr. Maciej S. Kumosa, my thesis advisor, for his guidance throughout this work. I am grateful to Professors David G. Atteridge and Jack H. Devletian for examining my dissertation. Special thanks are due to Professor Wesley M. Jarrell for his valuable suggestions in ion leaching analysis and for evaluating my thesis. I also wish to recognize Drs. Margaret Ziomek-Moroz and Antony Moroz for their constructive advises in the study of crack-tip chemistry.

I thank Mr. Lorne Isabelle, Mr. Wentai Luo, Ms. Zhihong Cui, Ms. Sheryl Martin, and Mr. Tim Mayer in the Department of Environment Science and Engineering for their assistance in chemical analysis and Ms. Kristine Roley in Library for her best efforts in searching the literature for this work. I greatly appreciate the help I received from all of the faculty, staff, and students in the Department of Materials Science and Engineering during my four-year study at Oregon Graduate Institute of Science & Technology.

I wish to express my deep gratitude to Dr. Daniel W. Walsh and his family for their friendship and continuous encouragement over the years. I am grateful to my husband, Wei Cheng, and my son, Cheng Cheng; without their love and support, my today's achievement is impossible.

TABLE OF CONTENTS

TITLE PAGE	i
APPROVAL PAGE	ii
DEDICATION	iii
ACKNOWLEDGEMENT	iv
TABLE OF CONTENTS	v
LIST OF TABLES	ix
LIST OF FIGURES	x
ABSTRACT	xv
INTRODUCTION	1
CHAPTER 1 CRITICAL REVIEW	5
1.1 Development of GRP Insulators	5
1.1.1 Historical Background	5
1.1.2 Insulator Construction	6
1.1.3 Insulator Materials	12
1.1.3.1 GRP Composites	12
1.1.3.2 Insulator Housing	17
1.1.3.3 End Fittings	19
1.1.4 Insulator Manufacture	20
1.1.4.1 Composite Rod Fabrication	20
1.1.4.2 Insulator Assembly	20
1.2 Brittle Fracture of GRP Insulators	22
1.2.1 Field Experience	22
1.2.2 Brittle Fracture Phenomenon	23
1.3 Stress Corrosion of GRP Composites	25

1.3.1	Fracture Morphology	25
1.3.2	Physical Fracture Theories	29
1.3.2.1	Fracture Models	29
1.3.2.2	Fracture Stresses	33
1.3.2.3	Crack Growth Rate	36
1.3.3	Chemical Deterioration Theories	38
1.3.3.1	Environmental Influence on Composites	38
1.3.3.2	Acid Leaching of Glass Fibers	42
1.4	Failure Mechanisms of GRP Insulators	48
1.4.1	Mechanical Stresses	49
1.4.2	Environmental Stresses	50
1.4.2.1	Acid Rain	50
1.4.2.2	Organic Acids	52
1.4.3	Electric Stresses	54
1.5	Summary	56
 CHAPTER 2 EXPERIMENTAL PROCEDURES AND RESULTS		 58
2.1	Insulator Failure Analysis	58
2.1.1	Insulator Configuration	58
2.1.2	Insulator Materials	60
2.1.3	Preliminary Examination	60
2.1.4	Fractographic Characterization	69
2.1.5	Chemical Analyses	83
2.1.6	Fracture Stress Estimation	94
2.2	Stress Corrosion Experiments	106
2.2.1	Materials	106
2.2.2	Constant K_I Specimen	107
2.2.3	Experimental Arrangement	109
2.2.4	Test Solutions	113

2.2.5	Stress Corrosion Behavior of Composites	113
2.2.5.1	Acid Type Effect	113
2.2.5.2	Acid Concentration Effect	115
2.2.5.3	Mechanical Load Effect	115
2.2.5.4	Materials Effect	120
2.2.5.5	Water Effect	124
2.2.6	Fracture Morphology	125
2.3	Electrical Discharge Experiments	128
2.3.1	Polymer Discharge Tests	129
2.3.2	High-Voltage Fracture Tests	134
2.3.2.1	Moisture Effect	137
2.3.2.2	Fracture Morphology	140
2.4	Acid Corrosion Behavior of E-Glass Fiber	140
2.4.1	Fiber Specimen	145
2.4.2	Acid Immersion Experiments	146
2.4.3	Fiber Weight Loss	146
2.4.4	Ion Depletion Behavior	147
2.4.5	Fracture Morphology	152
2.4.5.1	Surface Morphology	152
2.4.5.2	Cross-Section Morphology	160
2.5	Crack Tip Chemistry	165
2.5.1	Samples and Materials	166
2.5.2	Extraction Tests	166
2.5.3	Thermal Stability Test	174
2.5.4	Immersion Test	176
CHAPTER 3 DISCUSSION		179
3.1	Brittle Fracture Mechanisms of GRP Insulators	179
3.1.1	Fracture Mode	179

3.1.2	Electric Stress Influence	181
3.1.3	Service Environments	185
3.1.4	Fracture Model	191
3.2	Acid Corrosion of E-glass Fiber	196
3.2.1	Ion Depletion Behavior	196
3.2.2	Fracture Mechanism	202
3.3	Crack Tip Chemistry	208
3.3.1	Acid Leaching of Glass Fibers	208
3.3.2	Dissolution of Composites in Aqueous Solutions	212
3.3.3	Thermal Effects	214
CHAPTER 4 SUMMARY		215
4.1	Conclusions	215
4.2	Recommendations	219
4.3	Future Research	221
REFERENCES		222
VITA		236

LIST OF TABLES

Table 1.1	Nominal composition of E-glass fiber	14
Table 1.2	Representative properties of E-glass fiber	14
Table 1.3	Aspects of property deterioration in GRP composites	40
Table 2.1	Service conditions for as-received insulators	59
Table 2.2	Chemical compositions of the black substance inside the damage zone and the nearby materials	87
Table 2.3	Fiber diameter and mirror size measurements	99
Table 2.4	Average fracture stresses in the selected fields	105
Table 2.5	Number of the fractured fibers in 24 hours as a function of pH produced by oxalic acid	116
Table 2.6	Major constituents identified in the byproducts of discharged polyester resin	133
Table 2.7	Major constituents identified in the byproducts of discharged E-glass fiber/polyester composite	133
Table 2.8	Chemical composition of the E-glass fiber	146
Table 2.9	Comparison of fiber weight losses	151
Table 2.10	Major constituents identified in the deposits	176
Table 2.11	Fiber weight measurements	177

LIST OF FIGURES

Figure 1.1	Suspension insulators in service	7
Figure 1.2	Schematic construction of the insulator	9
Figure 1.3	Cross-section configuration of the insulator	10
Figure 1.4	Structure of a cone-designed end fitting	11
Figure 1.5	Fracture morphology of insulators	24
Figure 1.6	Single fiber fracture	27
Figure 1.7	Matrix fracture markings	28
Figure 1.8	Schematic representation of crack growth in unidirectional composites in acids	31
Figure 1.9	Influence of resin toughness on crack propagation behavior . . .	32
Figure 1.10	Schematic representation of fiber corrosion in acids	44
Figure 1.11	Annual average distribution of the weighted mean pH of precipitation in the United States and Canada for 1980	53
Figure 2.1	Damage zones found inside the high-voltage end	62
Figure 2.2	Black substance in the damage zone and on the inner surface of the metal casting	63
Figure 2.3	Circumferential cracks in the epoxy/sheath interface region	64
Figure 2.4	Damaged composite rod found inside the high-voltage end	65
Figure 2.5	Fracture morphology of insulator #6	66
Figure 2.6	Internal crack network formed outside the high-voltage end	68
Figure 2.7	Surface cutting on the weathershed	70
Figure 2.8	Morphology of the insulator fracture surfaces	72
Figure 2.9	Fiber fracture morphology	73
Figure 2.10	Fractured fibers with large mirror sizes	74
Figure 2.11	Glass wedge caused by crack bifurcation	75
Figure 2.12	Resin decomposition on the fracture surface	76

Figure 2.13	Depth profile on the local fracture surface	78
Figure 2.14	Localized resin decomposition	79
Figure 2.15	Surface morphology of the melted fibers	80
Figure 2.16	Deposits formed on the insulator fracture surface	82
Figure 2.17	Morphology of secondary transverse cracks	84
Figure 2.18	Fracture surface taken from the internal crack network	85
Figure 2.19	Fiber fracture morphology on the stepped fracture surface	86
Figure 2.20	EDS analysis on a transverse crack surface	89
Figure 2.21	EDS analysis on a longitudinal delamination surface	90
Figure 2.22	EDS analysis on a rod surface at the rod/sheath separation	91
Figure 2.23	EDS analysis on the bare surface of a fractured fiber	92
Figure 2.24	EDS analysis on a large particle deposited on the fracture surface	93
Figure 2.25	Calcium/silicon ration as a function of the distance to the fractured fiber surface	95
Figure 2.26	Aluminum/silicon ratio as a function of the distance to the fractured fiber surface	96
Figure 2.27	Fracture surface in insulator #5	98
Figure 2.28	Fiber diameter distribution	100
Figure 2.29	Mirror size distribution	101
Figure 2.30	Comparison between mirror size and fiber diameter distributions	102
Figure 2.31	Configuration of the constant K_I specimen	108
Figure 2.32	Schematic representation of the stress corrosion experimental arrangement	110
Figure 2.33	Acoustic emission output recorded during the stress corrosion experiments	112
Figure 2.34	Number of fractured fibers in the pH 3 nitric and oxalic acid solutions	114

Figure 2.35	Crack growth rate as a function of pH produced by oxalic acid	117
Figure 2.36	Rate of acoustic emission ringdowns as a function of tensile load in the pH 2 oxalic acid solution	119
Figure 2.37	Crack growth rate as a function of tensile load in the pH 2 oxalic acid solution	121
Figure 2.38	Crack growth rate as functions of exposure time and acid solution pH in E-glass fiber/polyester composite	122
Figure 2.39	Crack growth rate as functions of exposure time and acid solution pH in E-glass fiber/epoxy composite	123
Figure 2.40	Transverse cracks developed in the stress corrosion experiments	126
Figure 2.41	Surface morphology of stress corrosion fracture	127
Figure 2.42	AC electrical discharge cell	130
Figure 2.43	Reconstructed ion chromatogram for the byproducts of discharged polyester resin	131
Figure 2.44	Reconstructed ion chromatogram for the byproducts of discharged E-glass fiber/polyester composite	132
Figure 2.45	Configuration of the high voltage system	135
Figure 2.46	Scheme of the electrical control unit	136
Figure 2.47	Side view of the notch root region	138
Figure 2.48	Transverse crack developed under wet conditions	139
Figure 2.49	Fracture surface morphology generated under wet conditions . . .	141
Figure 2.50	Melted fibers on the fracture surface	142
Figure 2.51	Surface morphology of the melted fibers	143
Figure 2.52	Resin decomposition on the fracture surface	144
Figure 2.53	Fiber weight loss as functions of acid type and acid solution pH .	148
Figure 2.54	Calcium ion concentrations in the resultant acid solutions	149
Figure 2.55	Aluminum ion concentrations in the resultant acid solutions	150

Figure 2.56	Surface morphology of as-received E-glass fibers	153
Figure 2.57	Axial cracks generated in the pH 1 oxalic acid solution	154
Figure 2.58	Internal circumferential crack developed with axial cracks in the pH 1 oxalic acid solution	155
Figure 2.59	Spiral cracks generated in the pH 2 oxalic acid solution	157
Figure 2.60	Surface damage generated in the pH 3 oxalic acid solution	158
Figure 2.61	Fiber surface morphology generated in the pH 1 sulfuric acid solution	159
Figure 2.62	Surface particulate deposition induced in the pH 2 sulfuric acid solution	161
Figure 2.63	Surface morphology of glass fibers exposed to the pH 1 hydrochloric acid solution	162
Figure 2.64	Surface morphology of glass fibers exposed to the pH 1 nitric acid solution	163
Figure 2.65	Cross-section images of the fractured fibers	164
Figure 2.66	pH change of the extract obtained from the composite with the alumina trihydrate filler	168
Figure 2.67	Calcium and aluminum concentrations in the extract of the composite with the alumina trihydrate filler	169
Figure 2.68	pH change in the extract obtained from the composite with the calcium carbonate filler	171
Figure 2.69	Calcium and aluminum concentrations in the extract of the composite with the calcium carbonate filler	172
Figure 2.70	Surface morphology of the composite turnings before and after the extraction tests	173
Figure 2.71	Reconstructed ion chromatogram for the deposits	175
Figure 2.72	Fiber surface morphology before and after the immersion test	178
Figure 3.1	Fracture morphology comparison	186
Figure 3.2	Complex stress corrosion environments in insulator service	192

Figure 3.3	Failure model proposed for insulator brittle fracture	193
Figure 3.4	Fiber structure change in the radial direction	204
Figure 3.5	Crack tip chemistry in acid corrosion of composites	209
Figure 3.6	Localized environment at the crack tip	211

ABSTRACT

Brittle Fracture Mechanisms of Glass-Fiber Reinforced Polymer Insulators

Qiong Qiu

Oregon Graduate Institute of Science & Technology, 1995

Supervising Professor: Maciej S. Kumosa

The development of glass-fiber reinforced polymer (GRP) insulators represents a revolution in the electrical power industry. Although their design and manufacture remain relatively new technologies compared to conventional ceramic insulators, GRP insulators have shown a great potential to dominate the future insulator market. With increasing use of GRP insulators in service, particularly in high-voltage transmission applications, however, an unusual insulator failure designated as brittle fracture has been identified; the failure takes place catastrophically under 10-20% of the insulator load capacity in dry fracture, with the morphology of planar fracture perpendicular to the composite rod axis. Today, brittle fracture has become a major obstacle in their future applications of GRP insulators to high-voltage transmission.

To understand brittle fracture mechanisms, a systemic study was undertaken in five major phases: insulator failure analysis, stress corrosion experiments, electrical discharge experiments, acid corrosion behavior of E-glass fiber, and crack tip chemistry.

- Fractographic characterization of service-failed or -damaged insulators discovered both macroscopic and microscopic evidence of stress corrosion fracture, which was most likely initiated at structural damage inside the high-voltage end. However, unlike common stress corrosion fracture, irregular fiber and resin deformation characterized by melted fibers and resin decomposition, for first time, was identified on the insulator fracture surface, suggesting that service electrical activities were involved in the fracture process.

- The stress corrosion experiments revealed the effects of acid type and concentration, mechanical load, and material on the fundamental stress corrosion behavior of GRP composites. The results indicated that stress corrosion behavior of E-glass fiber/polymer composites was highly affected by the resin matrix; among polyester, epoxy, and vinyl ester composites tested in nitric acid, vinyl ester composite exhibited the highest stress corrosion resistance. Furthermore, water by itself could not initiate brittle fracture.
- Electrical discharge experiments verified that stress corrosion fracture could be generated in GRP composites subjected to the combined influence of mechanical load and electrical discharge in the presence of water, with the fracture morphology closely resembling the insulator fracture surface, particularly in the fracture initiation site.
- Acid corrosion of E-glass fiber was found primarily attributed to calcium and aluminum depletion. The formation of insoluble salts or complex ions between the anions in oxalic and sulfuric acids and some of the metal ions depleted from the glass accelerated fiber corrosion considerably. Axial and spiral crack morphologies were observed in fiber acid corrosion. The axial crack formation was most likely associated with a larger ion-depletion depth than the spiral crack formation.
- Crack tip chemistry was complex in nature, which could significantly differ from global environments to which GRP composites were exposed. The crack tip environment was determined by the chemistry of each composite component, the nature of global environments, and more importantly, the interaction between global environments and selective constituents in composites.

This study leads to a comprehensive understanding of the synergistic influence of mechanical, environmental, and electric stresses on the brittle fracture of GRP insulators. Major contributions resulting from this work include the development of brittle fracture mechanisms, an ion-depletion-depth theory for fiber surface cracking in acid corrosion, and a concept of crack-tip chemistry determination.

INTRODUCTION

An electrical power insulator with the dual functions of providing mechanical support and electrical insulation between conductors is a critical component in an electrical transmission system. In recent years, a revolution in insulator technology has taken place as conventional ceramic insulators have been gradually replaced by GRP insulators, which are also referred to in the literature under other terminologies, such as non-ceramic, fiber reinforced plastic (FRP), organic, or polymeric insulators. The generic structure of a GRP insulator consists of a composite rod, polymer housing, and end fittings, of which the composite rod serves as the major load-bearing component. GRP insulators exhibit significant advantages over ceramic insulators, the most appealing being their exceptionally high strength-to-weight ratio, improved damage tolerance, structural flexibility, and great impact resistance. The first application of GRP insulators on outdoor power transmission lines dates back to the early 1980s. Since then, their successful performance has made them widely accepted in the electrical power industry. Although their design and manufacture remain relatively new technologies, GRP insulators have shown great potential to dominate the future insulator market.

With increasing use of GRP insulators in service, particularly in high-voltage applications, however, some concerns have arisen regarding their long-term reliability; an unusual insulator failure designated as brittle fracture has been identified. This insulator failure takes place catastrophically under 10-20% of the insulator load-bearing capacity in dry fracture. The fracture morphology can be characterized by a planar fracture surface running perpendicular to the composite rod axis. Field experience reveals that the brittle fracture of insulators is always initiated either near or inside the high-voltage end, and service voltages associated with the failure are usually 145 kV or higher.

Since the brittle fracture phenomenon was initially recognized, little research has been conducted to understand its failure mechanisms. Simply inspired by their fractographic similarities, most researchers have agreed that the brittle fracture of insulators is most likely attributed to stress corrosion fracture of the composite rod in acidic environments, which may arise from acid rain caused by air pollution and/or from organic acids produced by internal partial discharge in voids embedded inside the composite rod. Stress corrosion of composites is virtually a corrosion-activated fiber fracture process. When a composite is exposed to an acid, the glass fiber in the composite will be corroded as a result of non-siliceous ion leaching due to the ion-exchange reaction, i.e., the non-siliceous ions in the fiber are replaced by hydrogen ions in the acid. For E-glass fiber, the most commonly used reinforcement material in the insulator composite rod, the major leachable non-siliceous constituents have shown to be calcium and aluminum ions. Because of acid leaching, the fibers lose their strength and thereby the composite will fail at a much lower mechanical stress than that in dry fracture, leading to stress corrosion fracture. The brittle fracture of insulators is an extremely complex stress corrosion process, primarily due to (1) the synergistic influence of mechanical, environmental, and electrical activities in service and (2) the high degree of heterogeneity and anisotropy of composite structures. To date, most studies have focused on stress corrosion fracture of composites caused by the interaction of mechanical and environmental stresses; however, little attention has been devoted to electric effects. Failure mechanisms that control the brittle fracture of GRP insulators are still unclear.

The occurrence of brittle fracture has become a great concern in the electrical power industry today. Facing a dramatically increased demand for electrical power supply every year, the utilities in the United States have decided to expand the capability of existing power transmission systems by substantially elevating transmission voltages. Based on field experience, however, a higher service voltage means a greater likelihood of developing brittle fracture. Therefore, understanding the brittle fracture mechanisms and finding solutions to the problem become crucial to further utilization of GRP

insulators in high-voltage transmission systems. The study of insulator brittle fracture not only is of practical significance but also will benefit the advancement of GRP insulator technology.

The objective of this study was to investigate the synergistic influence of mechanical, environmental, and electric stresses on the in-service integrity of GRP insulators, thereby gaining an insight into their brittle fracture mechanisms. The study was undertaken in five major phases: insulator failure analysis, stress corrosion experiments, electrical discharge experiments, acid corrosion behavior of E-glass fiber, and crack tip chemistry.

- Insulator failure analysis fully characterized the fracture morphology of service-failed or -damaged insulators. A special effort was made to identify electrical damage on the insulator fracture surface.
- Stress corrosion experiments focused on the effects of acid type and concentration, mechanical load, and resin material on the stress corrosion behavior of composites. In addition, the water effect was explored.
- Electrical discharge experiments targeted two issues: the possibility of both oxalic acid formation in electrically discharged polyester and stress corrosion fracture of composites under combined mechanical and electric stresses.
- Acid corrosion behavior of E-glass fiber was evaluated with special emphases on non-siliceous ion depletion and fiber fracture morphology in hydrochloric, nitric, sulfuric, and oxalic acids.
- Crack tip chemistry was evaluated, intended to understand the nature of localized environments in composite systems under water and thermal attack.

This dissertation is organized in four chapters. Chapter 1 includes a comprehensive and critical review on the development of GRP insulators, the brittle fracture phenomenon, and the current research status in this field. The experimental procedures and results in

each of the five phases conducted in this study are presented in Chapter 2. Chapter 3 provides an in-depth discussion of the experimental results and further proposes failure mechanisms of insulator brittle fracture, an ion-depletion-depth theory for fiber surface cracking in acid corrosion, and a concept of crack-tip chemistry determination. In Chapter 4, the most important conclusions obtained from this study are summarized, and several recommendations are suggested for improving the in-service integrity of insulators as well as future research.

CHAPTER 1

CRITICAL REVIEW

1.1 Development of GRP Insulators

The introduction of GRP insulators represents a revolution in the electrical power industry. Superior to conventional ceramic insulators, GRP insulators offer significant advantages.¹⁻⁵ The most attractive is their exceptionally high strength-to-weight ratio, resulting in a 90% weight reduction that eases handling, reduces breakage and damage during construction, and lowers installation and transportation costs. GRP insulators also exhibit excellent resistance to vandal damage, better handling of thermal shock, structural flexibility, and improved transmission line aesthetics. A smaller surface area and longer leakage path further enhance the power frequency insulation strength of GRP insulators under wet and polluted conditions.

1.1.1 Historical Background

The development of polymeric insulators began in the 1940s when organic insulating materials were introduced to manufacture high-voltage indoor insulators.¹ In the 1950s, polymeric insulators for outdoor use were made feasible by the discovery that alumina trihydrate filler increases the tracking and erosion resistance of polymer materials. Early polymers used for insulators were bisphenol and cycloaliphatic epoxy resins; however, they did not gain the final acceptance for outdoor insulation applications, primarily due to their poor cold temperature performance and insufficient weight reduction. In the late 1960s, an insulator consisting of a glass fiber/epoxy composite rod with porcelain sheds

was developed. Although this insulator was not widely used, its concept a few years later led to the first generation of contemporary GRP insulators, in which the composite rods were protected by polymer sheds. The commercial GRP insulators finally came into use on high voltage outdoor transmission lines in the 1980s. Since then, GRP insulators have become popular, successively used in West Germany, the United States, France, Canada, England, Italy, and several countries in southern Africa.^{2,6-11}

The use of GRP insulators, due to their high cost, initially was limited to special applications, such as in areas with a high incidence of vandalism, severe contamination, or installation difficulty. In recent years, GRP insulator technology has advanced considerably; improved quality and reduced cost make GRP insulators more competitive with ceramic insulators. As a result, their usage has rapidly expanded into routine outdoor insulation applications,¹² capturing more than 20% of the transmission line market in the United States.⁶ Although their design and manufacture are still relatively new technologies, GRP insulators have shown a great potential to dominate the future insulator market.

1.1.2 Insulator Construction

A suspension insulator is a device with metal attachments, intended to provide flexible mechanical support to electric conductors and to insulate them from ground or other conductors.¹³ At present, three commercial classes of GRP insulators are available: suspension, line post, and station post insulators.⁸ In this study, the suspension GRP insulators are of primary interest. Relative to different loading conditions, these insulators can be further classified as I-string and V-string (Figure 1.1). The I-string insulator is usually subjected to a much higher tensile load than the V-string, but their configurations are identical.



Figure 1.1 Suspension insulators in service.

A common suspension GRP insulator consists of three major constituents: a GRP composite rod, insulator housing (polymer sheath and/or weathersheds), and end fittings. The schematic construction and the cross-section configuration of the insulator are shown in Figures 1.2 and 1.3, respectively. The composite rod, with high axial mechanical strength and dielectric strength, makes up the center core of the insulator and bears a majority of the load in service. To protect the composite rod from environmental influences, polymer housing is required, either with or without separate weathersheds. Some insulator designs employ a polymer sheath between the weathersheds and the composite rod as a part of the housing (Figure 1.2). Projecting from the polymer sheath, weathersheds are uniformly spaced along the composite rod to provide a longer current leakage distance, which becomes crucial in the high-voltage electrical insulation. In most applications, the slant contour is desirable for weathersheds because water can drop off them easily. Additionally, weathersheds can provide an interrupted path for water drainage so that the sheath sections shaded by weathersheds can remain relatively dry in wet weather, improving the electrical performance of the insulator. Designed to transmit mechanical loads to the composite rod, a fitting is placed on each end of the composite rod; the ground (or cold or tower) end connects the tower, and the high-voltage (or hot or line) end links to the electrical transmission line. The structure of a cone end-fitting is detailed in Figure 1.4. In this design, a potting material is firmly bonded to the composite rod and interfaces with the sheath. The metal casting, mechanically connected with the potting material, shields the end fitting from the external environment to reduce the attendant electric stresses in the surrounding air, thus minimizing the chance of corona discharge. For the same reason, metal grading rings are usually installed near the end fittings in high-voltage applications, particularly near the high-voltage end where electric stresses are highly concentrated.

Since the design methodologies of GRP suspension insulators have not been standardized, a wide range of constructions can be found in practice. Further information regarding currently available designs can be found elsewhere.^{2,6-10}

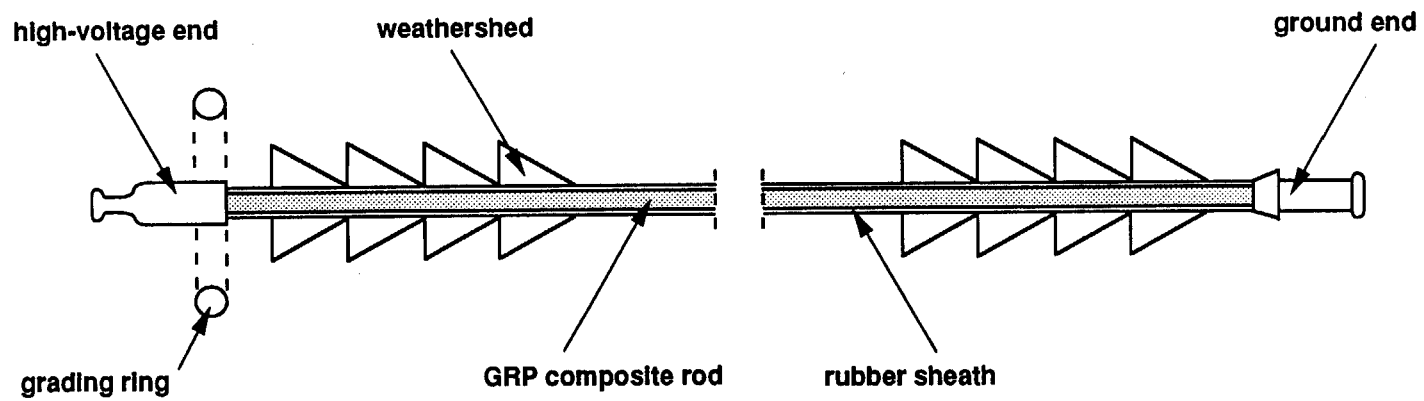


Figure 1.2 Schematic construction of the insulator.

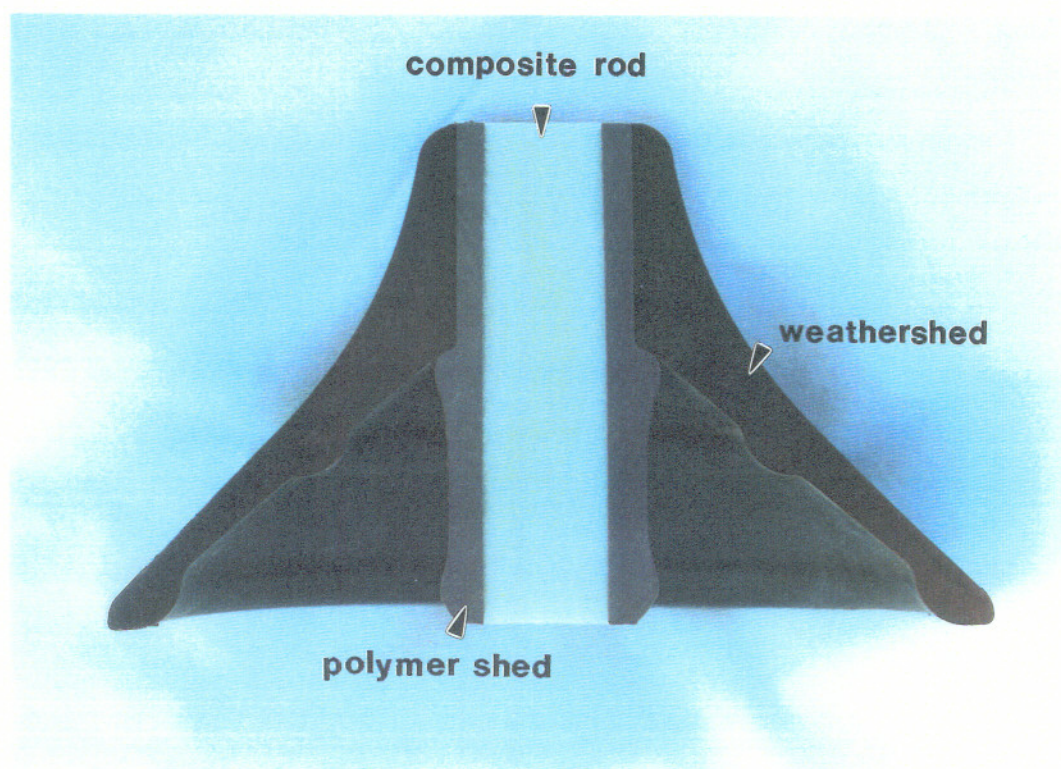


Figure 1.3 Cross-section configuration of the insulator.

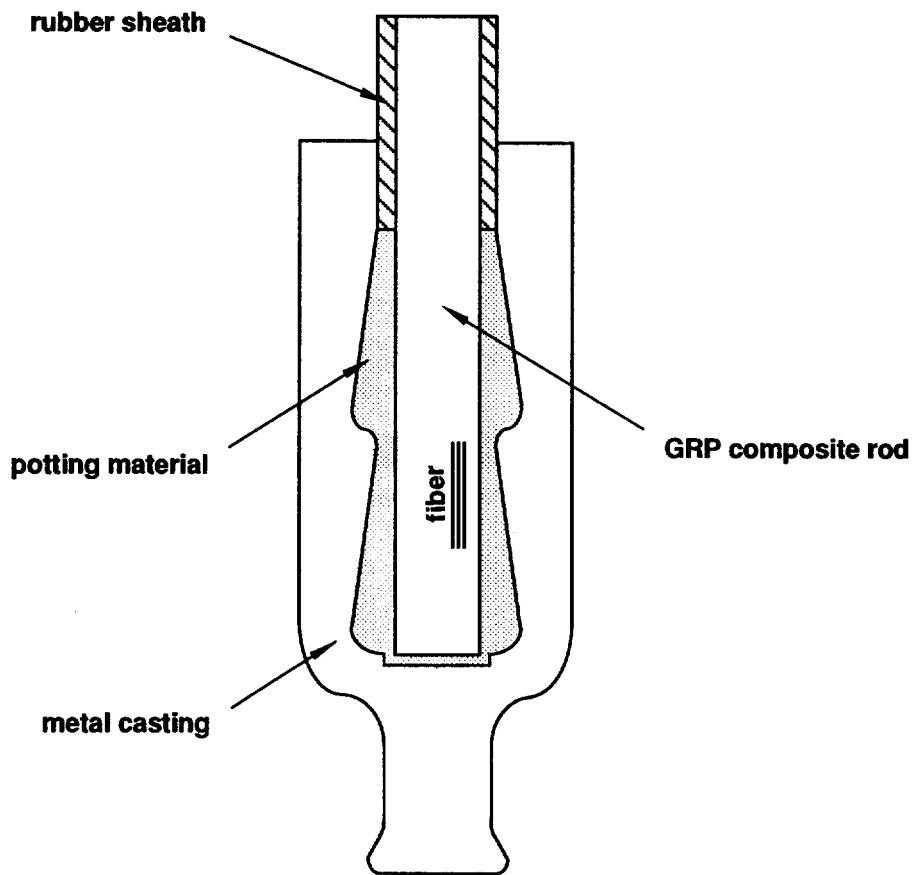


Figure 1.4 Structure of a cone-designed end fitting.

1.1.3 Insulator Materials

The mechanical and electrical performance of a GRP insulator are determined not only by its structural design but also largely relies on the material properties of each component of the insulator: the composite rod, the polymer housing, or the end fitting. In fact, every innovation in insulator development has been associated with the advent of new insulation materials or related technologies.^{1,6}

1.1.3.1 GRP Composites

Made from axially aligned, continuous glass fibers with a resin matrix, the composite rod constitutes the most important component of a GRP insulator. In general, glass fibers possess very high strength coupled with a low density; however, they are by themselves virtually useless in engineering applications. One approach to utilize the unique properties of glass fibers is to embed them in a resin matrix, forming a fiber-reinforced polymer composite. In this material structure, glass fibers provide almost all of the load-bearing characteristics, while the resin matrix binds the fibers into a monolithic form, transfers load to and between the fibers, and protects them from the environmental and handling damage. In practice, desirable properties of composites can be achieved by different combinations of glass fibers and resins.

Glass fibers

Inherently an amorphous structure, common glass fibers are silica based, about 50-70% SiO₂, with calcium, aluminum, boron, magnesium, sodium, or other minor oxides added either to improve the fiber formability or to obtain specific physical and chemical properties.^{15,16} Although many glass compositions have been formulated, only four types are used commercially to fabricate continuous glass fibers for manufacturing GRP composites. These are E-glass (calcium aluminoborosilicate), ECR-glass (calcium

aluminosilicate), S-glass (magnesium aluminosilicate), and C-glass (soda-lime-borosilicate), the designations of which stand for electrical grade, corrosion resistant E-glass, high silica content, and high corrosion resistance, respectively.

Currently, the dominant reinforcement material used in insulator composite rods is E-glass fiber because of its excellent electrical properties, dimensional stability, superior mechanical strength, and low cost. E-glass fiber also exhibits good resistance to moisture and fair resistance to alkalis; however, its acid resistance is relatively poor.¹⁷ The nominal composition and the representative properties of E-glass fiber are shown respectively in Tables 1.1 and 1.2. More recently, ECR-glass, a modified E-glass, has been developed to enhance the glass chemical resistance, particularly in acidic environments. The major changes in ECR-glass composition are a lower alkali content, the absence of boron and fluorine, and additions of zinc and titanium oxides.¹⁸ ECR-glass fiber is still under development, but it has shown a great potential to replace E-glass fiber in composites for insulator applications because of its exceptional corrosion resistance.¹⁷

Resin matrices

Although the type of glass fibers determine the potential ultimate strength of a composite, the stress transfer efficiency of the resin matrix controls the actual level of mechanical properties that can be realized. Furthermore, most physical and chemical properties of a composite, such as high-temperature performance, corrosion resistance, dielectric property, flammability, and thermal conductivity, are governed exclusively by the characteristics of the resin matrix.¹⁹ Therefore, selection of the resin and its formulation chemistry become critical, especially in the applications where the physical and chemical properties are concerned.

Table 1.1 Nominal composition of E-glass fiber, wt%¹⁶

Silica	Alumina	Calcium oxide	Boron oxide	Magnesia	Soda	Calcium fluoride	Minor oxides
54.0	14.0	20.5	8.0	0.5	1.0	1.0	1.0

Table 1.2 Representative properties of E-glass fiber¹⁶

Specific gravity	Tensile strength MPa	Tensile modulus GPa	Coefficient of thermal expansion $10^{-6}/^{\circ}\text{K}$	Dielectric constant α	Liquidus temperature $^{\circ}\text{C}$
2.58	3450	72.5	5.0	6.3	1065

Thermosetting resins have been the most popular matrix materials used in GRP composites. Due to their large molecule, covalently bonded, and crosslinked network structure, these resins, in addition to properties common to all polymers, exhibit adequate strength and rigidity as well as a relatively high thermal stability. Three principal thermosetting resin systems, widely used to construct continuous GRP composites, include unsaturated polyesters, epoxies, and vinyl esters.^{15,19} They differ in their chemical compositions. The cure chemistry of the unsaturated polyester and vinyl ester resins stems from the free radical polymerization of the double bonds present in the polymer chain, whereas the cure chemistry of epoxy resin is a condensation reaction between an epoxy group and the crosslinking agent, such as an amine, an organic acid, or an anhydride acid.²⁰ Because of their different chemistries, these three resins exhibit different mechanical properties, chemical resistance, and degrees of shrinkage.

Polyester resins possess good electrical properties as well as fair resistance to water, various chemicals, weathering, and aging. They can withstand temperatures up to 80°C and combine easily with glass fibers. Given the high unsaturation of polymer chains and the resultant high crosslink density, however, polyesters shrink between 4% and 8% on curing, which in turn increases their susceptibility to microcracking. An alternative to polyesters, vinyl esters are often used when higher corrosion resistance and elevated temperature capability are required. Compared to polyesters, vinyl esters have a lower crosslink density and hence greater toughness properties, such as shear and impact strength, but they usually cost 75% more than polyesters due to slower process speed. Of the three resin systems, epoxies are superior to polyesters and vinyl esters in mechanical properties as well as electric and thermal puncture strengths. In general, epoxies exhibit high cantilever strengths, thermal stability, excellent electrical properties, low shrinkage (about 3%) on curing, and good resistance to moisture and other environment influences. However, composites made with epoxy resins are known for their poor toughness because of the epoxy's rigid structure, even though epoxies have

increased continuous-use temperatures up to about 150°C. In addition, epoxies are approximately six times more costly than polyesters.

Depending on the chemical structures of curing agents, the additions of modifying reactants, and process conditions, a series of resins in each resin system can be formulated to tailor the base resin properties to the levels desired for specific applications. Resins available to the current GRP insulator market include standard medium reactivity isophthalic-based polyester, modified isophthalic-based polyester, high strength vinyl ester, high heat resistant modified vinyl ester, and high strength heat resistant epoxy.²¹

Fiber/resin interfaces

In a GRP composite, the glass fiber/resin interface is of great importance because the internal surface area introduced by the interface is extensive and because the interface characteristics directly affect mechanical behavior and temperature- or diffusion-controlled properties of the composite.¹⁵ The glass fiber/resin interface, more precisely the glass fiber/resin interfacial zone,²² usually consists of a sizing, a surface coating applied to the fibers to protect them from contact damage during fiber fabrication.

Glass fiber sizing is usually made of water-based emulsion, which contains two major ingredients: a film-forming polymer and a silane coupling agent.^{15,23} Possessing superior wetting and spreading properties, a film-forming polymer can produce a continuous and uniform coating on glass fibers, thus minimizing potential contact damage. Because of its inherently high polarity, however, a film-forming polymer is hydrophilic in nature. As a result of sizing, the fiber/resin interface becomes permeable to water, thereby reducing the interface bonding strength, or even damaging the glass fiber. To improve the moisture durability of composites, adhesion promoters, in particular silanes, are added to the sizing.

Commercial silanes are constituted by multi-functional groups with a general chemical formula X_3Si-R ,¹⁵ where X is a hydrolyzable group bonded to silicon such as chloro-, methoxy-, or ethoxy-, and R is an organic group such as -vinyl, -aminopropyl, or -methacryloxypropyl, which is compatible with the matrix resin. The X groups are hydrolyzed in aqueous size solutions to give trihydroxy silanols. These silanols are attached to the glass surface by hydrogen bonds. When the sized fibers are dried, water is removed, leaving a polysiloxane layer against the glass surface and an outer polymeric layer rich in R groups. During the curing process the R groups react directly with functional groups in the matrix resin, forming covalent bonds.

In practice, sizing formulation is highly empirical. Although the contribution of silanes to moisture resistance has long been recognized, the mechanisms involved are not well understood. The basic function of silane was early thought to be the formation of a simple chemical coupling between the glass fiber and the resin. More recently, several researchers^{23,24} have suggested that silane constructs the initial, open network on the glass substrate, then the matrix polymer, together with the film-forming polymer, penetrates into the silane network, forming an entangled polymer network in the interfacial zone between the glass fiber and the resin matrix. This new concept presents a more realistic picture of the adsorbed silane interface, but it still does not explain how silane protects the interface from moisture attack.

1.1.3.2 Insulator Housing

Insulator housing, consisting of a sheath and/or weathersheds, is made of polymer compounds. Like any other organic materials, housing polymers readily experience environmental aging, which is especially severe when they are used in an outdoor high-voltage insulation application. Therefore, the properties of housing polymers, such as tracking, erosion, and weathering resistance, become limiting factors in both the mechanical and electrical performance of GRP insulators.^{12,25-30} For outdoor high-voltage

insulation applications, insulator housing materials are generally required to have (1) good resistance to electrical tracking and discharge, (2) high dielectric strength to minimize erosion damage, (3) fair mechanical strengths, (4) good resistance to weathering, particularly ultra-violet radiation and oxidation, and (5) superior surface hydrophobicity, the ability to repel water, as well as fast hydrophobicity recovery after its temporary loss.

Four major polymer systems are currently used for insulator housing: epoxy, ethylene/propylene rubber (EPR), silicone rubber, and ethylene propylene diene monomer (EPDM)/silicone alloy.^{1,6,10,12,29} In the epoxy system, cycloaliphatic epoxy polymers are most commonly used, but their inherently low tensile strength prevents them from use in suspension insulators. Recent efforts have been made to improve the mechanical and electrical properties of epoxies by adding suitable filler materials. EPR designates both ethylene propylene monomer (EPM) and EPDM. Compounded with different fillers and additives, a variety of EPMs and EPDMs have been formulated, each offering a specific combination of characteristics. EPRs are generally among the best weathering resistant synthetic rubbers. By selecting the particular compounding chemistry, EPDMs can provide improved mechanical properties, superior aging and color stability, together with outstanding resistance to the effects of sunlight, oxygen, and ozone. However, there are disadvantages to EPDMs, particularly their high susceptibility to surface electrical discharges. Silicone rubbers, with both organic and inorganic ingredients, exhibit a combined organic/inorganic behavior. Relative to their vulcanizing temperature, they can be further identified as room-temperature-vulcanized silicone rubbers, RTVs, or high-temperature-vulcanized silicone rubbers, HTVs. The most beneficial properties of silicone rubbers are an exceptionally high surface hydrophobicity and the fast recovery of surface hydrophobicity after its temporary loss, which make them attractive for outdoor insulation applications, particularly in heavily contaminated areas. Silicone rubbers also maintain dielectric strength at elevated temperatures, but compared to EPRs, they possess lower mechanical strengths and higher susceptibility to

mishandling damage and vandalism. The newest development in insulator housing materials is represented by EPDM/silicone alloys, which inherit EPDM's superior mechanical properties and silicone rubber's high hydrophobicity.

Polymer characteristics depend not only on base polymers but also on filler and additive materials. In a polymer compound, a variety of fillers and additives, with up to 65% of the total polymer formulation by weight, can be incorporated into the polymer to enhance its physical and mechanical properties or to impart certain processing characteristics.²⁹ Generally, fillers can be classified into two groups: reinforcing and extending. The reinforcing filler improves hardness and mechanical properties, particularly the abrasion and erosion resistance of a polymer. The two most commonly used reinforcing fillers are carbon black and fine particle mineral pigment, such as silica. An extending filler, a non-reinforcing material, often is added to a polymer to optimize polymer physical characteristics or to reduce cost. Alumina trihydrate is an extending filler, used for its ability to suppress both electrical track development and flame generation. In addition to fillers, numerous additives can be compounded with polymers for special applications.^{19,29} Important categories of additives include curing agents for optimizing mechanical properties and processibility; coagents for inhibiting base polymer/curing agent bond degradation; ultra-violet stabilizers for improving weatherability; pigments for coloring; antidegradants for enhancing resistance to oxygen, ozone, and heat; coupling agents for strengthening the filler/base polymer chemical bond; processing acids for easing mold releases; plasticizers for lowering viscosity or increasing flexibility at low temperature; and other functional additives. A variety of options also are available in each of the preceding categories.

1.1.3.3 End Fittings

Materials used for end fitting construction vary with the end-fitting designs. Metal castings, essential to every end-fitting design, can be made of cast iron, steel, or

aluminum. To enhance their corrosion resistance in service environments, all of the ferrous materials, except for stainless steels, normally are hot-dip galvanized in accordance with ASTM A153.³¹ Adequate ductility is also required for the metal casting to prevent it from brittle failure. For some end-fitting designs, potting materials, usually epoxies, are utilized to achieve mechanical connection between metal castings and composite rods.

1.1.4 Insulator Manufacture

The manufacture of GRP insulators is a complex process. For the purposes of this study, only the two principal aspects of the process, composite rod fabrication and insulator assembly, are described here.

1.1.4.1 Composite Rod Fabrication

GRP composite rods are manufactured by the pultrusion process, an automated process for forming composite materials into continuous, constant cross-sectional profiles.¹⁹ In this process, reinforcing glass fibers are preimpregnated with a liquid thermosetting resin and pulled through a heated mold or die to cure the resin. Fiber placement, resin formulation, catalyst level, die temperature, and pulling speed are critical processing parameters. The pultruded composite rod used for insulators usually contains 70-80% glass fibers by volume, exhibiting the maximum mechanical strength along the rod.

1.1.4.2 Insulator Assembly

Insulator assembly, particularly the end-fitting assembly, is critical to the overall performance of insulators. Since the insulator design differs from one manufacturer to another, even for the same insulation application, a variety of assembly technologies have been developed.

For the suspension insulator with separate polymer sheath and weathersheds, a sheath is extruded on the composite rod first. To ensure firm bonding between the rod and sheath, the rod/sheath interface is usually vulcanized. Some manufacturers may use adhesives and greases as the rod/sheath interface bonding agents for the same purpose. In most cases, the sheath extends inside the end fitting. After the sheath is formed on the rod, each individually molded weathershed is slipped onto the sheath, and then the sheath/weathershed joint may be completely or partially vulcanized into place.

The load carrying capacity of insulators is usually limited by the strength of their end connections.³² The metal castings can be attached to the rod by different techniques,^{6,7,33} depending on the end-fitting design. The earliest glue design, the gluing of the metal casting to the rod, has been discredited because of pull-off problems. Cone, wedge, and compression end fittings are the most widely used designs today. In the cone design, the inner surface of the metal casting is shaped in a single or multiple-stepped cone contour. After the metal casting is capped on the rod end, the epoxy potting material is poured into the tapered cavity inside the end fitting through a port on the casting and then cured, bonding firmly both to the rod surface and the polymer sheath. Since the inner surface of the metal casting is precoated with a release agent, the bonding between the potting material and the metal casting is prevented. Finally, the port on the casting is sealed to avoid moisture penetration. In this design, both the rod and the potting material slip as a unit against the metal casting when a tensile load is applied to the rod. Given the conical inner contour of the metal casting, the rod end bonded with the potting material is secured inside the end fitting, thus achieving the load transfer. In the wedge design, a metal wedge is longitudinally inserted into the rod end, and under load, the slippage of the metal casting forces the metal wedge to lock into place, transferring the load to the rod. A more advanced design is compression end fitting, in which a metal shell is crimped directly onto the rod end during assembly. This design provides insulators with a higher torsion strength and better moisture resistance.

1.2 Brittle Fracture of GRP Insulators

During the past fifteen years, successful applications of GRP insulators have made them widely accepted in the power transmission industry. With the increasing use of GRP insulators in high voltage applications, however, an unusual insulator failure, later designated "brittle fracture", has been identified. Service voltages associated with these failures range from 145 to 420 kV.^{17,34-42}

1.2.1 Field Experience

Brittle fracture of GRP insulators was first reported in 1980.³⁴ Since then, this failure has been found successively by power utilities from several countries. Field experience in South Africa showed that brittle fracture was particularly significant in insulators used in 275 to 400 kV transmission networks.^{35,37} In a population of 6,000 insulators installed on 275 kV lines, 13 had failed within four years. In Germany, seven insulators broke in a brittle fashion between 1967 and 1982.³⁸ Brittle fractures of GRP insulators have also been reported in France, Italy, the United Kingdom, and North America.³⁹⁻⁴²

Since the first incident, brittle fracture of insulators has become increasingly severe with each year. Unfortunately, few statistics have been made available to the public because of commercial pressure. In 1989, one American utility company began to construct a 345 kV transmission line using GRP insulators. During the first four-year service, 14 complete brittle fractures out of 1,756 insulators were reported, and an additional 200 insulators were suspect. All of the insulator brittle fractures appeared catastrophic in nature and resulted in the complete outage of transmission systems. Today, brittle fracture of GRP insulators has caused such great concern regarding their long-term reliability that their further utilization in high-voltage insulation is challenged.

1.2.2 Brittle Fracture Phenomenon

When a composite rod is subjected to pure mechanical stresses in the dry-air condition, its fracture surface exhibits a broom-like appearance. In brittle fracture, however, the fracture surface appears essentially planar and runs perpendicular to the rod axis. Common brittle fracture morphologies of insulator rods are illustrated in Figure 1.5.⁴³ The typical fracture surface is characterized by a smooth region and a rough region (Figure 1.5a). Although the proportion of the rough region varies with cases, all of its characteristics are identical to those found in the pure mechanically fractured rods. Quite often, several transverse cracks initiate simultaneously at different locations along the rod, thus creating separate fracture planes linked by longitudinal delaminations in the rod (Figure 1.5b). Under certain circumstances, a planar fracture surface can be interrupted by a series of longitudinal delaminations (Figure 1.5c). A stepped fractography is also possible as a result of mixing the "b" and "c" fracture morphologies (Figure 1.5d).

In addition to the planar fracture morphology, other important evidence relevant to brittle fractures has also been found.^{8,17,35,43-45} Generally, brittle fractures of GRP insulators

- took place at 10 to 20% of the insulator load-bearing capacity in the dry-air condition,
- likely occurred either near or inside the high-voltage end,
- were often associated with high voltage applications,
- initiated from the external surface of composite rods, and
- seemed only related to specific manufacturing designs.

However, the occurrence of brittle fracture in service appears unpredictable. Based on field experience, brittle fractures of GRP insulators could occur within one month or 15 years later after installation. This behavior suggests that the insulator brittle fracture is likely controlled by a progressive deterioration mechanism in which other influences besides mechanical loads must be involved.

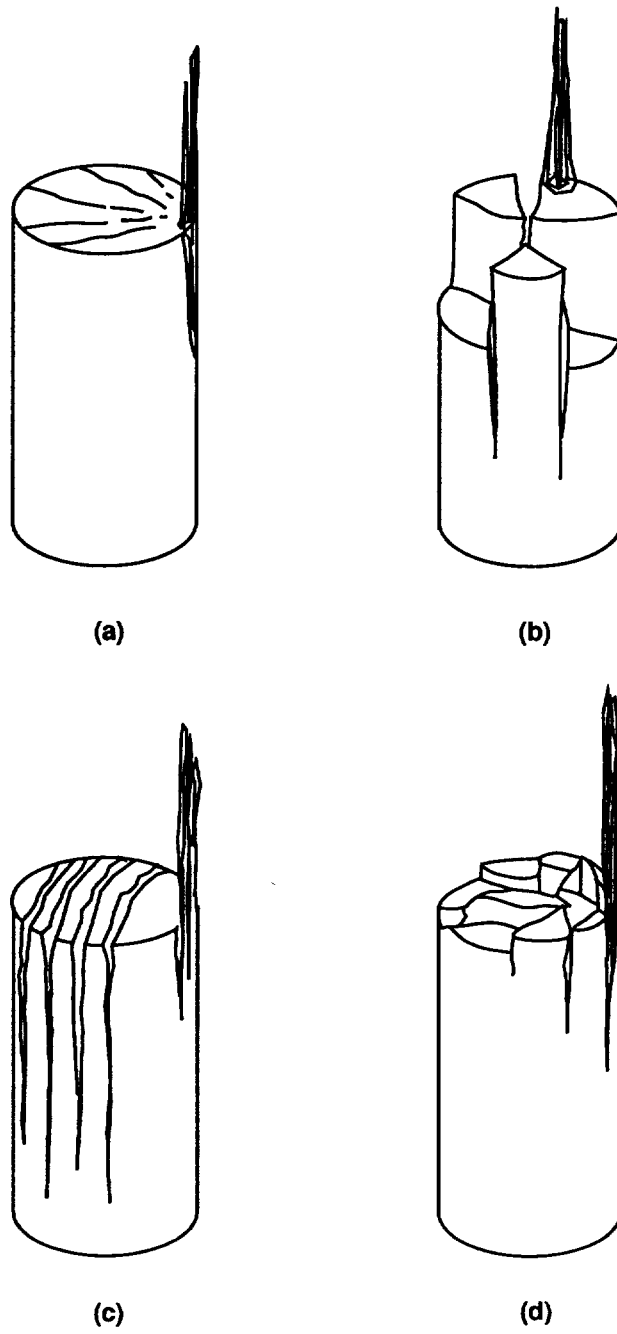


Figure 1.5 Fracture morphology of insulators.

Since the brittle fracture phenomenon was first recognized, some research has been conducted to understand its failure mechanisms.^{17,35,44-49} Inspired by the fractographic similarities between insulator brittle fracture and stress corrosion cracking of GRP pipelines and tanks,⁵⁰⁻⁵⁴ most of investigators have agreed that the brittle fracture of insulators are likely attributed to stress corrosion fracture of the composite rod in acidic environments. The fracture process is probably generated at the composite rod surface by environmentally induced cracking. Initial crack growth is controlled by the chemical deterioration of the glass fibers and tends to be slow, forming a smooth fracture region. As the crack advances further, the remaining load-bearing area on the rod cross-section becomes smaller, and the fiber/resin interface fracture becomes pronounced due to an increase in stress intensity at the crack front. Eventually, the insulator rod fails in a purely mechanical fashion, leaving a broom-like fracture region with extensive fiber pull-out and longitudinal splitting.

1.3 Stress Corrosion of GRP Composites

In recent years, intensive investigations have been undertaken on the stress corrosion behavior of GRP composites.⁵⁰⁻⁷³ An important conclusion that has emerged indicates that GRP composites are susceptible to stress corrosion cracking, especially in acidic environments. Generally, the stress corrosion phenomenon of composites has three features in common: (1) the fracture surface appears planar in nature, (2) the process is driven at much lower stresses than those required for dry fracture, and (3) the fracture of composites is controlled by a progressive fiber deterioration mechanism, resulting in a relatively slow crack growth.

1.3.1 Fracture Morphology

The most distinctive feature of stress corrosion in unidirectional GRP composites is the planar fracture morphology. Assisted by corrosive environments, a stress corrosion

process can take place at a low mechanical load so that the fiber/resin interface fracture, such as interfacial debonding and fiber pull-out, is limited. As a result, the stress corrosion fracture is restricted at the point of environmental attack, and the fiber fracture is usually co-planar with the resin fracture, leading to a clear-cut fracture surface.

Microscopically, a fiber fracture surface can be characterized by the classic mirror, mist, and hackle regions (Figure 1.6a), which have been well documented in glass fracture.⁷⁴⁻⁷⁶ The mirror refers to the smooth region on the fractured fiber surface. The region with radiating ridges and valleys is defined as the hackle region. Located between the mirror and the hackle, the mist appears slightly rough with micro-cracks. Fracture of individual fibers always initiates at the focus of the mirror zone and radiates to the mist region. As the crack becomes unstable, it bifurcates from the mist region, resulting in a hackle fracture appearance and sometimes forming a wedge between the two crack planes (Figure 1.6b).

Promoted by the fiber fracture, the matrix fracture features river lines and a polygonal network (Figure 1.7), although irregular fiber distribution can lead to complex matrix fracture morphology. Price,⁵⁰ who attempted to explain the matrix marking formations by assuming an idealized square fiber array, suggests that the river lines are derived directly from the ridges in the fiber hackle region to maintain the continuity of the crack front, and that the polygonal network is formed where the matrix cracks from adjacent fibers meet.

Fractography of individual fibers and local matrix not only reveals their fracture characteristics but also provides the information of the overall crack initiation and propagation. As a rule of thumb, the crack initiation site is always located in the region of fibers with relatively large mirror sizes, and the crack propagation direction can also be deduced from fiber and matrix surface markings.⁵⁰ In some cases, wide variations exist in the direction of local crack growth; some of these variations coincide with

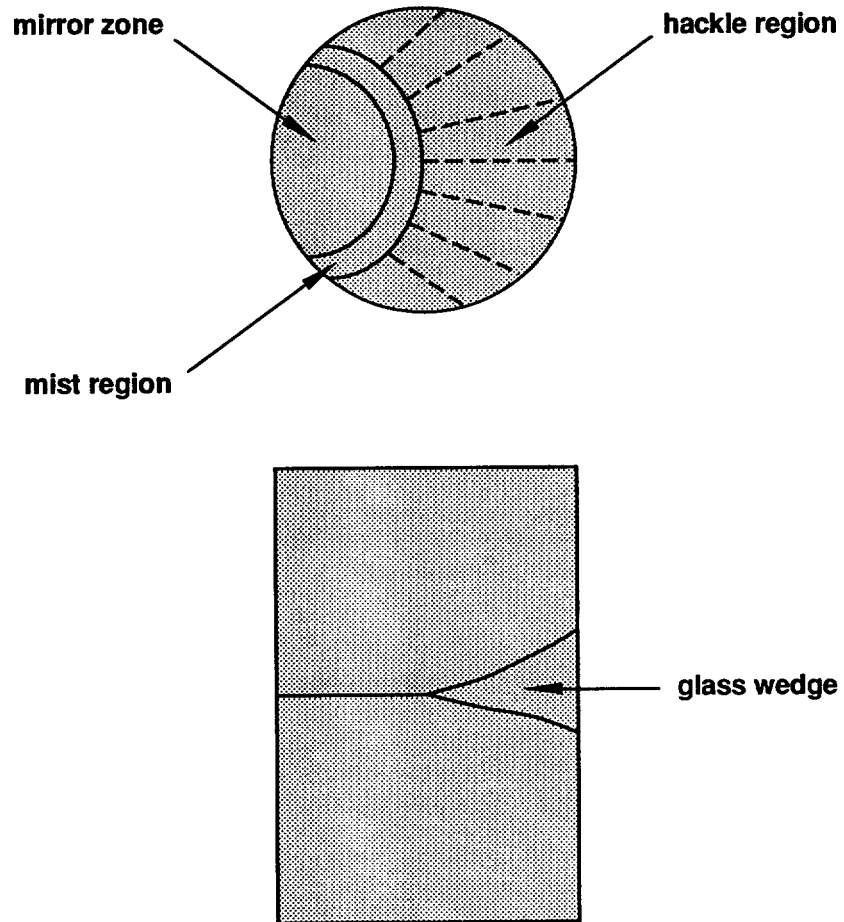


Figure 1.6 Single fiber fracture.

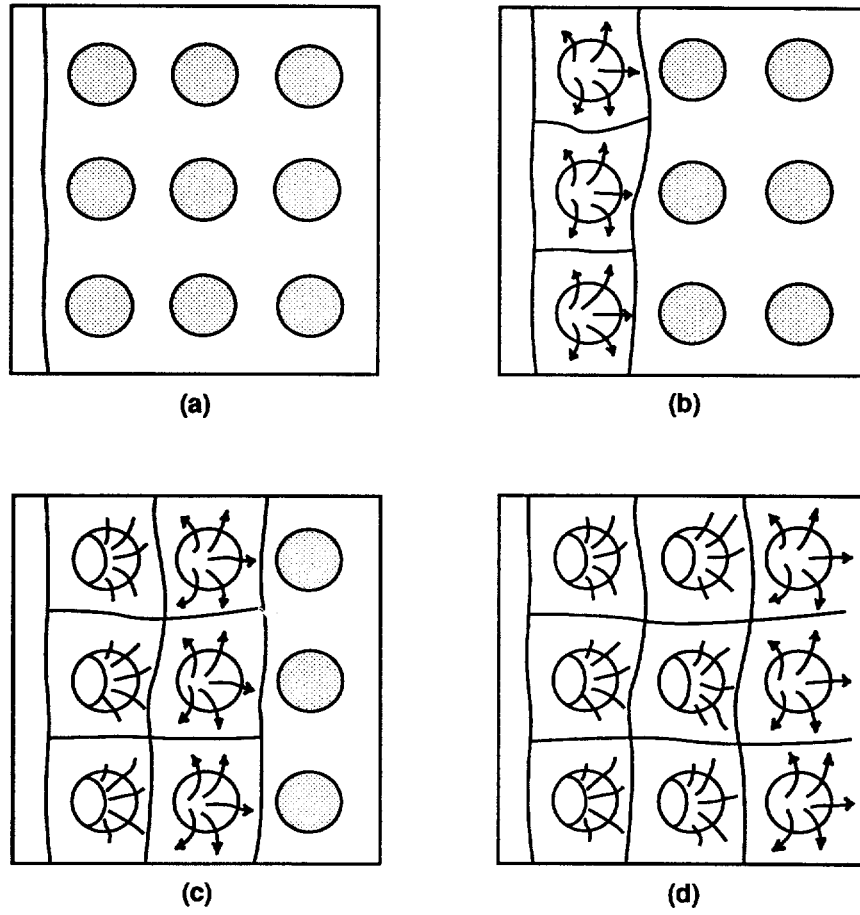


Figure 1.7 Matrix fracture markings.

macroscopic features, such as steps, on the fracture surface, while others may be associated with either local irregularity in fiber packing or resin-rich regions.⁶²

1.3.2 Physical Fracture Theories

The planar nature of fracture surfaces implies that stress corrosion fracture is primarily attributed to fiber fracture and matrix fracture. Generally, matrix fracture is physical in nature; while fiber fracture is controlled by chemical deterioration.

1.3.2.1 Fracture Models

Stress corrosion in composites consists of two stages: crack nucleation and crack propagation. Early studies suggest that a stress corrosion crack is likely to be initiated at the weakest point, usually at a flaw on the fiber surface.⁷⁷ However, this concept has been challenged by the existence of the planar fracture phenomenon, which requires that the surface flaw in each fiber ahead of a crack be aligned with the growing crack. Lhymn and Schultz,⁷⁸ who examined stress corrosion cracking in short-fiber reinforced composites, propose that acidic attack may produce etch pits, which act as stress raisers to promote fiber fracture. However, no evidence of such etch pits has ever been found on the fractured fiber surfaces.⁷⁹ At present, the demineralization on the fiber surface at the crack front has emerged as the crack initiation mechanism. Because the crack nucleation stage is insignificant compared to the crack propagation stage in composite systems, most research has been devoted to crack propagation behavior.^{62,63,66-68,80}

Stress corrosion of a composite virtually is a fiber fracture phenomenon.⁵⁵ Because glass fibers are shielded by a resin matrix, the accessibility of corrosive environments to the fiber becomes a controlling factor in the crack propagation mechanisms. Price and Hull⁶⁶ suggest two means by which corrosive media can reach the fibers: (1) direct access through micro-cracks or voids in the matrix and (2) indirect access by diffusion through

unfractured resin. The nature and extent of resin matrix cracking will determine which of these processes predominates.

An initial qualitative representation for crack propagation, presented by Hogg and Hull⁶⁰ on the basis of the idealized unidirectional composites loaded in uniaxial tension along the fiber direction, depicts a micro-mechanical stress corrosion mechanism (Figure 1.8). This model proposes that initial fiber fracture, assisted by chemical attack, occurs at such a low mechanical load that the crack-front stress intensity is insufficient to promote fiber/resin debonding. Immediately following the first fiber fracture, the surrounding matrix may crack, creating a channel through which corrosive media can gain access to the contiguous fiber. Consequently, crack propagation proceeds along a single microscopic plane until the stress at the crack front, which increases with the crack length, becomes high enough to initiate fiber/resin debonding. This model assumes that the fibers are weakened in an acidic environment by ion-exchange reactions. A further implicit assumption in this preliminary model is that crack propagation is achieved by mechanical cracking of the surrounding resin web after fiber fracture at the crack front.

Further understanding of the matrix influence on crack propagation behavior has led to the development of the diffusion-controlled crack propagation mechanism (Figure 1.9), an improved model proposed by Hogg and Hull⁶⁸ based on their study of stress corrosion crack growth in pipes with different resin matrices. This model suggests that the fracture toughness of resin matrix is a critical parameter in determining crack propagation behavior. If the matrix is brittle, fiber fracture may simultaneously result in resin fracture, the stress corrosion crack progressing directly to the next fiber. If the matrix is tough, however, fiber fracture may not cause complete fracture of the surrounding resin web, separating the crack front from the next fiber. In this event, further acid diffusion through the unbroken resin is required to fracture the next fiber, and the crack propagation will become diffusion limited. Moreover, once the second fiber eventually fails, the resin web may or may not remain intact. Under certain circumstances,

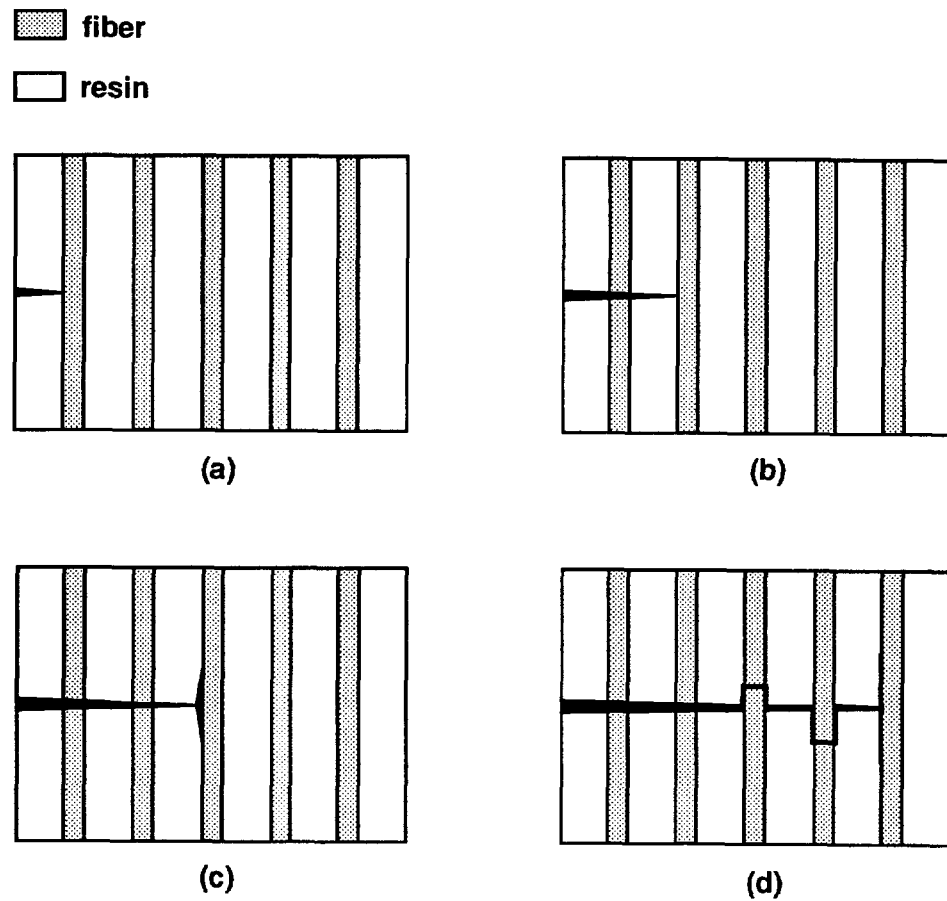


Figure 1.8 Schematic representation of crack growth in unidirectional composites in acids: (a) initial fiber and matrix fracture, (b) fracture of adjacent fibers owing to acid attack at the crack front followed by matrix fracture, (c) limited interface debonding caused by the stress at the crack front, and (d) crack growth involving increasing amount of out-of-plane fracture.

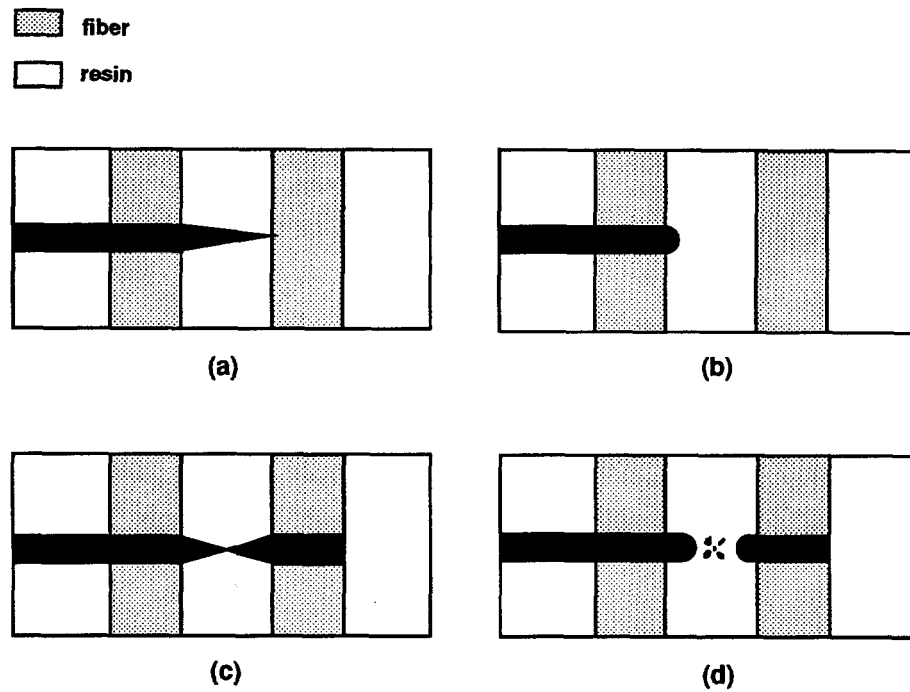


Figure 1.9 Influence of resin toughness on crack propagation behavior: possible sequence of events at the crack front for (a) brittle resin, (b) tough resin, (c) tough resin after the second fiber break leading to resin-bridge fracture, and (d) very tough resin after the second fiber break without resin-bridge fracture.

subsequent fracture of the second fiber may lead to back-cracking through the resin behind the crack front, thus coalescing the fiber fracture surfaces. If the matrix is sufficiently tough, however, fracture of the second fiber may not be able to break the resin ligaments, leaving plastic flow and cavitation between the fibers. To advance the crack, therefore, additional energy would be needed to tear apart those ligaments.

This model has been supported subsequently by several studies on the stress corrosion fracture morphology of various GRP composite systems.⁶⁶⁻⁶⁸ The results obtained from these studies reveals that the matrix effect on crack propagation may be attributed to the resin modifying the stress field at the crack front; the stress at fracture on individual fibers is generally higher for brittle resins than for tough resins. Using the equations proposed by McClintock to calculate the stresses acting on the fibers at the crack front, Hogg⁶⁷ further suggests that stress modification because of tough resins is achieved by limited yielding in a constrained resin layer parallel with fibers at the advancing crack front. Although tougher resins can effectively reduce the crack growth rate, they usually exhibit poorer chemical resistance and higher diffusion coefficients than brittle resins. The optimum resin for a stress corrosion resistant composite, therefore, represents a compromise between its diffusion coefficient or chemical resistance, and fracture toughness.

1.3.2.2 Fracture Stresses

The fracture morphology of a fiber, the mirror size in particular, provides a measure of the tensile stress acting on the fiber at fracture.⁵⁰ In general, the larger the mirror size, the lower the fracture stress that the fiber experiences.

The terminology of mirror size originated from fractographic studies of glasses and ceramics, later becoming an important concept in fracture mechanics of brittle materials. Through the years, many studies have been conducted to correlate the mirror size with

the fracture stress, fracture energy, or critical flaw size.⁷⁴⁻⁷⁶ For glasses and ceramics free from residual stresses, the relationship between the mirror size, r , and fiber fracture stress, σ_f , can be expressed by the following empirical equation:

$$\sigma_f r^{1/2} = A , \quad (1.1)$$

where A is a material-dependent mirror constant, and r is measured by the mirror radius, the distance from the fracture origin to the mirror/mist boundary (Figure 1.4). When residual stresses are involved, however, the simple relationship defined above becomes invalid. Kerper and Scuder⁸⁴ studied tempered and semi-tempered glass and found that the exponent of the mirror radius was not equal to 0.5 but changed with residual stresses. Kirchner and Gruver⁸⁵ and Shinkai and Hara,⁸⁶ in separate studies, concluded that Equation 1.1 must be modified when residual stress (σ_r) is present:

$$(\sigma_f + \sigma_r) r^{1/2} = A , \quad (1.2)$$

where the residual stress could be either tensile or compressive. This relationship was later validated by Mecholsky and Drexhage's study on compressively clad glass rods.⁸⁷

More recently, Jaras and Norman,⁸⁸ who have performed the mirror size/strength calibration on different types of glass fibers with diameters greater than or equal to $12\mu\text{m}$, confirmed that the inverse square root relationship is also applicable for glass fibers. The mirror constant obtained is $1.47 \text{ MPa m}^{1/2}$ for E-glass fibers. In dry fracture, fiber mirror sizes are usually too small to be measured; however, in stress corrosion fracture, they are measurable so that fiber fracture stress can be evaluated directly from fiber fracture markings. In the same study, Jaras and Norman also applied mirror size measurements to the direct estimation of fiber failure strength in glass-fiber reinforced composites, providing a potential technique to study the change in fiber strength distribution with time and to evaluate the failure strengths of composites.

Because of the complexity of a unidirectional composite structure, it is extremely difficult to predict the failure stress of a composite rod. To the first approximation, however, the macro-stress at failure for the composite rod, σ_c , can be estimated from the rule of mixtures:

$$\sigma_c = E_m \epsilon_m V_m + E_f \epsilon_f V_f , \quad (1.3)$$

where E is the Young modulus, ϵ is the strain, and V is the volume fraction. The subscripts m and f in the equation stand for matrix and fibers respectively. When a GRP composite rod is subjected to an elastic deformation under uniaxial tension, the following relation is assumed to be valid:

$$\epsilon_m = \epsilon_f = \epsilon_c = \sigma_f / E_f . \quad (1.4)$$

Strictly speaking, Equation 1.4 holds true only if the fiber and the resin adhere perfectly and have the same Poisson ratio. Combining Equation 1.3 and 1.4, the fracture stress for the composite rod can be estimated by

$$\sigma_c = \sigma_f [E_m / E_f (1 - V_f) + V_f] , \quad (1.5)$$

where the volume fraction of voids in the composite is neglected. It should be noted that the failure stress obtained by using Equation 1.5 might be either underestimated or overestimated given that the restrictions for each of the above equations cannot be fully fulfilled in reality. In addition, Equation 1.3 is not necessarily valid for stress analysis when stress is highly concentrated. The rule of mixtures has been verified for composite modulus measurements but has proven to be inaccurate for strength measurements.¹⁵ Currently, the finite element technique is the only effective method available for stress analysis in a high stress situation, such as the stress distribution at a crack front.

1.3.2.3 Crack Growth Rate

The validity of fracture mechanics, when applied to the crack growth in GRP composite materials, has been subject to some debate.^{89,90} The poorly defined crack front and large damage zone, normally associated with the crack growth in the composites, are major concerns leading to the invalidation of the fracture mechanics. In stress corrosion fracture, however, these problems do not arise; the crack front is usually sharp, with only a small damage zone.

The possibility of applying fracture mechanics to the stress corrosion fracture of unidirectional composites has been demonstrated by Aveston and Sillwood⁹¹ and Price and Hull.⁶² Both groups found that stress corrosion crack growth, normal to the fiber direction, obeys a simple power law:

$$da/dt = A K_I^n, \quad (1.6)$$

where A and n are material constants, K_I is the Mode I stress intensity factor, and da/dt is the crack growth rate. This relation can be converted into a linear relationship in a double-logarithmic scale.

Because of the high degree of heterogeneity and anisotropy of composite materials, the stress intensity factor in Equation 1.6 cannot be directly calculated from the simple equations that exist for homogeneous, isotropic materials. As is mentioned above, however, linear elastic fracture mechanics remains valid for the analysis of stress corrosion crack growth in composites because of a small damage zone at a crack front, particularly in the early stage of stress corrosion fracture.⁶² The stress intensity factor can, therefore, be derived from its relation to the strain energy release rate, G , in the plane strain condition:

$$K_I^2 = E G / (1 - \nu^2) , \quad (1.7)$$

where E and ν represent Young's modulus and Poisson's ratio along the fiber direction, respectively. The strain energy release rate can be determined by the change in compliance, C , with the crack length, a , experimentally:

$$G = (P^2/2t) (dC/da) , \quad (1.8)$$

where P is the applied load and t is the width of the crack front. Substituting G in Equation 1.7 with Equation 1.8, hence,

$$K_I^2 = [E / (1 - \nu^2)] [P^2 / (2t)] dC/da . \quad (1.9)$$

The validity of this approach for composite stress corrosion applications is discussed in detail elsewhere.⁶²

Stress corrosion crack growth in composites is also influenced by material, environmental, and mechanical variables. A systematic study conducted by Hogg and Hull^{67,68} showed a significant effect of resin types on the crack growth rate. Their results suggested that the resin's toughness, rather than its chemical resistance, control the rate of stress corrosion crack growth. B. Noble *et al*⁴⁷ studied the crack propagation behavior of GRP composite rods in various acidic environments and found that crack growth rate also was highly dependent on acid concentration, stress level, and ease of acid access to the fiber surface. The higher acid concentration at the crack front, the lower stress intensity was required to maintain a given crack propagation rate. Additional work performed by Price and Hull,⁶² revealed large variations on microscopic crack growth, although the crack growth rate appeared constant on a macroscopic scale. These variations were probably related to the mechanism of crack extension, particularly to secondary cracking parallel to the fibers. The occurrence of secondary cracking

lessened crack propagation rate. Price and Hull also stressed the influence of fiber volume fraction on the crack propagation rate; an increase in fiber volume fraction led to a reduction of the crack growth rate for a given stress intensity factor.

1.3.3 Chemical Deterioration Theories

The environmental deterioration of composites, particularly reinforcing glass fibers, has received great attention in recent years. Various mechanisms have been proposed to explain the chemical degradation of glass fibers in acidic environments.^{77,92-98} The most predominant is the diffusion-controlled dissolution of non-siliceous constituents in glass by ion-exchange reactions.

1.3.3.1 Environmental Influence on Composites

GRP composites are constructed of three microstructural components: glass fiber, resin matrix, and fiber/resin interface. Largely because of their material nature, these components exhibit different susceptibilities to environmental attack.⁸⁰⁻⁸³ Some environments cause only reversible changes in their physical or mechanical properties, while others may lead to irreversible damage, which becomes especially severe when environments interact chemically with composite components. Property changes induced by various environmental phenomena in each of the components are summarized in Table 1.3.⁸⁰ Very few of the listed phenomena are understood in detail, and little work has been done on the effect of these changes on composite properties.

glass fiber

Glass fiber has proven to be the component most susceptible to environmental degradation in GRP composites.^{50,55,63,80,99-101} Under the influence of water, acid, or alkali, properties of glass fibers may degrade, to a greater or lesser extent. Chemical

Table 1.3 Aspects of property deterioration in GRP composites⁸⁰

Materials Feature	Reversible Change	Irreversible Change
Resin	(1) Water swelling (2) Temperature flexibilizing (3) Physical ordering of local molecular regions	(1) Chemical breakdown by hydrolysis (2) Chemical breakdown by UV radiation (3) Chemical breakdown by thermal activation (4) Chemical breakdown by stress induced effects associated with swelling and applied stress (5) Physical ordering of local molecular regions (6) Chemical composition change by leaching (7) Precipitation and swelling phenomena to produce voiding and cracks (8) Non-uniform de-swelling to produce surface cracks and crazes (9) Chemical effect of thermoplastic polymer content on long term stability
Fiber-resin interface	Flexibilizing interface	(1) Chemical breakdown as above (1-4) (2) Debonding due to internally generated stresses associated with shrinkage and swelling and applied stress (3) Leaching interface
Fiber		(1) Loss of strength due to corrosion (2) Leaching of fiber

Note: the relative importance of these effects will depend on environmental test conditions.

attack mechanisms on glass fiber have been described as a leaching and/or an etching process.^{77,92,100,101} Leaching, more common in acidic media, is governed by ion-exchange reactions, i.e., the selective removal of non-siliceous constituents from glass. Etching is a first-order reaction that involves hydration followed by total dissolution of the glass. This process is more frequently found in alkaline media. The reactions that occur between glasses and solutions highly depend on the chemical composition of the glass.

Pure silica glass, an amorphous SiO_4 network structure, exhibits excellent acid resistance⁵⁰ and low solubility (0.02 wt%) in water,¹⁰¹ although it is susceptible to strong base attack. The addition of other intermediate and network modifying oxides to silica glass, however, will make it potentially vulnerable to water or aqueous acid attack. The fibers used in GRP composites are usually aluminoborosilicate E-glass, which contains about 45% non-siliceous oxides. Simple immersion of E-glass fibers in water or alkali is unlikely to cause serious degradation. By contrast, the consequences of acid exposure can be much more severe, the severity relying on the nature and concentration of acids. Metcalfe *et al*⁹² showed that bare E-glass fibers in dilute hydrochloric acids were subjected to spontaneous cracking, even in the absence of external stresses. This phenomenon is actually attributed to the non-siliceous ion removal from glass fibers by ion exchange mechanisms, which will be addressed in Section 1.3.3.2.

Resin matrix

Thermosetting resins, common matrix materials, are chemically inert with respect to reinforcing glass fibers. In early studies, resin matrices were thought to play a protective role in shielding glass fibers from environmental attack;^{45,63,80,91} more recently, however, they have been shown to be only partial barriers to water and aqueous acids.^{56,58,64,104,105} Research conducted by Marshall *et al* on a variety of resins using radioactive tracer techniques¹⁰⁵ indicates that water readily diffuses through resin systems, the average diffusion coefficient being around 10^{-8} cm²/s. The solvent diffusivity in resins depends

depends primarily on the resin type, temperature, and the nature of solvents, their polarity in particular.^{50,106,107} Noble and his colleagues,⁴⁷ in their study on stress corrosion cracking of pultruded GRP rods in hydrochloric acids, found cracked fibers surrounded by unfractured resin at a crack tip, convincing that stress corrosion fracture of fibers can be achieved by aqueous acid diffusion through the resin matrix. Similar evidence was observed by Hogg and Hull on the fracture surface of unidirectional lamina after stress corrosion cracking in acid.⁸⁰ An alternative to resin diffusion, corrosive media can reach the fiber by resin micro-cracking. This mechanism is especially effective when either the resin matrix is brittle or localized stresses are high. Noble *et al*⁴⁷ suggested that resin diffusion likely takes place in the early stages of the stress corrosion process, but resin micro-cracking may become increasingly important in the later stages with an increase in the stress intensity at the crack front. Furthermore, solvent absorption in resin itself, either directly or indirectly, will affect its susceptibility to cracking, although this process normally occurs slow at room temperature. Solvent attack on resin can be chemical or physical in nature:¹⁰⁸⁻¹¹³ chemical degradation is generally restricted to hydrolysis or oxidation, while physical deterioration often results from swelling, leaching, or plasticization. Due to both a low solubility and an extremely slow absorption rate, solvent absorption does not exhibit significant influence on resin mechanical properties at room temperature but may lead to serious resin degradation at elevated temperatures as a result of a combined chemical and physical effects. When resins are exposed to hot water, leaching of low molecular weight constituents will occur¹¹³, which may lead to a reduction of resin fracture toughness¹¹⁴ as well as the formation of disc-shaped internal cracks.¹¹⁰ Consequently, resins become more prone to cracking.

Fiber/resin interface

Fiber/resin interface, mechanically the weakest component in composites, is also sensitive to environmental damage. Early coupling materials were usually degraded by water

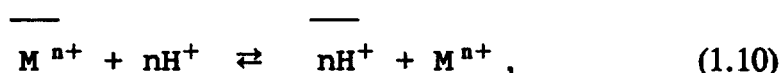
attack because of hydrolysis of interfacial bonds. The use of silane coupling agents has shown the improvement of interfacial integrity in a variety of corrosive environments.^{111,113,115} The deterioration of fiber/resin interface is a complex process that is not exclusively determined by the bonding material but significantly impacted by the resin and fiber degradation behavior. Menges and Gitschner¹¹⁶ indicate that the resin swelling could generate internal stress in the transverse direction and thus cause severe stress concentration at the fiber-resin interface, leading to the interfacial debonding. Alternatively, osmotic pressures have been suggested to be effective in the formation and extension of the interfacial debonding.¹¹¹ During environmental attack, solvents or soluble salts from fiber or resin corrosion may collect in voids or existing debonding at the interface, thus developing osmotic pressures in the interfacial zone. The evidence that solutions, such as brine, are less aggressive than distilled water is actually attributed to the osmotic effect. In the stress corrosion of composites, fiber/resin debonding will have a detrimental influence on mechanical properties of composites, and more importantly, provide a short path for corrosive media to access the glass fiber.

1.3.3.2 Acid Leaching of Fibers

Stress corrosion of GRP composites in acids results primarily from the chemical deterioration of glass fibers. This deterioration is ascribed to the leaching of non-siliceous constituents from glass, which may not only be controlled by the acid concentration but also be influenced by the anions associated with acids.

Leaching mechanisms

Acid leaching of glass fiber is achieved chemically by preferential exchanges between the non-siliceous constituents in glass and the hydrogen ions in acids.^{101,103} Since the non-siliceous constituents in E-glass is dominated by metal ions, the ion-exchange reaction in acid leaching can be simplified into the following expression:



where the bar denotes the species associated with the glass phase. When a fiber is immersed in aqueous acids, metal ions in non-siliceous oxides are readily extracted from the fiber surface, and to maintain electroneutrality, hydrogen ions in acids simultaneously diffuse into the fiber. This ion exchange results in the formation of a sheath that is depleted of metal ions in the fiber surface.^{58,92,117} Since the hydrogen ion is much smaller in size than the replaced metal ions, the depleted sheath tends to shrink; however, this shrinkage is restricted by the intact fiber core. Consequently, a tensile stress is generated in the sheath. Such a stress, with the growth of the sheath, becomes higher and eventually exceeds the sheath fracture strength, promoting spontaneous surface cracking.⁹² This process is accelerated if an applied stress is present.⁷⁷ A schematic representation of fiber corrosion in acids is shown in Figure 1.10.⁵⁰

Because of its low silica content, E-glass fiber contains insufficient SiO groups to screen the soluble constituents from the acid, leading to high leachability. Originally, the acid leaching of E-glass fibers was attributed to the ion exchange between alkali ions in the glass and hydrogen ions from the acid, as first proposed by Metcalfe *et al* based on their study of stress corrosion in E glass filaments.⁹² They also suggested that if glass fiber contains less than 5% of alkali ions by weight, surface corrosion cracking can be inhibited. Recently, however, further studies^{52,118-120} have confirmed that the leaching of calcium and aluminum ions, rather than alkali metal ions, is responsible for the acidic corrosion of E-glass fiber. Work by Aveston and Sillwood⁹¹ showed that zirconia glass, which contained almost no calcium and aluminum oxides but 11% of alkali oxides by weight, appeared immune to concentrated sulfuric acid solutions. In fact, all other non-siliceous constituents, in addition to calcium and aluminum, possess a certain leachability in acids^{96,101,118,121,122} However, given their low contents in the glass, the removal of these ions has no significant effect on the acidic corrosion behavior of E-glass fiber.

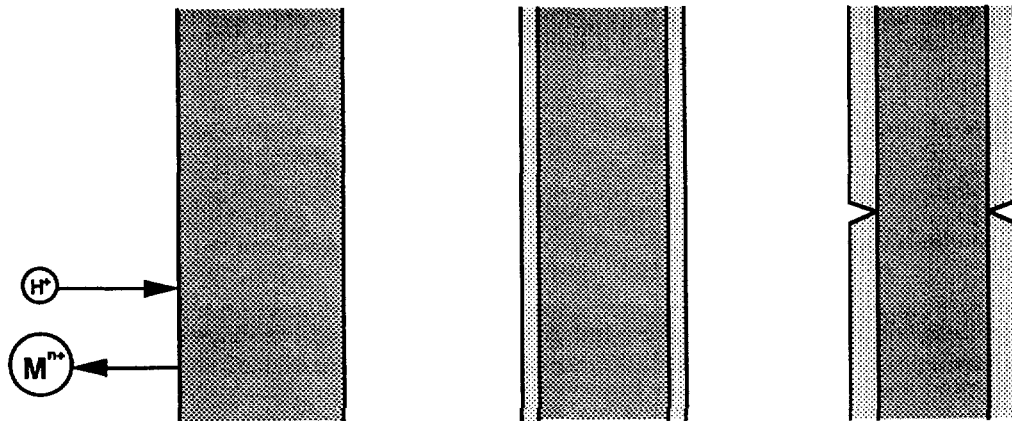


Figure 1.10 Schematic representation of fiber corrosion in acid: (a) ion exchange of metal ions, M^{n+} , from glass with hydrogen ions, H^+ , from acid; (b) sheath depleted of M^{n+} ions around a intact fiber core, producing a surface shrinkage stress, σ_s ; (c) sheath growth followed by surface cracking when shrinkage stress exceeds sheath fracture strength, σ_{fs} .⁵⁰

Leaching kinetics

Acid leaching controlled by ion-exchange reactions is an interdiffusion process;¹¹⁷ non-siliceous ions diffusing out from glass fiber and simultaneously hydrogen ions diffusing into glass fiber. Chandler and Jones⁹⁵ suggested that the rate limiting step in ion exchange could be diffusion of ions either through the liquid phase, a film-diffusion controlled process, or through the solid phase, a particle-diffusion controlled process. Because of the relatively compact structure of glass, leaching was most likely controlled by particle diffusion.

Caddock *et al*¹¹⁷ studied the influence of ion diffusion behaviors on leaching rate and found that acid leaching was characterized by two distinct stages. In each stage, the diffusion coefficient was constant, but the diffusion coefficient in the early stage was much higher than that in the later stage. They presumed two possible mechanisms responsible for this phenomenon: (1) The diffusion rate change was associated with the non-uniform glass structure along the fiber radius, being porous near the surface and denser in the core, and (2) The leaching was dominated by the metal ion diffusion in the early stage, but by the hydrogen ion diffusion in the later stage.

From a different perspective, Tian *et al*¹²¹ proposed that the leaching process is driven by two competing mechanisms: ion exchange and hydrogen ion diffusion. The early stage of leaching is governed by ion-exchange reactions because in this stage the diffusion rate of hydrogen ions is higher than the speed of ion-exchange reactions. Non-siliceous ion leaching results in the formation of a silicon-rich layer in the fiber surface, which acts as a barrier to hydrogen ion diffusion. When the leaching process proceeds, this layer becomes thicker and denser, making the hydrogen ion diffusion more difficult. In the later stage, therefore, the leaching process is limited by the diffusion rate of hydrogen ions.

Since leaching is primarily a diffusion-controlled process, its rate is highly sensitive to diffusion-related factors. As a general rule, the increase of acid strength, which is usually expressed by the hydrogen ion concentration, accelerates the leaching process. The temperature also has a great effect on leaching. For most silicate glasses, the leaching rate is nearly double for every 8 to 15°C increment, depending on the glass composition.¹⁰¹ This effect can be attributed to increased ion mobility at higher temperatures.

Anion influence

Acid strength was considered to be the only driving force in fiber corrosion until the recent discovery of the anion influence made by Chandler and Jones.^{95,96} After a series of studies on the corrosion behavior of E-glass fiber in various inorganic and organic acids, they found that the anions present in acids also play an important role, particularly when the anions can form insoluble salts or complex ions with the metal ions depleted from the glass. Such an insoluble salt or complex ion formation can effectively remove the leached metal ions from the right hand side of Equation 1.10, favoring the forward direction of the ion-exchange reaction and thus accelerating fiber corrosion.

This theory has been supported by the finding of severe corrosion effects of oxalic and mesoxalic acids.⁹⁵ On the basis of acid strength, the relatively weak organic acids are not expected to be very corrosive, this concept being true for most organic acids. However, organic acids, oxalic and mesoxalic, are in fact extremely corrosive to E-glass fiber because they can form insoluble calcium salts and/or aluminum complex ions and therefore assist the leaching of calcium and aluminum ions from the glass. The same effect has been observed with sulfuric acid, which can form low solubility calcium sulphate.⁹⁷ Additional evidence was provided by the observation that fiber corrosion was considerably suppressed by the addition of selective metal ions, such as aluminum or calcium ions, to neutralize the negative atmosphere in the acids.⁹⁵ Furthermore, the

formation of complex ions also gives a rational explanation for the corrosion of E-glass fibers in neutral phosphate solutions.⁹³

Passivation phenomenon

In general, the higher the acid concentration, the faster and more severe corrosion the glass fiber suffers. However, recent studies have shown that this rule holds true only within a specific range of acid concentrations.^{56,95-97} When the acid strength exceeds a critical value, the fiber becomes more acid resistant with a further increase in acid concentration. This abnormal behavior is called the passivation phenomenon, wherein the critical concentration varies with the nature of acids but in most cases exists below pH 1.

The passivation phenomenon primarily occurs in anion-controlled corrosion,^{56,96} in which the anions in acids tend to form insoluble salts or complex ions with the major metal ions depleted from the glass, such as calcium and aluminum ions. The formation of these insoluble salts or complex ions actually has two opposite functions: hastening the fiber corrosion by removing the free metal ions in the acid solution and inhibiting the fiber corrosion by forming a protective film on the fiber surface. When acid concentration is below the critical value, the former function is predominant because the amount of insoluble salts or complex ions is insufficient to form the dense surface film; however, when acid concentration is above the critical value, the formation of the surface film is favorable,⁹⁶ and therefore, the latter function becomes dominant.

Surprisingly, Jones and Chandler^{95,97} have recently reported the passivation phenomenon in hydrochloric and hydrobromic acids, in which fiber corrosion is controlled by acid strength, although the anions present can also form complex ions with the minor metal ions in the glass. They suggest that formation of ferric complex ions on the fiber surface hinders the fiber corrosion process. However, this passivating mechanism is challenged

by the extremely low availability of ferric ions in E-glass fiber. A better interpretation of the passivation phenomenon in acid corrosion, particularly in acid-strength controlled corrosion, can be made via the polymerization theory,¹²² which was originally established by Elmer to explain the surface area decrease of the leached fibers in strong nitric acids. During acid attack, the fiber surface experiences leaching, which makes it porous and rich in silica, and meanwhile undergoes polymerization:



which causes not only a restructure of the silica skeleton but also colloidal deposition in the pores of leached glass. Consequently, the fiber surface structure becomes denser, thereby increasing difficulty in ionic diffusion and eventually retarding fiber corrosion. Since the high hydrogen ion concentration favors the disruption of Si-O bonds, the polymerization effect is significant only in highly concentrated acids.

1.4 Failure Mechanisms of GRP Insulators

Brittle failure of GRP insulators is attributed to the deterioration of the composite rod. In service, insulators experience the combined actions of environmental, mechanical, and electric stresses. Due to the ultraviolet degradation, long-term hydrolysis, and gunshot or power arc damage of polymer housing, the composite rod may lose its protection and become exposed to the external environment. Further mechanical stress and environmental effects can lead to stress corrosion fracture of the rod. When service electrical activities are involved, the rod deterioration process becomes even more complex, given that the electrical activity can modify both the stress distribution and the corrosive environment.

1.4.1 Mechanical Stresses

Mechanical stresses, in particular tensile stress, play an important role in the stress corrosion fracture of GRP insulators, although fracture stress has been found to be only 10 to 20% of the insulator strength in dry fracture. Studies have shown that chemical attack alone does not cause serious loss of composite properties, but that the interaction between chemical attack and mechanical stress leads to a rapid deterioration of composites.^{63,91,97} Mechanical stress can accelerate a corrosion process in four possible ways:^{50,58,117} reducing the leaching-induced stress level required for the fiber fracture, increasing the diffusivity of moisture or aqueous acids in the resin, promoting interfacial debonding and matrix cracking to speed up the acid transfer, and accelerating the rate of stress-activated chemical reactions.

In insulator service, mechanical stresses primarily result from two sources: external loads and residual stresses in composite rod. External loads applied to the insulator rod mainly arise from the weight of transmission lines, aeolian vibrations, and installation stresses. Although the overall loading is dominated by tension, it will certainly be affected by other mechanical stresses such as vibration, torsion, or bending. Because of the superimposition of various stresses in service, external loading can be either static or cyclic in nature. In most cases, mechanical stresses induced by external loads are concentrated inside the end fitting of insulators, largely due to its structural complexity and the existence of dissimilar material interfaces. Additionally, the character and distribution of stresses in the rod will alter with the end-fitting design.³³ In the cone end fitting, shear stresses are predominant.

Residual stresses inside the composite rod can be generated during manufacture due to different thermal expansion coefficients between the glass fiber and resin. They become particularly high when resin is not completely cured. These localized stresses in the rod can be intensified by such manufacturing defects as fiber misalignment, matrix voids, and

fiber/resin interface debonding. Furthermore, microscopic residual stresses can be induced to glass fibers as a result of a fast cooling rate and high drawing stress during fiber fabrication. The cooling rate, which usually rises up to 10^4 °K/s, leads to an open glass structure, whereas the high drawing stress, assisted by fast cooling rates, leads to an anisotropic frozen-in network deformation.¹²⁸ Because the fiber surface experiences the fastest cooling rate and highest drawing stress, residual stresses are expected to be concentrated in the fiber surface layer.

1.4.2 Environmental Stresses

Previous studies have suggested that acidic environments in insulator service may arise from two sources: (1) acid rain from external environments, and (2) organic acids produced by internal partial discharge.

1.4.2.1 Acid Rain

Acids can form naturally in the atmosphere as a result of the dissolution of carbon dioxide in water or the oxidation of neutral sulphur and nitrogen compounds. In ambient air, the acidity of natural rainwater will stabilize near pH 5.6, due to its equilibrium with atmospheric carbon dioxide. Therefore, acid rain is usually referred to as rainfall with an acidity below pH 5.6.¹²³

Acid rain primarily results from emissions of sulphur oxides (SO_x) and nitrogen oxides (NO_x), which can come from either natural or anthropogenic sources.¹²⁴ The natural SO_x emission can be generated by seaspray containing sulfates, hydrogen sulfide from volcanic eruptions, and biogenic sulfur compounds originating from the bacterial decay of organic matter. However, the principal natural source of gaseous NO_x appears to be chemical decomposition of nitrides. In general, the natural emission of SO_x or NO_x occupies at least 50% of total global emissions. Although natural inputs of SO_x and NO_x

may be significant, they are well distributed globally, whereas manmade emissions tend to be concentrated near population centers. The anthropogenic emissions of SO_x and NO_x largely arise from fossil fuel combustion, industrial processes, and transportation. Of these sources, fossil fuel combustion and industrial processes are the major ones for manmade SO_x emission, while fossil fuel combustion and transportation make up a great portion of the NO_x emission. Reported by the National Emission Data System,¹²⁴ total anthropogenic emissions for SO_x and NO_x in the United States for 1982 are 29.1 and 24.0 million tons, respectively.

Different chemical pathways exist for oxidizing SO_x and NO_x to sulfuric acid and nitric acid in the atmosphere, depending on where the reaction takes place.¹²⁵ Both acids can be formed homogeneously in the gas phase and in the liquid phase, such as cloud water and rainwater, or heterogeneously on the surfaces of liquid or solid aerosols. Kinetically, the acid transformation rate is highly dependent on not only the composition of the polluted air but also the presence of solar radiation. Once the acids are developed in the atmosphere, they can be deposited onto transmission line hardware by either "wet deposition," in which acids precipitate in the forms of rain, snow, and fog; or "dry deposition," in which pollutant gases and particles, such as fly ash, sulfates, and nitrates, are first deposited onto the hardware surfaces and then converted into aqueous acids when they contact water.¹⁷

In addition to sulfuric and nitric acids, hydrochloric acid may be involved in the formation of acid rain. Average rainwater acidity in the northeastern United States has been reported to result from 62% sulfuric acid, 32% nitric acid, and 6% hydrochloric acid.¹²⁴ To date, the sources and formation mechanisms of hydrochloric acid have not been completely identified. The natural sources of chloride include salt spray from oceans, volcanic gases, and upper atmospheric reactions. Manmade chlorine and chlorides are emitted from various manufacturing processes, particularly in chlorine

gas and hydrochloric acid production. Coal combustion can also release chlorides into the atmosphere.

Figure 1.11 depicts the annual average distribution of the weighted mean pH of precipitation in the United States and Canada for 1980.¹²⁵ Notably, the precipitation in some regions may reach an acidity of pH 4.08. In some local regions, the precipitation can be even more acidic; for instance, acid fog with an acidity of as low as pH 1.7 has been observed in California.¹²⁴ Globally, acid rain has also become an increasing problem. In Sweden, rain acidity of pH 3.0 to 3.5 is not unusual, and under certain circumstances, rainwater can be as acidic as pH 1.¹²⁶

1.4.2.2 Organic Acids

The formation of organic acids within GRP insulators may occur in service because of to electrical partial discharge.^{17,35,46} The phenomena and mechanisms of partial discharge will be discussed in more detail in a later section.

Partial discharge within air-filled voids embedded inside insulator composite rods can produce N^+ , O_2^+ , O_3 , and other reactive species. Further reactions between these species generate a series of nitrogen oxides, such as N_2O , NO_2 , and N_2O_4 . Reactive oxygen species and nitrogen oxides are powerful oxidizing agents and are able to oxidize polymer chains into the most highly oxidized state: CO_2 and H_2O . During the intermediate stages of the process, however, the polymer carbon backbone is broken at various places, producing a mixture of low molecule weight organic acids of the sort:⁴⁶



Next to the final oxidation stage, the species most likely to predominate is oxalic acid ($n=0$), which may be formed in a polymer chain by the reaction:

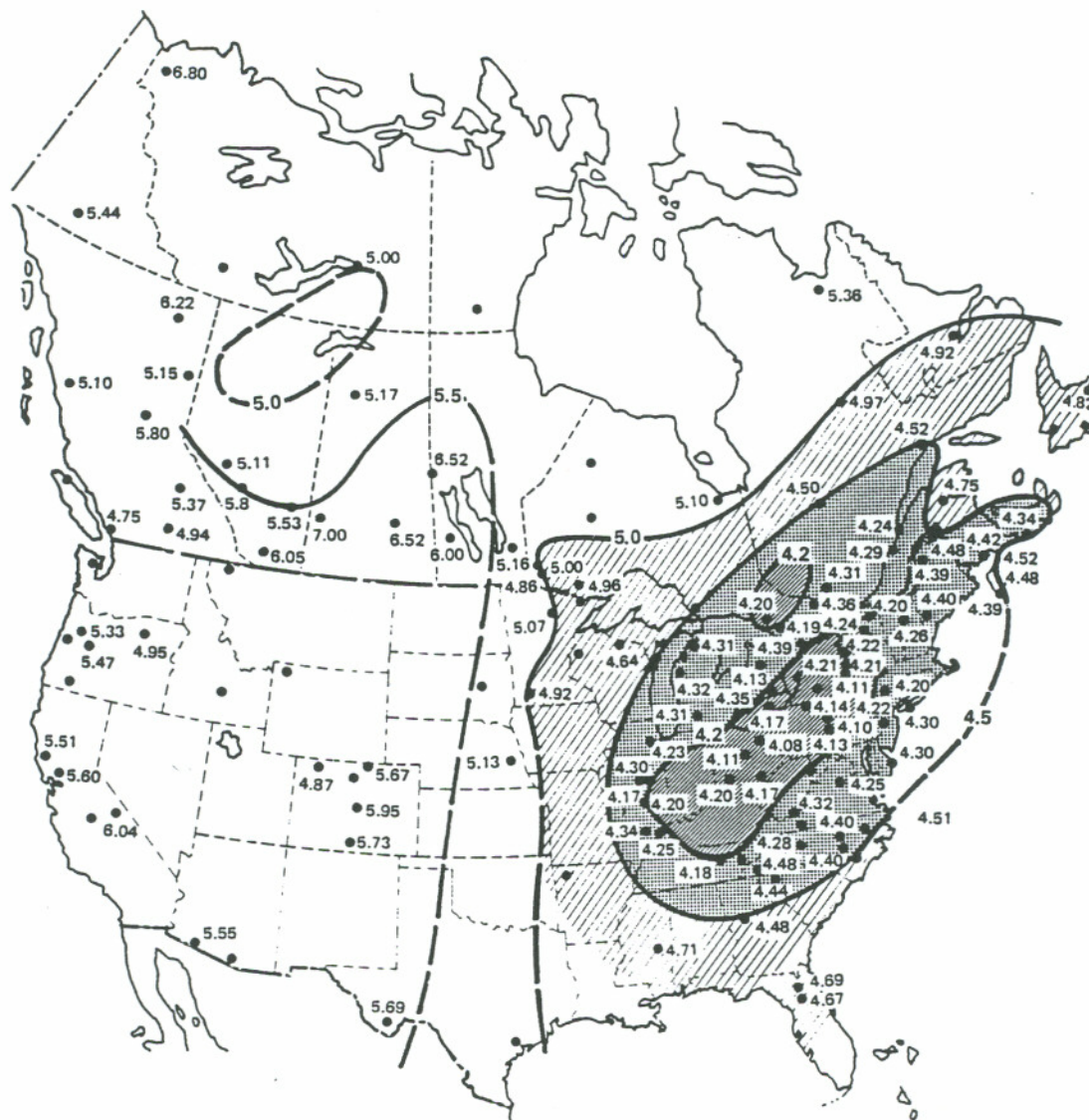
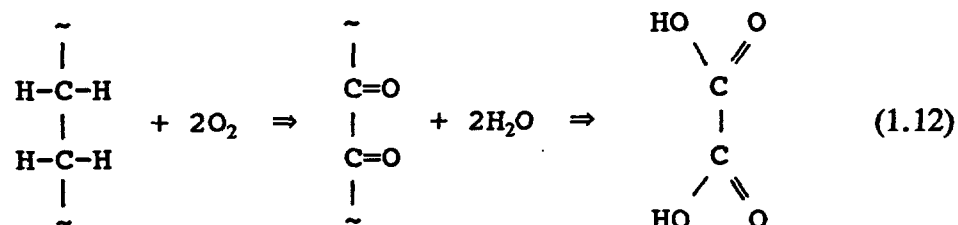


Figure 1.11 Annual average distribution of the weighted mean pH of precipitation in the United States and Canada for 1980.¹²⁵



This acid can then further react with O_2 to form CO_2 and H_2O . Although most organic acids in the above group are weak acids, oxalic acid ($n=0$) and mesoxalic acid ($n=3$) can be extremely corrosive.⁹⁶ A study conducted by Chandler and Reynders³⁵ revealed that oxalic acid actually was much corrosive to E-glass than nitric acid.

The polymer oxidation theory has been supported by direct evidence. McMahon¹²⁷ found that electrical discharge on polyethylene did produce appreciable quantities of oxalic acid. Similar to polyethylene in structure, the polymers used to construct GRP composites, such as polyester and epoxy resins, would also be expected to be prone to such degradation. In fact, Chandler and Reynders,³⁵ who exposed an artificial cavity between two thin epoxy sheets to the partial discharge, found that oxalic acid was formed inside the cavity. This finding suggests that it is possible to generate oxalic acid inside the composite rod, particularly in micro-voids located in either the resin matrix or the fiber/resin interface.

1.4.3 Electric Stresses

Most brittle fractures of GRP insulators have been reported as occurring either near or inside the high-voltage ends,^{17,35,44,45} where electrical stresses are concentrated. This fact suggests that insulator brittle fracture is an unusual stress corrosion process, in which not only corrosive environments and mechanical stresses but also electrical activities are present.

In high-voltage applications, insulators may receive significant damage in the form of erosion, puncturing, tracking, melting, burning, and displacement of both glass and polymer phases, either by electrical activities alone or under the combined influences of electrical activities and attendant environments.^{8,35,44,45} Early concern with electrical activities was restricted to their damage to polymer housing materials, which may lead to the exposure of the composite rod to the external environment, thereby initiating the stress corrosion of insulators. However, the latest development has revealed that internal discharges associated with insulators could result in the formation of organic acids,^{35,127} although the influence of electrical activities on the stress corrosion mechanisms is still unclear.

Partial discharge occurs when some form of electrical activity within a material system causes a rapid change of the electric field configuration.¹²⁹ To generate partial discharge in air-filled voids, two requirements have to be met. First, the electric field in a gas void must be raised beyond the minimum breakdown field, under which free electrons can be produced to initiate a discharge event. Second, the initiating free electrons must be sufficiently far from the wall of the void so that the electron multiplication may achieve a critical avalanche size before the wall is reached, i.e., a critical void size exists. A quantitative theory of the void-induced partial discharge in a dielectric system has been discussed in detail elsewhere.¹³⁰

Internal partial discharge basically is a void-induced electrical phenomenon. The major source of voids in an insulator exists in the composite rod. During the pultrusion process, by which the composite rod is manufactured, glass fibers are pulled through a resin bath and then through a heated forming die. Air is forced out of the space between individual fibers and resin. If glass fibers are not completely wetted, however, air bubbles are likely to be trapped in the rod, resulting in oblong air-filled voids in the fiber/resin interface along the fiber direction. Besides the interfacial voids, longitudinal cracks can develop as a result of more rapidly curing in the outside of the rod than in the

interior. This situation usually occurs when the die temperature is too high for a given pulling speed. Furthermore, mishandling during installation and mechanical loading in service may cause rod/housing debonding or longitudinal cracks along the composite rod.

In service, a higher applied voltage generally requires a longer insulator for the insulation purpose. By increasing the insulator length, however, voltage distribution along the rod will become nonuniform, with maximum electric stress occurring at the high-voltage end. On a microscopic scale, the electric field in a small air-filled void is always greater than the adjacent glass fibers by a factor of the glass dielectric constant, which is about 5.8 for E-glass.⁴⁶ If the void is sealed inside the rod, the pressure in the void, which is determined by the vapor pressure of the most volatile component in the coupling agent, can be lower than one bar at room temperature, leading to an additional increase of the electric stress in the void.³ As a result of the above three factors, the electric stress in the void can be sufficiently high to initiate partial discharge activity inside the composite rod near the high-voltage end.

1.5 Summary

The resemblance of fracture surfaces of GRP insulators in service to those generated in laboratory stress corrosion conditions indicates that insulator fracture is an environmentally assisted process. However, it is unlikely that highly concentrated mineral acids from acid rain prevail in the service environment. The probability of electrical activities playing a role in the failure mechanism, therefore, becomes stronger. An interesting mechanism, recently proposed for the brittle fracture of GRP insulators in high-voltage applications, suggests that resin can be degraded under the influence of partial discharge activity, producing organic acids and thus creating an internal corrosive environment. This mechanism gives a reasonable mode for the crack initiation. However, it is difficult to understand how this mechanism alone can account for crack propagation and the extremely planar nature of the fracture surface because internal

partial discharge is such a localized activity. The stress corrosion fracture of GRP insulators is an extremely complex process, primarily due to (1) the synergistic influence of mechanical, environmental, and electrical activities in service, and (2) the high degree of heterogeneity and anisotropy of GRP composite structures. To date, most studies have been concerned only with the interaction between mechanical and environmental stresses; however, little attention has been devoted to the influence of electrical activities on stress corrosion of insulators. Failure mechanisms that control the brittle fracture of GRP insulators have not been fully explained.

CHAPTER 2

EXPERIMENTAL PROCEDURES AND RESULTS

2.1 Insulator Failure Analysis

Insulator failure analysis aimed to characterize the fractography of service-failed or damaged GRP insulators, and thereby to identify the failure mode of brittle fracture. Seven GRP suspension insulators were fully examined in this failure analysis. The service conditions for as-received insulators are summarized in Table 2.1. Insulators #1, #2, and #3 had operated in service only for several months; the service lives for the other insulators were not available.

In this failure analysis, a special attempt was made to estimate the fracture stress of composite rod on the basis of the rule of mixtures and the empirical relationship of the fiber mirror size with the fiber strength by direct measurement of fiber mirror sizes on the actual fracture surface.

2.1.1 Insulator Configuration

The insulators examined in this failure analysis had the same configuration as shown in Figure 1.2, consisting of a composite rod, polymer housing, and metal end fittings. In this specific design, the cone end fitting was employed, and the housing was composed of separate rubber sheath and weathersheds (Figure 1.4). All the composite rods were approximately 16 mm in diameter, except for insulator #7 with a rod diameter of 32 mm.

Table 2.1 Service conditions for as-received insulators

Insulator No.	Insulator type	External status	Service voltage, kV	As-received
1	I-string	intact	345	insulator
2	I-string	intact	345	insulator
3	V-string	intact	345	insulator
4	I-string	intact	345	high-voltage end section
5	I-string	failed	345	high-voltage end section
6	I-string	failed	345	insulator
7	N/A*	failed	115	high-voltage end section

* N/A: the insulator type is not provided.

2.1.2 Insulator Materials

The generic material information of major insulator components is listed below:

- Insulator rod: unidirectional E-glass fiber reinforced polyester composite
- Rubber sheath: ethylene propylene diene monomer (EPDM)
- Weathershed: silicone rubber
- Metal end fitting: cast iron with zinc coating
- Potting material: epoxy resin

The detailed material composition was not available for this failure analysis. In the high-voltage end construction, asphalt print, a release agent, was sprayed onto the inner surface of the metal casting to prevent the bonding between potting material and the metal casting.

2.1.3 Preliminary Examination

Visual examination was conducted on the external integrity of the insulators, including composite rods, rubber sheaths, and weathersheds. For the failed insulators, the location of the major fracture was determined. For the externally intact insulators, both high-voltage and ground ends were initially sectioned along the center line of the composite rod. Subsequently, the exposed internal surfaces of the rod, as well as the rod/sheath and epoxy/sheath interfaces, were subjected to optical examination.

Damage zone in the rubber sheath

As-received insulators #1, #2, and #3 appeared externally intact. After removing the metal castings, no visible internal damage was observed either in two end fittings of the V-string, insulator #3, or in the ground ends of the I-strings, insulators #2 and #3.

Damage zones, however, were exposed in the high-voltage ends of both I-strings (Figure 2.1). Developed on the rubber sheath surface, these damaged zones were located adjacent to the epoxy/sheath interface. Further examination revealed that the damage zone in insulator #3 formed a notch down into the rubber sheath but did not penetrate to the composite rod underneath (Figure 2.1b). In addition, a black substance was found both inside the damage zone and on the inner surface of the metal casting (Figure 2.2).

Interface debonding and transverse crack

Similar to insulators #1 and #2, the high-voltage end of insulator #4 also exhibited no external damage in the as-received condition, but the removal of the metal casting revealed multiple circumferential cracks in the epoxy/sheath interface region (Figure 2.3a); they existed either along the interface or in the epoxy potting material (Figure 2.3b). The crack region was confined to one side of the rod and covered an approximate 180° arc. White powders and rust-colored substances were also found in the proximity of the crack region. By sectioning the high-voltage end normal to the longest circumferential crack, a flat transverse crack was unveiled, along with a longitudinal delamination (Figure 2.4a). Careful examination confirmed that the transverse crack was actually co-planar with the epoxy/sheath interface debonding (Figure 2.4b).

Fracture morphology

In all the failed and damaged insulators examined in this study, the main fracture occurred in the region from the epoxy/sheath interface to the first weathershed (Figures 1.2 and 2.5). The fracture surfaces in completely failed insulators can be characterized by the morphologies shown in Figures 1.5a and 1.5b. In most cases, the fracture surface exhibited two distinct regions (Figure 1.5a): one region appeared



(a)



(b)

Figure 2.1 Damage zones found inside the high-voltage end of insulator #3.

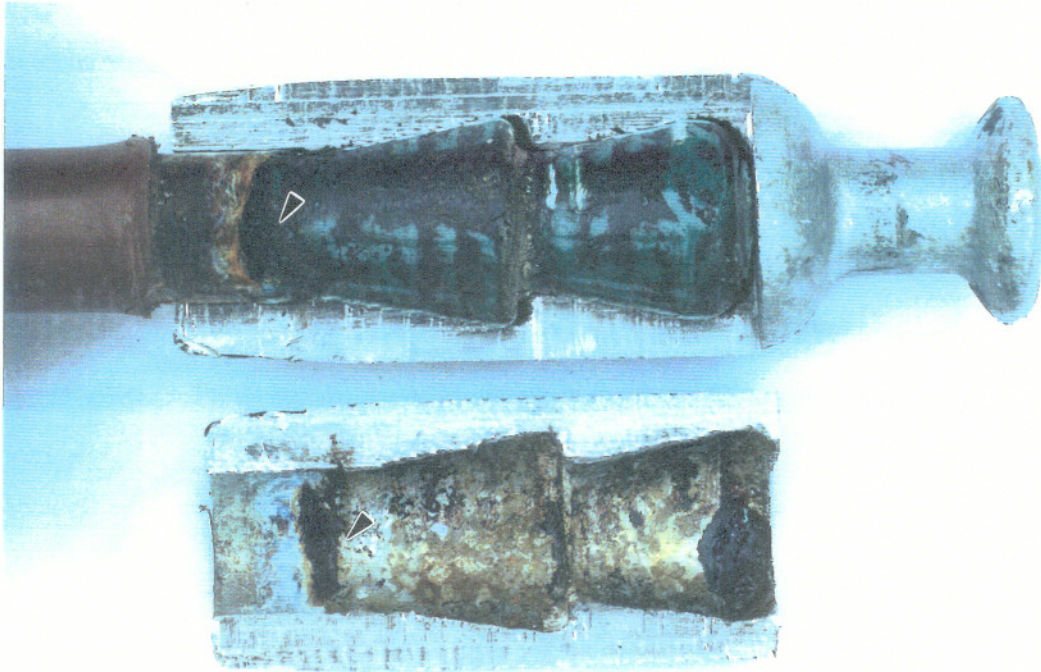
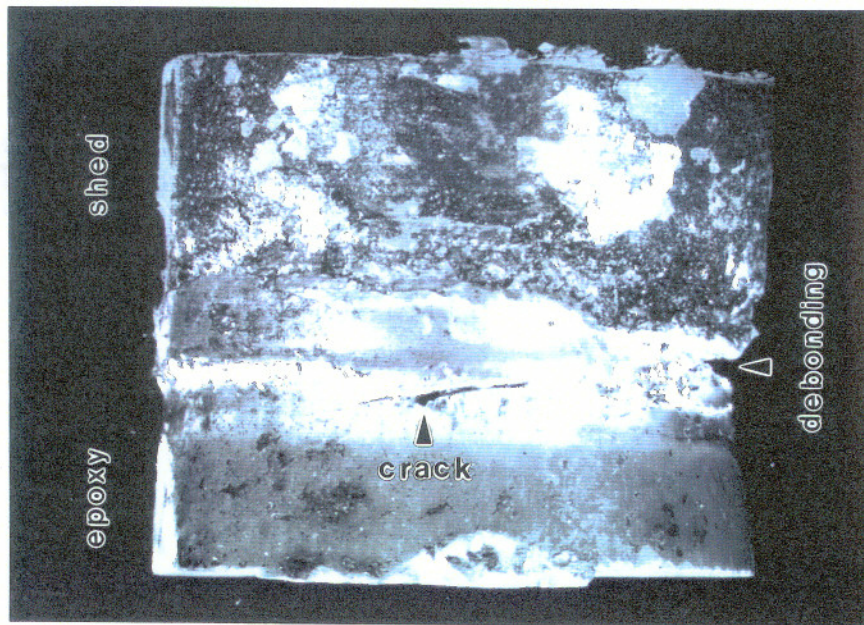


Figure 2.2 Black substance in the damage zone and on the inner surface of the metal casting.

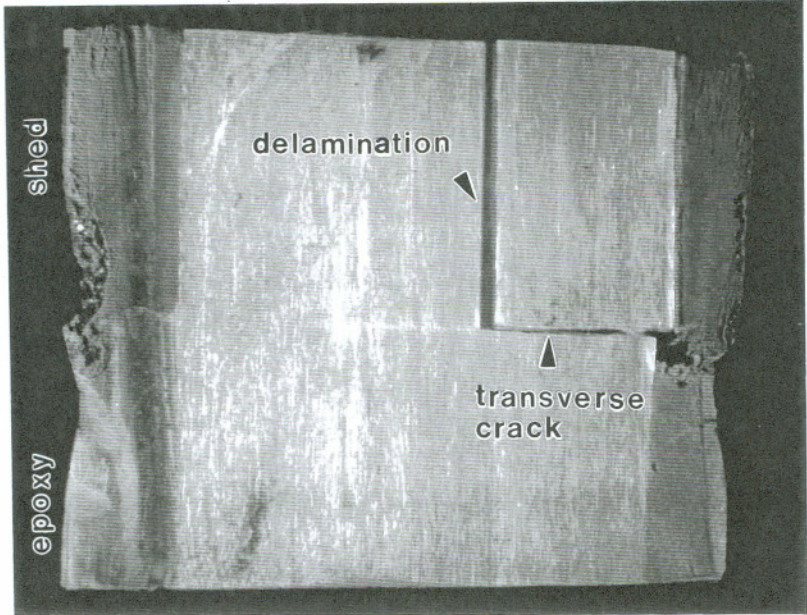


(a)



(b)

Figure 2.3 Circumferential cracks in the epoxy/sheath interface region.



(a) Transverse crack



(b) Epoxy/sheath interface debonding

Figure 2.4 Damaged composite rod found inside the high-voltage end.

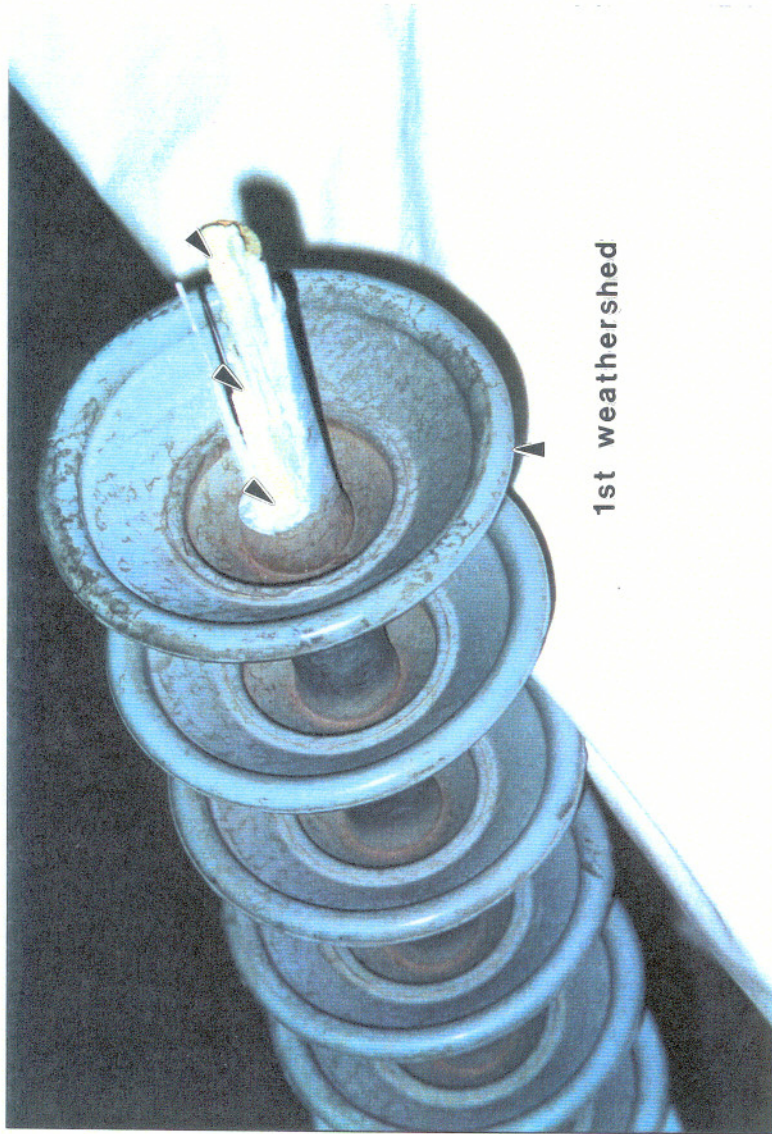


Figure 2.5 Fracture morphology of insulator #6.

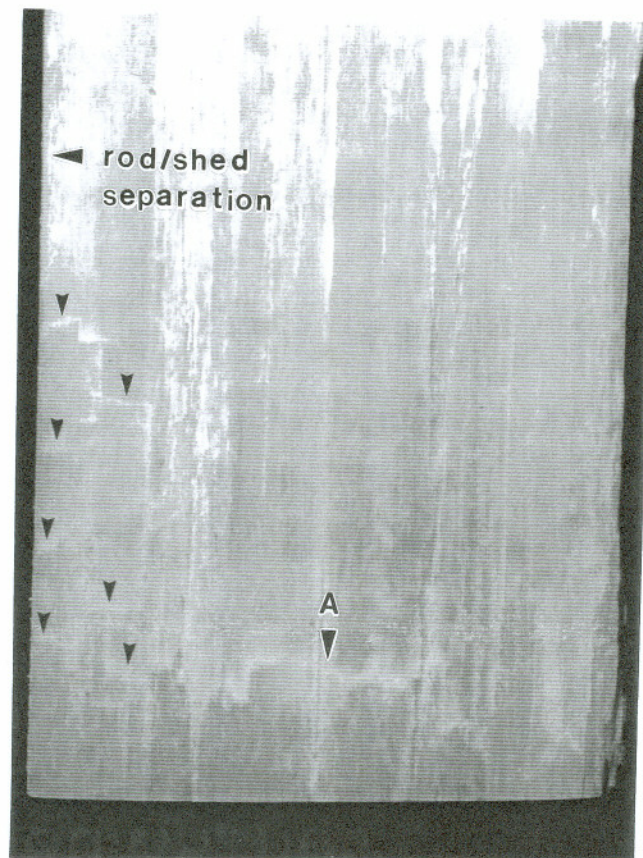
planar and ran perpendicularly to the composite rod, while the other displayed a broom-like morphology with extensive longitudinal splitting. A unique fracture morphology was observed in insulator #6, in which three transverse fracture planes were located at different locations along the rod (Figure 2.5). Visual examination revealed that all three transverse cracks were connected to the external surface of the composite rod.

Longitudinal delamination

Longitudinal delamination is a common phenomenon associated with the brittle fracture of composite rods. In insulator #4, longitudinal delamination developed along the rod/sheath interface, starting from the epoxy/sheath interface debonding inside the high-voltage end and extending all the way up to the 15th weathershed along the same fracture plane. By separating the sheath from the rod in the delamination region, a thin composite layer was found adhering to the inner surface of the sheath (Figure 2.4b). This evidence verified that the delamination did not exist at the exact rod/sheath interface, but rather inside the composite rod. Similar longitudinal delamination was also observed in insulator #5.

Internal crack

Since the longitudinal delaminations observed in this failure analysis were linked to the epoxy/sheath interface debonding, their formation likely created a channel for the external environment to access the internal composite system, thereby damaging the composite rod adjacent to the delaminations. In insulator #4, an internal crack network (Figure 2.6), comprised of a series of small transverse and longitudinal cracks, was formed in the composite rod outside the high-voltage end where the rubber sheath appeared intact. This network likely started from the rod surface, where the longitudinal delamination occurred, and travelled towards the rod center.



2 mm

Figure 2.6 Internal crack network formed outside the high-voltage end.

Discoloration

Discoloration of composite rods was, on several occasions, observed in this study; however, it was difficult to photograph under the regular illumination conditions in an optical microscope. In insulators #6 and #7, the color of the major fracture and delamination surfaces turned yellowish. More severe discoloration of the composite rod occurred in insulator #4. The rod discoloration essentially accompanied the longitudinal delamination somewhere above the epoxy/sheath interface to the 15th weathershed. Examination of the rod cross-sections, taken at intervals up along the rod, indicated that the discoloration area became larger the farther from the high-voltage end it was measured.

Surface cutting

In insulators #4 and #6, surface cutting was discovered on the weathersheds near the high-voltage end. The cutting always existed along the rod direction in which the electric field was distributed. Figure 2.7 shows the surface cutting found at the root of the 3rd weathershed above the high-voltage end in insulator #4. In this case, the cutting penetrated through the weathershed but stopped at the sheath/weathershed joint. However, further cutting of the rubber sheath may be also possible in service.

2.1.4 Fractographic Characterization

To obtain a high magnification and quasi-three-dimensional image of the fracture surface, scanning electron microscopy (SEM) was employed for the fractographic characterization. The SEM specimens were prepared by removing the fracture surfaces from failed or damaged insulators. In this process, precaution was taken to avoid any mechanical damage or surface contamination to the fracture surfaces. Since GRP composites are electrically non-conductive, a thin layer of gold/palladium alloy



Figure 2.7 Surface cutting on the weathershed.

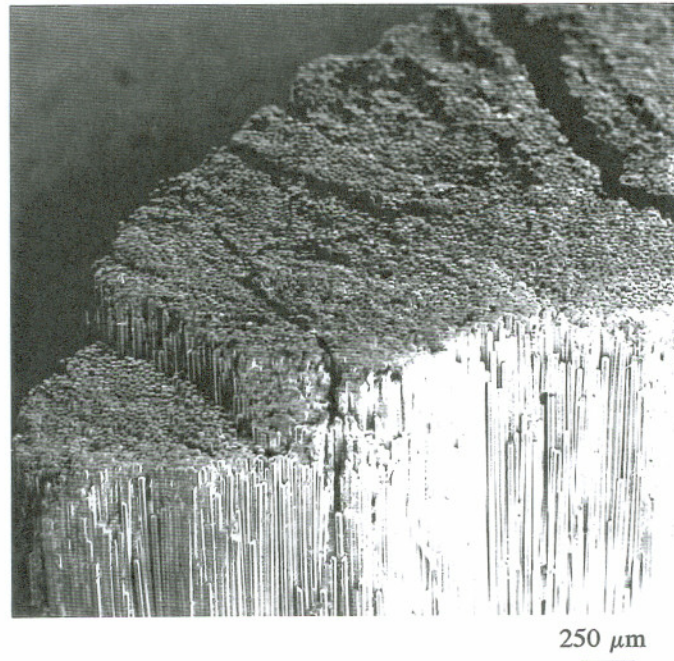
was deposited on each specimen in vacuum to minimize electrical discharge during SEM examination. The fracture morphology was characterized in a Zeiss DSM-960 scanning electron microscope operated at an accelerating voltage of 10 kV.

Planar fracture surface

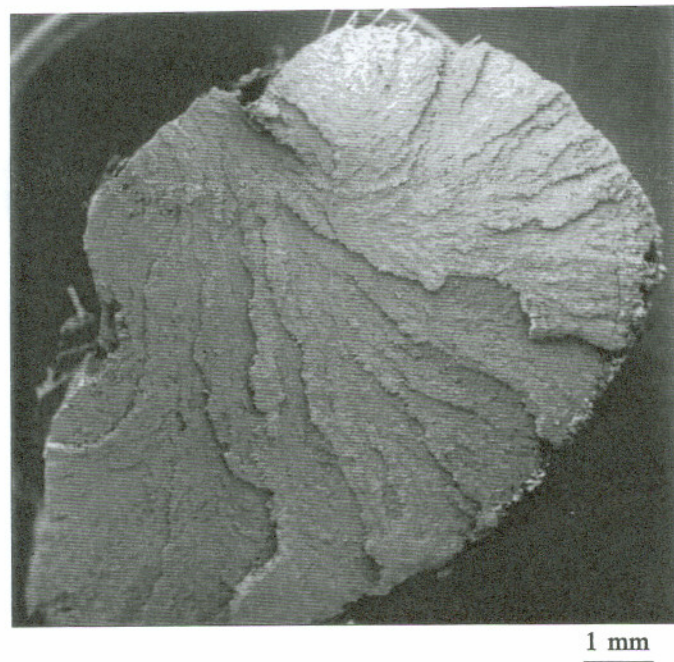
The main fracture surface in insulator composite rods appeared planar in nature and perpendicular to the rod (Figure 2.8). Although some micro-steps were present parallel to the fiber axis, the fracture surface was essentially free from fiber pull-out. In insulator #6, the micro-steps on the fracture surface were generated from the same origin and twisted in a similar orientation, forming a spiral staircase pattern (Figure 2.8b). The overall fracture morphology observed in this study resembles the stress corrosion fractography in unidirectional GRP composites under tension.^{47,48,51,64}

Fiber fracture morphology

On a microscale, fiber fracture surfaces exhibited the classic mirror, mist, and hackle regions (Figure 2.9). This micro-fracture behavior, particularly the formation of well-defined mirror zones, was identical to the characteristic of stress corrosion fracture of individual fibers in composites exposed to acids.^{47,51,79} As a trend, the region on the fracture surface with relatively large mirror sizes always located adjacent the external surface of composite rods; the fiber mirror sizes, in some cases, were found to be as large as the fiber diameter (Figure 2.10). Based on the relationship described in Equation 1.1, the fiber fracture stress was expected to be extremely low in this region, and therefore it was likely the initiation site of stress corrosion fracture. Moreover, the glass wedge in the hackle region (Figure 2.11), a result of the crack bifurcation, was a common feature observed throughout the fiber fractures.

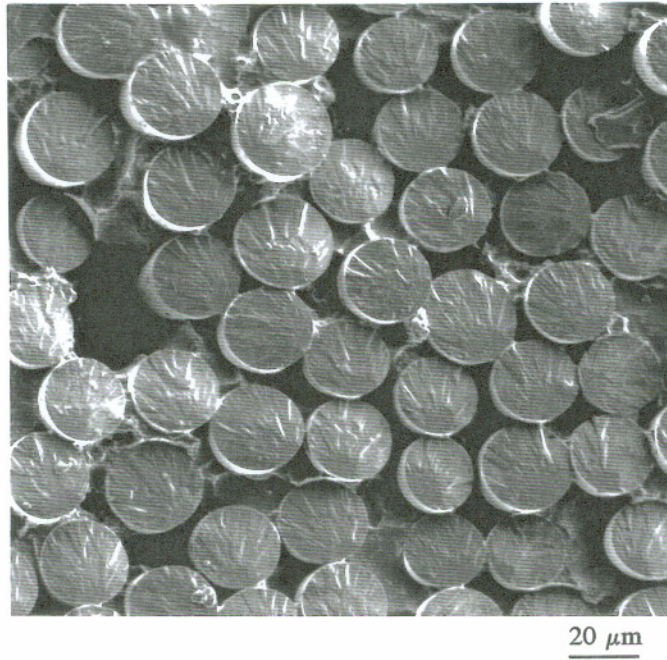


(a) Insulator #5

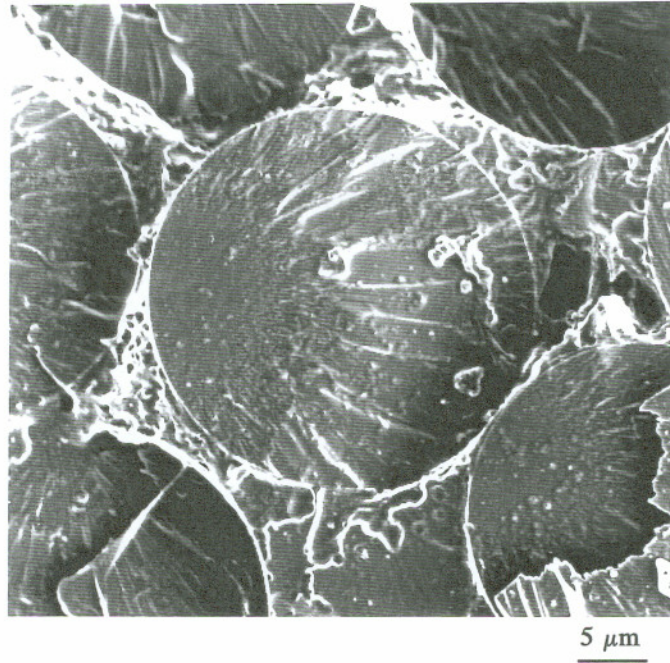


(b) Insulator #6

Figure 2.8 Morphology of the insulator fracture surfaces.

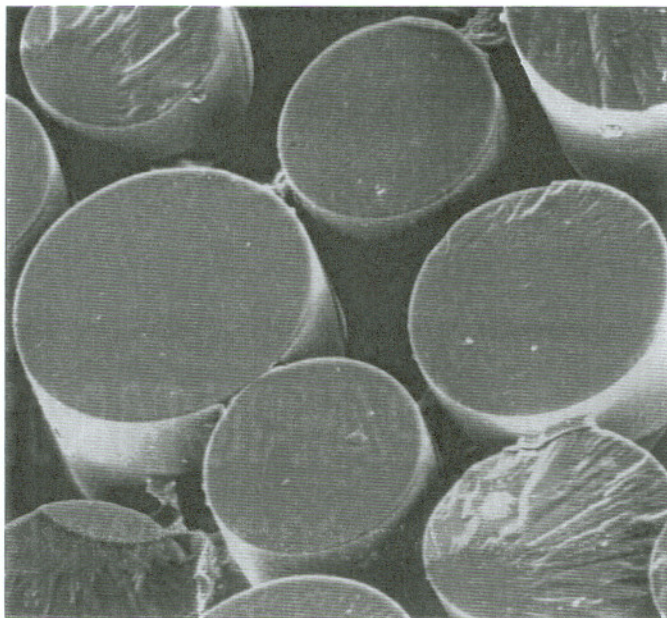


(a)



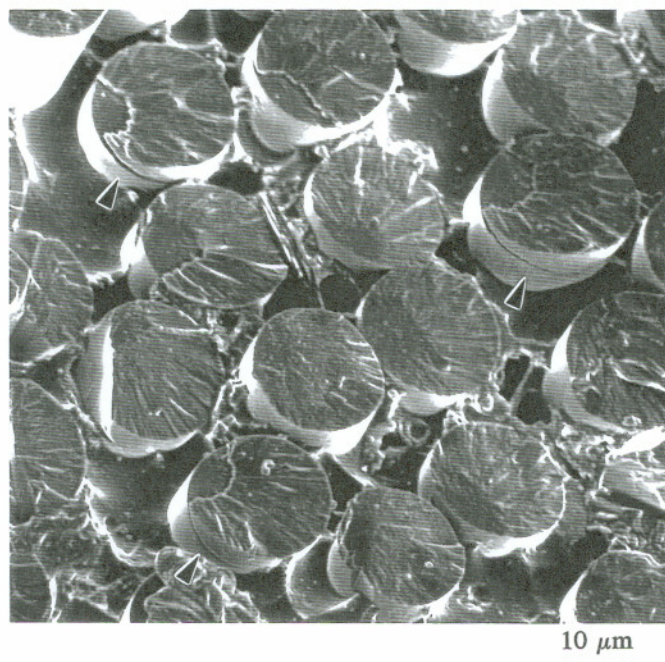
(b)

Figure 2.9 Fiber fracture morphology.

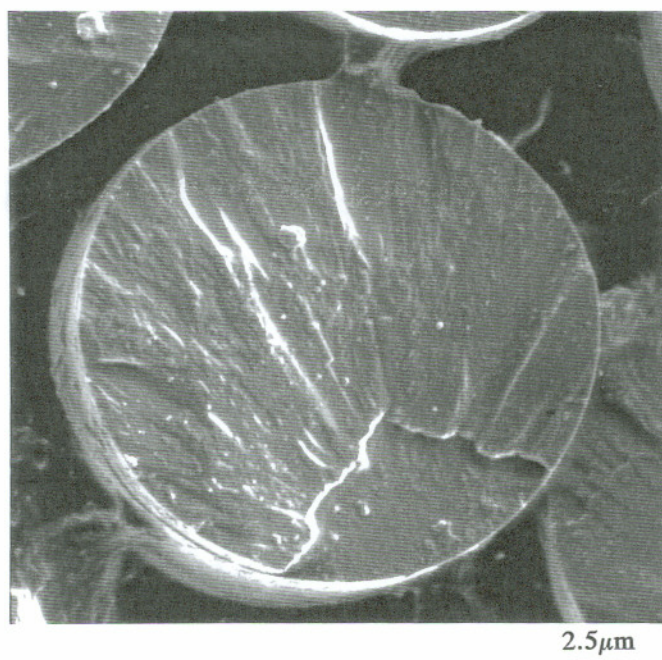


10 μm

Figure 2.10 Fractured fibers with large mirror sizes.



(a)



(b)

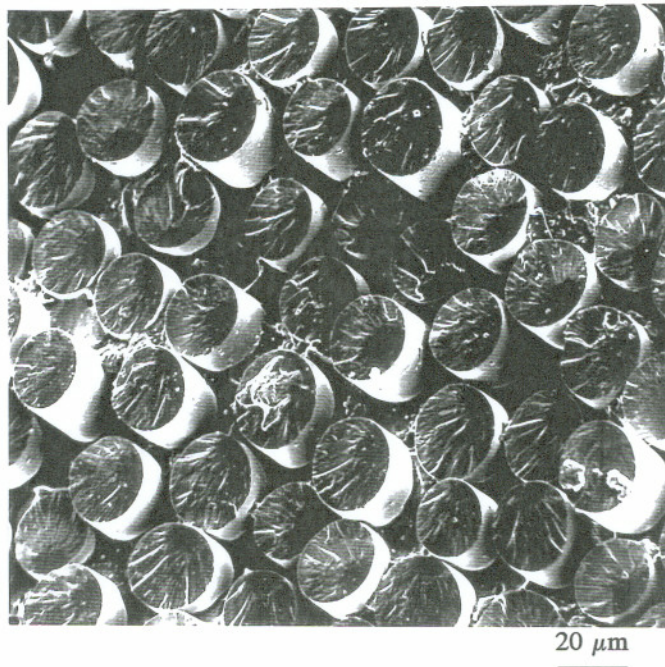
Figure 2.11 Glass wedge caused by crack bifurcation.

Resin decomposition

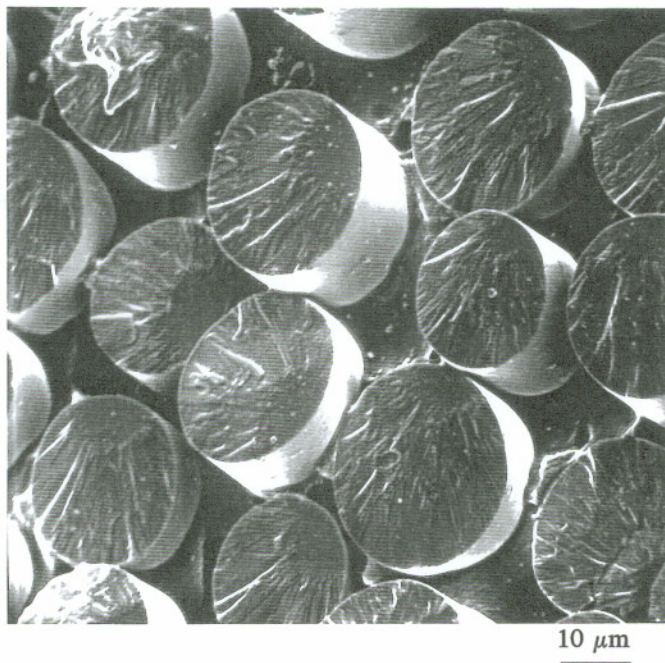
In this failure analysis resin decomposition was identified, for the first time, on the insulator fracture surfaces. Figure 2.12 shows the fracture surface morphology in insulator #5, taken at a tilt angle; the resin matrix over the entire fracture surface was significantly depressed relative to the fiber fracture surfaces. This feature disagreed with the typical stress corrosion fracture of GRP composites, in which the fiber fracture is always co-planar with the resin fracture (Figures 1.8 and 1.9). A depth profile along a line between two adjacent fiber ends on the fracture surface indicated that the resin level was approximately 30 μm below the fractured fiber surfaces (Figure 2.13). Further examination confirmed that resin decomposition was not an unusual phenomenon in the brittle fracture of insulators. On the internal fracture surface in insulator #4, resin decomposition was also observed. In this case, however, the decomposition did not cover the entire fracture surface but remained localized in several scattered regions (Figure 2.14). The decomposition in those regions was much more severe than that found across the fracture surface of insulator #5. Resin decomposition is a thermally activated process. In general, the resins used for the matrix materials in GRP insulators are thermosetting polymers. One characteristic of these polymers is that they will decompose instead of melt when subjected to certain critical temperatures, usually 200°C or lower, depending on the resin composition. Since the resin decomposition did not alter the planar character of the fracture surface, it most likely occurred after the fracture surface was formed.

Melted fibers

Similar in nature to the resin composition, melted fiber was another important finding associated with high temperature involvement in the brittle fracture of insulators. On the fracture surface of insulator #5, 10 to 15 melted fibers were observed near the external surface of the composite rod (Figure 2.15). These fibers completely lost



(a)



(b)

Figure 2.12 Resin decomposition on the fracture surface.

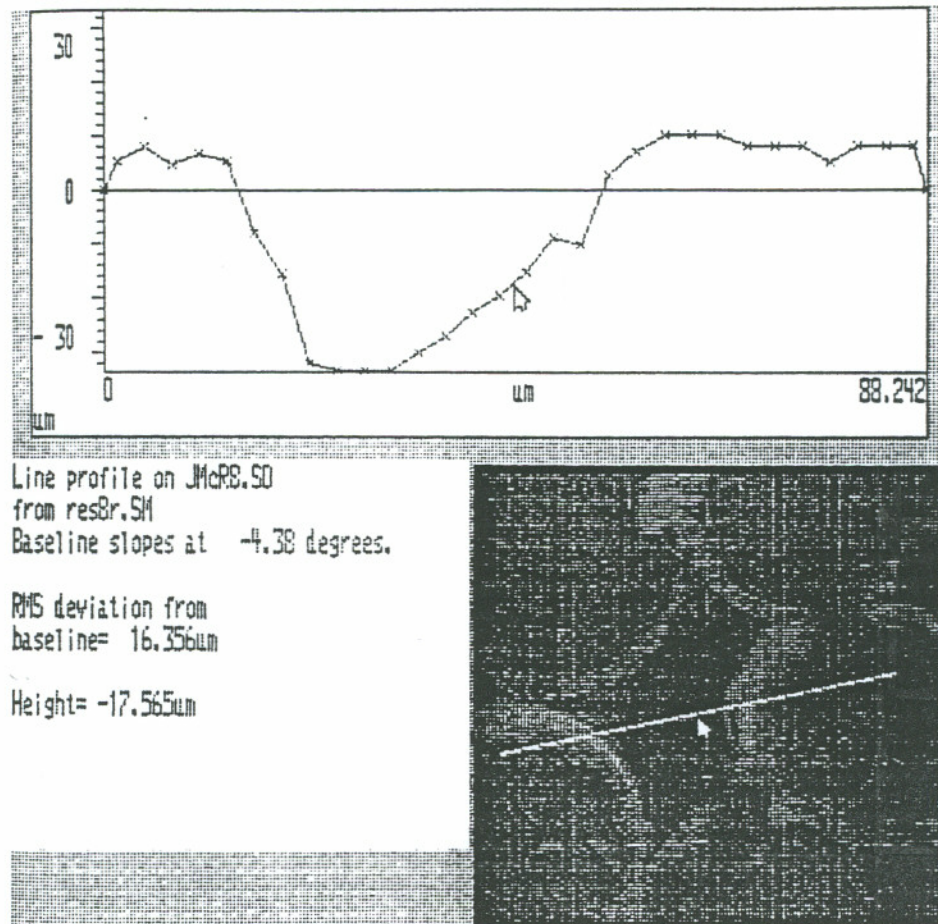
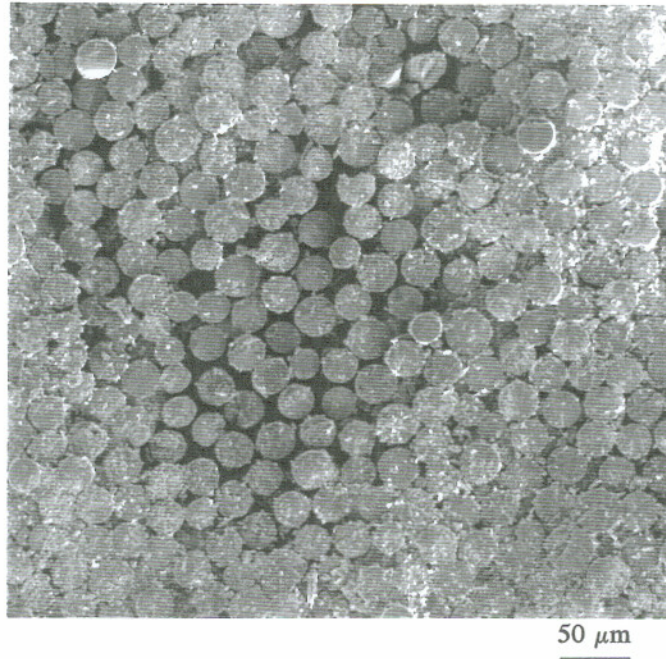
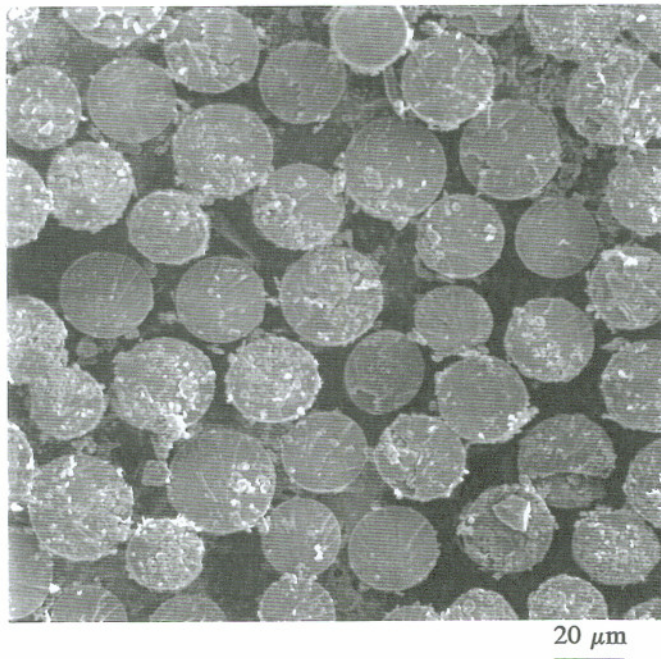


Figure 2.13 Depth profile on the local fracture surface.

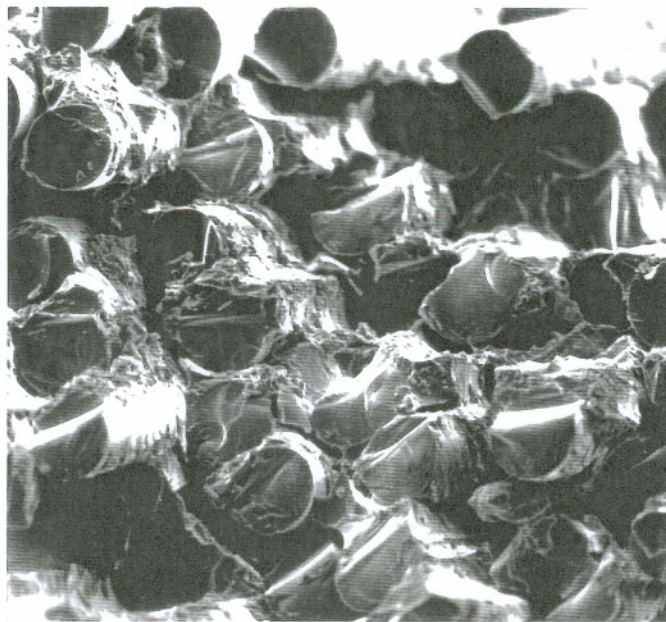


(a)



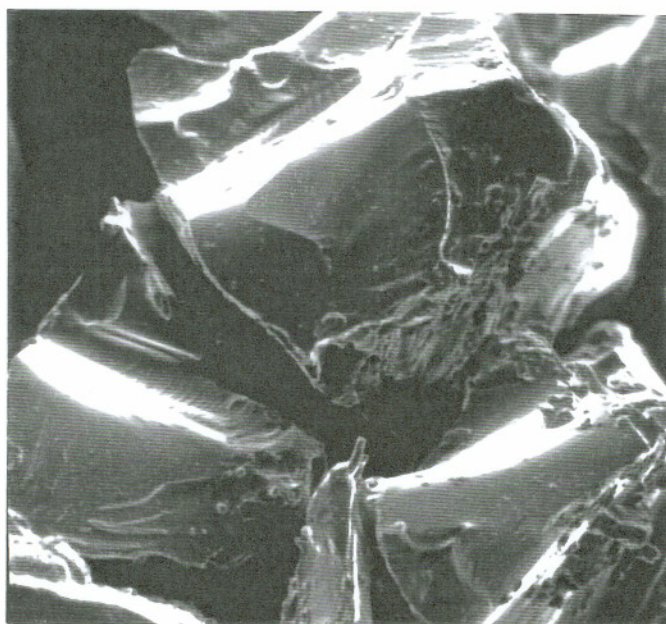
(b)

Figure 2.14 Localized resin decomposition.



20 μm

(a) Irregular fiber deformation



7.5 μm

(b) "Flow mark"

Figure 2.15 Surface morphology of the melted fibers.

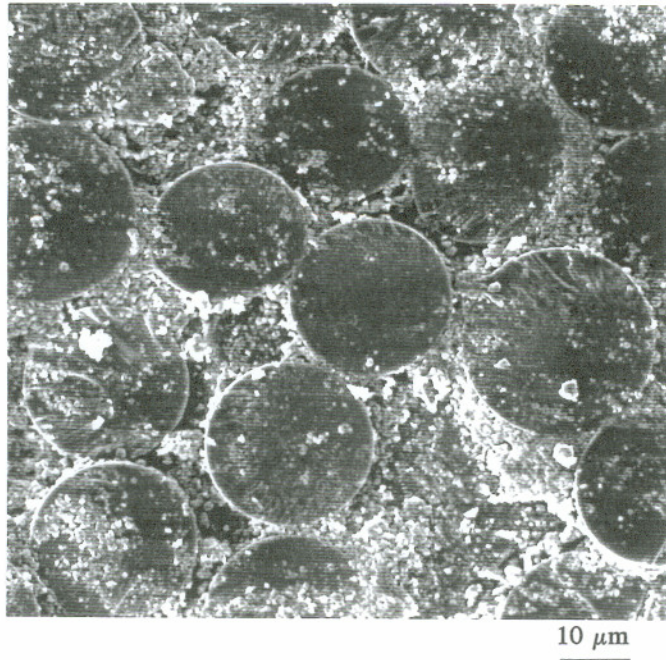
their cylindrical geometries, and the fiber deformation appeared extremely irregular. At high magnification, "flow marks" were discerned on the surface of the melted fibers (Figure 2.15b). Since melted fibers were found adjacent to the region where the fibers with huge mirror sizes were located, their formation may be associated with the initiation of insulator brittle fracture. Furthermore, melted fibers were also found on the fracture the fracture surface in insulator #7. Fiber melting, a high temperature behavior, is impossible unless the temperature exceeds about 1,065°C, the glass transition temperature of E-glass.¹³ In service, such localized high temperatures can be induced only by electrical activities, especially electrical discharges.

Post-failure damage

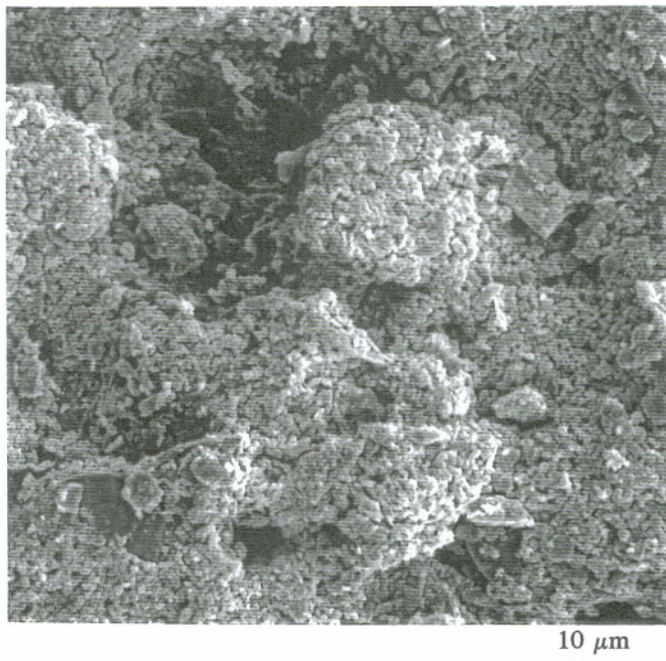
Surprisingly, all of the insulator fracture surfaces examined in this failure analysis were free from any post-failure surface damage (Figure 2.8), which is often observed on the stress corrosion fracture surface of GRP composites exposed to acids.^{50,51,79,118} Controlled by the diffusion process, the formation of post-failure surface damage primarily relies on the acid concentration as well as the exposure time of the fracture surface to aqueous acids. The fact that post-failure surface damage was eliminated from insulator fracture surfaces implies that the corrosive media in service might be not concentrated enough or only temporarily in contact with the fracture surface during the stress corrosion process.

Surface deposits

Another common feature of the insulator fracture is surface deposits. In almost all cases, the fracture surfaces were, more or less, covered with deposits (Figure 2.16). The deposits tended to be distributed non-uniformly over the fracture surface; the highest density of deposit was always located near the external surface of the



(a) Sparse region



(b) Dense region

Figure 2.16 Deposits formed on the insulator fracture surfaces.

composite rod, where the deposit layer could be so dense that the fractured fiber ends beneath it were completely obscured (Figure 2.16b).

Secondary cracks

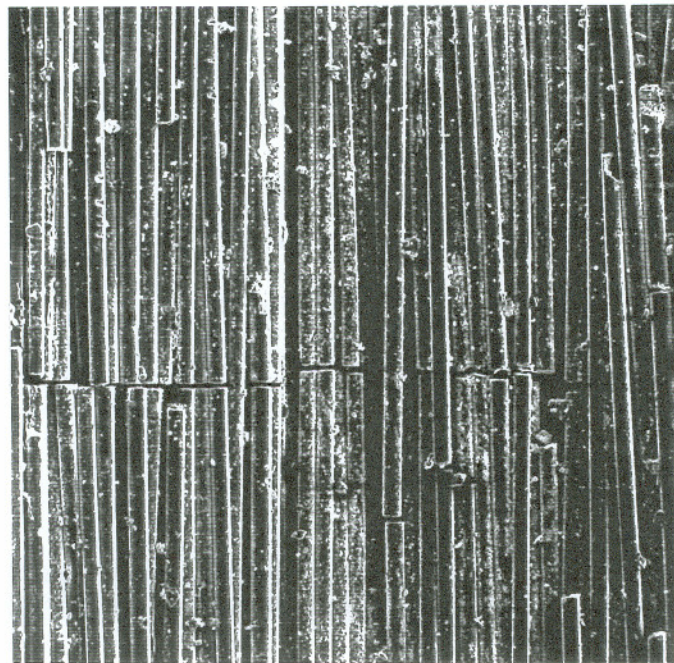
In addition to the main fracture, secondary cracks were found in the composite rod. Figure 2.17 shows one of the three transverse cracks detected on the external rod surface near the main fracture in insulator #5, which followed microscopically straight lines. As was described in the preliminary examination, secondary cracks were sometimes found to be interrupted by short longitudinal delamination, forming a crack network. Figure 2.18 displays the internal fracture surface taken from region "A" in the crack network (Figure 2.6). The entire fracture surface in this region exhibited a highly irregular morphology, consisting multiple steps. However, the fracture surface on each step was planar in nature, and the fractured fibers exhibited large mirror sizes (Figure 2.19).

2.1.5 Chemical Analyses

The chemical analysis conducted in this study was limited primarily to three areas: the black substance observed inside the damage zone on the rubber sheath, the deposit on the insulator fracture surfaces, and the depth distribution of major leachable metallic ions, calcium and aluminum, in the fractured fiber end.

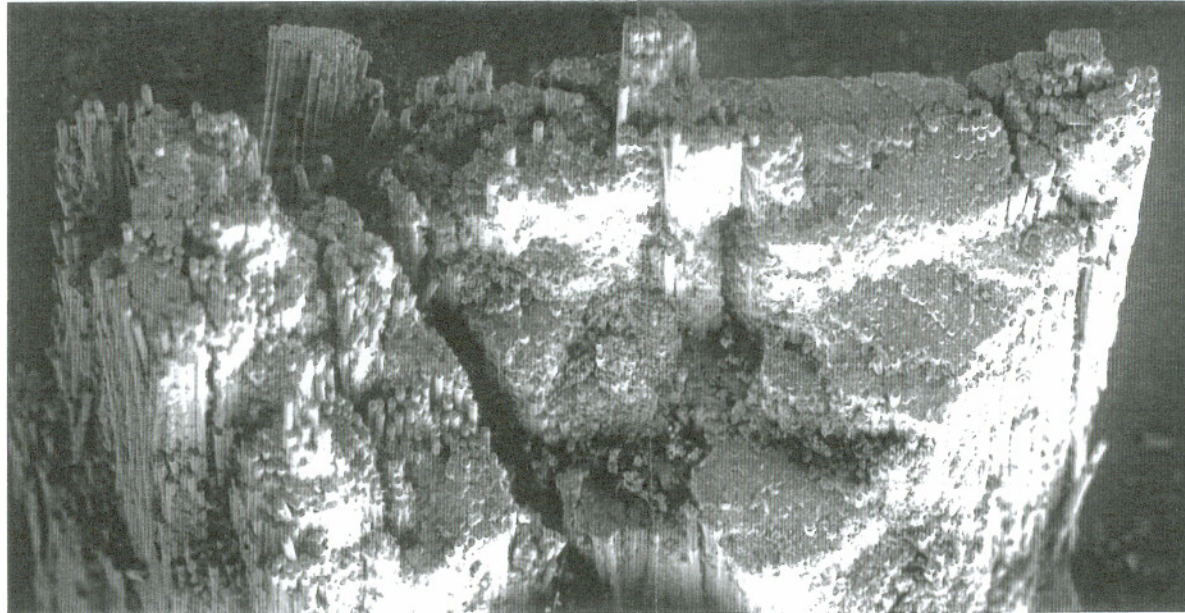
Black substance inside the damage zone

In both of the externally intact I-string insulators #1 and #2, damage zones were formed in the rubber sheath adjacent to the epoxy/sheath joint inside the high-voltage end (Figures 2.2, and 2.3). To determine the nature of the damage to the rubber sheath, chemical analysis was conducted on the black substance taken from the



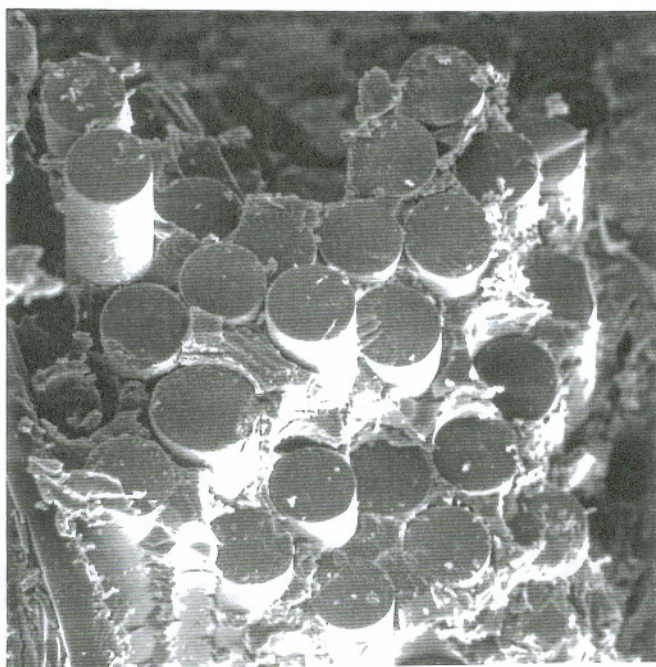
100 μm

Figure 2.17 Morphology of secondary transverse cracks.



200 μm

Figure 2.18 Fracture surface taken from the internal crack network.



20 μm

Figure 2.19 Fiber fracture morphology on the stepped fracture surface.

damage zone in insulator #2. For purposes of comparison, the materials near the damage zone, including rubber sheath, epoxy, and asphalt print, were also examined. The chemical analysis was performed on a CARLO ERBA Nitrogen-Carbon-Sulphur analyzer (NA 1500, Series 2), focusing on the amounts of carbon, hydrogen, and nitrogen.

The elemental contents of carbon, hydrogen, and nitrogen by weight percentage in each of the above components are presented in Table 2.2. As expected, the carbon content in the black substance is significantly higher than that in the rubber sheath. This result supports the hypothesis that the notch formation in the rubber sheath likely resulted from erosion induced by electrical discharge. Since the asphalt paint might partially cover the sheath surface, the interaction of electrical discharge with the asphalt paint was also possible.

Table 2.2 Chemical composition of the black substance inside the damage zone and the nearby materials, wt%

Material	C	H	N
Black substance	83.31	10.10	2.13
Rubber sheath	27.76	7.01	0.72
Epoxy	46.47	4.67	2.88
Asphalt paint	81.59	9.79	1.26

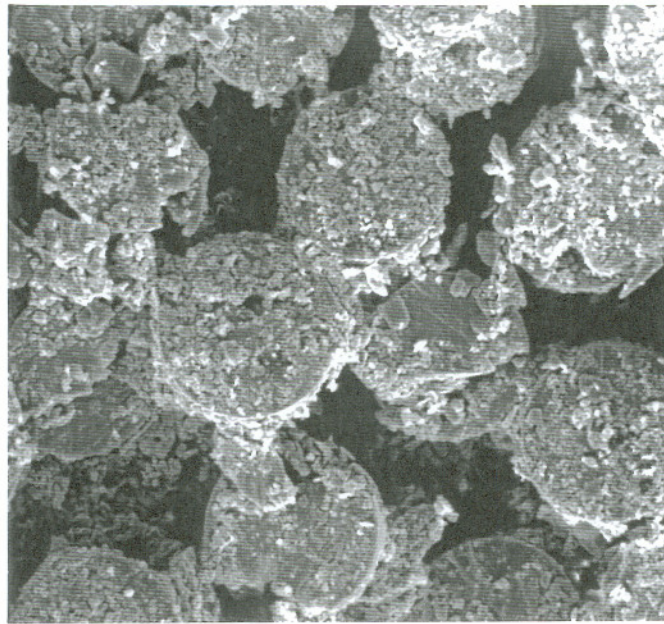
Deposits on the fracture surface

The deposit formation on the fracture surface is a common phenomenon in insulator brittle failure. To gain an insight into the stress corrosion process in service, a quantitative chemical analysis was performed on the deposits. Three fracture surfaces in insulator #4 (Figures 2.5) were selected for the chemical analysis: a transverse crack surface, a longitudinal delamination surface inside the rod, and a rod surface at the rod/sheath separation. Energy dispersive X-ray spectrometry (EDS), coupled with SEM, was used to identify the deposits forming on the fracture surfaces. Given that the deposits might contain some light elements, ESD was operated in the "no window" mode.

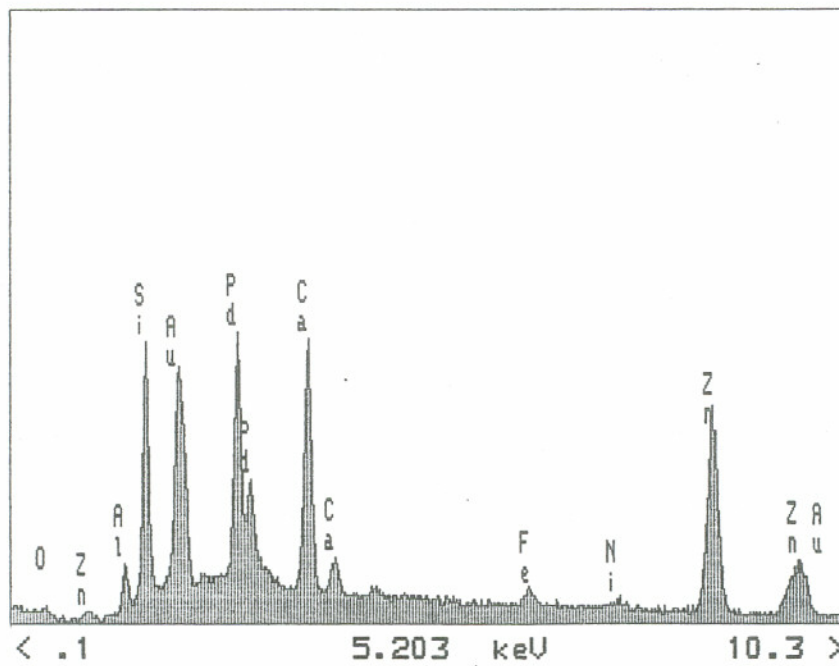
Figures 2.20 to 2.22 show the EDS analysis result on each of the examined surfaces, respectively. In addition to glass constituents (silicon, calcium, and aluminum) and surface coating materials (gold and palladium), zinc and iron were detected on all three surfaces. The chemical analysis on both the bare surface of a fractured fiber and a large deposit particle on the transverse fracture surface further confirmed that zinc was concentrated in the surface deposit (Figures 2.23 and 2.24). Since zinc and iron could only come from the metal casting and its coating, their presence on the fracture surface suggested that the metal casting may be corroded in the insulator fracture process. This finding also implied that water, either in liquid or vapor form, must have been present inside the high-voltage end, acting as a carrier to transport zinc and iron internally along the fracture surface to the region away from the high-voltage end.

Elemental depth distribution in the fractured fiber end

Numerous studies have been conducted on the stress corrosion behavior of glass fibers or GRP composites in aqueous organic or inorganic acids under laboratory

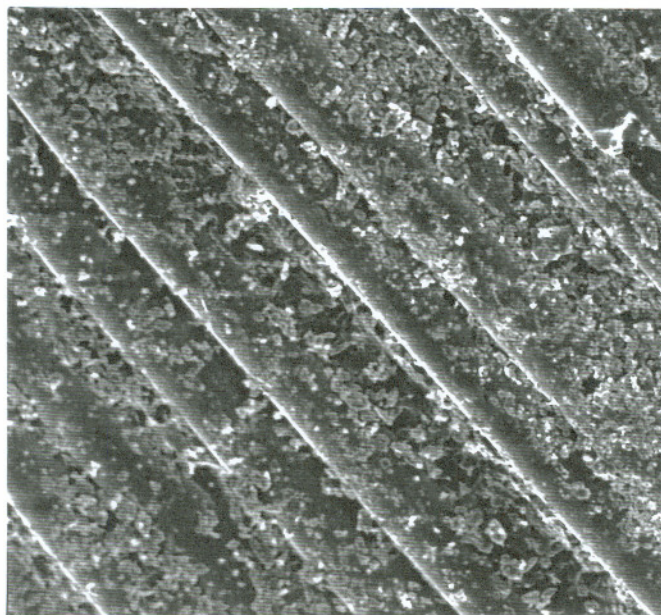


(a) SEM micrograph

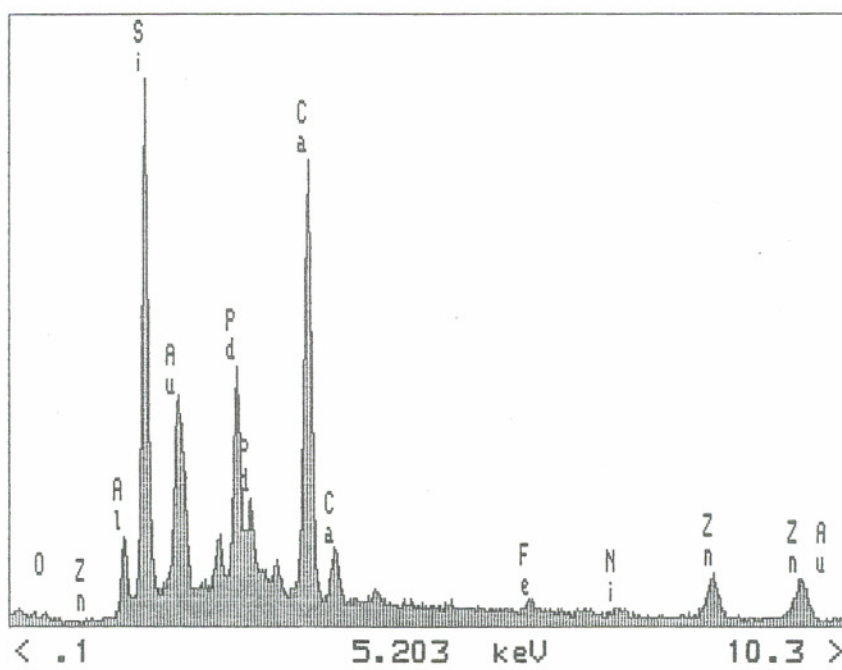


(b) EDS spectrum

Figure 2.20 EDS analysis on a transverse crack surface.

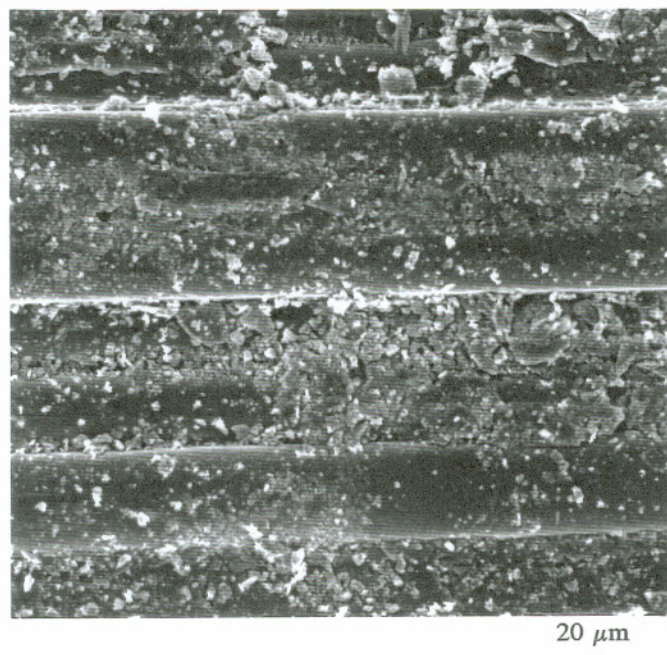
20 μm

(a) SEM micrograph

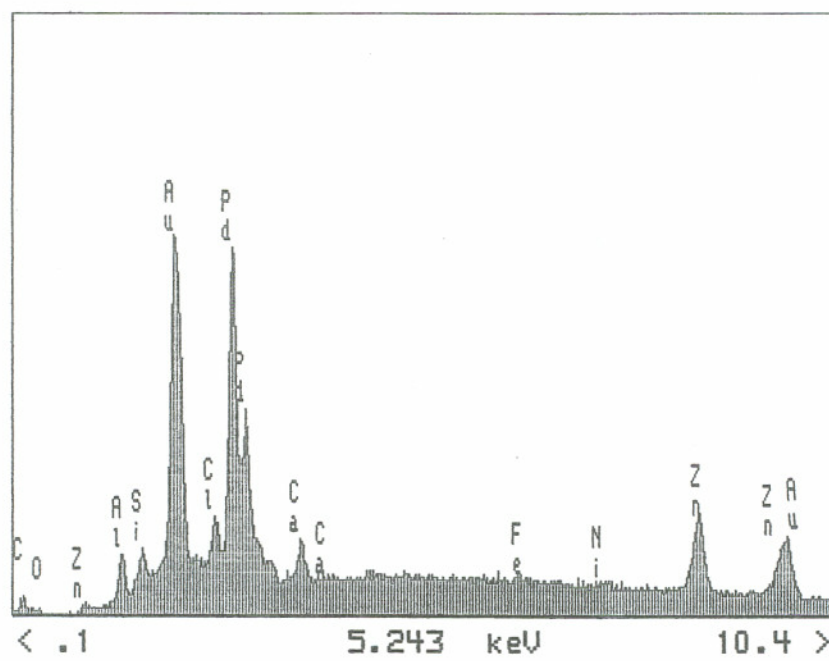


(b) EDS spectrum

Figure 2.21 EDS analysis on a longitudinal delamination surface.

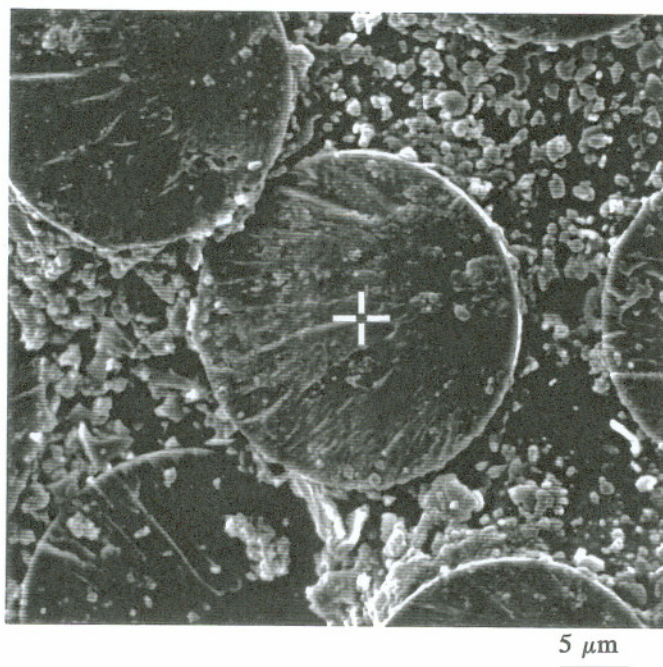


(a) SEM micrograph

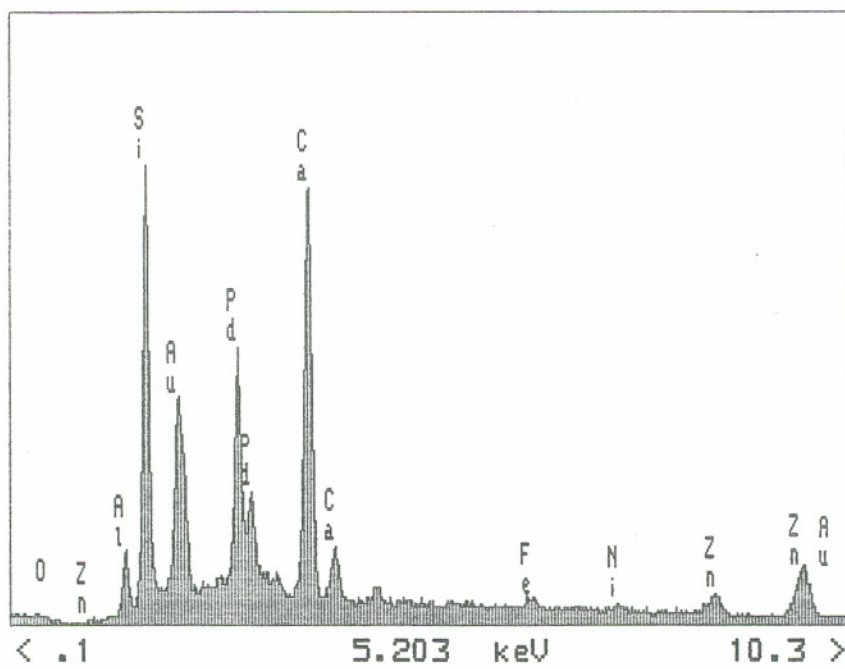


(b) EDS spectrum

Figure 2.22 EDS analysis on a rod surface at the rod/sheath separation.

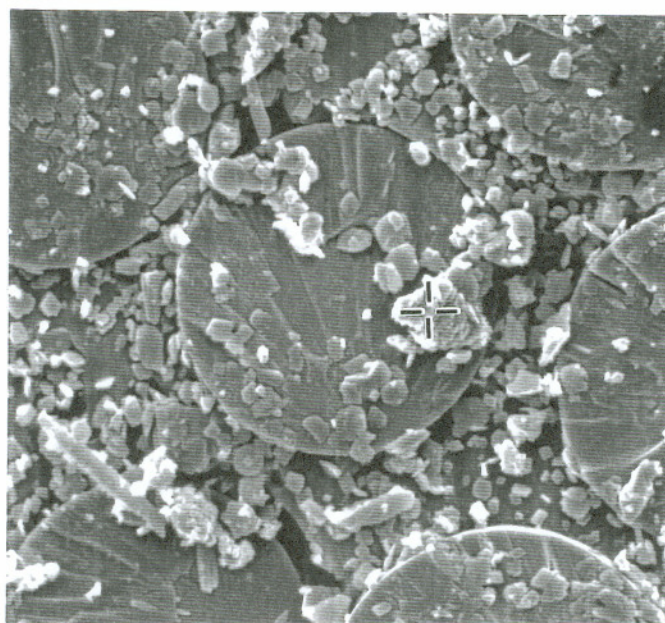


(a) SEM micrograph



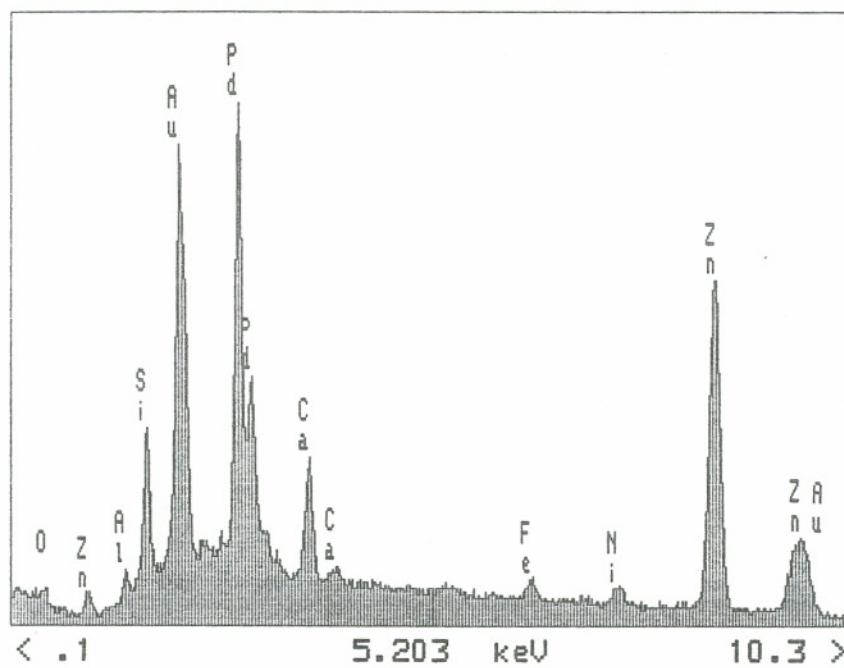
(b) EDS spectrum

Figure 2.23 EDS analysis on the bare surface of a fractured fiber.



5 μ m

(a) SEM micrograph



(b) EDS spectrum

Figure 2.24 EDS analysis on a large particle deposited on the fracture surface.

conditions.^{47,50-52,94-98,118-120} The results obtained from these studies have led to the same conclusion that calcium and aluminum depletion from glass fibers are responsible for stress corrosion of E-glass/polymer composites. Thus far, however, no direct evidence of calcium and aluminum depletion has been found on the actual fracture surface developed in the composite rod of field insulators. In this failure analysis, an attempt was made to determine the calcium and aluminum depth profiles in the fractured fiber end on the fracture surface in insulator #5.

Considering the limitation of low depth resolution inherent in the EDS technique, scanning Auger microscopy (Auger) of high surface sensitivity was selected for determining elemental depth distribution in the fiber ends on the fracture surface of insulators.¹³¹ The analysis was accomplished in micro-steps from the surface of a fractured fiber end down to its interior along the fiber axis, with the aid of the ion sputtering technique.

The results indicate that both the calcium and aluminum contents changed as functions of the distance to the fractured fiber surface (Figures 2.25 and 2.26). With an increase in the distance, calcium or aluminum content first increased and then reached a constant value, i.e., calcium or aluminum content in an intact fiber, at the distance of about 1 μm for aluminum or 2 μm for calcium, provided that silicon was distributed uniformly along the fiber. This trend verified the occurrence of acid corrosion during the insulator fracture process. Furthermore, it was evident that calcium depletion was more pronounced than aluminum depletion.

2.1.6 Fracture Stress Estimation

In this failure analysis, an effort was made to estimate the fracture stresses on both a single fractured fiber and the a failed composite rod by applying Equations 1.1 and 1.5, respectively, based on the direct measurement of fracture mirror sizes. To

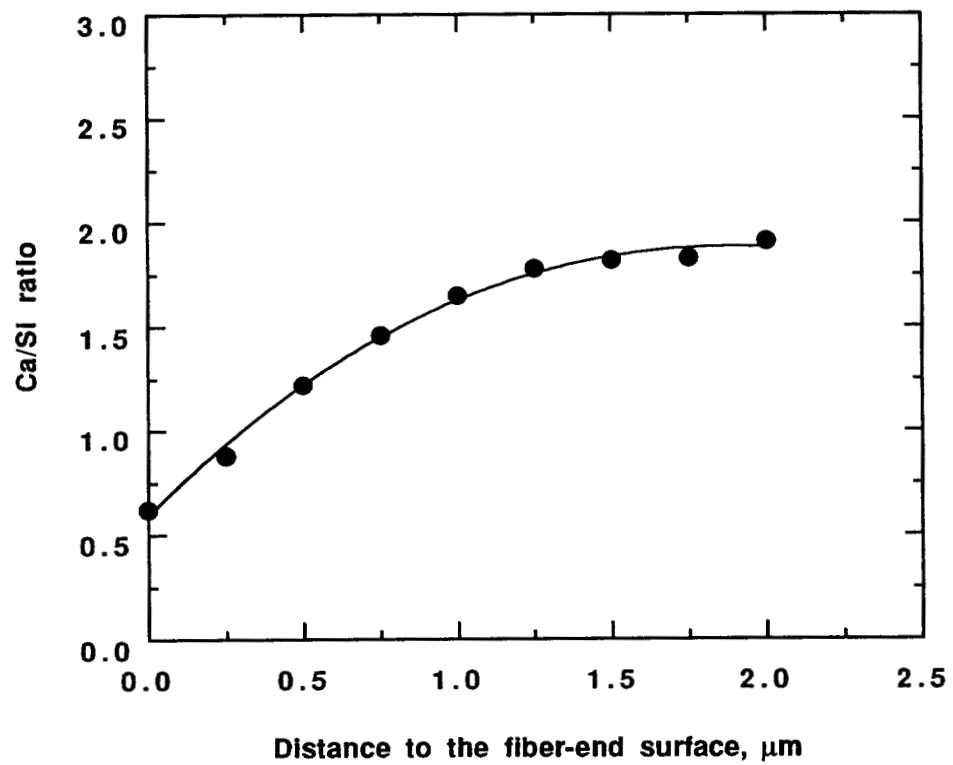


Figure 2.25 Calcium/silicon ratio as a function of the distance to the fractured fiber surface.

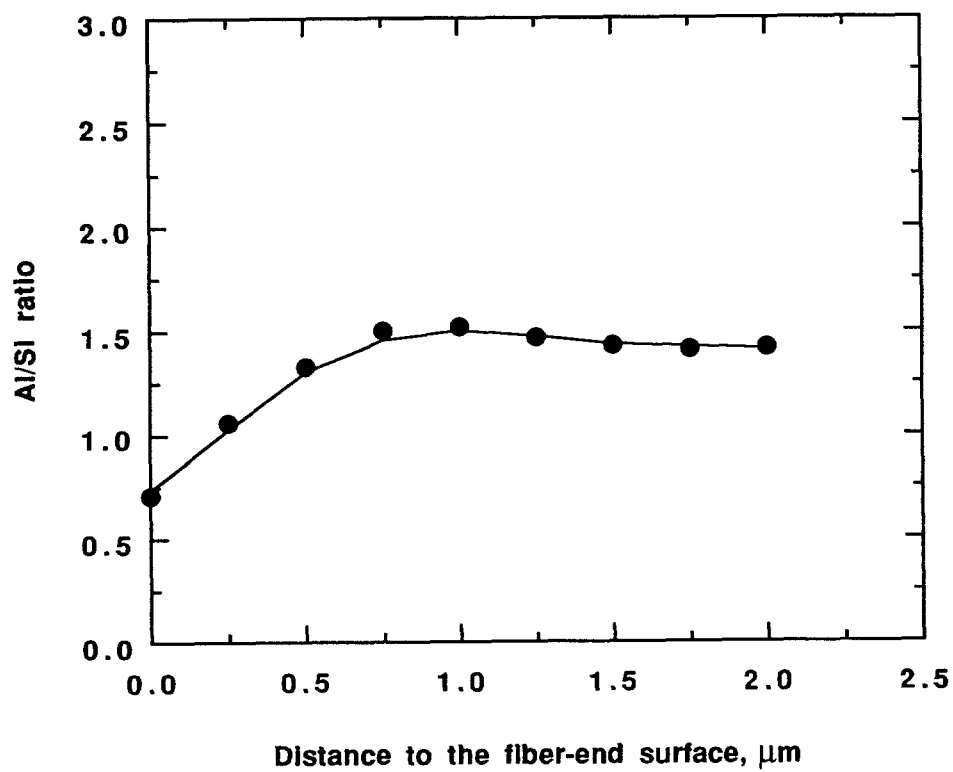


Figure 2.26 Aluminum/silicon ratio as a function of the surface to the fractured fiber surface.

perform the estimates, two parameters were essential: the mirror size on the fractured fiber and the fiber volume fraction in the composite rod, which were measured using SEM. In light of the assumption that the fiber volume fraction can be approximated by the fiber area fraction on the rod cross-section for a unidirectional composite rod, the fiber volume fraction was evaluated directly on the SEM images taken from the fracture surface under a LECO 2001 imaging analyzer.

The fracture stress estimation was performed on the fracture surface in insulator #5. To evaluate the fiber mirror size and the fiber volume fraction, ten fields were randomly selected on the fracture surface (Figure 2.27), with each field possessing approximately ten fractured fiber ends.

Mirror size and fiber diameter measurements

Mirror size and fiber diameter measurements of individual fibers in the selected fields are listed in Table 2.3. The corresponding mirror size and fiber diameter distributions on the basis of 100 fibers are depicted respectively in Figures 2.28 and 2.29. The fiber diameter obeys a Gaussian distribution. If the mirror size distribution is plotted on a semi-logarithmic scale, it can also be described as a Gaussian distribution (Figure 3.29b). The calculated mean value from each distribution appeared to be $23.22 \mu\text{m}$ for the fiber diameter and $6.88 \mu\text{m}$ for the mirror size. Furthermore, the distributions of the average mirror size and the average fiber diameter in each selected field was compared (Figure 2.30). As expected, the average fiber diameter remained nearly constant within the ten fields; however, the average mirror size varied significantly from one field to another, with the smallest value of $4.71 \mu\text{m}$ in field 3 and the largest average value of $14.38 \mu\text{m}$ in field 9.



Figure 2.27 Fracture surface in insulator #5.

Table 2.3 Fiber diameter (D) and mirror size (r) measurements, μm

Number		1	2	3	4	5	6	7	8	9	10
Field 1	D	23.6	21.8	22.9	22.5	21.5	22.5	23.6	20.4	23.2	22.2
	r	6.3	5.2	4.9	10.9	8.8	6.7	6.3	12.3	6.0	7.0
Field 2	D	20.1	21.5	22.9	22.2	22.5	21.8	22.5	23.2	22.9	26.4
	r	6.7	7.0	9.1	9.1	7.0	10.5	7.7	5.2	8.4	6.0
Field 3	D	21.1	21.8	22.5	21.5	21.1	19.4	19.7	21.1	24.7	21.6
	r	3.5	5.6	4.5	5.2	6.0	4.9	5.2	3.5	4.2	4.5
Field 4	D	29.2	19.7	20.4	21.1	21.5	20.4	20.1	20.8	20.4	21.8
	r	7.0	6.7	8.8	11.2	8.4	9.1	14.4	7.7	6.3	6.3
Field 5	D	21.4	23.2	24.3	24.3	23.2	25.7	26.8	25.4	25.0	22.2
	r	3.8	6.7	5.2	4.9	4.2	6.7	4.9	6.0	6.3	4.5
Field 6	D	22.5	22.5	23.6	23.6	22.9	22.2	22.2	22.2	22.9	25.0
	r	8.4	8.1	5.2	9.5	9.1	6.0	7.4	5.2	8.1	9.8
Field 7	D	23.2	24.0	24.7	23.6	23.6	23.2	22.9	23.6	22.9	22.2
	r	7.0	6.0	4.5	3.8	3.5	4.9	5.6	6.0	4.9	2.8
Field 8	D	26.8	23.6	22.9	24.0	26.4	22.9	22.2	20.8	24.3	22.2
	r	5.2	7.4	7.4	4.2	3.5	7.0	4.5	4.9	4.2	6.7
Field 9	D	24.4	23.6	25.0	24.0	26.1	24.7	24.7	24.3	25.7	24.3
	r	16.2	11.6	11.2	10.5	15.1	11.2	18.0	17.6	17.6	14.8
Field 10	D	25.0	2.0	25.4	25.4	24.7	24.7	25.0	24.7	24.7	24.7
	r	7.7	8.4	12.0	8.1	7.4	6.0	8.1	4.5	8.4	7.4

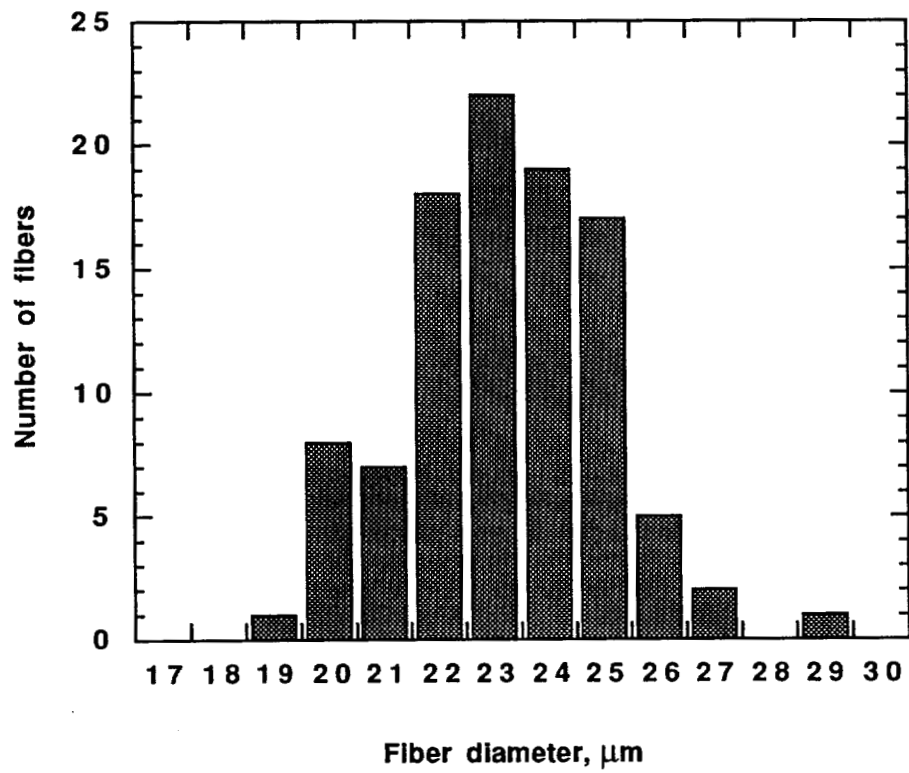
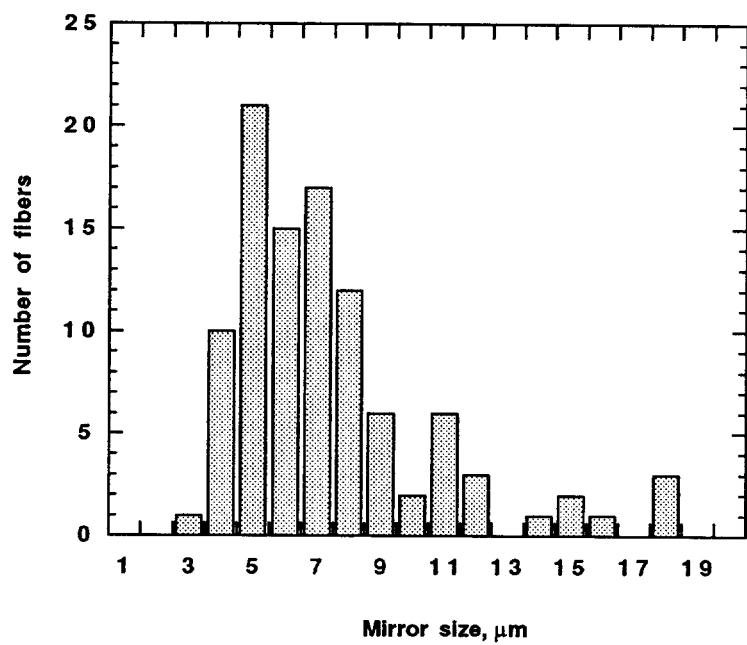
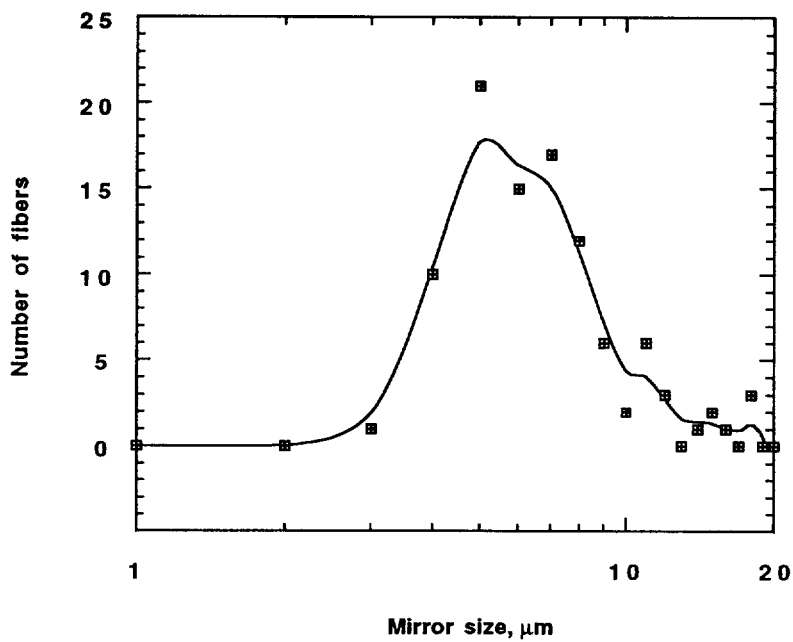


Figure 2.28 Fiber diameter distribution.



(a)



(b)

Figure 2.29 Mirror size distribution.

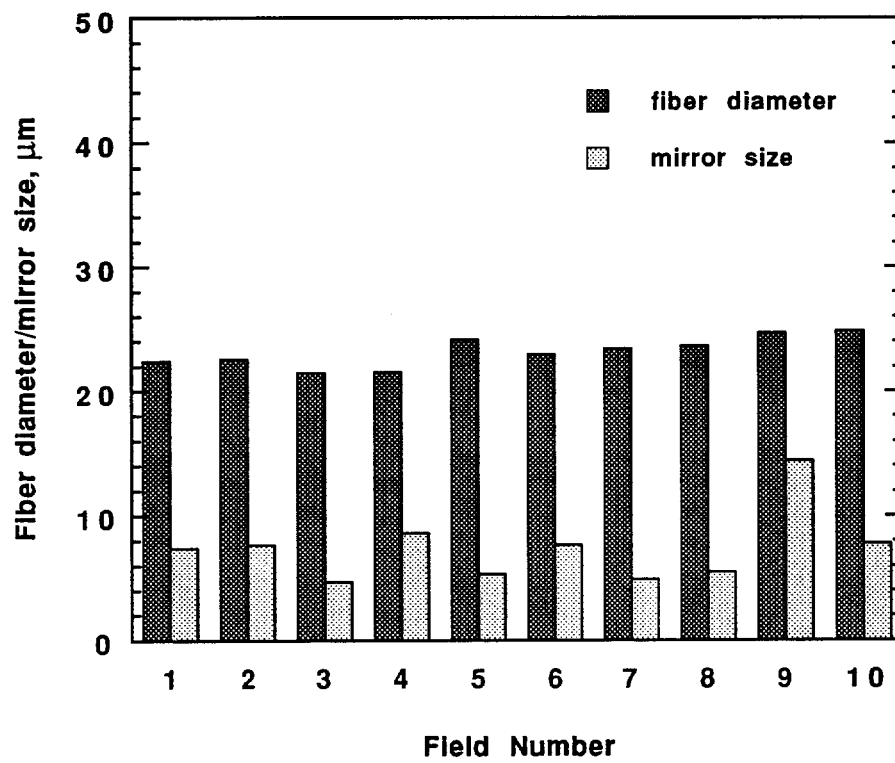


Figure 2.30 Comparison between mirror size and fiber diameter distributions.

Fiber volume fraction evaluation

By averaging the fiber area fractions in the selected fields on the fracture surface, the fiber volume fraction of the composite rod was estimated to be 75%, which fell within the range designated for common unidirectional GRP composites.

Fracture stress estimation

The fiber fracture stress was evaluated in each of the regions selected on the fracture surface (Figure 2.27). To make the estimated stress representative, the average mirror size, r_M , in each region, instead of the mirror size on a single fractured fiber, r , was chosen for the calculation. Equation 1.1 was thereby modified to

$$\sigma_F r_M^{1/2} = A , \quad (2.1)$$

where σ_F represents the average fiber fracture stress in the region. The mirror constant, A , was assumed to be 1.47 MPa m^{1/2} suggested by Jaras and Norman for E-glass fiber.⁸⁸

The fracture stress on the composite rod was estimated by applying Equation 1.5 based on the rule of mixtures. Since the average fiber fracture stress, σ_F , was employed, the equation was modified accordingly to

$$\sigma_C = \sigma_F [E_m/E_f(1-V_f) + V_f] , \quad (2.2)$$

where the Young moduli for resin matrix, E_m , and glass fiber, E_f , were assumed to be 3 GPa and 76 GPa, respectively,¹³² and the fiber volume fraction, V_f , was taken as 75%, the actual value obtained from insulator #5. In the stress analysis, an effort was also made to compare the fracture stress of the composite rod obtained from the above estimation with its ultimate tensile strength in the dry-air condition, σ_C^* , which was

calculated to be 146 MPa, given the fracture load of 2,724 kg (6,000 lbs)¹³³ and the rod diameter of 16 mm.

Both the estimated fiber and rod fracture stresses are summarized in Table 2.4. Notably, the estimated rod fracture stresses were approximately two to four times higher than its ultimate tensile strength in the dry-air condition, which were much higher than the values reported in the literature. The stress overestimate resulting from this approach may arise from two sources. First, the relationship expressed by Equation 2.1, originated from bare glass fibers, may not be valid for the fracture stress calculation on the fibers in composites. Constrained by a resin matrix, individual fibers in composites experience internal stress concentration at the fiber/resin interface, which primarily depends on the fiber volume fraction, the mechanical properties of both the fiber and the resin, and more importantly, the curing status of the resin. Second, the rule of mixtures may not work well for composite strength evaluation. In general, mechanical strengths of composites are highly structure-sensitive.¹⁵ During composite fabrication, fiber or resin structure may be changed, and due to considerable difference in their thermo-mechanical properties, residual stresses may be generated within the composite. These stresses could become large enough to cause the plastic deformation of the resin matrix, thereby considerably altering the stress state in the composite.

Although some success has been obtained in strength calculation of glass fiber-reinforced cement composites based on direct fiber strength measurements,⁸⁸ stress estimation conducted in this study suggests that this approach is not suitable for evaluating fracture stress of GRP composite rods in insulator brittle fracture.

Table 2.4 Average fracture stresses in the selected fields

Field number	r_M μm	σ_F MPa	σ_C MPa	σ_C/σ_C^*
1	7.44	538.93	409.59	2.80
2	7.67	530.79	403.40	2.76
3	4.71	677.34	514.78	3.52
4	8.59	501.56	381.19	2.61
5	5.32	637.32	484.36	3.31
6	7.68	530.44	403.13	2.76
7	4.90	664.08	504.70	3.45
8	5.50	626.81	476.38	3.26
9	14.38	387.65	294.61	2.01
10	7.80	526.34	400.02	2.73

2.2 Stress Corrosion Experiments

The purpose of these experiments was to understand the basic stress corrosion behavior of common GRP composites in actual insulator environments. In service, GRP insulators are likely surrounded by an acidic medium, containing nitric acid, oxalic acid, or hydrochloric acid. Therefore, these acids were selected for the test solutions. In these experiments, the effects of acid type, acid concentration, mechanical stress, and materials on stress corrosion fracture were of primary interest.

Moreover, the existence of moisture or water is inevitable in service environments. It is well known that GRP composites can be damaged when exposed to water.^{22,50,134-137} However, no conclusive answer has been found to the question whether or not water itself, i.e., without the presence of any other corrosive media, can cause stress corrosion cracking of composites. In this experiment, water influence on stress corrosion behavior of composites was also explored.

2.2.1 Materials

Three GRP composite systems, supplied by GlasForms Inc., were investigated in the stress corrosion experiments. Made in the form of pultruded plates, these composites were all reinforced by E-glass fibers, but constructed by different matrix materials, including polyester, epoxy and vinyl ester.

All experiments focused on E-glass/polyester composite. Only in the study on the material effect, were E-glass/epoxy and E-glass/vinyl ester composites involved in addition to E-glass/polyester composite.

2.2.2 Constant K_I Specimen

The modified cantilever specimen, which is usually referred to as the constant K_I specimen, was employed in the stress corrosion experiment. The geometry and dimensions of the specimen are illustrated in Figure 2.31. The specimen was machined from an unidirectional composite plate in such a way that the fibers were parallel to the load direction. To reduce the width of the crack front, a pair of grooves were made on the sides of the specimen along the center line. Before the testing, a pre-crack of about 1 mm in length was introduced at the notch root with a scalpel blade to minimize the crack initiation time, and the sides of the specimen were coated with vaseline to prevent acid attack ahead of the crack front.

Price and Hull have shown that this specimen geometry ensures that both the stress intensity factor, K_I , will remain constant within the first 15 mm of crack growth⁶² and that the stress corrosion crack will propagate from the notch root of the specimen in the direction perpendicular to the fiber. For a stress intensity lower than 4.8 MPa $m^{1/2}$,⁵¹ or more conservatively 4.0 MPa $m^{1/2}$,⁶² the fracture surface will appear essentially planar, and the extent of fiber/matrix interface debonding and fiber pull-out will be limited.

The geometry and dimensions of the specimen used in this study were identical to those employed by Price and Hull,⁶² except for the thickness of the specimen at the grooves, which was reduced from 1.0 mm to 0.5 mm. Further finite element analysis¹³⁸ and a compliance calibration experiment¹³¹ verified that the constant K_I assumption remained valid for the reduced-thickness specimen. Results obtained from the compliance calibration experiment also suggested that the constant K_I region, in this case, was lessened to approximately the first 8 mm of crack growth.

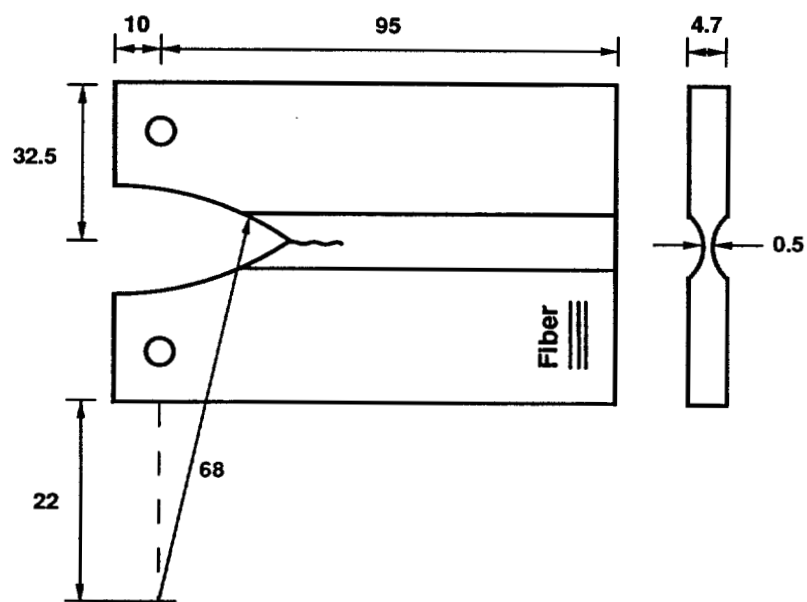


Figure 2.31 Configuration of the constant K_I specimen (all dimensions in mm).

2.2.3 Experimental Arrangement

Stress corrosion experiments were conducted based on the concept introduced by Price and Hull.⁶² The distinct advantage of their test technique is that mechanical stresses in acting on the specimen can be accurately controlled, allowing for the correlation of stress intensity to crack growth behavior. The experimental arrangement used in the stress corrosion experiments consisted of three basic parts: a stress-corrosion test unit, a load cell, and an acoustic emission unit. The detail of the arrangement is presented in Figure 2.32.

Stress-corrosion test unit

The stress-corrosion test unit contained a cantilever mechanical device, a solution storage tank made of PMMA plexiglass, and a travelling optical microscope. In the experiments, the constant K_I specimen was immersed in the test solution to a level slightly above the grooves. The tensile load was simultaneously applied to the specimen through its two arms by the cantilever mechanical device. The travelling optical microscope, pointing to the notch root, was used to measure the crack length during the experiments.

Load cell

To control the tensile load applied to the constant K_I specimen, a load cell was inserted into the loading path in the cantilever mechanical device and connected to a bridge amplifier. The accuracy of load cell was calibrated to a tenth of a pound.

Acoustic emission (AE) unit

To monitor the stress corrosion process quantitatively, acoustic emission technique was employed in the experiments. An AC 375L piezoelectric transducer was positioned

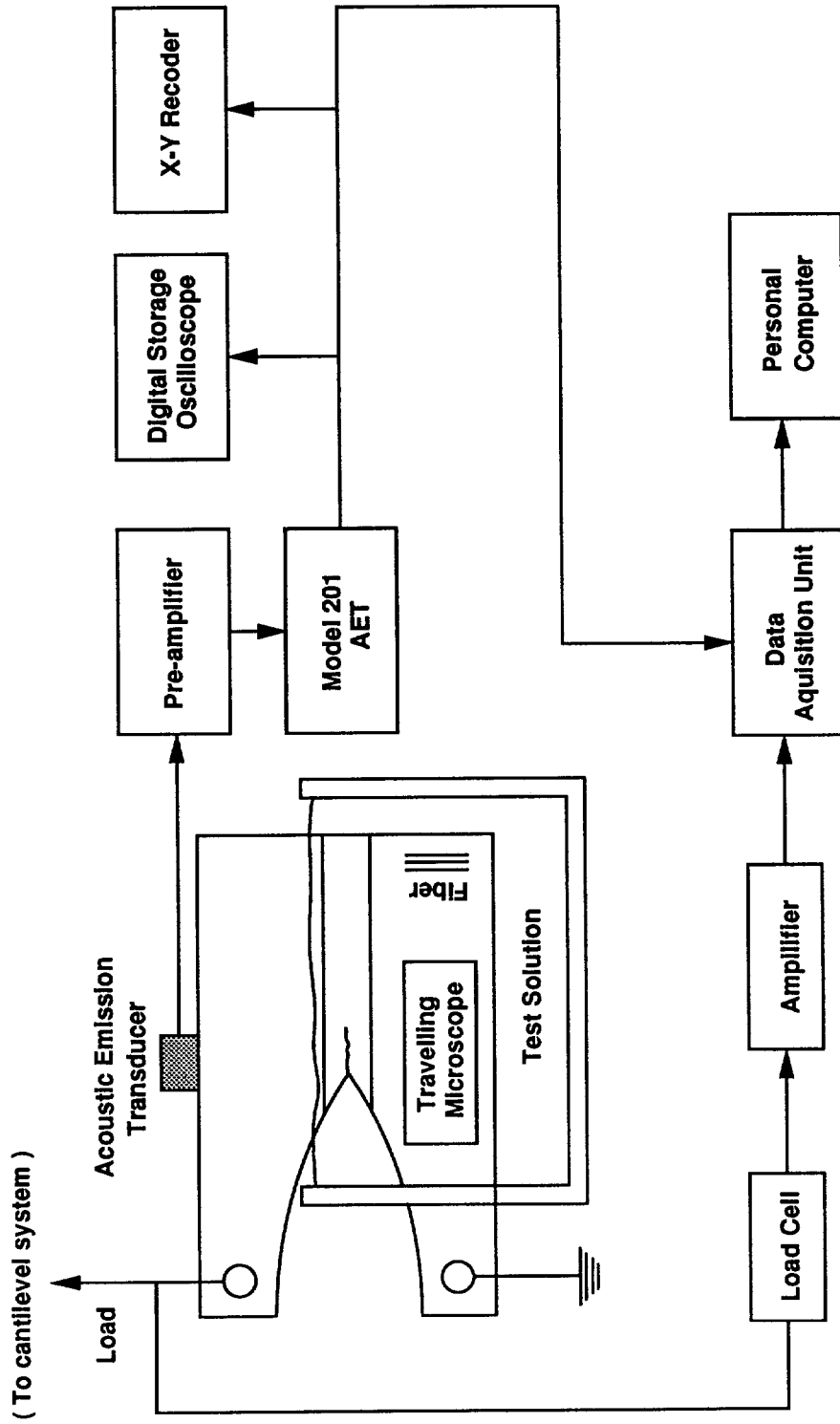


Figure 2.32 Schematic representation of the stress corrosion experimental arrangement.

on the upper edge of the specimen directly above the crack front (Figure 2.32). The specimen surface in the contact area was polished and coated with vaseline, which serviced as a coupling agent between the transducer and the specimen. During the stress corrosion experiment, acoustic emission induced by crack propagation was detected by the transducer, and the number of acoustic emission ringdowns was recorded on a X-Y plotter. The acoustic emission technique has been found to be a useful tool to estimate the number of fractured fibers in the stress corrosion fracture of composites.^{139,140} A study conducted by Kumosa *et al*¹³⁹ has shown when the stress corrosion fracture in unidirectional GRP composites are subjected to low stress intensities at the crack front, two types of acoustic emissions are produced: high-energy signals generated by fiber fracture and low-energy signals induced by matrix fracture. If the total gain of the acoustic emission system is sufficiently low, however, it is possible to record only the high-energy signals associated with fiber fracture. Based on this principle, the acoustic emission system in the study was adjusted to the total gain of approximately 80 dB, at which a one-to-one correlation between fractured fibers and high-energy signals, recorded as ringdowns, was established. Figure 2.33 shows the acoustic emission output recorded from the stress corrosion test in 0.5N hydrochloric acid. The large steps in the curve correspond to the high-energy signals produced by fiber fracture.

The stress corrosion experiments were performed at room temperature. A fixed tensile load of 9.08 kg (20 Lbs) was employed in all of the experiments, except for the study on mechanical load effect, in which the tensile load was a variable. This particular load was chosen to achieve the possibly highest crack growth rate under conditions of limited fiber/matrix interface debonding at the crack front, thus reducing the test duration. The calibration of the constant K_I specimen used in this experiment¹³⁸ further revealed that the tensile load of 9.08 Kg (20 Lbs) resulted in the stress intensity of approximately 4.3 MPa m^{1/2} at the crack front, which approximated the upper limit suggested by Price and Hull for the formation of a planar stress corrosion crack in acidic environments.^{51,62}

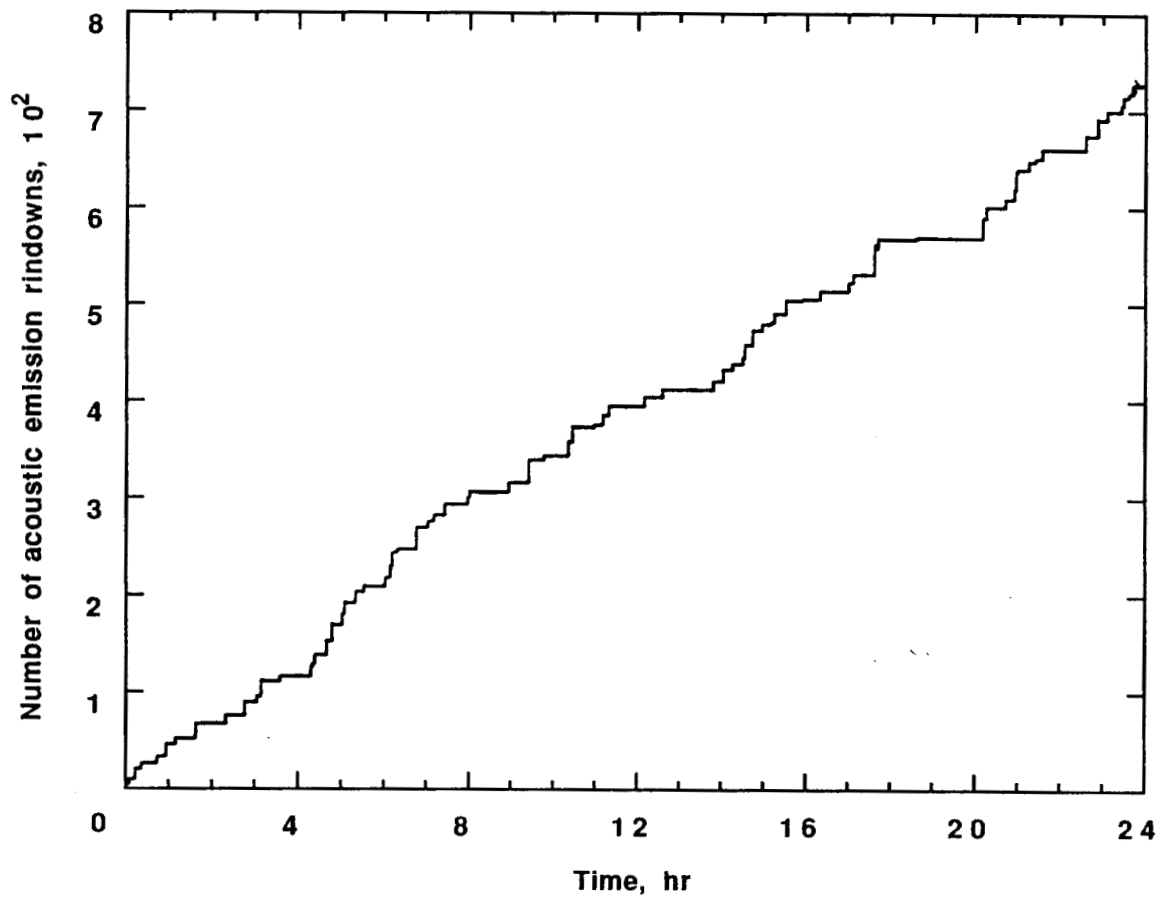


Figure 2.33 Acoustic emission output recorded during the stress corrosion experiments.

Therefore, the stress corrosion experiments performed in this study were conducted in a highly accelerated condition.

2.2.4 Test Solutions

In the experiments, nitric acid (HNO_3), oxalic acid ($\text{H}_2\text{C}_2\text{O}_4$), and hydrochloric acid (HCl) with different concentrations, as well as tap water of pH 6.8, were chosen for the test solutions. All the acid solutions were prepared by mixing analytical-grade acid reagents with deionized water.

2.2.5 Stress Corrosion Behavior of Composites

The stress corrosion behavior of GRP composites is affected by many factors. Among the most fundamental are acid type, acid concentration, mechanical load, and composite materials. The effects of these factors on stress corrosion behavior of composites were explored in the experiments. Additionally, the influence of water was also considered.

2.2.5.1 Acid Type Effect

The acid type effect was examined in nitric and oxalic acids; the former is an inorganic acid and the latter is an organic acid. The concentration of each acid was fixed at pH 3. The test duration in each solution was 24 hours.

The experimental results are given in Figure 2.34. Within 24 hours, the number of fractured fibers induced by stress corrosion in the oxalic acid solution appeared approximately three times higher than that in the nitric acid solution, suggesting that oxalic acid was more corrosive to E-glass/polyester composite relative to nitric acid at equal pH. These results are consistent with those observed by Chandler *et al* on corrosion behavior of E-glass fiber in nitric and oxalic acids.⁴⁶

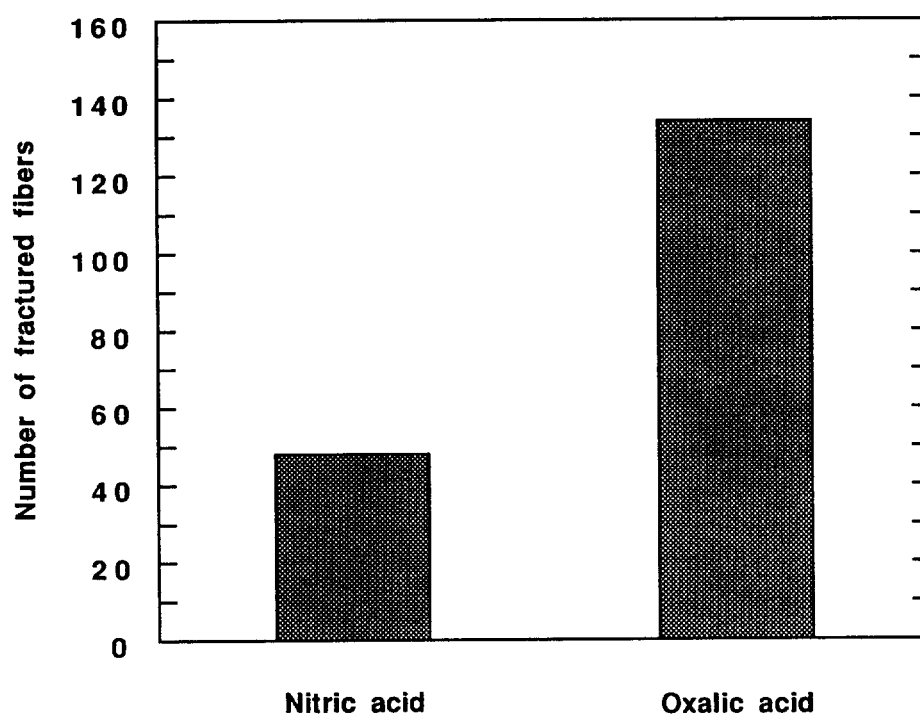


Figure 2.34 Number of fractured fibers in the pH 3 nitric and oxalic acids.

2.2.5.2 Acid Concentration Effect

Acid concentration influence on stress corrosion behavior of composites were examined in aqueous solutions of oxalic acid, from pH 5 down to pH 1 at intervals of one pH value. The experiment in each solution lasted 24 hours. It should be noted that the relationship between acid concentration and pH value is not linear, rather logarithmic; for every reduction of one pH value, the acid concentration will become ten times higher.

The number of fractured fibers and the crack growth rate as a function of oxalic acid concentration, expressed by the pH value, is presented respectively in Table 2.5 and Figure 2.35. Apparently, the severity of stress corrosion in E-glass/polyester composite, under a constant mechanical load, is highly dependent on the acid concentration; a higher acid concentration, i.e., a lower pH value, led to a larger number of fractured fibers. Furthermore, there likely existed a critical concentration of oxalic acid, between pH 4 and pH 5, below which the crack propagation was inhibited. It should be noted that the critical acid concentration for stress corrosion fracture of composites may vary with the applied mechanical load, the acid type, as well as the composite material.

2.2.5.3 Mechanical Load Effect

The mechanical load effect was evaluated in the aqueous oxalic acid of pH 1. The experiment was conducted over 24 hours for each applied mechanical load, with the load ranging from 6.81 kg (15 lbs) to 9.08 kg (20 lbs) in increments of 0.454 kg (1 lb).

Previous studies^{47,62,66} have suggested that in the stress corrosion fracture of unidirectional GRP composites, the relationship between the crack growth rate, da/dt , and the applied stress intensity, K_I , or the applied tensile load, P , obeys a simple power law:

$$da/dt = A K_I^n, \quad (2.3)$$

Table 2.5 Number of fractured fibers in 24 hours as a function of pH produced by oxalic acid

pH	Number of fractured fibers
1	532
2	288
3	143
4	31
5	0
6	0

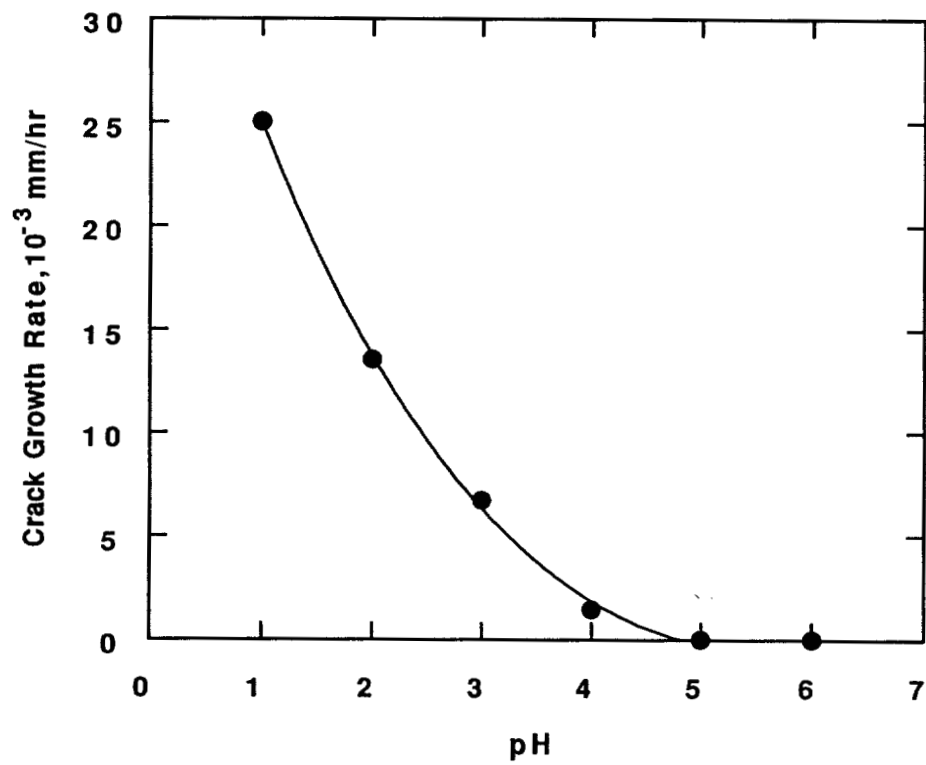


Figure 2.35 Crack growth rate as a function of pH produced by oxalic acid.

or

$$da/dt = B P^m, \quad (2.4)$$

where A, n, B, and m are constants. Assuming that each high-energy AE signal corresponds to a single fiber fracture, the frequency of high-energy signals induced by fiber fracture, $d(AE)_f/dt$, and the applied load, P, should comply with a similar power relationship:

$$d(AE)_f/dt = B^* P^{m^*}, \quad (2.5)$$

where B^* and m^* are also constants.

Figure 2.36 depicts the frequency of high-energy signals, expressed by the rate of AE ringdowns, as a function of the applied tensile load in the pH 2 oxalic acid solution, which satisfies the relationship described by Equation 2.5 and can be specified as

$$d(AE)_f/dt = 2.5e^{-27} P^{21}. \quad (2.6)$$

For the constant K_I composite specimen, the crack growth rate, da/dt , can be further derived from

$$da/dt = 1/(w V_f) d(AE)_f/dt, \quad (2.7)$$

where w is the thickness of the specimen at the grooves, and V_f is the fiber volume fraction. Substituting w and V_f with 0.5 mm and 75%, respectively, Equation 2.7 becomes

$$da/dt = 6.7 e^{-27} P^{21}, \quad (2.8)$$

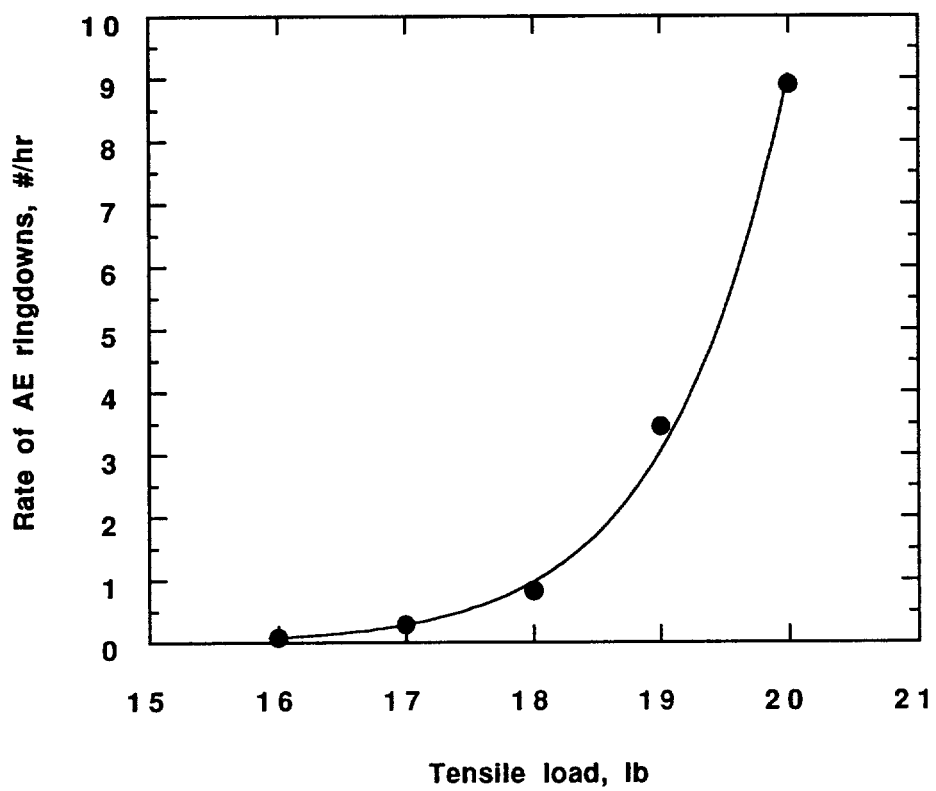


Figure 2.36 Rate of acoustic emission ringdowns as a function of tensile load in the pH 2 oxalic acid solution.

which implies that on a double-logarithmic scale, the crack growth rate should be linearly correlated to the applied load. As expected, this linear relationship was also observed in the oxalic acid experiments (Figure 2.37).

Notably, the results confirmed that the acoustic emission technique provided a reliable method for estimating crack growth rate in the stress corrosion fracture of unidirectional GRP composites.

2.2.5.4 Materials Effect

The stress corrosion behavior of E-glass fiber/polyester, E-glass fiber/epoxy, and E-glass fiber/vinyl ester composites were studied in nitric acid solutions of pH 3, pH 3.5, and pH 4. The experiment on each composite material at each acid concentration took ten days.

The crack growth rates as a function of the acid exposure time for different nitric acid concentrations in E-glass fiber/polyester and E-glass fiber/epoxy composites are shown in Figures 2.38 and 2.39, respectively. Apparently, the E-glass fiber/epoxy composite exhibited much higher resistance to stress corrosion cracking in nitric acid compared to the E-glass fiber/polyester composite; the crack growth rate in the E-glass fiber/epoxy composite specimen exposed to the pH 3 nitric acid was found to be about ten times less than in the E-glass fiber/polyester composite specimen. Furthermore, there may have existed a critical acid concentration between pH 3 and pH 4, under which the crack propagation could not be initiated in the E-glass/polyester composite (Figure 2.38); however, this phenomenon was not clearly identified for the E-glass fiber/epoxy composite (Figure 2.39).

Superior to both E-glass fiber/polyester and E-glass fiber/epoxy composites in the stress corrosion resistance, no signal of fiber fracture was recorded by the AE system during

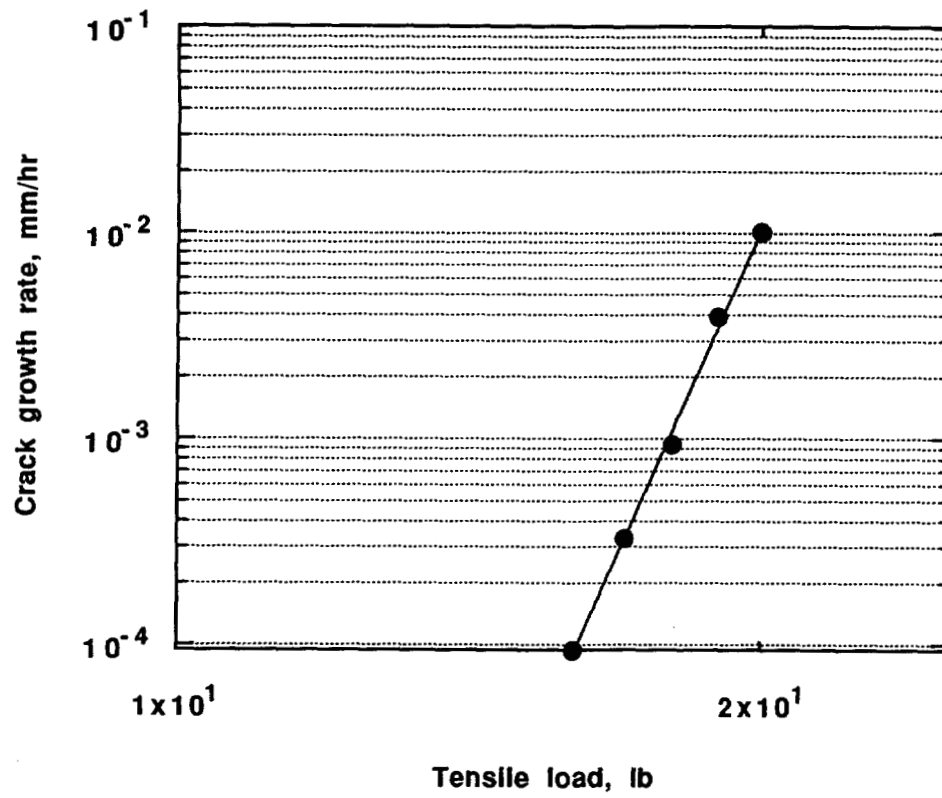


Figure 2.37 Crack growth rate as a function of tensile load in the pH 2 oxalic acid solution.

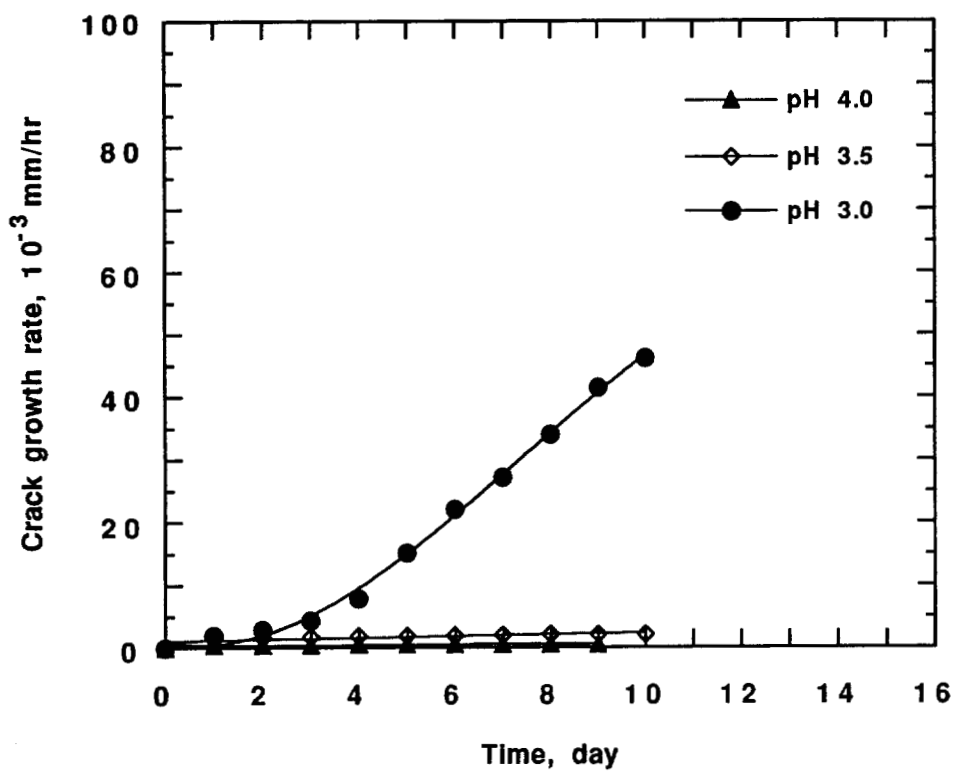


Figure 2.38 Crack growth rate as functions of exposure time and acid solution pH in E-glass fiber/polyester composite.

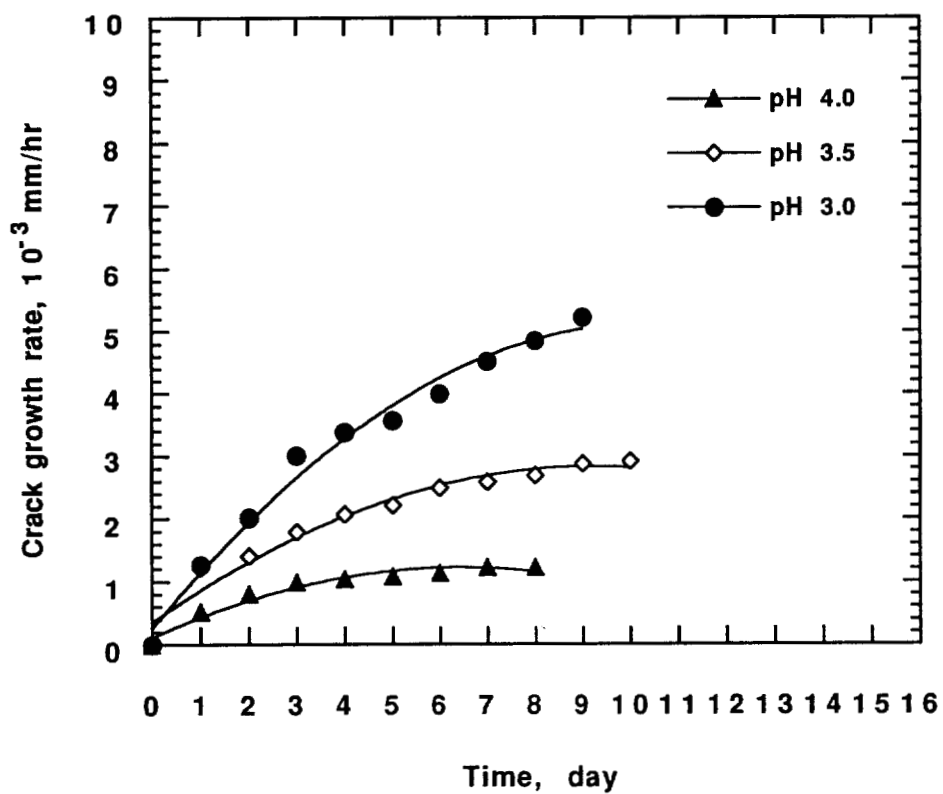


Figure 2.39 Crack growth rate as functions of exposure time and acid solution pH in E-glass fiber/epoxy composite.

the exposure of the E-glass fiber/vinyl ester composite specimen to the pH 4, pH 3.5 and pH 3 nitric acid solutions. Further study revealed that the stress corrosion fracture in the E-glass/vinyl ester composite specimen could be initiated only if the pH value was less than 2.5.

Crack propagation behavior of composites subjected to stress corrosion fracture in acids has been suggested to be a function of the chemical resistance and fracture toughness of resin matrices.^{58,59} Tougher resins can effectively reduce the crack growth rate; however, they usually possess poorer chemical resistance as well as higher acid diffusion coefficients, which in turn may facilitate crack propagation. Among the three composite systems tested, the fracture toughness of the resins increases in the sequence of epoxy, vinyl ester, and polyester, while their chemical resistance or acid diffusion coefficients follow the opposite order. The much higher crack growth rate observed in E-glass fiber/polyester composite than in E-glass fiber/epoxy composite implies that the influence of the chemical resistance of resins on crack propagation may outweigh that of their fracture toughness. Furthermore, it is a good combination of chemical resistance and fracture toughness of vinyl ester that makes E-glass fiber/vinyl ester composite to be of the best stress corrosion resistance.

2.2.5.5 Water Effect

The water test was conducted in the same manner as the acid stress corrosion experiments. The pH value of tap water was measured around 6.8. Given that tap water is much less corrosive than acid solutions, the composite specimen was tested in water for a half year, a much longer time than that in the acid experiments.

Although some damage, such as fiber/resin interface debonding, developed in the notch root region due to water attack, no transverse crack was initiated, indicating that tap water was not corrosive enough to generate stress corrosion cracking in unidirectional

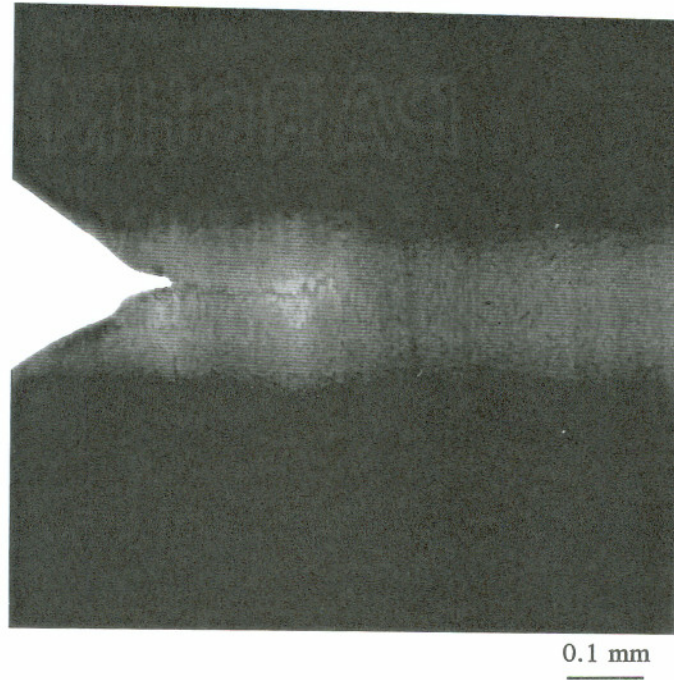
E-glass/polyester composite at room temperature. This observation is in accordance with the result obtained by Grag¹⁴¹ that water shows negligible influence on stress corrosion behavior of glass fiber reinforced epoxy composites at room temperature.

2.2.6 Fracture Morphology

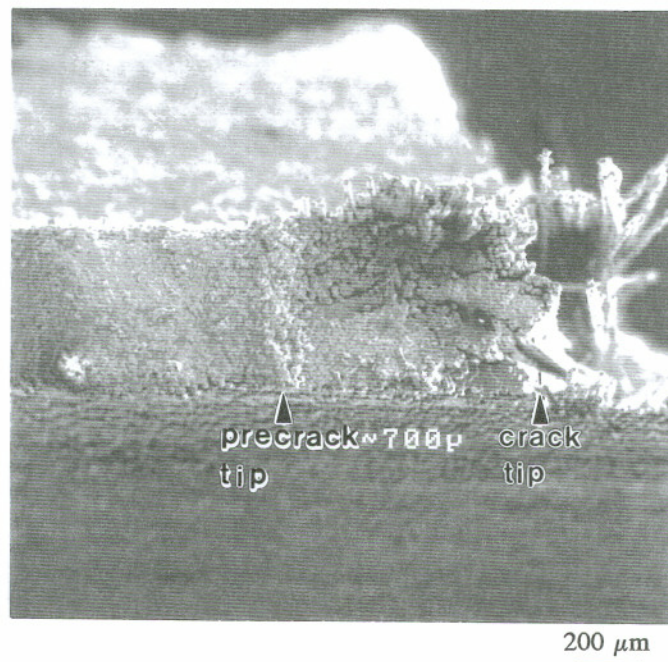
The surface fracture morphology of the stress corrosion cracks that developed during the experiments was characterized using SEM. The sample was prepared for SEM examination in the following sequence. First, the constant K_I specimen, after being disconnected from the test unit, was rinsed in deionized water and dried in air. Second, Scotch tape was placed on the both sides of the notch root region to cover the stress corrosion crack, preventing the crack from any contamination or mechanical damage in the procedure. Third, the notch root region was cut off from the specimen with a jewelry saw, and the matching fracture surfaces were obtained by mechanical separation of the specimen along the crack. Finally, the fracture surface was deposited with a gold/palladium conductive layer in a vacuum sputtering coater.

All of the stress corrosion cracks obtained from different acid experiments exhibited a similar macro-fracture morphology, although their growth rates varied with acid type, acid concentration, applied mechanical load, and composite material. A typical crack morphology could be characterized by an essentially straight line or planar surface, which initiated at the notch root of the constant K_I specimen and propagated perpendicular to the fiber direction along the center of the grooves (Figure 2.40).

The micro-fracture characterization was focused on the fracture surfaces in E-glass/polyester composite induced by stress corrosion cracking in both nitric and oxalic acids, since these acids were major sources of the corrosive environment in insulator service. Figure 2.41a shows the fracture surface morphology of a crack generated in the pH 3 nitric acid under the stress intensity of $4.3 \text{ MPa m}^{1/2}$. Evidently, the fractured fiber

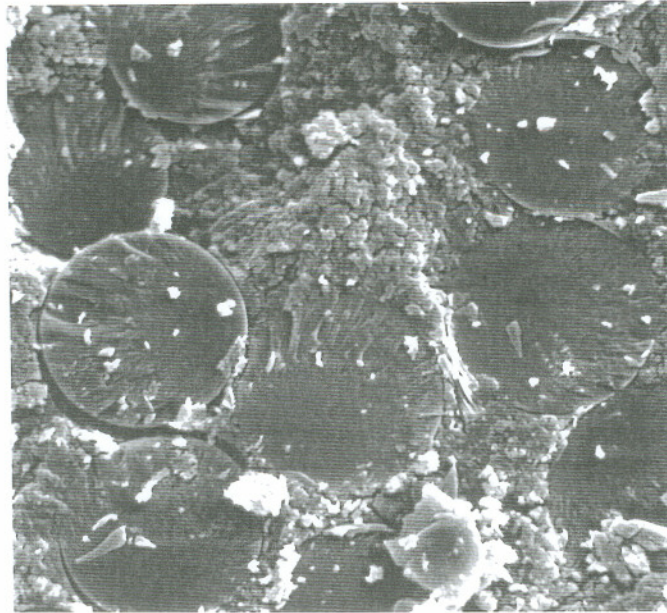


(a)

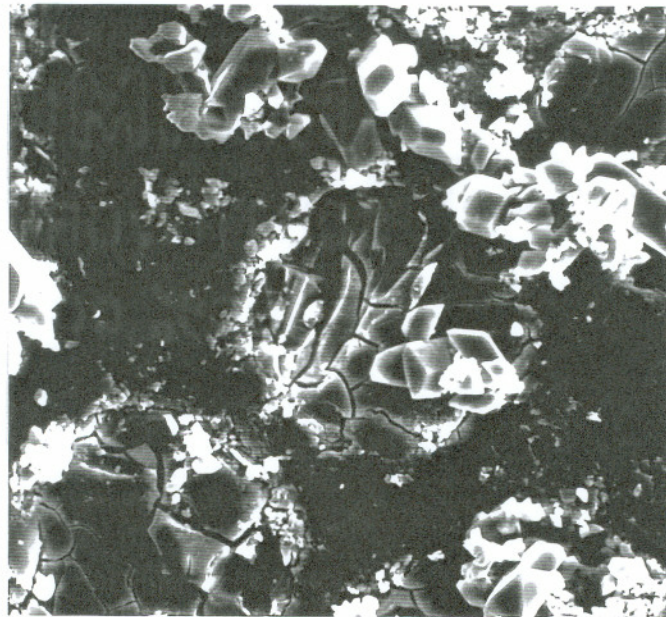


(b)

Figure 2.40 Transverse cracks developed in the stress corrosion experiments.



(a) In nitric acid



(b) In oxalic acid

Figure 2.41 Surface morphology of stress corrosion fracture.

surfaces exhibited large mirror sizes, and the entire fracture surface was free from any post-failure damage, which resembled two of the critical features identified on the fracture surface in field insulators. In contrast, the fracture surface produced by the pH 2 oxalic acid under the same stress intensity showed severe post-failure damage, which completely destroyed the initial markings on the fractured fiber surfaces (Figure 2.41b). As indicated earlier, the post-failure damage actually resulted from acid corrosion of glass fibers. Controlled by ion diffusion, post-failure damage is also expected to occur on the fracture surface generated in the less concentrated oxalic acid solutions, but over relatively longer time. The fracture morphology differences caused by nitric and oxalic acids were further verified by the acid corrosion study of E-glass fiber, which will be discussed in Section 2.4.

To further examine the possibility of generating post-failure damage in nitric acid, a specimen of the fracture surface, originally developed in the pH 3 nitric acid, was immersed in the same solution for one month. No visible surface damage was observed.

2.3 Electrical Discharge Experiments

The brittle fracture of GRP insulators is caused by a complex stress corrosion process, in which service electrical activities may play a crucial role. To understand the electrical effect on stress corrosion fracture of E-glass/polyester composite insulators investigated in this study, two issues were anticipated to be resolved by the electrical discharge experiments: the possibilities of both the formation of oxalic acid in polyester and the initiation of stress corrosion cracking in E-glass fiber/polyester composite under electrical discharge. These issues were studied in the electrical discharge test and the high-voltage fracture test, respectively.

2.3.1 Polymer Discharge Test

The formation mechanisms of organic acids, particularly oxalic acid, under the interaction between polymer and partial discharge is pertinent to the investigation of the brittle fracture of insulators. Previous studies have shown that oxalic acid can be produced from polyethylene and epoxy resins under the influence of electrical discharge.^{35,127} However, no direct evidence has ever been found of the oxalic acid formation in polyester resin subjected to electrical discharge. In this test, the surface discharge phenomenon on both polyester and E-glass fiber/polyester composite was investigated to explore the possibility of the oxalic acid formation in these materials.

The surface discharge test was conducted on 1-mm thick polyester and E-glass fiber/polyester composite disks in an AC electrical discharge cell (Figure 2.42). Placed on the bottom electrode in the cell, the disk specimen was separated from the top electrode at a distance of about 2 mm. During the test, the upper surface of the specimen was subjected to electrical discharge in air under the applied voltage of 6 kV at 60 Hz.

The electrical discharge byproducts, collected from the discharged area on the specimen surface, were subsequently analyzed by gas chromatography in a Finnigan 4021 gas chromatograph mass spectrometer data system.¹³⁸ Using a DB-5 methyl silicone column, the analysis was performed at the programmed rate of 20°C/min from 50 to 200°C after maintaining an initial temperature of 50°C for one minute. The solvent and the derivitizing agent used in this analysis were pyridine and bis(trimethylsilyl) trifluoroacetamide. The gas chromatographic results for the byproduct samples collected from discharged polyester and E-glass fiber/polyester composite are presented in Figures 2.43 and 2.44, respectively. Further identification of the major constituents in each reconstructed ion chromatogram is listed in Table 2.6 for polyester resin and Table 2.7

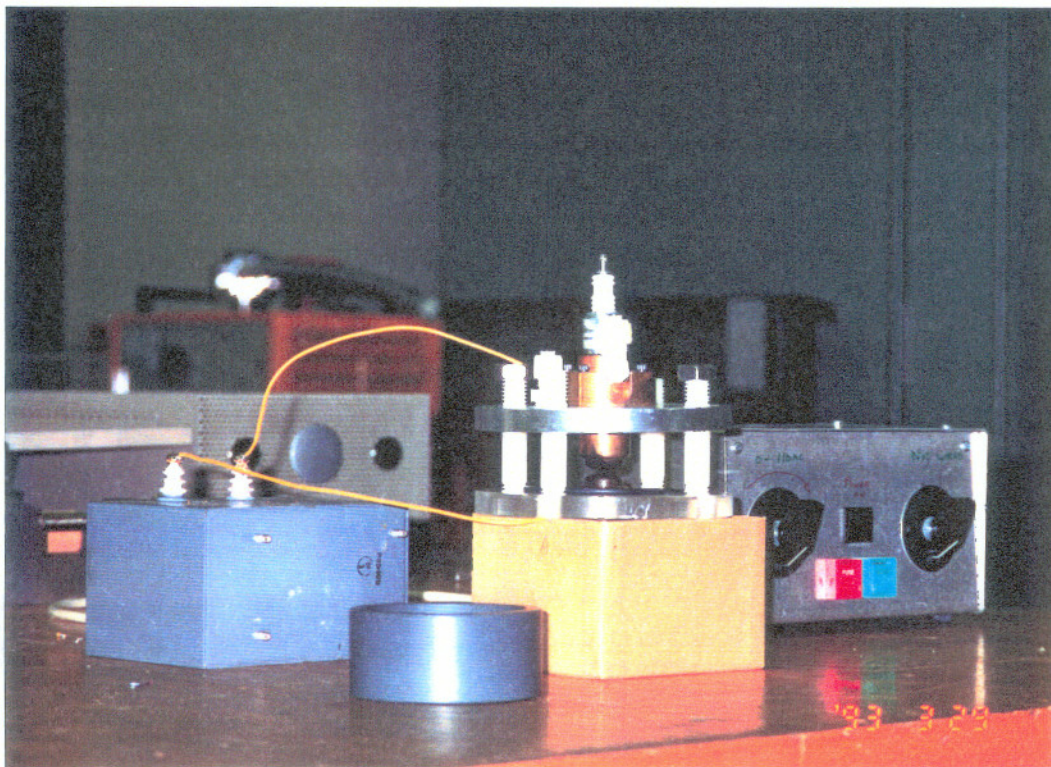


Figure 2.42 AC electrical discharge cell.

75776.

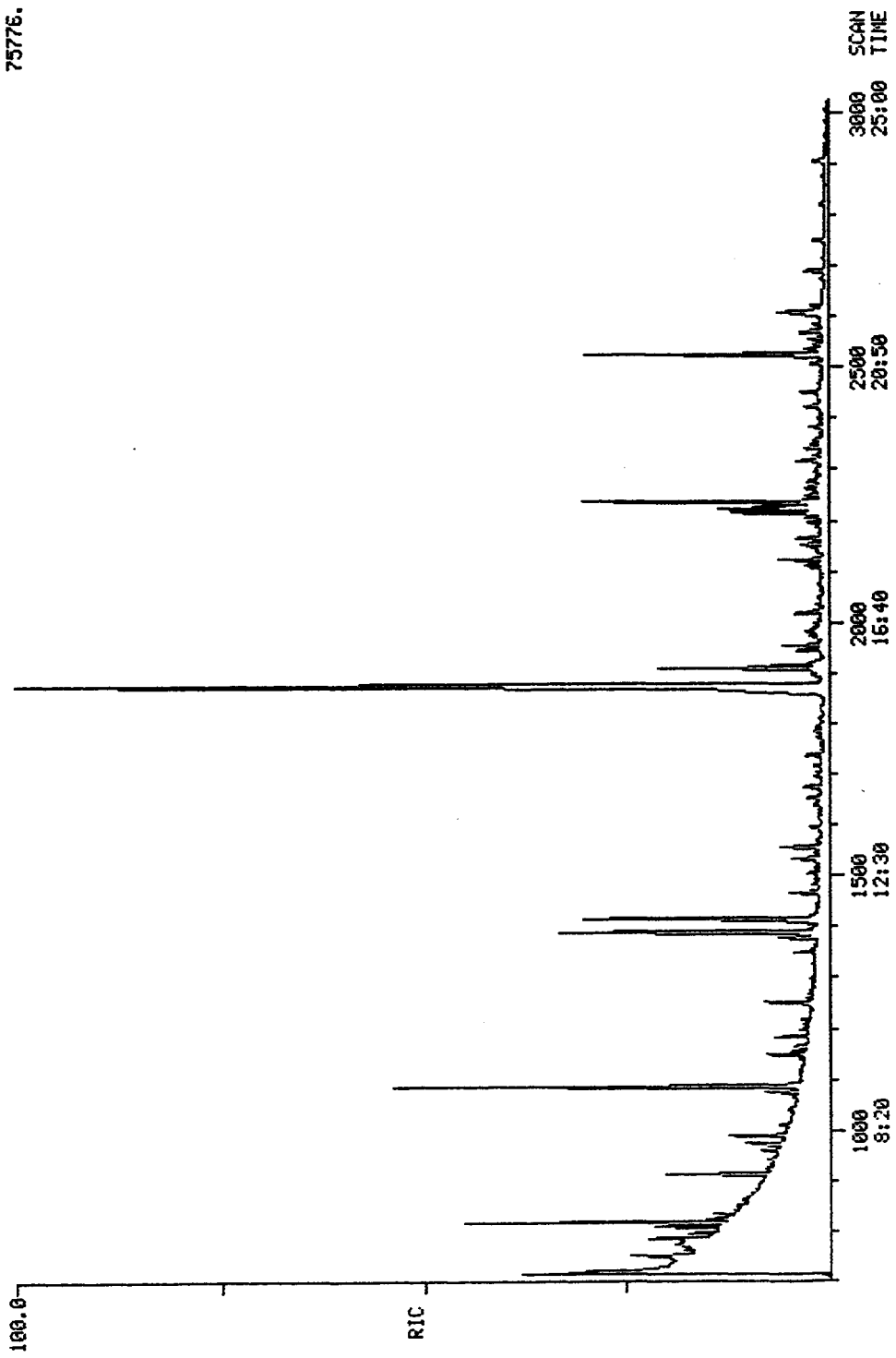


Figure 2.43 Reconstructed ion chromatogram for the byproducts of discharged polyester resin.

150784.

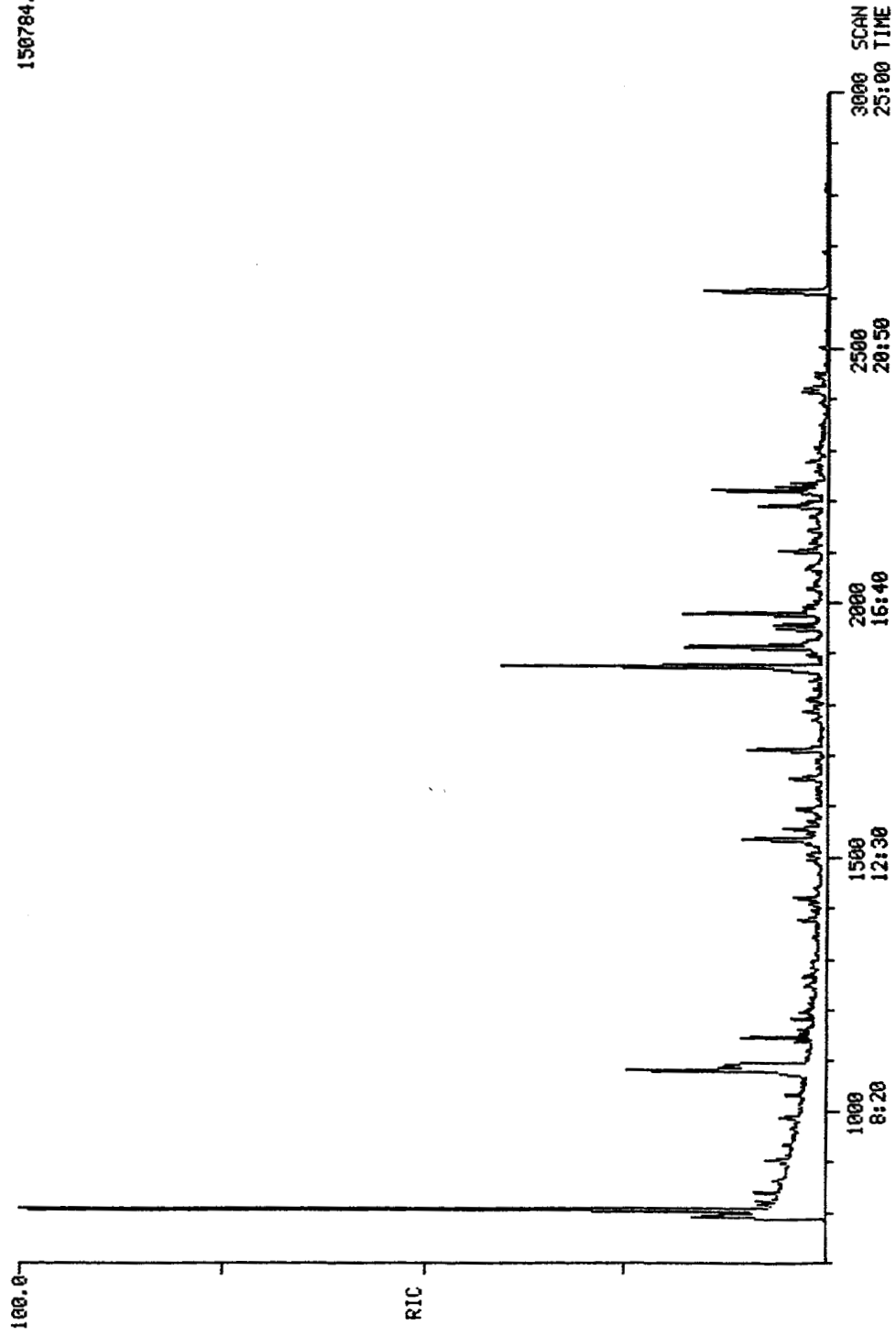


Figure 2.44 Reconstructed ion chromatogram for the byproducts of discharged E-glass fiber/polyester composite.

Table 2.6 Major constituents identified in the byproducts of discharged polyester resin

Peak number	Constituents
1089	silanol
1392	benzeneacetic acid
1417	dimethyl phthalate
1879	phthalic acid

Table 2.7 Major constituents identified in the ion chromatogram for discharged E-glass fiber/polyester composite

Peak number	Constituents
1085	silanol
1152	trimethylsilyl ether glycerol
1879	phthalic acid
1915	tri(trimethylsilyl) borate
1981	tetradecanoic acid

for E-glass fiber/polyester composite. Phthalic acid was identified in both polyester and E-glass fiber/polyester composite samples; however, oxalic acid was not detected. Phthalic acid is an organic acid used in manufacturing polyester resin. Because its dissociation constant, $10^{-3.51}$, is substantially lower than that of oxalic acid, $10^{-1.23}$, phthalic acid is expected to be much less corrosive than oxalic acid.

2.3.2 High-Voltage Fracture Test

To investigate the influence of electrical discharge on the stress corrosion fracture of composites, a high voltage system was constructed. Designed on the basis of the constant K_I specimen geometry, the system consisted of four basic parts: a loading unit, a syringe pump unit, an electrical control unit, and an AE unit (Figure 2.45). The specimen loading in this system was achieved by applying dead weight. To initiate electrical discharge at the notch root, a positively charged needle, controlled by a X-Y positioner, was placed at a close distance to the notch root, about 0.5 mm, and the opposite side of the specimen was electrically connected to the ground pole. The creepage distance, the distance between the needle tip to the ground, was adjusted by moving the clamp at the ground end along the grooves. Figure 2.46 shows the scheme of the electrical control unit. This electrical layout allowed the system to achieve the maximum voltage capacity of 14 kV. To modify the notch root environment externally, a syringe pump unit was installed, making it possible to transfer test solutions to the notch root at an adjustable rate. Similar to the stress corrosion system, the high voltage system was also equipped with an acoustic emission unit to monitor the fracture process. For insulating purposes, a wave-guide glass bar was employed to bridge the AE transducer to the specimen, eliminating possible electrical discharge on the transducer. More detailed information on the high voltage system can be found elsewhere.¹³⁸

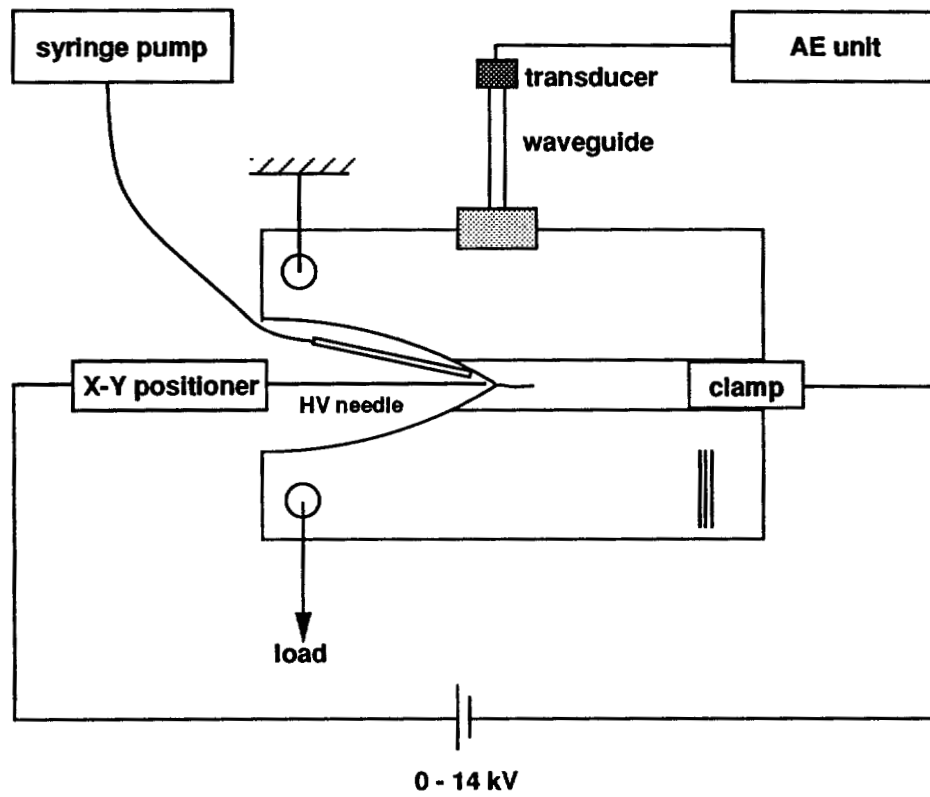


Figure 2.45 Configuration of the high voltage system.

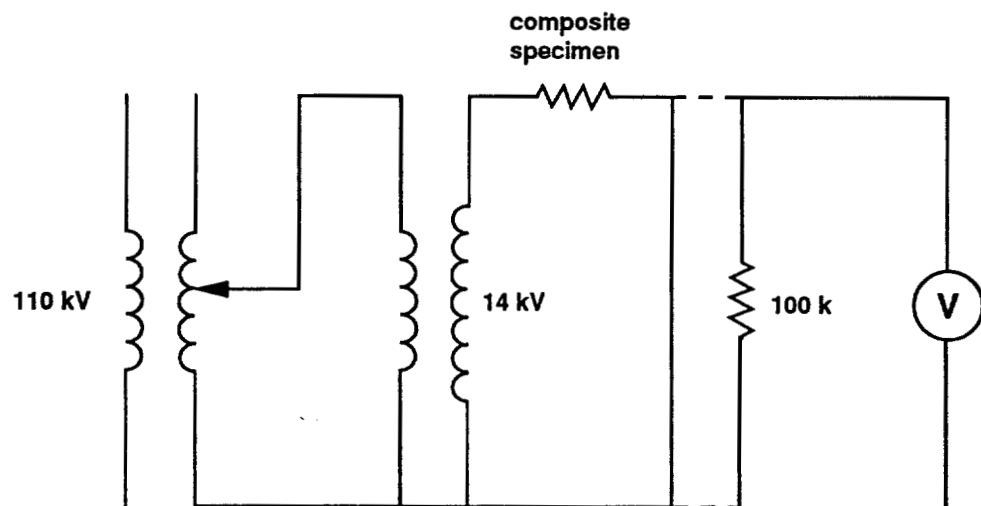


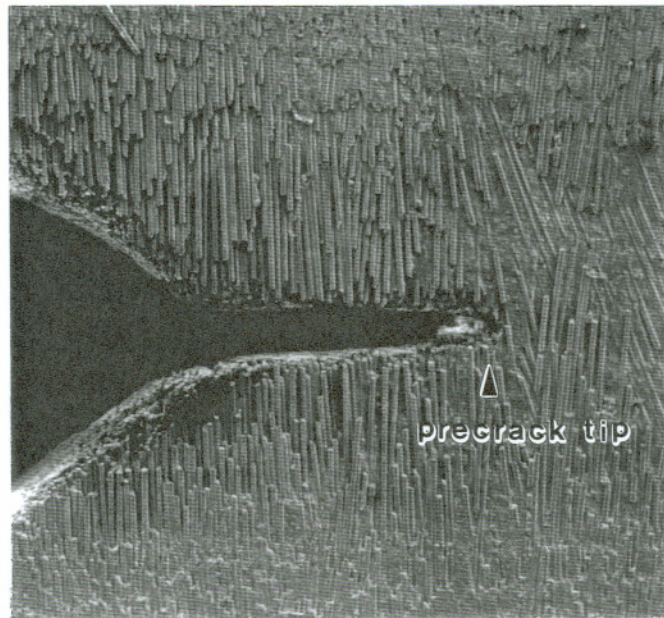
Figure 2.46 Scheme of the electrical control unit.

The high-voltage fracture test was conducted on the constant K_I specimen made of E-glass fiber/polyester composite. The specimen geometry was similar to that used in the stress corrosion experiment, previously defined in Section 2.2.2. Mechanically loaded under 9.08 kg (20 lbs), the specimen was subjected to electrical discharge at 12 kV, which corresponded to the creepage distance of approximately 15 mm. Two specimen conditions were considered: the dry condition in which the specimen was kept in the normal atmosphere, and the wet condition in which the specimen was immersed in tap water for one month prior to the test.

2.3.2.1 Moisture Effect

Under dry conditions, the notch root of the specimen was exposed to electrical discharge for one month. Figure 2.47 shows the side view of the notch root region. The notch root region was significantly affected by electrical discharge, exhibiting severe resin decomposition. No crack initiation, however, was observed at the pre-crack front.

In sharp contrast, the wet condition promoted cracking initiation from the pre-crack front only a few days after the test started, reaching approximately 2 mm in length within ten days (Figure 2.48). Comparable to the transverse crack developed in the stress corrosion experiment, the crack observed in this test also propagated perpendicular to the fiber direction. This evidence revealed that the transverse crack could be generated in E-glass fiber/polyester composite under the combined influence of mechanical and electrical stresses in the presence of moisture. Similar results were obtained from the test, in which tap water was periodically injected at the notch root of the specimen during electrical discharge.¹³⁸



200 μ m

Figure 2.47 Side view of the notch root region.

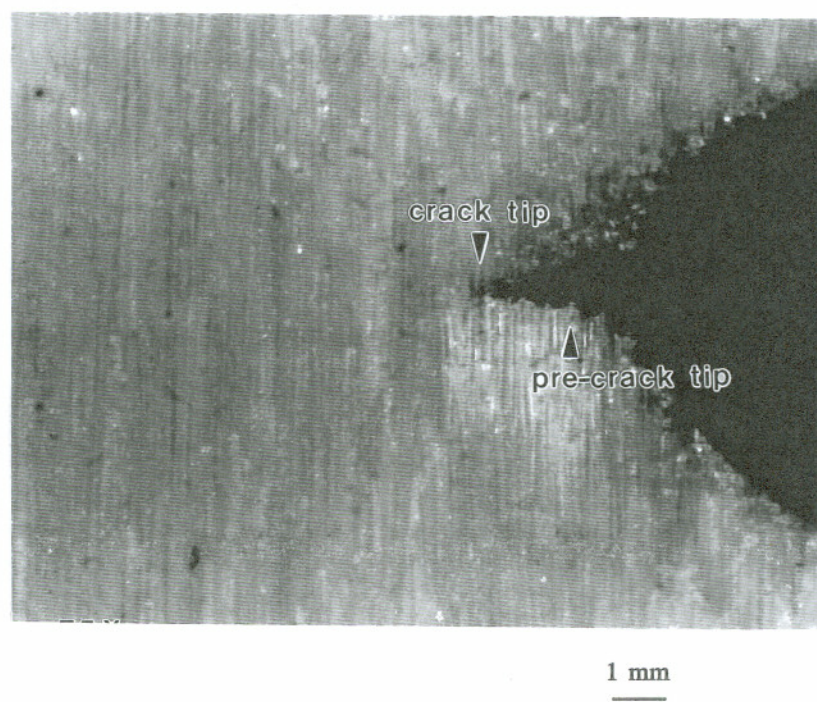


Figure 2.48 Transverse crack developed under wet conditions.

2.3.2.2 Fracture Morphology

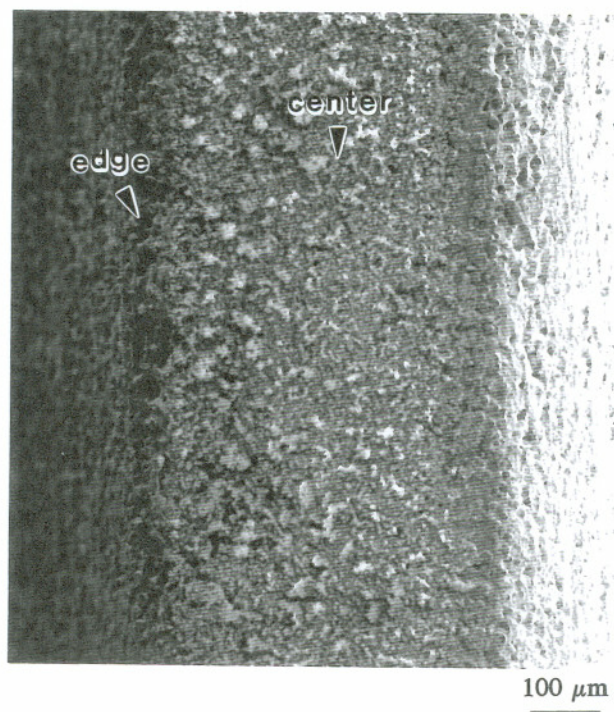
The fracture surface generated in the high-voltage fracture test was characterized using SEM. The same methodology described in Section 2.2.6 was employed for the sample preparation in this SEM examination.

The transverse crack generated under wet conditions exhibited planar fracture morphology, which was similar to that observed on the fracture surface of an acid-induced stress corrosion crack (Figure 2.48). Two well-defined regions were identified on the fracture surface: the center and the edge regions (Figures 2.49a). In the center region the fracture surface was covered by a dense deposit layer (Figure 2.49b); however, the surfaces in the two edge regions were free from deposit, the fractured fibers in these regions being clearly visible (Figure 2.49c). The formation of these two distinctive regions were likely associated with both the trajectory of the electric wind relative to the specimen and the availability of oxygen supply.

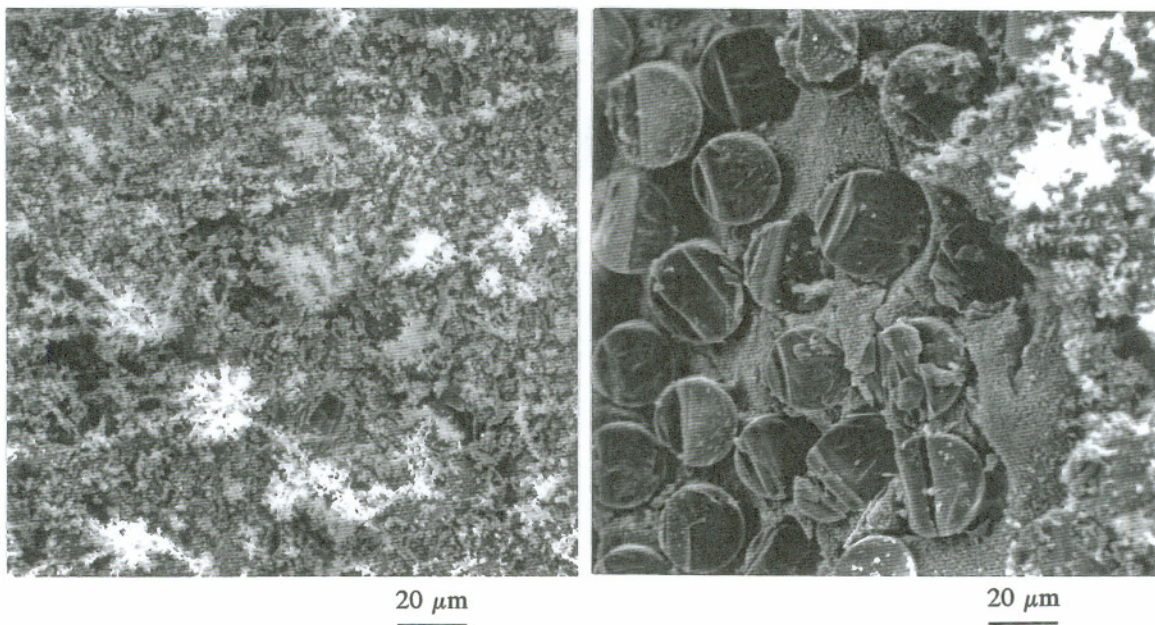
On a microscale, partially or completely melted fibers were observed on the fracture surface (Figure 2.50). Most of them were detected in the region close to the notch root. In fact, the partially melted fibers exhibited a surface morphology similar to that found on the fracture surface of field insulators (Figure 2.51). Furthermore, in both the center and edge regions the polyester resin was severely decomposed, especially in the edge regions near the notch root. (Figure 2.52). This feature was also identified on the fracture surface of field insulator (Figure 2.12).

2.4 Acid Corrosion Behavior of E-Glass Fiber

Stress corrosion fracture of GRP composites is primarily attributed to the chemical deterioration of glass fibers by ion-exchange reactions. Therefore, the fundamental investigation on acid corrosion behavior of glass fibers in aqueous acids, which is similar



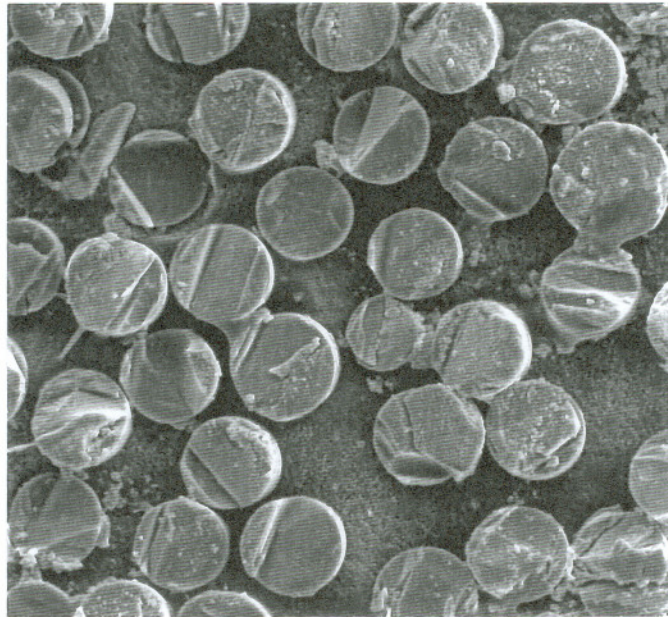
(a)



(b)

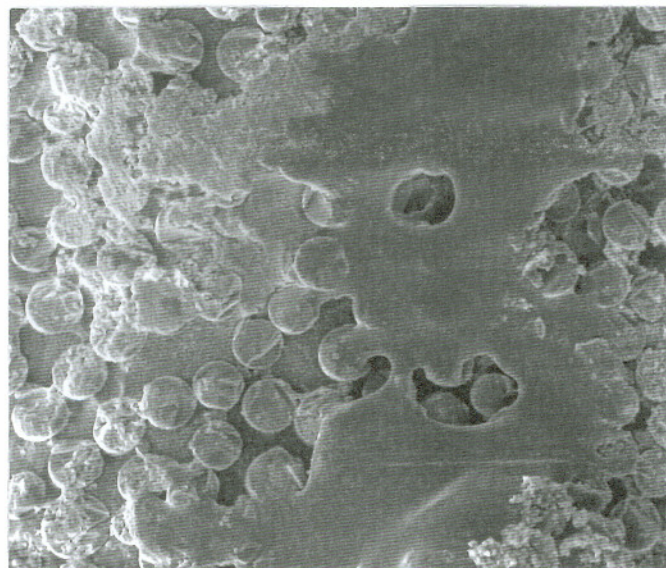
(c)

Figure 2.49 Fracture morphology generated under wet conditions.



10 μm

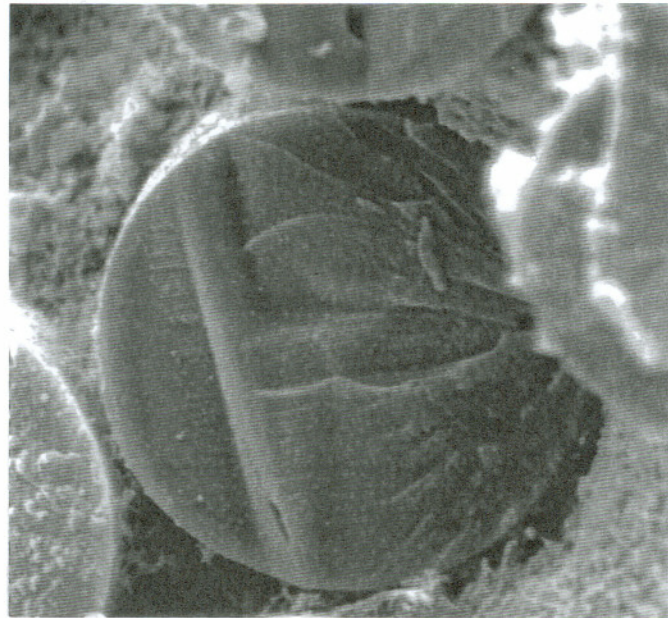
(a) Partially melted fibers



20 μm

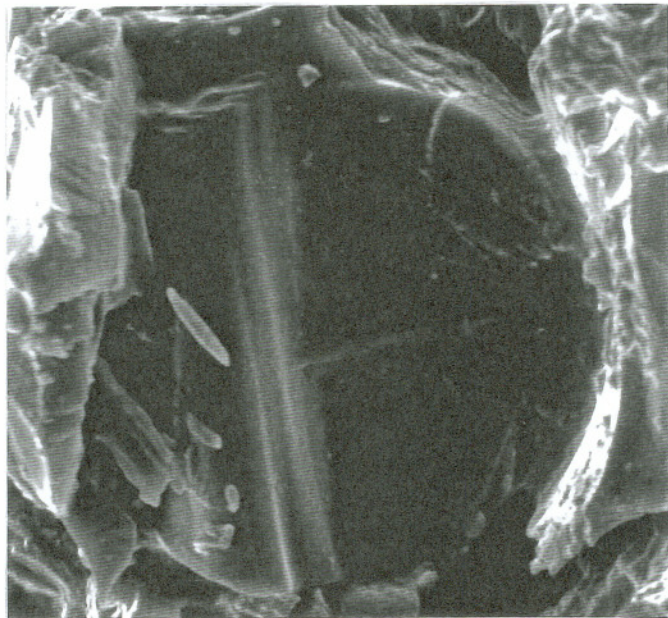
(b) Completely melted fibers

Figure 2.50 Melted fibers on the fracture surface.



2.5 μm

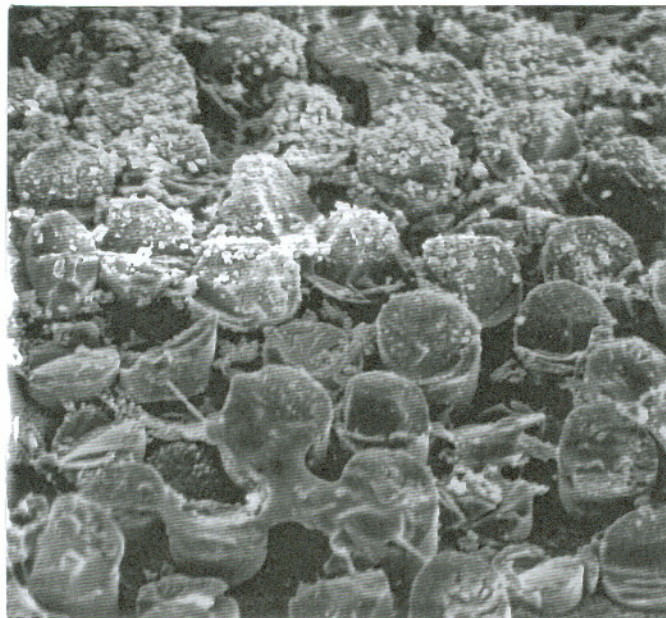
(a) Melted fiber generated by electrical discharge



2.5 μm

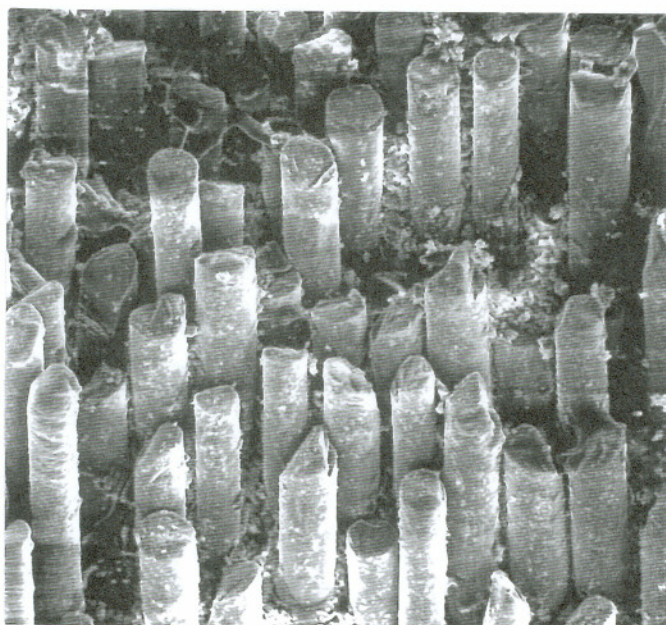
(b) Melted fiber on the insulator fracture surface

Figure 2.51 Surface morphology of the melted fibers.



10 μm

(a) In the center



20 μm

(b) Near the edge

Figure 2.52 Resin decomposition on the fracture surface.

in nature to service environments of insulators, becomes essential to understanding the stress corrosion mechanisms of GRP insulators. Arising from either acid rain or byproducts of partial discharge in polymers, the potential service environments would be nitric acid, oxalic acid, sulfuric acid, hydrochloric acid, or the combination of these. In this study, the influences of the above acids on the acid corrosion behavior of E-glass fiber, particularly on the fiber surface deterioration and the non-siliceous ion depletion, were investigated.

Another motivation for this study was to evaluate the tendency to form post-failure damage in composites exposed to the above four acids, and thereby to determine which of these acids is likely dominant in service environments. From the insulator failure analysis, it was evident that all of the fracture surfaces were free from post-failure damage, which is a common phenomenon in stress corrosion fracture of composites. Post-failure damage is caused by non-siliceous ion leaching from fractured fiber ends during a prolonged exposure of existing fracture surfaces to relatively concentrated acids.⁷⁹ Therefore, it is rational to assume that the tendency to form post-failure damage can be evaluated by the susceptibility of glass fiber to acid-induced surface cracking, which is controlled by exactly the same mechanism as that in the process of post-failure damage.

2.4.1 Fiber Specimen

The glass fiber used in this study, supplied by GlasForms Inc., was the E type with the chemical composition shown in Table 2.8. The average fiber diameter was approximately 12 μm . To maintain compatibility with various resin systems, the glass fiber was sized with silane agent. Cut from a fiber strand, each fiber specimen was about 10 cm in length and contained about 2,500 fibers. The weight of fiber specimens ranged from 70.2 mg to 83.5 mg.

Table 2.8 Chemical composition of the E-glass fiber, wt%

SiO ₂	CaO	Al ₂ O ₃	B ₂ O ₃	MgO	Na ₂ O & K ₂ O	TiO ₂	Fe ₂ O ₃	CaF ₂
52.58	16.25	12.16	5.10	0.50	0.20	0.00 to 0.08	0.05 to 0.40	0.00 to 0.01

2.4.2 Acid Immersion Experiments

The acid immersion experiments were performed in nitric, oxalic, sulfuric, and hydrochloric acids. For each acid, four solutions were prepared using deionized water with concentrations changing from pH 1 to pH 4 in increments of one pH value. In the experiments, a fiber specimen was completely immersed for two weeks in each of the sixteen acid solutions, which were stored in Teflon bottles to avoid any possible chemical reactions between the acid solution and the container material. After the experiments, the fiber specimen was removed from the solutions, rinsed immediately in deionized water, and dried in air.

2.4.3 Fiber Weight Loss

The weight loss estimation was conducted on each fiber specimen by comparing its weight before and after the acid immersion test. The sensitivity of the balance used for the weight measurement was on the order of 1/10,000 of gram.

The fiber weight loss results obtained from the acid immersion experiments are illustrated in Figure 2.53. Notably, the fiber weight loss was significantly affected by both the acid type and the acid concentration; however, the acid type influence seemed more pronounced. Of the four acids, oxalic acid led to the highest weight loss in all tested acid concentrations. The fiber weight losses in nitric and hydrochloric acids were similar to one another but insignificant compared to the value in either oxalic or sulfuric acid of the same concentration. It was also evident that for all the acids tested, the relationship between fiber weight loss and the acid concentration followed a general rule: the fiber weight loss became intensified with increasing acid concentration, i.e., reducing the pH value.

2.4.4 Ion Depletion Behavior

Acid corrosion of E-glass fibers mainly results from calcium and aluminum ion depletion.^{52,118-120} To evaluate the leachability of these ions in the selected acids, atomic absorption and colorimetric spectrophotometry were utilized. Both calcium and aluminum contents in the resultant solutions from the acid immersion experiments were determined using either a Perkin-Elmer 603 atomic absorption spectrophotometer or a Perkin-Elmer Lambda 6 UV/VIS colorimetric spectrophotometer. For the solution containing precipitates, a 0.1 μm polycarbonate membrane filter was employed to separate the precipitates from the solution. The precipitates were then dissolved in a 0.1N hydrochloric acid solution. The calcium and aluminum measurements were carried out in the filtrate and the acidified precipitate solution independently.

As expected, both calcium and aluminum depletion from E-glass fiber were found in the acid immersion experiments (Figures 2.54 and 2.55). The results further revealed that the leachability of calcium or aluminum ions was highly dependent on both acid type and acid concentration, exhibiting a similar trend to the fiber weight loss (Figure 2.53). For all of the acid concentrations, both calcium and aluminum ion depletion in oxalic and

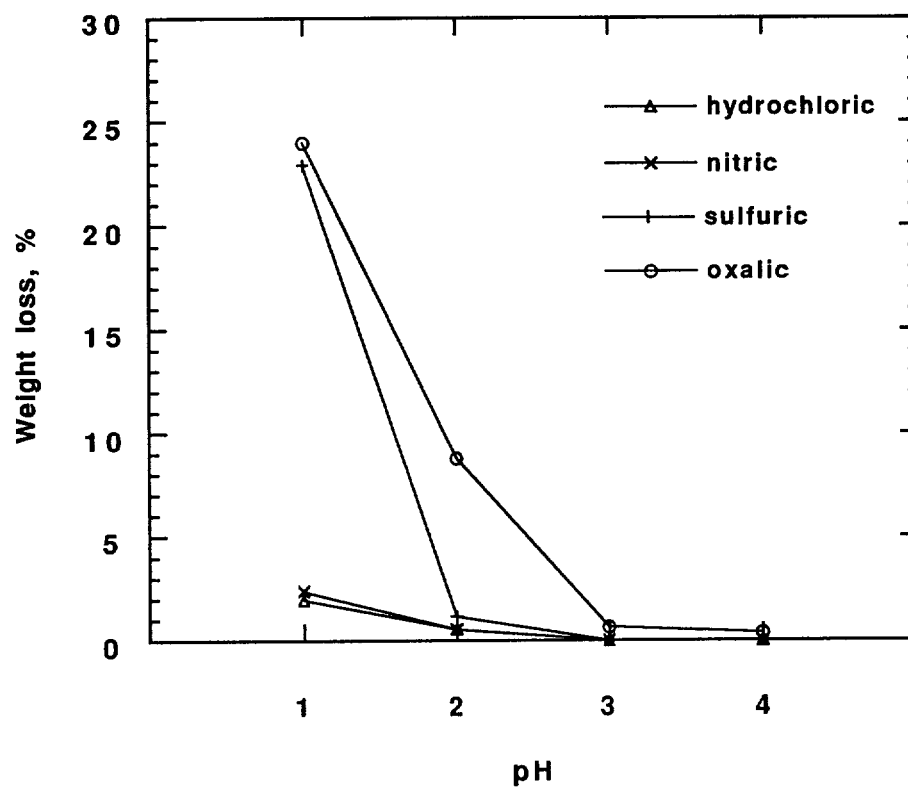


Figure 2.53 Fiber weight loss as functions of acid type and acid solution pH.

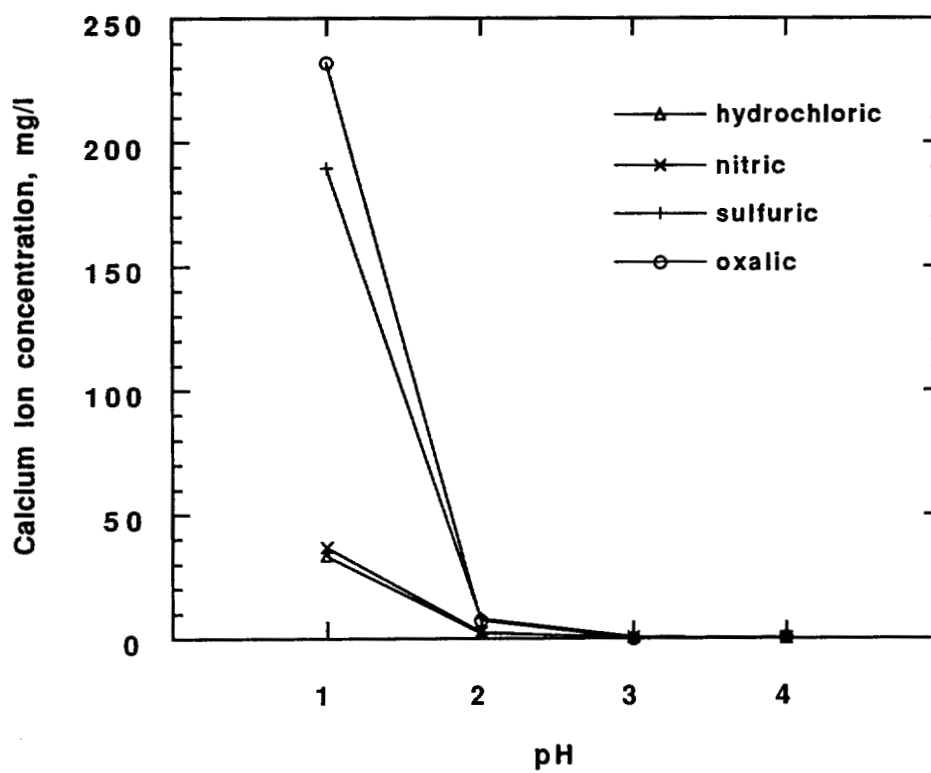


Figure 2.54 Calcium ion concentrations in resultant acid solutions.

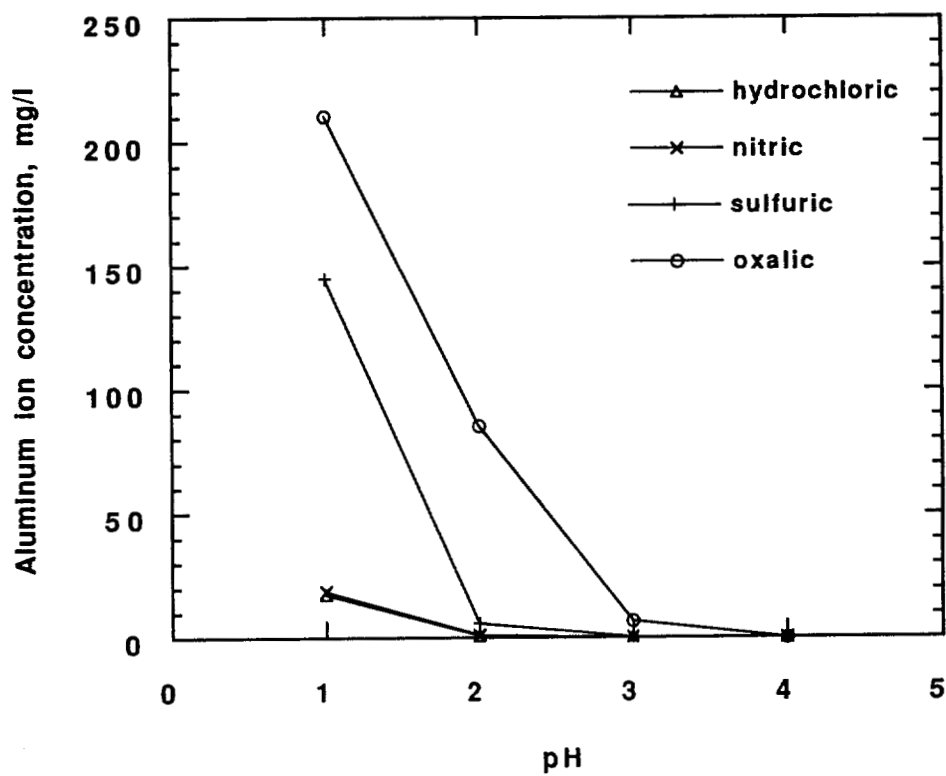


Figure 2.55 Aluminum ion concentrations in resultant acid solutions.

sulfuric acids were more severe than in nitric and hydrochloric acids and in each acid, a higher acid concentration resulted in greater ion depletion. Moreover, calcium ions depleted from the fibers appeared higher in quantity than aluminum ions in all the acid solutions, excluding the pH 2 oxalic acid solution in which the opposite result was observed.

Furthermore, an attempt was made to calculate the fiber weight loss caused by the removal of calcium and aluminum oxides. The calculation was performed based on both calcium and aluminum depletion results and relative contents of calcium and aluminum oxides in the glass fiber (Table 2.8). Table 2.9 shows the comparison of the measured fiber weight losses, $wt_m\%$, with the calculated fiber weight losses, $wt_c\%$, in each of the four pH 1 acid solutions tested. Clearly, a good agreement was reached between the measured and calculated weight losses in both nitric and hydrochloric acids. A lower calculated weight loss relative to the measured value, however, was found in both oxalic and sulfuric acids. The discrepancy is likely caused by discounting the depletion of other non-siliceous ions, particularly boron ions. E glass contains 5.10% of boron oxide by weight. Because boron ions reside in the silica network, their depletion may disturb the glass structure and thus make it unstable, facilitating the depletion of other non-siliceous ions.

Table 2.9 Comparison of fiber weight losses

Acid, pH 1	Hydrochloric	Nitric	Sulfuric	Oxalic
$wt_m\%$	1.98	2.40	22.93	24.98
$wt_c\%$	1.98	2.46	14.88	19.95

2.4.5 Fracture Morphology

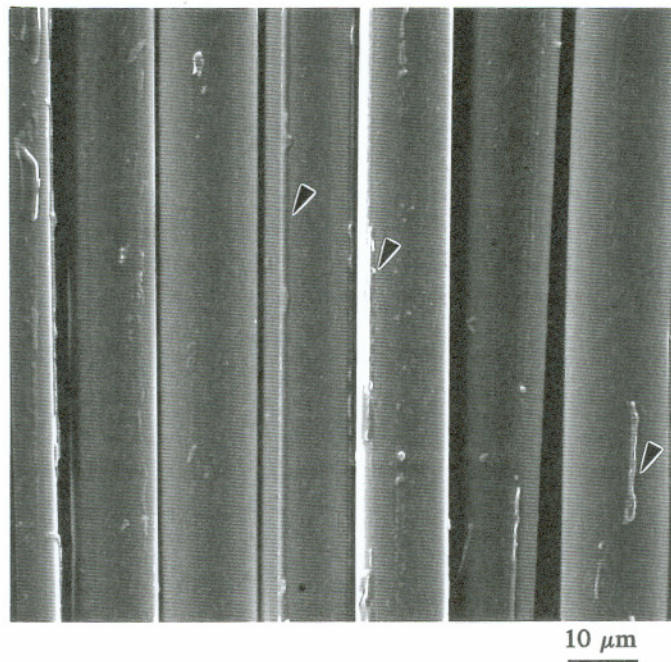
After the acid immersion experiments, the surface and cross-section morphology of the fibers was examined in a Zeiss DSM-960 SEM at an accelerating voltage of 10 kV. Samples for the surface morphology examination were prepared by laying single fiber layer on the surface of pre-taped sample stubs. For the cross-section morphology examination, the fibers, supported by a coil clip, were mounted in epoxy. Mounted samples were then ground with 240, 320, 400, 600, 800, and 1200 grit silicon carbide papers successively. Final polishing was carried out on the lapping films from size 9 μm , 3 μm , to 1 μm . To avoid electrical discharge, carbon was sputtered on each sample before SEM examination.

2.4.5.1 Surface Morphology

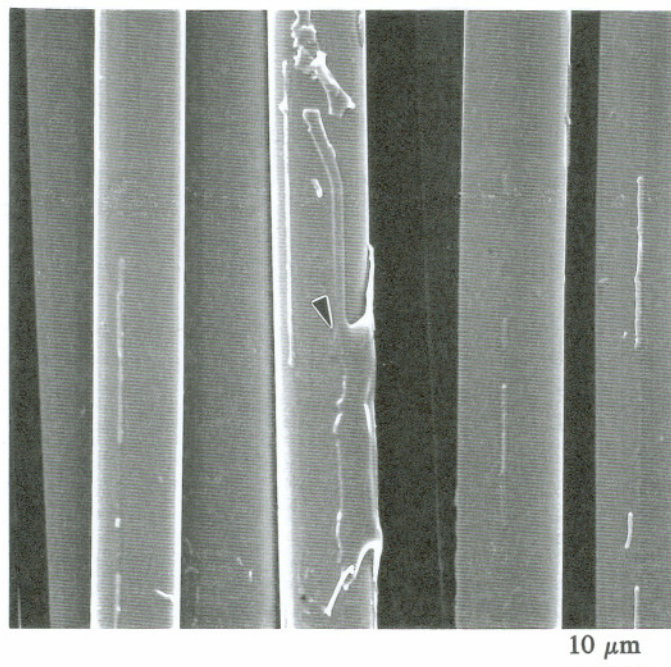
In the as-received condition the fiber surface appeared intact, with the exception of some superficial irregularities, such as axial lines or extrusion patches (Figure 2.56). These defects were likely introduced to the fiber surface during fiber fabrication. After the acid immersion experiments, the fiber surface deterioration was observed to various degrees, depending on the acid type and concentration. The characterization of the fiber surface morphology is summarized below based on the acid type.

Fibers immersed in oxalic acid solutions

The surface morphology of the fibers immersed in the pH 1 solution was characterized by axial cracks, which ran through the entire fiber length (Figure 2.57). This crack morphology implied that the principal surface stress was axial in nature. Further observation revealed that each axial crack was usually accompanied by an circumferential crack underneath (Figure 2.58). It is likely that during acid immersion the axial crack was initiated on the fiber surface and propagated towards the fiber center. Once the

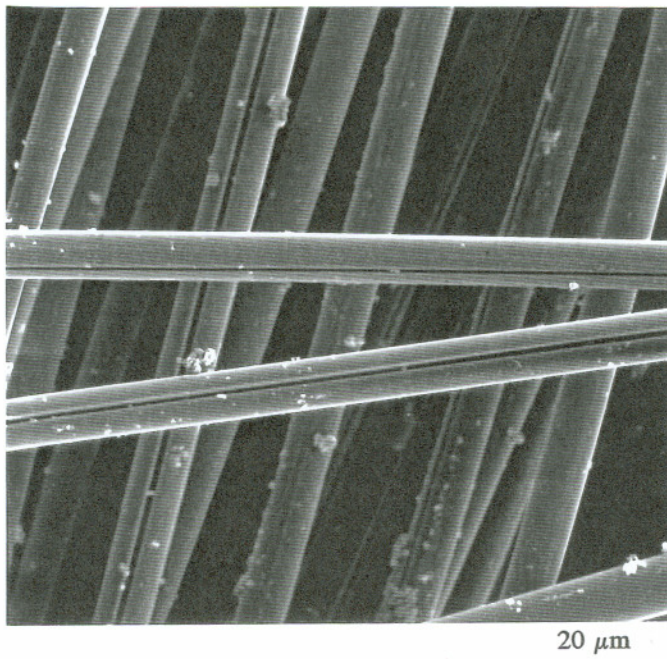


(a) Axial lines

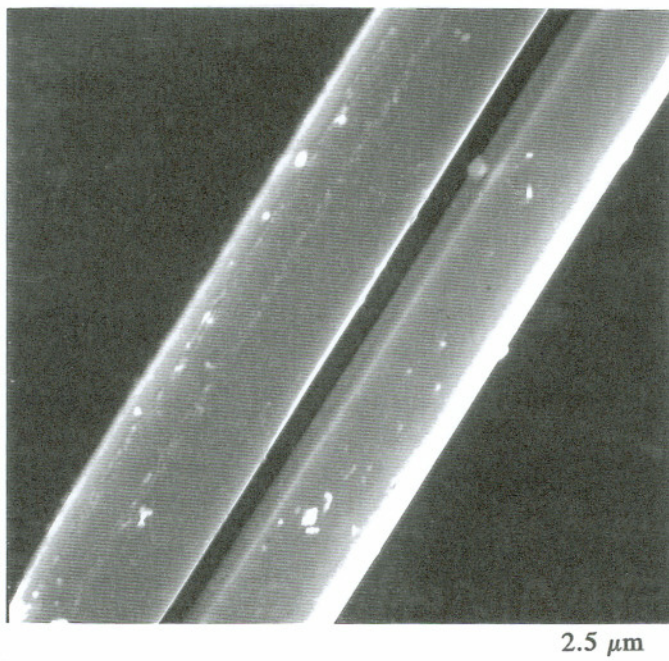


(b) Extrusion patches

Figure 2.56 Surface morphology of as-received E-glass fibers.

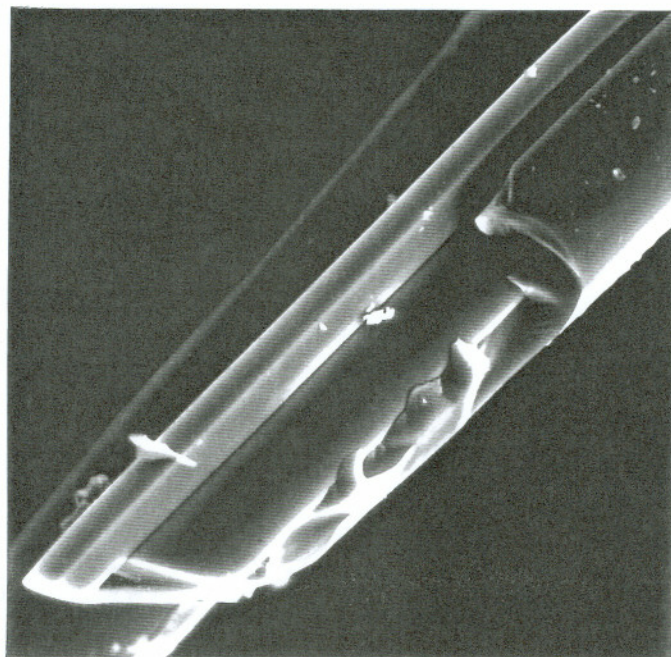


(a)



(b)

Figure 2.57 Axial cracks generated in the pH 1 oxalic acid solution.



5 μm

Figure 2.58 Internal circumferential crack developed with axial cracks in the pH 1 oxalic acid solution.

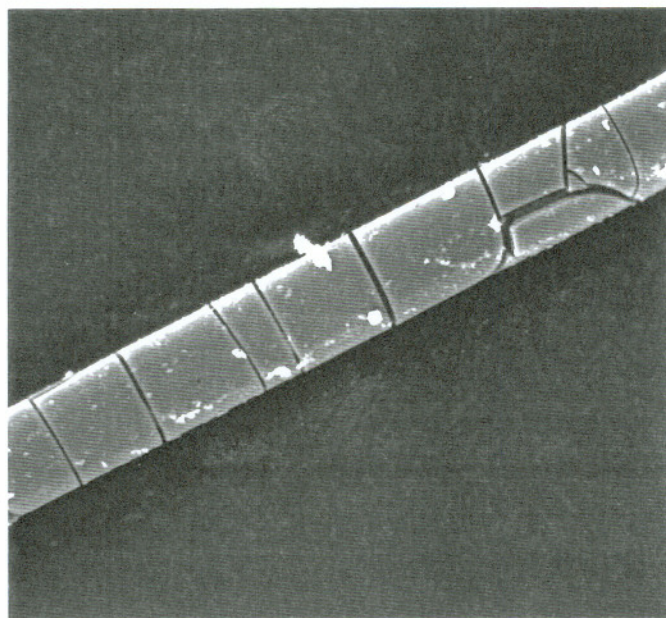
axial crack advanced to a certain depth, its further growth was prohibited in the radial direction and thereby turned to the tangential direction, forming an internal circumferential crack. Unlike the surface morphology induced by the pH 1 solution, ring or spiral surface cracks were formed on the fibers exposed to the pH 2 solution (Figure 2.59). The spiral spacing appeared non-uniform, and some small cracks were also found in various locations between spiral steps. The pitch angle of spiral cracks was found to be highly irregular. On most occasions, spiral crack propagation was terminated someplace along the fiber, where the crack propagation changed to the direction perpendicular to the fiber axis, i.e., the pitch angle became approaching to zero.

For the fibers immersed in the pH 3 and pH 4 solutions, however, no cracking was detected on the fiber surface, although a few fibers tested in the pH 3 exhibited spiral-like surface damage (Figure 2.60). This damage could be the initial indication of the spiral crack formation.

Fibers immersed in sulfuric acid solutions

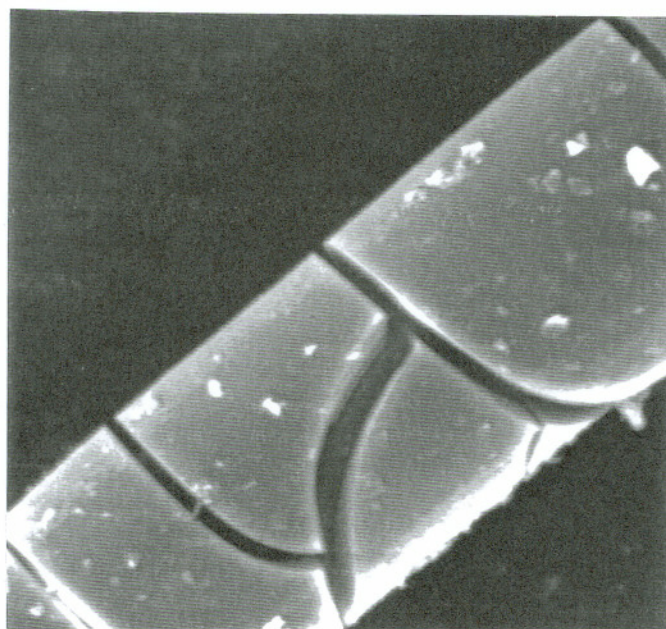
Similar to the fiber surface morphology formed in the pH 2 oxalic acid solution, spiral cracking was also found on the fiber surface exposed to the pH 1 sulfuric acid solution (Figure 2.61a). In this case, however, the spiral cracks were uniformly spaced, and their pitch angles appeared similar to one another. Some cracks ran through the entire fiber length, while others were discontinuous in the form of small segments. On several occasions, multiple short cracks were formed between two adjacent steps of a spiral crack and perpendicular to the spiral crack (Figure 2.61b).

Although no surface cracking was generated on the fibers in the pH 2 solution, particulate deposition was found on the surface of several fibers (Figure 2.62). For less concentrated pH 3 and pH 4 solutions, no visible surface damage could be identified on the fibers under SEM observation.



10 μm

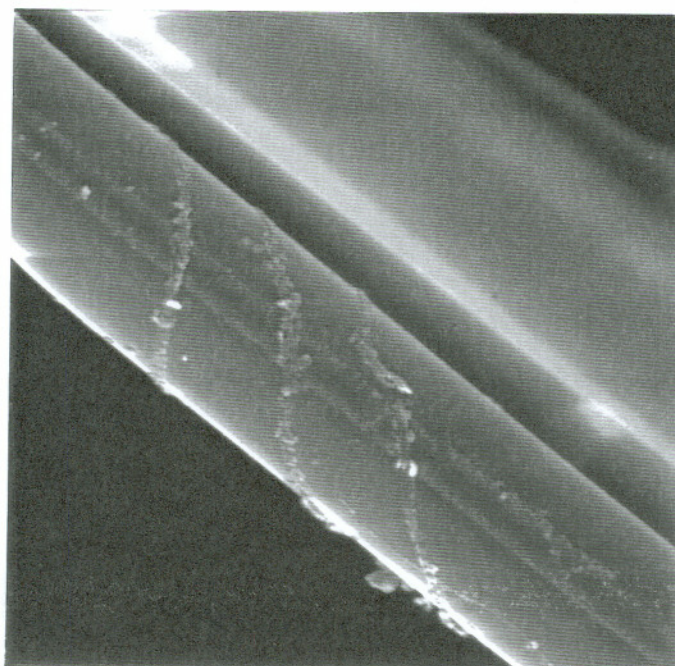
(a)



2.5 μm

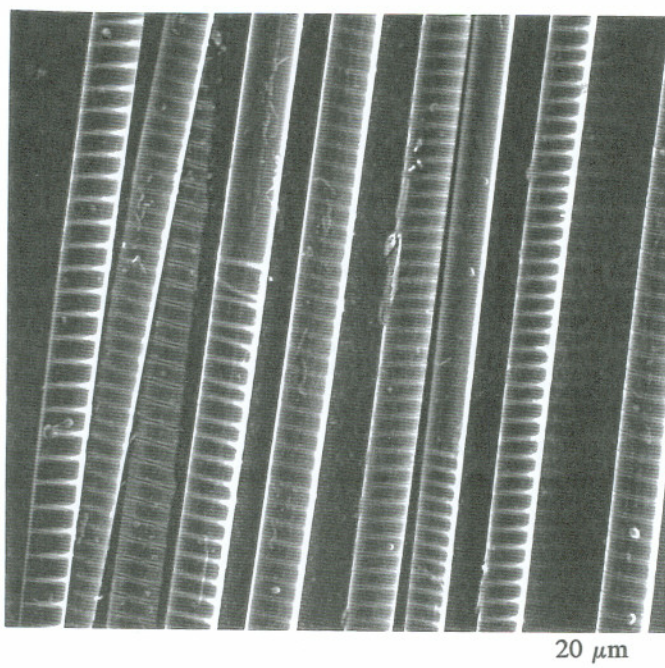
(b)

Figure 2.59 Spiral cracks generated in the pH 2 oxalic acid solution.

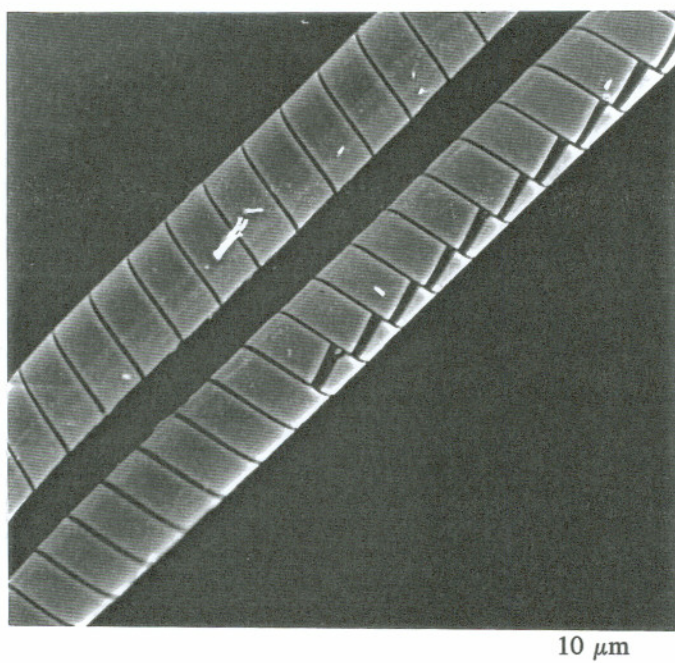


5 μm

Figure 2.60 Surface damage generated in the pH 3 oxalic acid solution.



(a) Spiral crack



(b) Multiple short cracks

Figure 2.61 Fiber surface morphology generated in the pH 1 sulfuric acid solution.

Fibers immersed in hydrochloric acid solutions

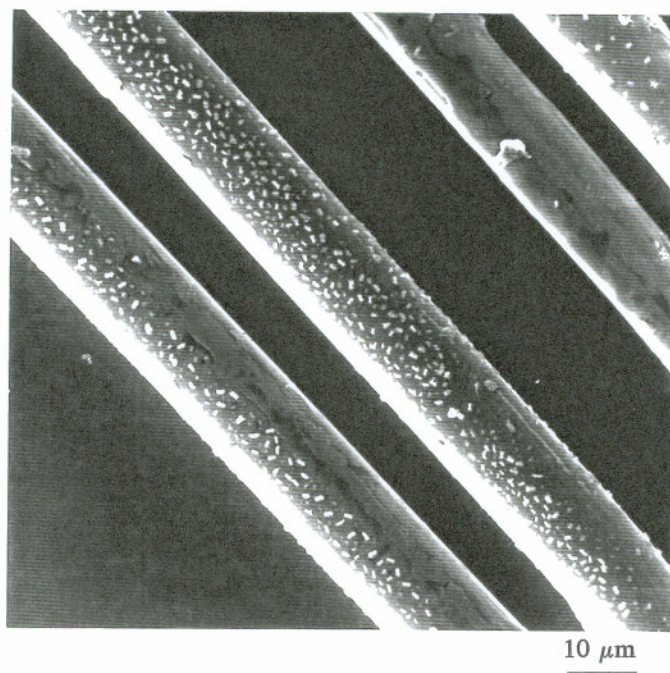
Compared to oxalic and sulfuric acids, hydrochloric acid appeared to be less corrosive to E-glass fiber. Surprisingly, no surface crack or damage developed on the fibers exposed to every hydrochloric acid solution for two weeks, even in the pH 1 and pH 2 solutions (Figure 2.63). This observation contradicted the results obtained from earlier studies,⁵⁰ which indicated that hydrochloric acid at pH 1 or lower could generate spiral cracks on E-glass fiber within 24 hours. In general, the acid corrosion resistance of glass fibers should rely primarily on their chemical composition. In practice, however, the composition of E-glass fiber varies from one manufacturer to another. The high corrosion resistance of the fibers to hydrochloric acid observed in this study may be attributed to the specific fiber composition and/or the sizing agent applied.

Fibers immersed in nitric acid solutions

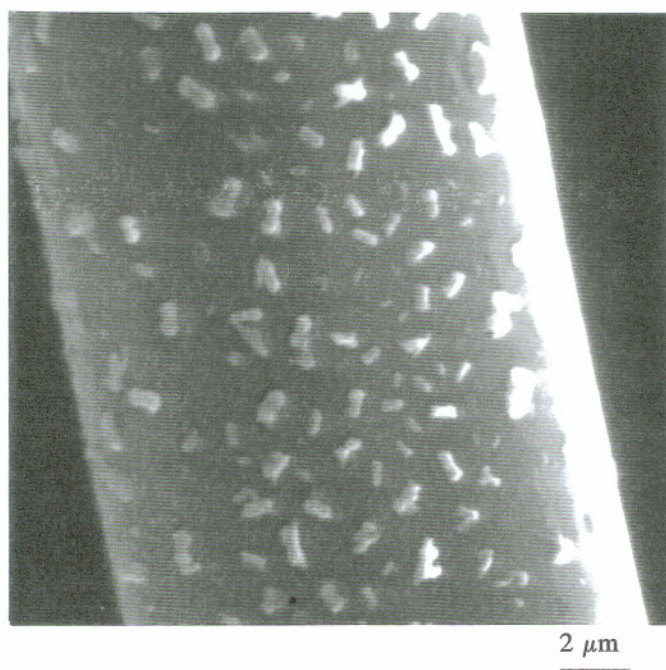
Similar to the results obtained from the hydrochloric acid immersion tests, no surface damage was observed on the fibers tested in every concentration of nitric acid solutions for two weeks (Figure 2.64).

2.4.5.2 Cross-Section Morphology

To further identify crack penetration depth, cross-sections of the fibers with axial and spiral surface cracks, which were generated in the pH 1 oxalic acid and the pH 1 sulfuric acid respectively, were examined. Figure 2.65a illustrates the cross-section image of an axial crack in the fiber exposed to the pH 1 oxalic acid. The average penetration depth of axial cracks was estimated to be 3 μm . In all cases, the axial crack was arrested by an internal circumferential crack. This finding was consistent with the observation shown in Figure 2.58. Furthermore, the circumferential crack appeared symmetric in relation to the axial crack, and its angular length ranged from 150 to 180

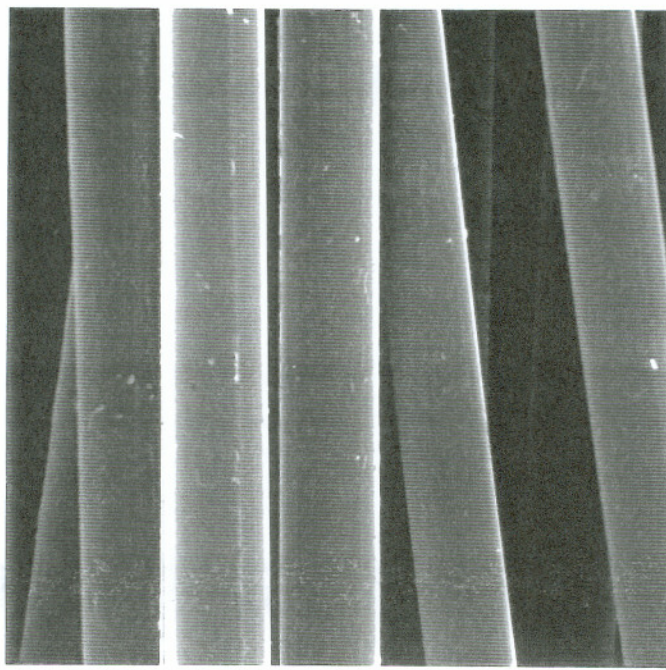


(a)



(b)

Figure 2.62 Surface particulate deposition induced in the pH 2 sulfuric acid solution.



10 μm

Figure 2.63 Surface morphology of glass fiber exposed to the pH 1 hydrochloric acid solution.

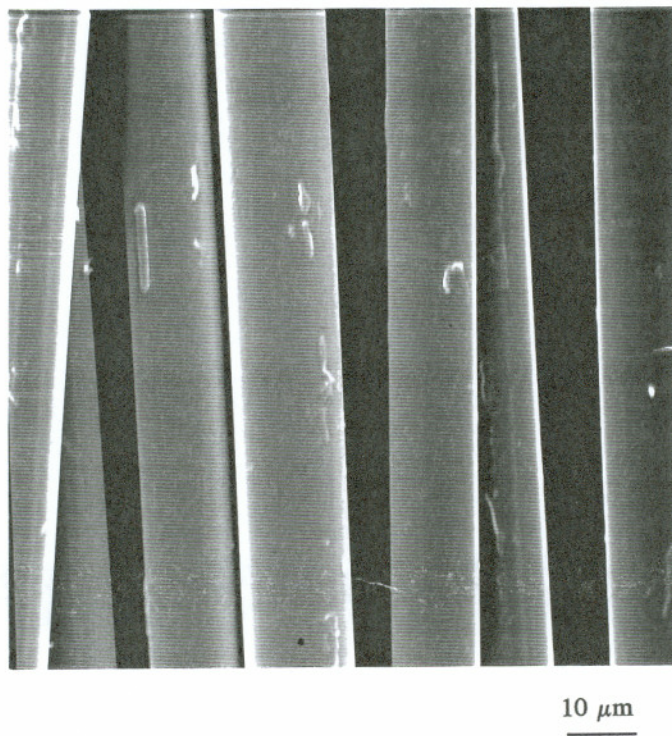
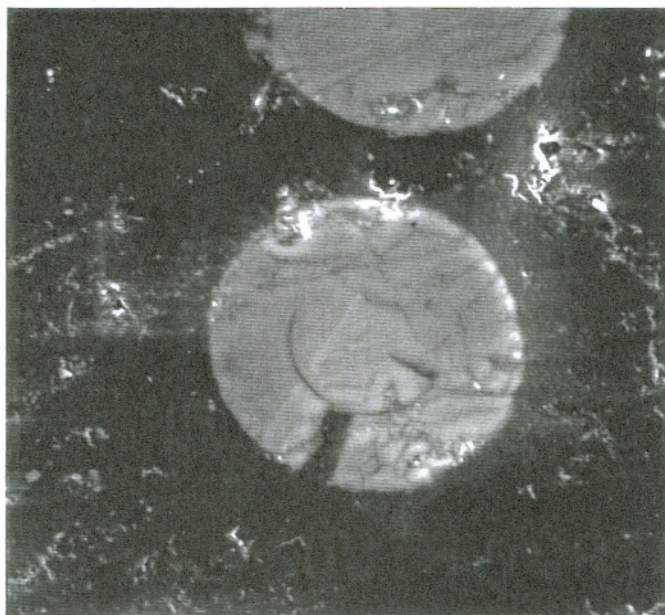
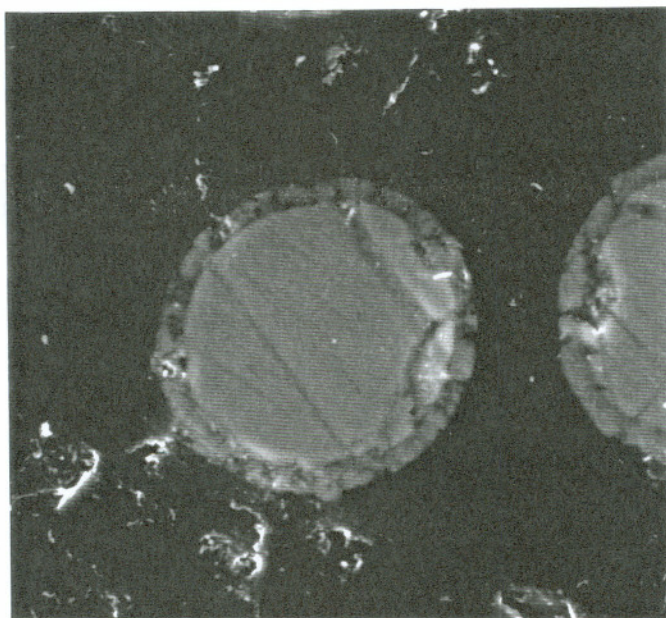


Figure 2.64 Surface morphology of glass fibers exposed to the pH 1 nitric acid solution.



(a) Fiber with an axial crack



(b) Fiber with a spiral crack

Figure 2.65 Cross-section images of the fractured fibers.

in radian. For the fiber tested in the pH 1 sulfuric acid, a ring structure was observed (Figure 2.65b), which reflected the image of a spiral crack on the fiber cross-section. The average penetration depth of spiral cracks approximated $1\ \mu\text{m}$, which was two times smaller than that of axial cracks.

In addition, based on the literature, a core-sheath structure can develop on the cross-section of glass fibers undergoing long-term acid corrosion.^{92,117} The fiber outer sheath, depleted of non-siliceous ions, may be identifiable both optically and in SEM because of the change of refractive index in the sheath with respect to the intact fiber core.^{117,142} However, this core-sheath structure was not detected on the cross-section of acid-corroded fibers in this study.

2.5 Crack Tip Chemistry

Stress corrosion cracking of composites, dominated by crack propagation, is virtually driven by the stress intensity and the corrosive environment at the crack tip. Because a stress corrosion process involves localized corrosion at the crack tip, the crack tip chemistry can be further modified by corrosion products and thereby may become significantly different from the global environment. To gain a better understanding of the propagation behavior of stress corrosion cracking in GRP composites, the influence of the chemical composition of composite materials on the crack tip chemistry was investigated in this part of the study.^{131,138}

The investigation was conducted in two phases: the water extraction test and the thermal stability test. The first phase aimed to explore the influence of water on the internal chemical environment in composites. Water, being inevitable in the service environment of insulators, can exist in gaseous, liquid and/or solid states. Due to its relatively small molecule size, water can easily penetrate into many resin matrices used in GRP insulators. The presence of water in composites may lead to the dissolution of water

soluble compounds, thereby changing the internal chemical environment. The second phase was devoted to the inspection of the thermal stability of composites. In insulator service environments, electrical activities may generate heat in the insulator system, which may in turn decompose the resin matrix in the composite rod and even promote chemical reactions.

Furthermore, the extraction of water soluble compounds from the composite turnings may lead to the pH change in the extract. To examine the influence of the extract, particularly the alkaline extract, on glass fiber, an additional immersion test was designed.

2.5.1 Samples and Materials

Test samples were obtained by chipping composite rods into small turnings. Two composite systems were employed for the crack tip chemistry investigation. Made of E-glass fibers and polyester resin, these composites only differed in the filler material used in the resin: one containing alumina trihydrate, and the other calcium carbonate. The chemical composition of E-glass fiber was the same as given in Table 2.8. However, the chemical formulation of the polyester resin was not available.

2.5.2 Extraction Tests

The extraction tests were conducted in a Soxhlet apparatus, following the standard procedure. In the test, deionized water with a pH value ranging from 5.6 to 5.8 was used as the initial solvent. To ensure test consistency, the sample weight and the water volume used in each test were fixed at 17 g and 170 ml, respectively. During the test, a small amount of the solution was periodically removed from the apparatus for the pH measurement, which was performed at room temperature. The extraction test was finally stopped when the solution reached a constant pH value.

After the test, calcium and aluminum ion concentrations in the extracts were determined by atomic absorption and colorimetric spectrophotometry. Both atomic absorption and colorimetric spectrophotometers employed for the chemical analysis were the same as those described in Section 2.4.4. The analysis was performed respectively on a filtered precipitate and an unfiltered sample for each extract. The filtered precipitate sample was prepared by collecting the precipitates suspended in the extract through a 0.2 μm polycarbonate membrane filter and acidifying them in 0.1N hydrochloric acid, while the unfiltered sample was directly treated with 0.1N hydrochloric acid to dissolve the precipitates in the sample, thereby obtaining the total ion concentration in the extract.

For purposes of clarity, the results from the extraction tests are presented separately, based on the filler material used in the resins.

Composite with the alumina trihydrate filler

The change in the pH value relative to the extraction time for the extracts is shown in Figure 2.66, in which two independent test results are included. Within the first 10 hours, the pH value of the solution tended to increase over time, reaching the maximum value after approximately 10 hours. Further increasing the extraction time led to a rapid reduction of pH. Eventually, the pH value stabilized at approximately 5.0 when the extraction time exceeded 40 hours.

The chemical analysis of extracts indicated that not only aluminum but also calcium species were extracted from the composite with alumina trihydrate filler (Figure 2.67). It was also evident that the extracts contained much more calcium than aluminum species. The comparison between the filtered precipitate and the unfiltered samples further revealed that in the extracts most of aluminum species existed in the form of precipitates; in contrast, calcium species were essentially water soluble.

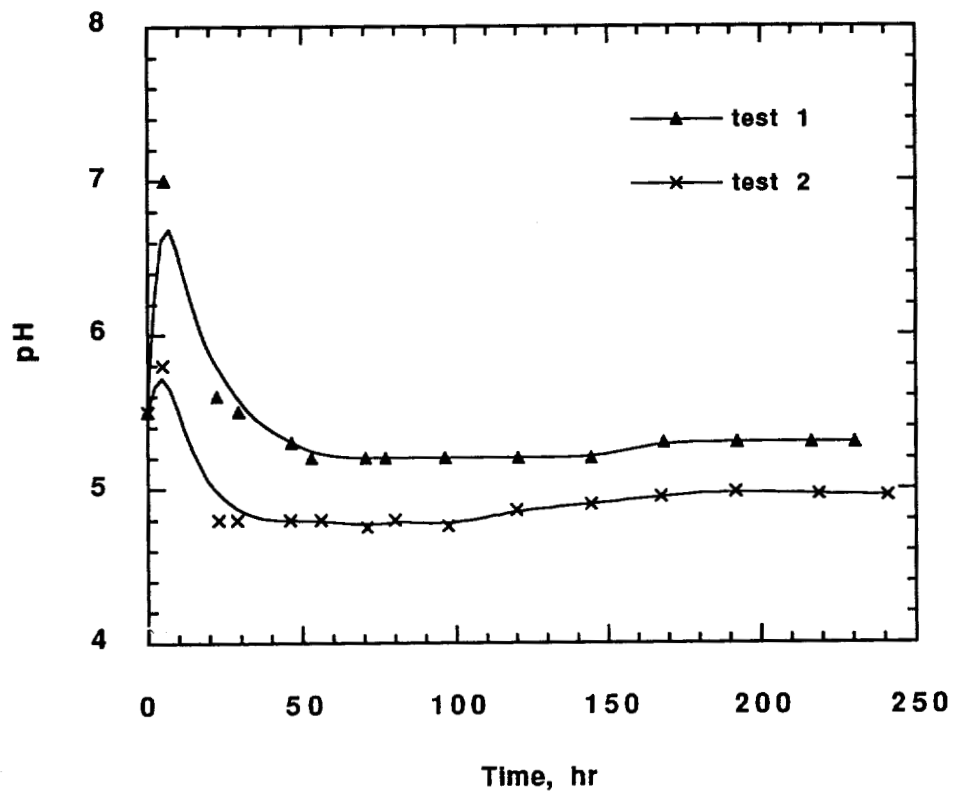


Figure 2.66 pH change of the extract obtained from the composite with the alumina trihydrate filler.

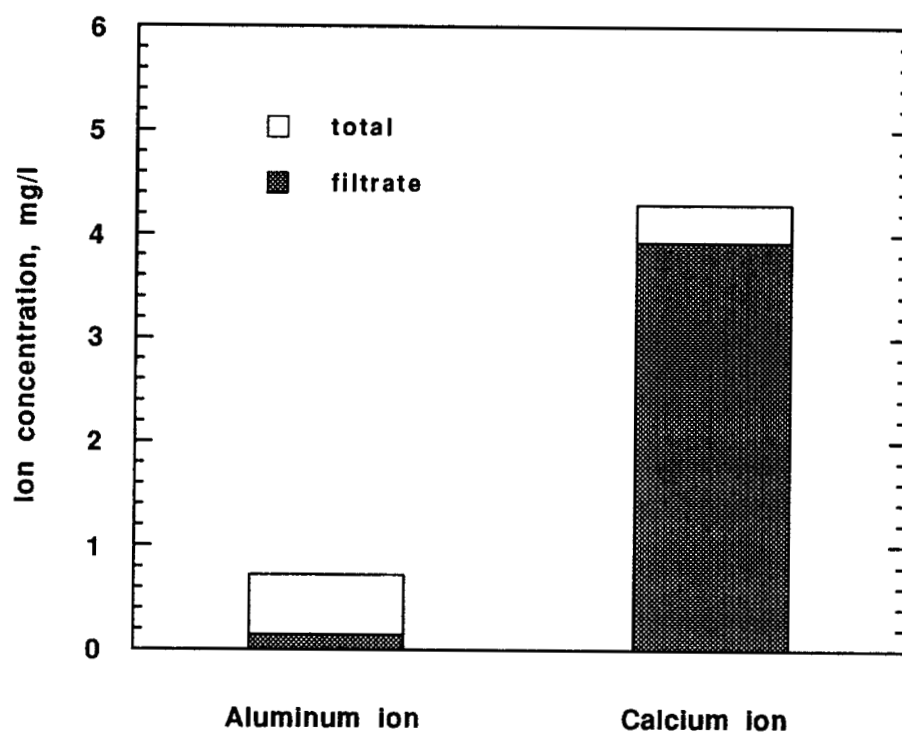


Figure 2.67 Calcium and aluminum concentrations in the extract of the composite with the alumina trihydrate filler.

Composite with the calcium carbonate filler

The change in the pH value of the extracts from the composite turnings was found to be a function of the extraction time (Figure 2.68). After an initial increase, the pH value stabilized around pH 10. Similar to those from the composite with the alumina trihydrate filler, the extracts from the composite with the calcium carbonate filler also contained both aluminum and calcium species, but at considerably higher concentrations (Figure 2.69). In the extracts, aluminum species existed in the precipitates, but most of the calcium species were dissolved in the solution.

Additional SEM examination was conducted on the turnings before and after the extraction test (Figure 2.70). Evidently, the extraction process did not cause any visible damage to the glass fibers, but the resin around the fibers appeared seriously diminished. This observation implies that the high concentrations of calcium and aluminum in the extract might not be attributed largely to calcium and aluminum depletion from the glass fibers but rather to that from the resin system or the sizing agent. This concept was further supported by the fiber immersion test results, which are given later in Section 2.5.4.

In summary, the results obtained from the extraction tests reveal that the composite itself under the influence of water could reach an internal chemical stability in a relatively short period of time, which may provide the composite a capability to accommodate the external aqueous environment. The significantly higher calcium concentrations with respect to aluminum concentrations observed in the extracts from composites with both fillers further indicated that the internal chemical stability in a composite system was not solely determined by the filler material, and that other factors, possibly organic or inorganic additives in the resin, may also have great influences. For instance, the stable pH value of about 5.0 obtained from the extraction of the composite with the alumina trihydrate filler might result from the dissociation of some organic acids, which were

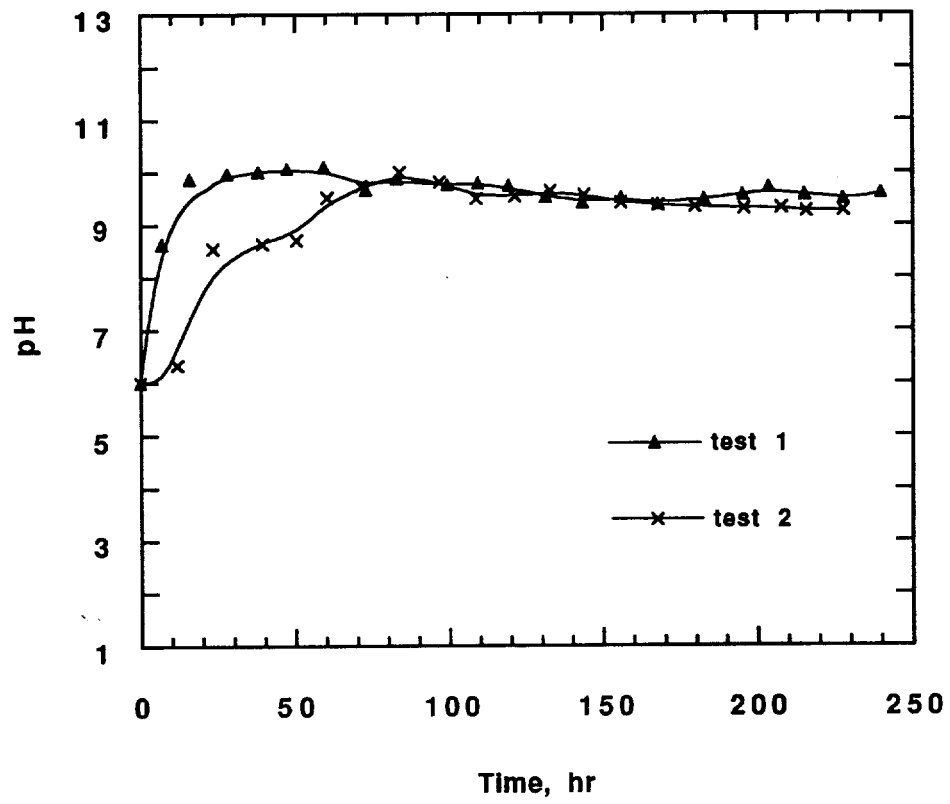


Figure 2.68 pH changes of the extract obtained from the composite with the calcium carbonate filler.

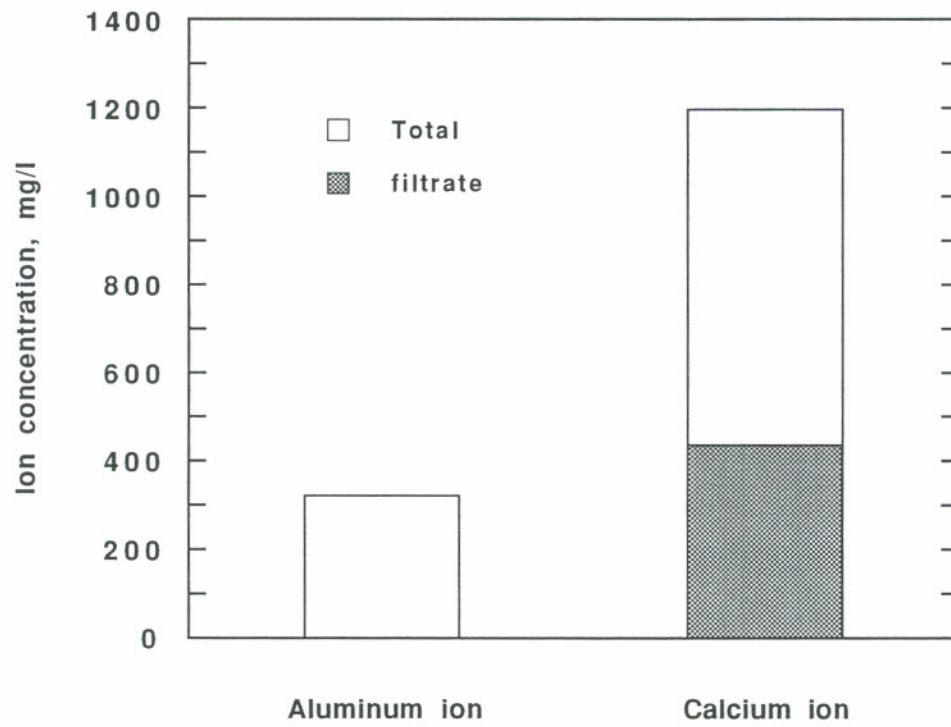
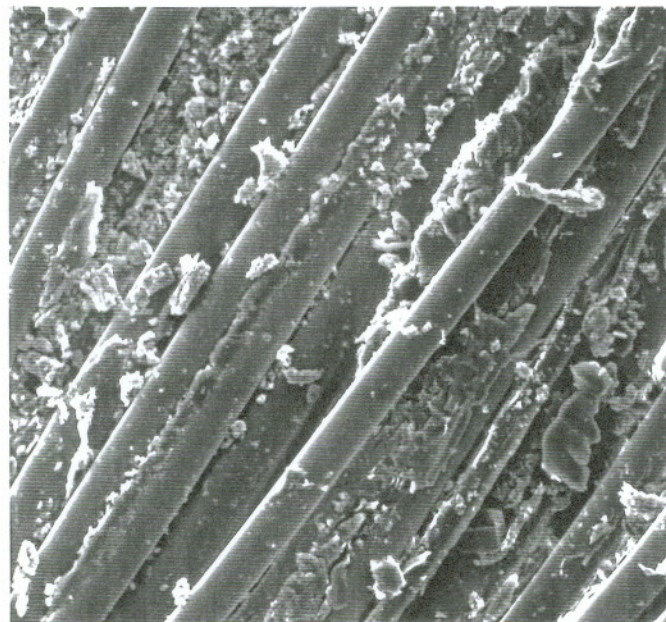


Figure 2.69 Calcium and aluminum concentrations in the extract of the composite with the calcium carbonate filler.



(a) Before the test



(b) After the test

Figure 2.70 Surface morphology of the composite turnings before and after the extraction test.

added to the resin during the resin formulation. It should be emphasized that calcium and aluminum were not the only species in the extract, and given the chemical complexity of the resin and fiber sizing formulations, a variety of other ions might also exist.

2.5.3 Thermal Stability Test

The thermal stability test was performed only on the composite containing the alumina trihydrate filler. In the test, the composite turnings were placed in a beaker, which was covered with a watch glass and heated in a heat jacket set at 100°C. To monitor the temperature during the test, a thermometer was inserted inside the composite turnings, but far from the wall of the beaker. The deposit collected on the watch glass was subsequently removed for chemical analysis.

The compounds in the deposit, which was derivitized with a dizomethane freshly distilled from dimethyl ether, were identified by gas chromatography in a Finnigan 4021 gas chromatograph mass spectrometer data system.

The thermal stability test revealed that E-glass fiber/polyester composite was thermally unstable. A few hours after the test started, light brown crystalline deposits were formed on the watch glass. During the test, the temperature of the composite turnings initially stayed at 100°C for the first several days, then gradually increased, and finally reached a constant value of 160°C. This phenomenon was probably caused by exothermic chemical reactions within the composite system.

The reconstructed ion chromatogram obtained from the deposits is shown in Figure 2.71. The major constituents identified are organic acids (Table 2.10), which either in a mixture or independently could serve as solvent to enhance further the degradation of composites.

68096.

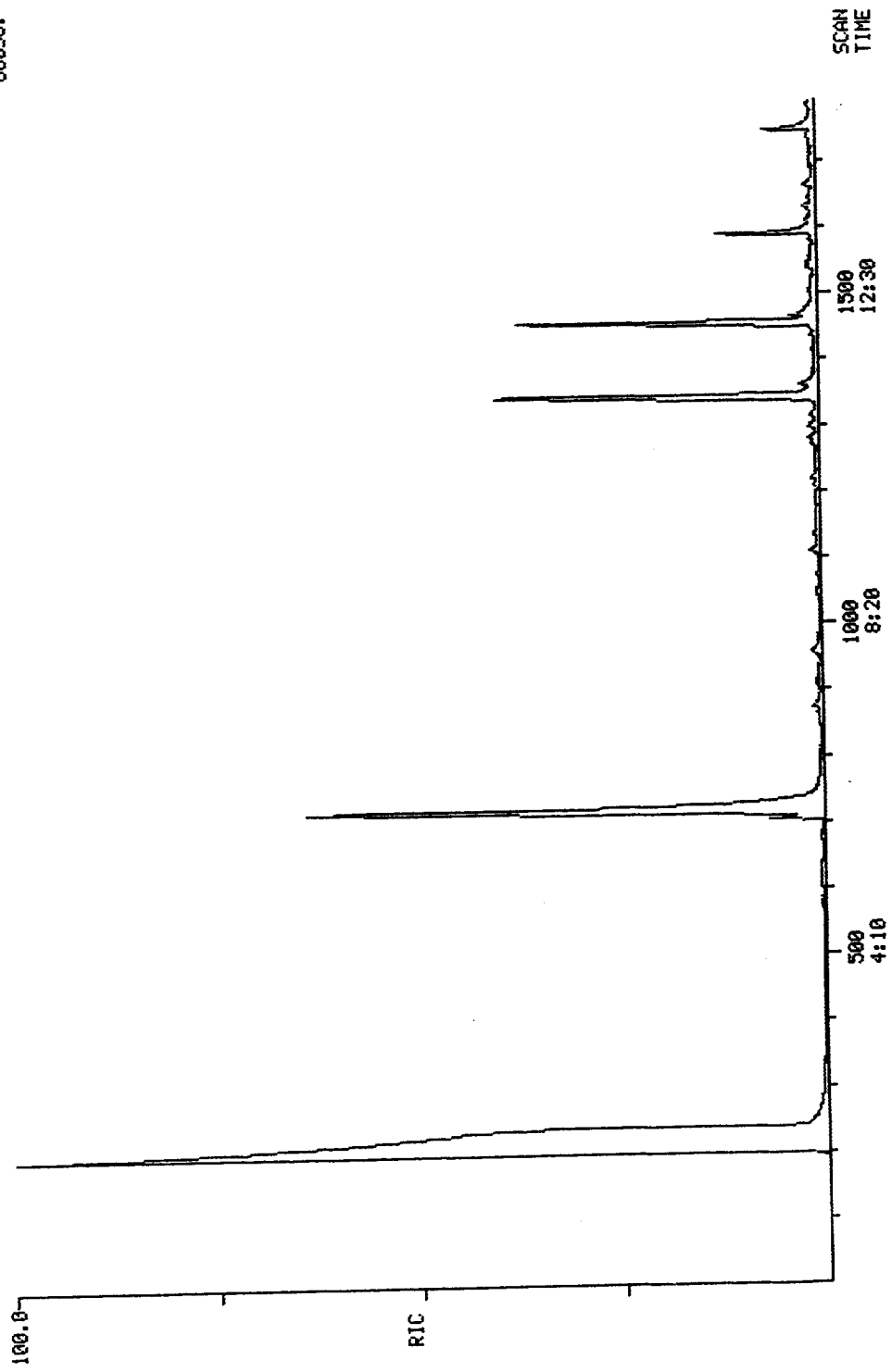


Figure 2.71 Reconstructed ion chromatogram for the deposits.

Table 2.10 Major constituents identified in the deposits

Peak number	Constituents
722	benzoic acid
1347	phthalic acid
1458	isomeric benzenedicarboxylic acid
1592	erythrocentaurin

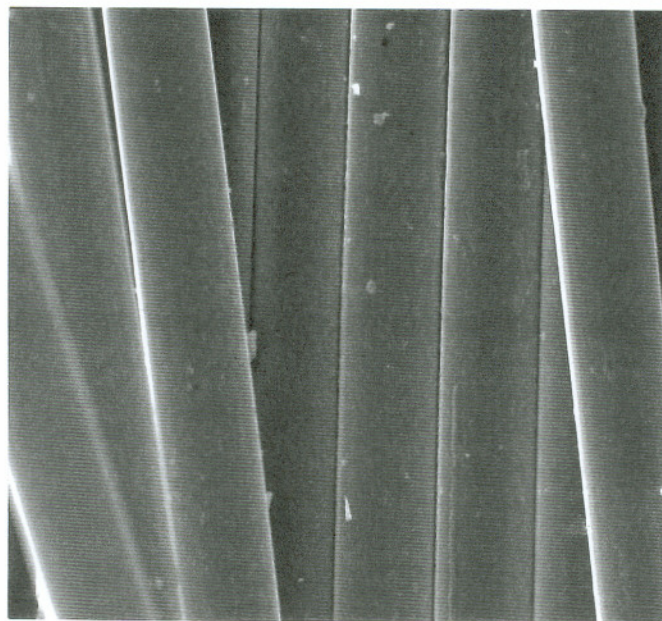
2.5.4 Immersion Test

In the immersion test, E-glass fibers, identical to those used in the extracted composite turnings, were immersed for one month in the extract of pH 10, which was obtained from the composite with the calcium carbonate filler. Fiber weight as well as the fiber surface morphology were compared before and after the immersion test.

During the immersion test, no visible damage developed on the fiber surfaces (Figure 2.72), suggesting that the internal alkaline environment created by the interaction of the composite with water may not be corrosive enough to cause stress corrosion fracture of E-glass fiber. Supporting evidence could be found from the fiber weight measurement results from two independent tests (Table 2.11); a negligible difference existed in the fiber weight before and after the test. The minor weight gain of the fibers may be due to the deposition of the suspended precipitates in the extract onto the fiber surface (Figure 2.72b).

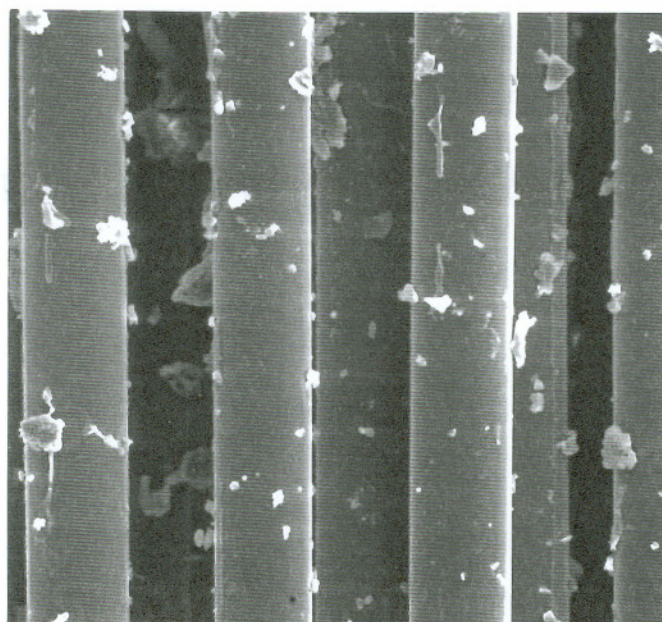
Table 2.11 Fiber weight measurements

Weight before test, mg	Weight after test, mg	Weight gain, mg
62.9	63.5	0.6
63.9	64.8	0.9



10 μm

(a) Before the test



10 μm

(b) After the test

Figure 2.72 Fiber surface morphology before and after the immersion test.

CHAPTER 3 DISCUSSION

3.1 Brittle Fracture Mechanisms of GRP Insulators

3.1.1 Failure Mode

In dry-air conditions, the fracture morphology of GRP insulators primarily depends on the end-fitting designs,³³ because they control how external loads can be transferred to the GRP rods. When a GRP insulator is subjected to a tension load, the free span of the composite rod experiences a uniform tensile stress; however, the stress near or inside the end fitting is complex in nature and non-uniformly distributed, with the highest stress concentrated near the end-fitting edge (Figure 1.4). Therefore, dry-fracture of insulators always starts on the external surface of the rod near the end-fitting edge, propagating towards the inside of the rod. For the cone end fitting, which is a common end-fitting design used in suspension GRP insulators, the stress concentration is estimated by a factor of two.¹⁷ The typical fracture morphology associated with this design is dominated by a 45° type fracture; rod fracture first runs approximately 45° to the rod axis, about 50% of its cross-section area, and then turns into longitudinal splitting.^{32,43} Mier-Maza *et al*,³² who developed a general model for calculating stresses induced by the end fitting, suggest that in the cone end fitting, shear stresses can approach 150 MPa, which is sufficiently high to fracture the rod. On a microscale, the dry-fracture surface is extremely irregular, with extensive fiber pull-out and longitudinal splitting.⁴³

The brittle fracture phenomenon of GRP insulators was first identified in the early 1980s.³⁴ The distinctive differences between dry fracture and brittle fracture exist in the orientation and the roughness of fracture surfaces. Unlike dry fracture, the fracture surface in brittle fracture always exists perpendicular to the rod axis and appears microscopically smooth (Figure 2.8). These features indicate that brittle fracture is dominated by tensile stresses, and more importantly, that other factors in addition to mechanical loads must be involved in the fracture process. Furthermore, brittle fracture is most likely to occur in the rod section between the high-voltage end and the first weathershed, producing a multi-stepped morphology because of a uniform tension distribution (Figures 2.5 and 2.6). Under certain circumstances, however, the fracture surface can also develop inside the end fitting (Figure 2.4) or above the first weathershed.⁴⁴ In this study, a spiral staircase morphology was observed on the fracture surface generated inside the high-voltage end of insulator #6 (Figure 2.8b), suggesting that some torsion stress was superimposed on the tensile stress inside the end fitting.

Suspension GRP insulators are given a maximum design rating of approximately 30% of the tensile fracture load (with end-fittings), with a design life of 30 to 50 years.¹⁷ A daily load applied to insulators commonly ranges from 12% to 24% of their load capacities; for the 16-mm round rods, by which the failed insulators studied in this study were constructed, the daily load approximates 1,362 kg (3,000 lb) to 2,724 kg (6,000 lb). The occurrence of insulator fracture at such low service loads further suggests that the brittle fracture is not caused exclusively by mechanical fracture but rather by environmentally assisted processes.

In this study, all of the fracture surfaces examined in service-failed or -damaged insulators appeared essentially planar and transverse to the rod axis (Figure 2.17). These features were identical to those found on fracture surfaces generated by stress corrosion of composites in acidic environments (Figure 2.40), signifying that stress corrosion likely is the fracture mode of brittle fracture in GRP insulators. This conclusion is further

confirmed by the observation of large mirror sizes on the fractured fiber ends (Figure 2.10), which is characteristic of stress corrosion of composites.

In general, stress corrosion of GRP composites virtually is a corrosion-assisted fiber fracture process. It is well documented that E-glass fiber, the most commonly used reinforcement in GRP composites, possesses excellent resistance to water and basic solutions.^{50,56,79,101} The fact that no crack was generated in a composite specimen subjected to both tensile load and water attack for 3 months, which was observed in this study, also favors the argument that GRP composites are not susceptible to stress corrosion in water. It is most likely, therefore, that stress corrosion in acidic environments is responsible for the brittle fracture of insulators. This rationale was supported by the presence of calcium and aluminum depletion, direct evidence of fiber acid leaching, found on the fracture surface of a service-failed insulator (Figures 2.25 and 2.26).

3.1.2 Electric Stress Influence

Electric stresses in service play a crucial role on the brittle fracture of GRP insulators, based on two important facts derived from field experience: (1) brittle fracture always occurs near the high-voltage ends of insulators,^{17,35,43-45} and (2) this fracture is not common on low-voltage but rather on high-voltage transmission lines, particularly in lines with a service voltage of 200 kV or above.⁴⁵ In general, stress corrosion fracture results from the simultaneous actions of tensile stresses and corrosive environments. In service, the distribution of mechanical stresses inside both high-voltage and ground ends should resemble one another, given their same structural design. Additionally, external service environments surrounding both high-voltage and ground end fittings are identical. If only mechanical stresses and corrosive environments are involved, brittle fracture should randomly occur in either end fitting. The predominance of brittle fracture in

the high-voltage end strongly argues for the involvement of electric stresses in the brittle fracture process.

Further evidence of electric stress influence was obtained by the observation of melted fibers (Figure 2.15) and resin decomposition (Figures 2.12 and 2.14) on the fracture surfaces of service-failed insulators in this study. In normal stress corrosion conditions, where only mechanical stresses and corrosive media are present, the fractured resin surface should be co-planar with the surfaces of fractured fiber ends; however, on some of the insulator fracture surfaces examined in this study, the fracture resin surface appeared significantly depressed. This unusual resin deformation is likely induced by a thermally activated process. Partially composed of organic materials, the thermal stability of GRP composites generally is quite low. At temperatures around 100°C, some organic compounds, primarily from the resin matrix and sizing, begin to decompose (Figure 2.72 and Table 2.9). Additionally, high electric stresses in service may cause a discharge in the gap between two crack surfaces in the composite rod or between the rod surface and the rubber sheath. When the electric field inside the gap builds so fast that the thermal conduction loss can be neglected, all of the heat generated will be consumed by rising surface temperatures, resulting in local thermal instability. Depending on the discharge intensity, the temperature caused by local heating can be high enough to promote resin decomposition or even fiber melting. The fractographic difference between brittle fracture of insulators and stress corrosion of composites, particularly the depressed resin surface, confirms the involvement of electric stresses in the brittle fracture of insulators.

In insulator applications, the length of an insulator varies with the service voltage. To eliminate electrical flashover, the higher the service voltage, the longer the insulator has to be. An increase in the insulator length will, however, lead to a non-uniform distribution of voltage along the rod, with the highest electric stress existing near the high-voltage end. In fact, this electric stress concentration is likely to localize in the

region from the end-fitting edge up to the first weathershed,¹⁴³ where the brittle fracture of insulators mostly occurs. According to the ladder network model established by Chandler *et al*,⁴⁶ the electric stress concentration, expressed by the ratio of maximum to average electric stress, is a function of the insulator length; a longer insulator will result in a higher electric stress concentration. For a 3-meter long insulator used in a 400 kV transmission network, the high-voltage end is expected to experience the maximum stress of 3 times greater than average stress elsewhere along the rod, which may exceed the ionization limit in air, thereby causing corona discharges near the high-voltage end. When the service voltage is higher than 230 kV, therefore, a grading ring is usually required at the high-voltage end to minimize the likelihood of corona discharge. However, the effectiveness of the grading ring is highly dependent on the ring dimension as well as its relative position to the end fitting. Although the attachment of the grading ring can significantly reduce the intensity of electric stresses around the high-voltage end, void-induced partial discharge is still possible because the reduced stress intensity may exceed the inception voltage for partial discharge.¹⁴³

In general, electric stress concentrated near the high-voltage end can assist the brittle fracture of insulators in two ways: (1) oxidizing polymer resins to generate acidic environments *in situ*, and (2) initiating the fracture by localized electrical damage to insulator components.

Oxidation of polymer resins by partial discharges is well documented in the literature.^{17,35,127} The detailed oxidation mechanism is described in Section 1.4.1.2. Under the influence of partial discharge, polymer resin that is designed to protect glass fiber from environmental attack may actually become a direct source for producing internal corrosive media, represented by oxalic acid and other organic acids. This mechanism provides a base for the self-initiated stress corrosion mechanism in insulator applications. Recently, Braun¹⁴³ has conducted a series of numerical simulations of electric field distributions in the high-voltage end region with longitudinal or transverse

cracks embedded inside the composite rod, assuming the insulator is operated in a 345 kV network. His study revealed that the introduction of cracks into the rod can readily intensify the electric stress at the crack front to the level above the partial-discharge inception voltage, even given a situation in which the crack extends inside the high-voltage end, where otherwise electric stresses should be absent. The intensification of electric stress at the crack front becomes particularly severe if the transverse crack is filled with air or the longitudinal crack is partially filled with contaminated water. Based on the Braun's study, it is reasonable to deduce that partial discharges move along the crack front when a crack is present in the rod. In this case, therefore, the corrosive byproducts induced by partial discharge are likely concentrated at the crack front and continuously replenished as the crack advances.

Under the influence of high electric stresses near the high-voltage end, insulator components, including weathersheds, rubber sheath, and composite rods, may suffer significant electrical damage in the form of melting, erosion, or vaporization. This damage can contribute to the initiation of brittle fracture in insulators. Field experience reveals that in all cases of brittle fracture, evidence of electrical damage is always found adjacent to the fracture initiation site.^{17,44,45,49} In insulator service, high electric stresses can breakdown the weathershed (Figure 2.7) and/or the rubber sheath (Figure 2.1) by electrical cutting or erosion, thereby exposing the composite rod to external moisture or contaminants and promoting stress corrosion fracture.⁴⁴ Under certain circumstances, further electrical damage to the composite rod is also possible.^{44,45} In this study, melted fibers induced by electrical discharge was found on the fracture surface contiguous to the external rod surface where the brittle fracture was initiated. Once the rod is exposed to external environments, electrical damage then tends to progress into the rod and eventually causes the rod to separate from the sheath with the assistance of moisture, thereby making it possible to generate multi-stepped cracks internally along the rod surface (Figures 2.5 and 2.6). Electric stresses evidently accelerate the crack initiation in the brittle fracture of insulators. However, their influence on the crack propagation

is still not clear. Recently, Akhtar *et al*¹⁶ studied the influence of an electric stress on stress corrosion behavior of bare GRP rods and found that the likelihood of failure for composite rods with and without introduced electric stresses are practically the same, suggesting that superimposing electric stresses on mechanical and environmental stresses may not further enhance crack propagation of the composite rod.

In this study, a special effort was made to investigate the influence of electric stresses on the stress corrosion fracture of composites. Preliminary results obtained from the high-voltage fracture experiments were encouraging. In fact, transverse cracks with planar fracture morphology, similar to those observed in stress corrosion fractures, were for the first time generated in an E-glass/polyester composite specimen subjected to both an mechanical stress and corona discharge in the presence of water. Fractographic examination further revealed that the fracture morphology produced in the high-voltage fracture experiments closely resembled that observed in service-failed insulators, particularly the morphology in the fracture initiation region where both melted fibers and resin decomposition were present (Figures 2.50, 2.51, and 2.52). By comparing the morphology of the fracture surfaces generated in service-failed insulators and in the stress corrosion and high-voltage fracture of composites (Figure 3.1), it is clear that the brittle fracture of insulators is not a simple but rather a complex stress corrosion process controlled by the synergistic influences of mechanical, environmental, and electric stresses. At present, the corrosive substances induced by corona discharge on the composite remains unidentified. Although these substances are likely to be nitric acids, as is suggested in the next section, further research is certainly needed to confirm this speculation.

3.1.3 Service Environments

The brittle fracture of insulators is attributed to stress corrosion of the composite rod in acidic environments. Previous investigations have suggested that acidic environment in

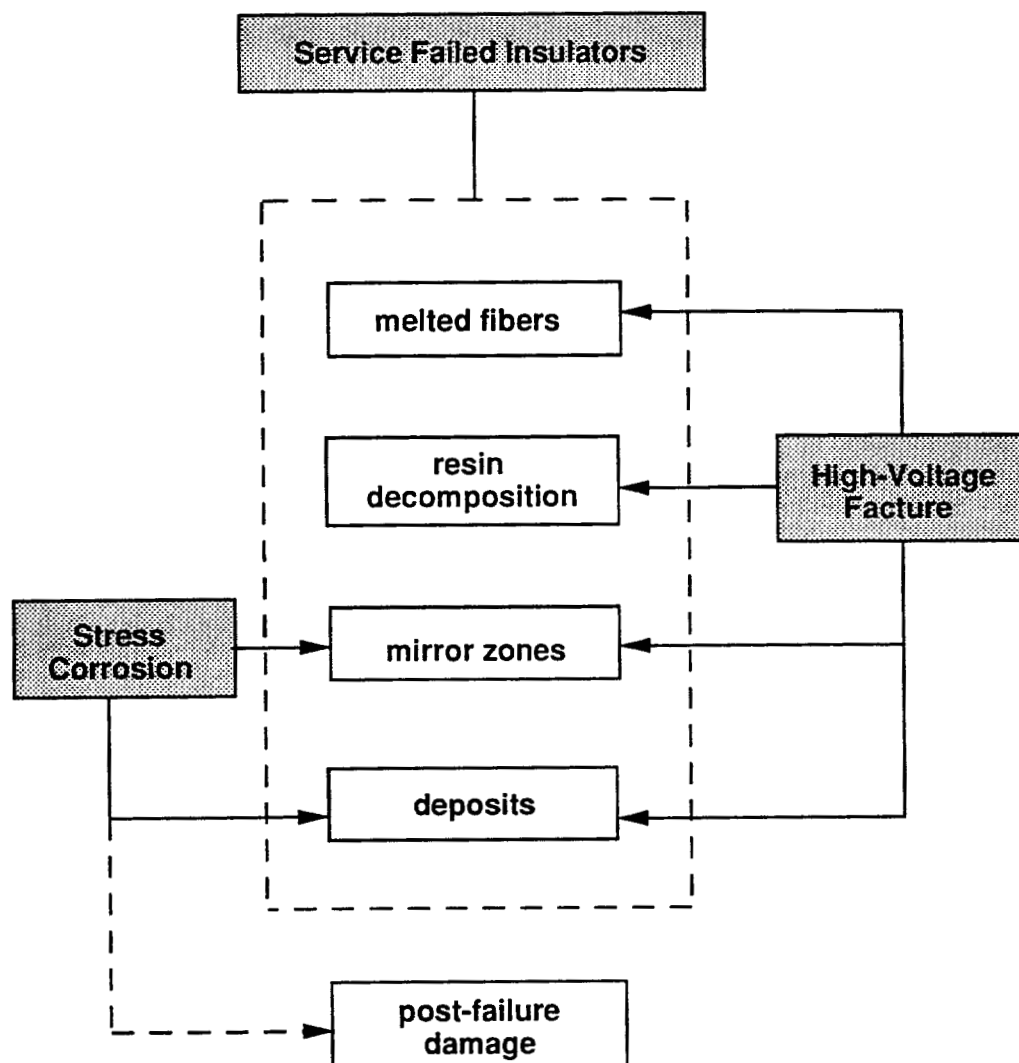


Figure 3.1 Fracture morphology comparison.

insulator service may arise from two sources.¹⁷ One is acid rain, which contains primarily sulfuric and nitric acids. On rare occasions, hydrochloric acid may be present. The other source may be polymer oxidizing byproducts induced by internal partial discharge, such as oxalic acid and other organic acids. Based on field experience, the presence of brittle fracture is always found to be associated with polymer housing damage, and hence acid rain or contaminated moisture attack to the composite rod is possible. However, it is hard to believe that acid rain alone could be responsible for brittle fracture of insulators because some of the incidents did occur in the areas where rain was not contaminated, i.e., the acidity of rainwater was around pH 5.6, the equilibrium value between natural rainwater and atmospheric carbon dioxide.¹²³ Therefore, electrical discharge-induced acids are more likely to be dominant in service environments. To date, the formation of oxalic acid in epoxy and polyethylene resins exposed to electrical discharge has been experimentally proven;^{35,127} however, no evidence has been found of oxalic acid formation in polyester or vinyl ester resin. In this study, an attempt was made to determine the chemistry of the oxidizing byproducts generated by electrical discharges in E-glass/polymer composite and pure polyester resin. Although some of weak organic acids were identified, no oxalic acid was found in the byproducts (Figures 2.46 and 2.47, or Tables 2.5 and 2.6).

In addition to acid rain and oxalic acid, another important source responsible for acidic environments in insulator service, namely surface discharge-induced nitric acid, is proposed in this study. The earliest discovery of surface discharge induced nitric acid was made by Chandler *et al* in 1983.⁴⁶ Intended initially to confirm the formation of internal discharge induced oxalic acid in epoxy resin, they exposed an artificial cavity made of thin epoxy sheets to electrical discharges. After four-day exposure, however, they not only found oxalic acid formed inside the cavity but also nitric acid produced on the cavity external surfaces, where oxygen and nitrogen were abundant. In recent years, internal discharge-induced oxalic acid has become a popular mechanism for producing

acidic environments in insulator service,^{17,35,46,96} but unfortunately the phenomenon of surface-discharge induced nitric acid appears to have been forgotten.

In service, electric stress distribution across the insulator surface in dry and unpolluted environments resembles the internal stress distribution, with the highest stress located at the high-voltage end. Due to the existence of weathersheds, however, the surface electric stress is generally much lower than the internal electric stress. Therefore, surface discharges are unlikely to take place on a dry insulator, except for the corona-induced surface discharge near the high-voltage end. In wet and polluted environments, pollutant deposition and wetting will leave a conductive layer on the insulator surface. Because of the discontinuity of this layer, dry bands form when the electric current flow through the layer. Consequently, the full voltage applied to the insulator will be concentrated on these dry bands, and the related surface areas will be highly stressed. Under such circumstances, surface discharge is possible, and arcing across dry bands may occur as well. In fact, dry band formation will cause not only high surface stress but also high internal stress beneath the surface. Therefore, surface discharge is often accompanied by internal discharge either in the rod or on the rod/sheath interface.

Surface discharge in an ambient atmosphere, on one hand, produces ions and activated neutrals. On the other hand, it forms a water layer on any exposed polymer surface, either by transporting water in air to the polymer surface, which becomes hydrophilic under surface discharge, or by producing water from the polymer itself under oxidation.^{145,146} During the surface discharge process, discharge-activated species readily react with and/or dissolve in the water. As a result, the water layer on the exposed polymer surface will become acidic,^{144,145,147} containing significant amounts of NO_x , HNO_2 , and HNO_3 . Meanwhile, both the vapor pressure and the electrical conductivity of the water will be increased.¹⁴⁴ Further studies indicate that acidification of the water is not dominated by ionized species, but rather by the activated neutrals, comprised of excited particles, radicals, and atoms from dissociated molecules.¹⁴⁶ Additionally, the

polarity of discharges may also influence the acidity of water. Goldman *et al* studied the acidity of distilled water exposed to electrical discharge with both polarities and found that water exposed to the negative discharge became more acidic than water exposed to the positive discharge and could reach an acidity as high as pH 3, which is acidic enough to promote stress corrosion fracture in E-glass polymer composite (Figures 2.38 and 2.39).

Driven by electric stresses, both surface and internal discharges can induce acidic environments in insulator service. However, these two processes completely differ in nature. Internal discharge in voids oxidizes polymers, producing organic acids;³⁵ while surface discharge changes the chemistry of surface water layers, acidifying the water.¹⁴⁴ Therefore, acidic environments induced by the former are highly dependent on the polymer involved, but those induced by the latter are unconstrained by the nature of polymers. Since surface discharge can occur on any exposed polymer, the formation of nitric acids will most likely occur in service environments, thereby being responsible for brittle fracture of insulators. In service, surface discharge readily occurs either on the external surfaces of an insulator, such as the surfaces of the weathersheds and rubber sheath, or on the internal surfaces, like the surfaces of internal cracks in the rod and between the rod and the rubber sheath, if the crack is exposed to external environments. In this study, an appreciable amount of zinc as well as a small amount of iron was detected on internal fracture surfaces (Figures 2.20, 2.21, and 2.22), suggesting that the metal casting was corroded probably prior to insulator brittle fracture. This corrosion might be associated with nitric acids produced by surface discharge on the rubber sheath near the high-voltage end.

Additional evidence that brittle fracture can be attributed to the nitric acid dominant environments exists in the fractographic similarity between brittle fracture and stress corrosion fracture of composites in nitric acid (Figures 2.16a and 2.41a). The most important characteristic is that both fracture surfaces are free from post-failure damage.

In general, stress corrosion fracture of composites in acids is often accompanied by post-failure damage; the fracture surface featuring multi-cracks on the fractured fiber ends and fiber/resin interface debonding. When the fracture surface that developed in stress corrosion cracking is continuously exposed to acids, non-siliceous ions will be leached out from the fractured fiber ends, eventually leading to the fiber shrinkage. This shrinkage can reach up to as much as 30% by volume and therefore, is often accompanied by fiber splitting, fiber/resin interface debonding, or a combination of both.⁵⁰ Since the formation of post-failure damage is primarily a fiber corrosion phenomenon, it is determined by the nature of acids.

As indicated earlier, acidic environments in insulator service may contain oxalic, nitric, sulfuric, and hydrochloric acids, which may arise from acid rain, internal discharge, or surface discharge. To evaluate the tendency of composites to develop post-failure damage in each of the above acids, the acid corrosion behavior of E-glass fiber, particularly its surface deterioration behavior, was investigated in this study. The results indicated that fibers immersed in both oxalic and sulfuric acids showed severe surface cracking, while to the contrary, fibers tested in nitric and hydrochloric acids appeared free from any visible surface damage. These behavior suggests that oxalic and sulfuric acids have a greater tendency to promote post-failure damage on the fracture surface of E-glass fiber reinforced composites. Therefore, they are unlikely to dominate acidic environments in service because of the absence of post-failure damage on all of the fracture surfaces in the field-failed or -damaged insulators examined in this study. Between the two acids left, nitric acid is believed to be the major component in service environments, given that hydrochloric acid is rarely present in acid rain. This perception is further supported by the fact that no post-failure damage developed on the fracture surface exposed to a pH 3 nitric acid solution for over one month. It should be noted that nitric-acid dominant environments in insulator service can be further complicated in chemistry by the contamination of sulfuric acid if acid rain is present, or oxalic acid if internal discharge in epoxy resin is involved.

3.1.4 Fracture Model

The brittle fracture of insulators is a complex stress corrosion process controlled by the combined influence of mechanical, environmental, electric stresses, which can be outlined in Figure 3.2. In this study, a generic fracture model is established on the basis of surface discharge-induced nitric acids together with external moisture or acid rain (Figure 3.3).

In an insulator structure, the high-voltage end is most vulnerable to stress corrosion fracture because maximum mechanical, environmental, and electric stresses are likely to be located in its vicinity. In fact, insulator failure analysis conducted in this study and previous investigations have both revealed that brittle fracture always occurs near the high-voltage end of insulators, or more precisely, in the region from the epoxy/sheath interface inside the high-voltage end up to the first weathershed (Figures 2.4, 2.5, and 2.6). In general, external acidic environments come in contact with the composite rod of insulators by three means: (1) epoxy/sheath interface debonding inside the high-voltage end,^{133,143} (2) circumferential cracking in the epoxy potting material near the rubber/epoxy interface,¹³³ and (3) electrical breakdown of the rubber sheath and weathersheds.^{44,45}

Based on the end-fitting design specific to the insulators investigated in this study (Figure 1.4), the high-voltage end consists of the composite rod, epoxy potting material, rubber sheath, and metal casting. Among the first three materials, an interface is formed between each of the two: the rod/epoxy, the rod/sheath, and the epoxy/sheath interface, all of which are mechanically weak links in the insulator structure. The relative strength of the interfaces primarily depends on the mechanical properties of the two materials with which they are interfaced, the bonding material used in between the two materials, and the interface geometry. Due to substantial differences in mechanical properties of the materials and the interface geometry, the epoxy/sheath interface appears to be the

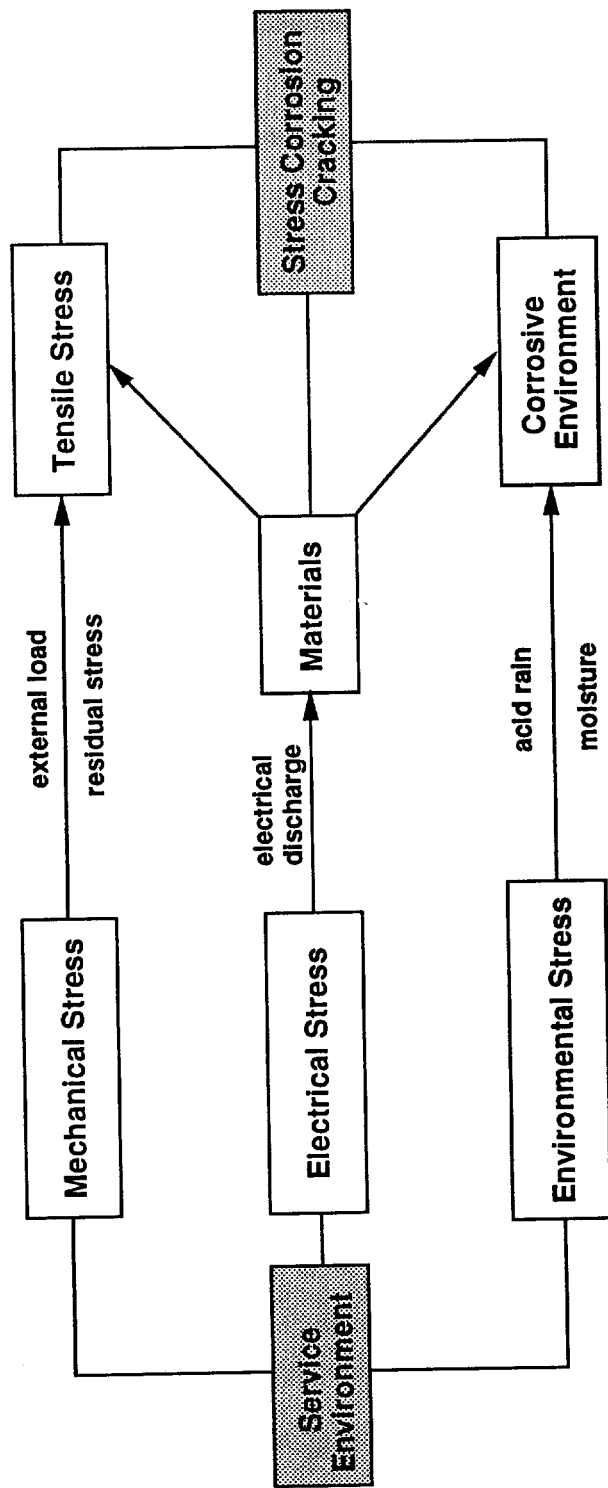


Figure 3.2 Complex stress corrosion environments in insulator service.

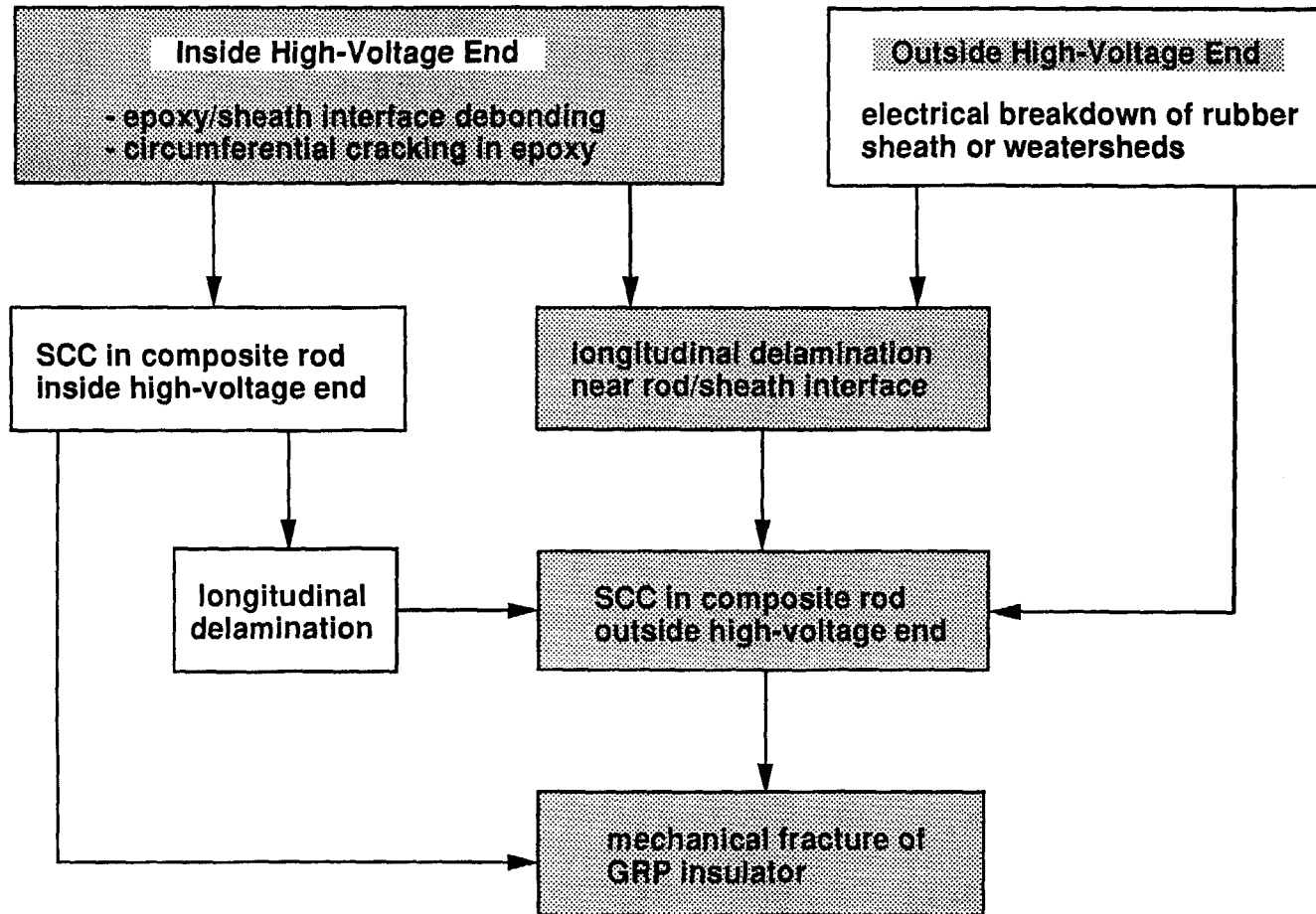


Figure 3.3 Failure model proposed for insulator brittle fracture.

mechanically weakest joint. When the applied mechanical stress on an insulator reaches a certain level, which may be much lower than the dry-strength of the composite rod, the epoxy/sheath interface may fail first (Figure 2.4). This failure can be enhanced if high temperatures induced by electrical discharge are present near the high-voltage end. Since a gap, based on the cone end-fitting design, exists between the rubber sheath and the metal casting (Figure 2.2), the epoxy/sheath interface debonding will then create an initial access for external acidic media to the interior composite rod. In addition to the epoxy/sheath interface debonding, circumferential cracking in the epoxy potting material (Figure 2.4) is commonly associated with the brittle fracture of insulators.¹³³ This cracking is always localized adjacent to the epoxy/sheath interface and often results in small crushing zones, short circumferential cracks paralleling with one another. Through the circumferential cracks in the epoxy the composite rod is exposed to external acidic environments. At present, the formation of the circumferential cracks in the epoxy material cannot fully be explained. Since these cracks are also found in the ground end of insulators, their formation is likely driven by mechanical stresses only. Epoxies are brittle materials¹⁴⁸ and thereby susceptible to impact fracture. During insulator proof loading tests or installation, the epoxy wedge may be pulled up against the metal casting instantly (Figures 1.4 and 2.2), i.e., subjected to a high impact stress, thus creating circumferential cracks or crushing zones in the epoxy material. Moreover, electrical breakdown of the rubber sheath and weathersheds can also expose the composite rod to external acidic environments. The formation of this damage is discussed in Section 3.1.2.

When external acidic environments come in contact with the composite rod inside the high-voltage end, two processes may occur simultaneously: (1) acid attacks the glass fibers in the composite rod, initiating stress corrosion fracture, and (2) solvent, particularly water, attacks the composite rod first, causing the longitudinal delamination in the rod near the rod/sheath interface by fiber/resin interface debonding, and then the delamination channels external acidic media into the interior of the composite rod.

Although stress corrosion fracture may develop from the rod surface being directly exposed to external acidic environments inside the high-voltage end, such as in the region of the epoxy/sheath interface debonding or the circumferential cracks in the epoxy material, on more occasions, the fracture is initiated internally on the rod surface outside the high-voltage end, where the rod is separated from the rubber sheath and experiences much higher electric stresses (Figures 2.5 and 2.6).

It is well known that a pultruded composite rod exhibits high axial tensile strength. However, its transverse tensile strength and shear strength are relatively low and will decrease with an increase in the fiber volume fraction. Further reduction in these strengths can result from water attack to composite components, primarily the resin matrix and the fiber/resin interface. Water absorption can cause swelling of the resin and degrade the sizing agent within the fiber/resin interfacial zone.^{50,116,134-137} In a unidirectional lamina, resin swelling in the axial direction will be severely restricted by the fiber, whereas extensive swelling occurs in the transverse direction, generating internal stresses in the fiber/resin interface.¹¹⁶ This effect appears insignificant at room temperature due to a low absorption rate but may eventually become detrimental to the mechanical properties of composites at high temperatures.¹⁴⁹ In fact, the internal stresses induced by the resin swelling, on their own, are sufficient to promote the fiber/resin interface debonding at temperatures even below 60°C. This temperature range is feasible in insulator service when electrical discharge is involved. Because of water attack, longitudinal delamination caused by the fiber/resin debonding always occurs near the rod surface, leading to a separation of the rod and rubber sheath. The delamination starts from either circumferential cracks in the epoxy potting material or from epoxy/sheath interface debonding and extends up to the outside of the high-voltage end along the same cylindrical fracture plane. In this case, external acidic environments can be transported through the longitudinal delamination by capillary effect to the area outside the high-voltage end, and meanwhile electrical discharge is also possible at the tip of the delamination.¹³⁸ Because the tensile stress outside the high-voltage end is uniformly

distributed, several stress corrosion cracks can be simultaneously generated along the rod surface and may propagate perpendicular to the fiber direction, thereby creating the stepped fracture morphology (Figures 2.5 and 2.6).

Furthermore, longitudinal delamination in the rod can be induced by the stress relief mechanism. The initiation of a stress corrosion crack causes stress concentration at the crack tip, which will be intensified as the crack grows.^{62,66,67} When the transverse crack propagates to the point where the stress exceeds the fiber/resin interface strength, longitudinal delamination will develop at the crack tip to release the stress. If the stress corrosion crack is initiated inside the high-voltage end, the longitudinal delamination can only propagate in the direction away from the high-voltage end (Figure 2.4) because the stress field in the opposite direction is compressive in nature. If the stress corrosion crack is generated outside the high-voltage end, however, the tensile stress field exists on the both sides of the crack, and thereby the longitudinal delamination readily propagates in either direction.

The final fracture of insulators results from the reduction of an unfractured rod cross-section. When the tensile stress in the unfractured rod cross-section, which becomes smaller as stress corrosion cracks propagate, reaches the ultimate tensile strength of the composite rod, the rod will fracture in a purely mechanical fashion, leaving broom-like fracture morphology.

3.2 Acid Corrosion of E-Glass Fiber

3.2.1 Ion Depletion Behavior

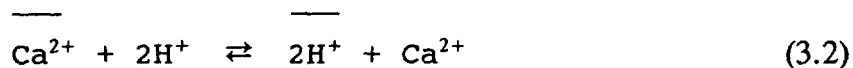
In a glass-acid system, the silica network in the glass is generally stable.^{101,150} Acid corrosion of the glass is essentially attributed to preferential leaching of non-siliceous oxides. The leachability of different glasses in acids can be evaluated by the Si/O ratio

formula proposed by Huggins *et al.*¹⁵¹

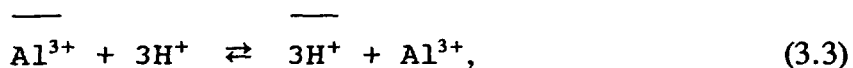
$$\text{Si/O} = \frac{\text{SiO}_2 / 100}{\text{mol}\{\text{SiO}_2\} \sum [(\text{M}_m\text{O}_n / 100) (\text{O}_n / \text{mol}\{\text{M}_m\text{O}_n\})]} \quad (3.1)$$

where M_mO_n refers to the weight percentage of oxides, $\text{mol}\{\text{M}_m\text{O}_n\}$ is the mole weight of oxides, and O_n equals to the number of oxygens in the oxide. A smaller Si/O ratio in the glass means more non-bridging oxygen ions, resulting in a lower stability of the silica network and thus a higher leachability of non-siliceous ions in acids. In E-glass, the amount of non-siliceous oxides is about 45% by weight. Such a high content of non-siliceous oxides leads to its relatively lower Si/O ratio (0.31) in comparison to those of other commonly used glasses, such as A-glass(0.41), C-glass(0.36), and S-glass(0.34).¹⁰¹ Therefore, E-glass is highly susceptible to acid attack.

Non-siliceous oxides in E-glass include calcium, aluminum, boron, magnesium, and other minor oxides. Since calcium and aluminum oxides alone make up about 35% by weight of the glass (Table 1.1), leaching of these metal ions is considered to be the major cause of acid corrosion of E-glass fiber. Acid leaching of glass is an ion-exchange process controlled by diffusion. Specific ion-exchange reactions for the calcium and aluminum depletion in acids can be expressed respectively by



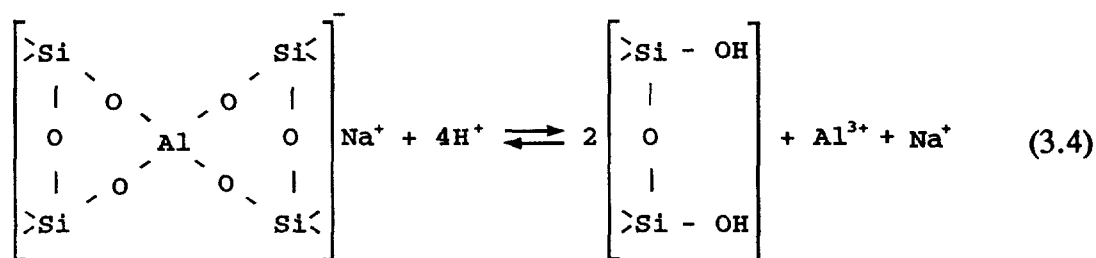
and



where the ions denoted by the bar are in the glass phase, and the other ions exist in the acid solution. Based on the ion-exchange mechanism,¹⁵² the tendency toward ion

depletion is highly dependent on the characters of the ion, particularly its bonding energy in the glass, valence state, hydrated volume, and the concentration and nature of the acid.

In a glass structure, calcium oxide, designated a network modifier, disrupts the continuity of the silica network; each divalent calcium cation produces two non-bridging oxygen ions.¹⁵³ Because it occurs as an interstitial in the glass, the calcium ion can diffuse readily through the silica network and exchange with hydrogen ions when the glass is exposed to an acid. Classified as an intermediate, aluminum oxide can either occupy the holes in between the SiO₄ tetrahedra or join the silica network provided enough alkali cations are available to neutralize the negative charge of the tetrahedral aluminum ion.¹⁵³ If the molar ratio R₂O/Al₂O₃ is greater than 1, where R refers to alkali ions such as sodium ions, aluminum exhibits a fourfold coordination and acts as a network former.^{101,154} Under such circumstances, the aluminum ion will be leached out along with the sodium ion in acid corrosion of glass. This leaching sequence can be described by the equation:⁹⁴



The presence of aluminum ions in the network will improve the chemical durability of the glass. However, if the molar ratio is smaller than 1, aluminum will pass into a sixfold coordination and act as a network modifier like the calcium ion.¹⁰¹ Given this ratio concept, aluminum in E-glass is unlikely to join the silica network but likely to remain as an interstitial ion in the silica network, since E-glass has a low alkali oxide content. In acid corrosion, the aluminum ion theoretically is more difficult to remove

from the glass because of its higher valence and smaller hydrated volume relative to the calcium ion, even if both calcium and aluminum ions in E-glass reside in between the silica network.

In this study, similar leachability of the calcium and aluminum ions was observed in the acid immersion experiments of E-glass fiber exposed to both hydrochloric and nitric acids (Figures 2.55 and 2.56), although the calcium content of the glass is much higher than the aluminum content. One reasonable explanation for this result is that the distribution of calcium and aluminum may be non-uniform along the radial direction of a glass fiber; the surface of E-glass fiber is rich in aluminum ions at the expense of calcium ions.¹⁰² The segregation of aluminum ions to the fiber surface can facilitate the aluminum ion depletion in acids, thereby increasing the leachability of the aluminum ion. Currently, the aluminum segregation phenomenon is not well understood. Eakins,¹⁵⁵ who studied the reactivity of various glass fiber surfaces, proposed that aluminum segregation results from its smaller atomic volume and lower electronegativity in comparison with the other ions in glasses. However, the finding of the calcium-rich surface in the magnesium-free E-glass fiber¹⁵⁶ further suggests that chemical segregation is a complex process in which ion interaction may play an important role.

The ion depletion of glass in acids generally can be characterized either by acid-strength-controlled leaching, in which hydrogen ion concentration is the driving force, or by anion-controlled leaching, in which the anion in the acid that can form insoluble salts and/or complex ions with the metal cations depleted from the glass is the determining factor. In this study, much higher calcium and aluminum depletion was found in oxalic and sulfuric acids than in hydrochloric and nitric acids at the same hydrogen ion concentrations (Figures 2.54 and 2.55). This evidence suggests that different leaching mechanisms were operative.

In hydrochloric and nitric acids, the anions associated with the acids, Cl^- and NO_3^- , have a negligible effect on the depletion behavior of calcium and aluminum ions because the anions form neither insoluble salts nor complex ions with these metal cations. Therefore, the calcium and aluminum depletion in these two acids should be determined only by the hydrogen ion concentration. In fact, depletion rates of calcium and aluminum ions in hydrochloric acid were found to be almost identical to those in nitric acid for each given pH value (Figures 2.55 and 2.56). This result indicated that the ion depletion in both hydrochloric and nitric acids was governed by the acid-strength-controlled leaching. Furthermore, it should be mentioned that the chlorate anion in hydrochloric acid may form a complex ion (FeCl_4^-) with the ferric ion depleted from glass.⁹⁵ Because of a small quantity of iron oxide in E-glass, however, this mechanism has little influence on the leaching behavior of E-glass fiber in hydrochloric acid.

Unlike hydrochloric and nitric acids, the anion in oxalic acid, $\text{C}_2\text{O}_4^{2-}$, can form both an insoluble salt with the calcium ion and stable complex ions with the aluminum ion. For the formation of the insoluble salt, the reaction can be expressed by



The solubility product (K_{sp}) of calcium oxalate is 2.34×10^{-9} . The oxalate anion can also form several complex ions with the aluminum ion,¹⁵⁷ two of which are dominant. The formation of these complex ions can be represented by the reactions:

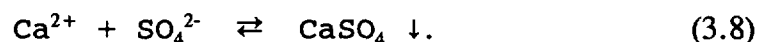


and



The equilibrium constants for these two reactions are $10^{6.1}$ and $10^{4.99}$, respectively. According to the ion-exchange reactions 3.2 and 3.3, the formation of the above insoluble salt and complex ions in oxalic acid will effectively remove both calcium and aluminum ions from the right side of the reactions, thereby accelerating the ion depletion, i.e., the fiber corrosion. Comparing the ion depletion behavior in oxalic acid with that in both hydrochloric and nitric acids (Figures 2.55 and 2.56), it is evident that the anion influence on the ion depletion in oxalic acid was much more significant than the acid concentration, which suggests that the ion depletion in oxalic acid is governed by the mechanism of the anion-controlled leaching.

Based on the same concept, the depletion of calcium ions in sulfuric acid is also ruled by the anion-controlled leaching because the sulfate anion, SO_4^{2-} , can form an insoluble salt with the calcium ion by



The solubility product of calcium sulfate is 7.10×10^{-5} . Since this value is lower than that of calcium oxalate, the leachability of calcium ions is expected to be higher in oxalic acid than in sulfuric acid (Figure 2.55). As for the aluminum ion depletion, its leaching behavior in sulfuric acid should be similar to that observed in hydrochloric and nitric acids, which is controlled by acid concentration, given that the sulfate anion in sulfuric acid can form neither insoluble salts nor complex ions with the aluminum ion. Surprisingly, relatively higher leachability of aluminum ions in sulfuric acid was evident in this study (Figure 2.56). The mechanism of this phenomenon is not clear at present. One speculation is that the calcium and aluminum depletion may not be two independent processes. The high calcium depletion in the sulfuric acid may reduce the stability of the glass structure, thereby facilitating the aluminum depletion. Recently, Jones and Rock observed similar corrosion effects of 0.5 NaHSO₄ (pH 2.2) and 0.5M H₂SO₄ (pH 0.21) on E-glass fiber and proposed that fiber corrosion in sulfuric acid may not obey the

simple ion-exchange reactions between the hydrogen ion in the acid and the metal cations in the glass.⁹⁸ In reality, the dissociation of sulfuric acid in an aqueous solution follows two steps: the first step,



and the second step,



The equilibrium constant of Equation 3.9 is much larger than that of Equation 3.10. The existence of the bisulfate ion, HSO_4^- , in aqueous sulfuric acid may also affect fiber corrosion by weakening the Si-O bonding because this ion is composed of both electron and proton donor sites.^{98,158}

3.2.2 Fracture Mechanism

Spontaneous surface cracking is a well-known phenomenon in acid corrosion of E-glass fiber.^{92,118-120,142} Typical fracture morphologies include axial, spiral (or helical), and radial cracks (Figures 2.57, 2.58, 2.59 and 2.61). At present, the formation mechanisms of these cracks is still unclear. Under acid attack, non-siliceous ions will be leached out continuously from the fiber surface to its interior. This leaching process gradually produces an outer depleted sheath and an inner intact core (Figure 1.10). The replacement of non-siliceous ions by hydrogen ions in the depleted sheath will cause a reduction of molar volume, leading to the shrinkage of the sheath. Because the shrinkage is restrained by the intact inner core, surface tensile stresses will be generated. This stress, increasing with the growth of the depleted sheath, can be high enough to fracture the fiber surface. The above concept was initially proposed by Metcalfe *et al*⁹² and later became well accepted by other investigators.^{50,63} Obviously, Metcalfe's model gives a

reasonable explanation to the formation of surface spiral cracks. For the formation of surface axial cracks, however, the model may be inadequate because in this case the hoop stress, rather than the tensile stress, should be responsible. Another concern with this model is that it does not consider the residual stresses induced in the fiber surface during fabrication, which may contribute substantially to the formation of surface cracks in acid corrosion. In this study, the ion-depletion-depth theory is proposed to correlate the surface crack morphology with the acid leaching process.

The surface crack morphology of acid-corroded fibers is directly dependent on the internal stress state in the fiber surface, which is determined by the balance of two different stresses: (1) the residual stress introduced during fiber fabrication and (2) the shrinkage stress caused by the corrosion-induced volume mismatch between the fiber surface and core.

Glass fiber is a frozen-in, thermodynamically unstable system.¹⁵⁹ Unlike isotropic bulk glass, glass fiber exhibits structural anisotropy, the extent of which is controlled by the thermal and mechanical prehistories of fiber fabrication, particularly the cooling rate and the drawing stress or speed.^{128,160} During processing, the cooling rate can rise to 10^5 °K/s.¹⁶⁰ Such a high cooling rate causes severely non-uniform distribution of temperature across a fiber, with the lowest temperature at the fiber surface and the highest in the fiber center. Conversely, the temperature-dependent viscosity of melted glass becomes higher towards the fiber surface. Under the influence of this viscosity profile, together with the applied drawing stress, a considerable thermal-stress gradient is set up, and the glass layers in a fiber are displaced at different viscosities in the radial direction (Figure 3.4), with higher stresses and velocities being concentrated near the fiber surface. As a result, the glass structure becomes more open, less dense, or even more axially oriented towards the fiber surface, and meanwhile extensive axial strain induced by the drawing stress, along with some radial strain induced by the thermal gradient, will be frozen in the fiber surface, thereby causing the fiber to lose its isotropic character.^{128,159,160} It should be

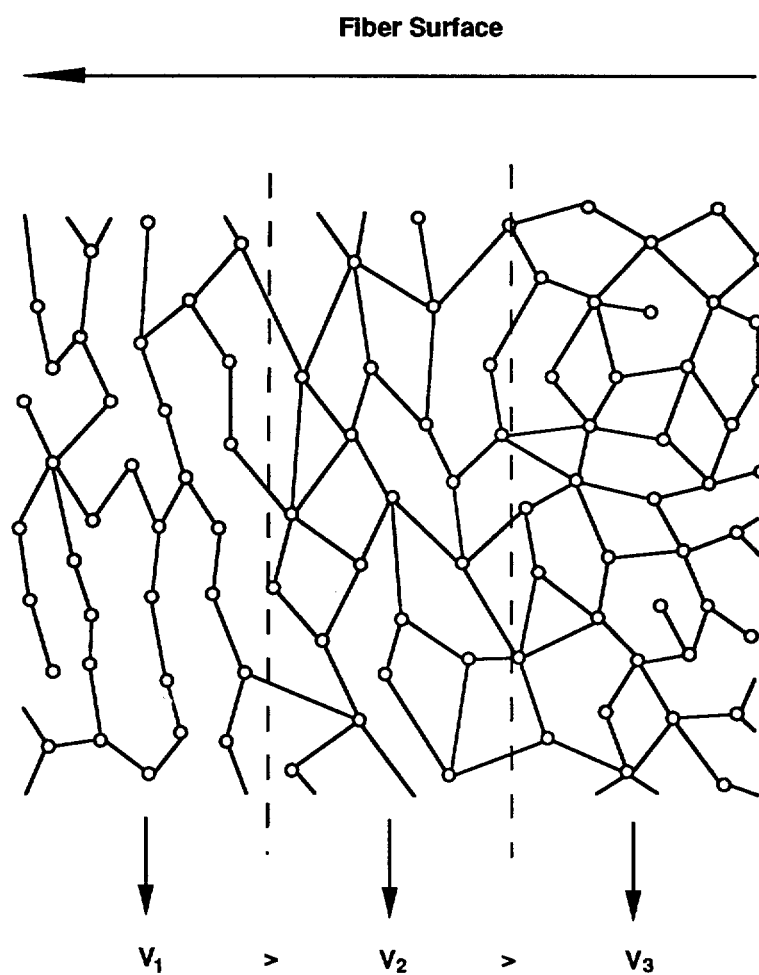


Figure 3.4 Fiber structure change in the radial direction.

noted that in general the structure-changed surface layer in a fiber does not completely coincide with the residual stress-loaded surface layer.¹²⁸ The extent of both layers is highly dependent on the mechanical prehistory. A faster drawing speed leads to a larger structure-changed surface layer but a smaller residual stress-loaded surface layer.

The anisotropy of the structure and deformation in a glass fiber, particularly the surface structure and residual stress state, has a significant influence on the acid corrosion behavior of the fiber. Because of the more open structure near the fiber surface, acid leaching in the surface layer is proven to be much faster than in the core.^{117,128} During a leaching process, the ion exchange of non-siliceous ions in glass with hydrogen ions in acid will simultaneously introduce two changes to the fiber surface. First, acid leaching will cause structural change in glass. The depletion of non-siliceous ions produces a silica-rich layer near the fiber surface and therefore causes a change in the reflective index of the material, resulting in a visual lumen formation,^{128,159} i.e., the development of the core-sheath structure described in Figure 1.10. Under certain circumstances, this core-sheath structure can also be identified on the fiber cross-section in SEM observation.^{64,117} Since the change of fiber radius is negligible in acid leaching,¹¹⁷ the sheath size grows when the leaching progresses.^{117,159} Second, acid leaching will induce a shrinkage stress to the fiber surface. Since this stress is caused by the volume mismatch between the surface layer and the core, it is three-dimensional in nature, containing the axial, hoop, and radial portions.

The surface cracking of glass fiber in acids is a stress-activated process, primarily driven by the residual and the shrinkage stresses. Therefore, the fracture criterion can be simplified by the expression:

$$\sigma_r + \sigma_s \geq \sigma_{fs} , \quad (3.11)$$

where σ_r and σ_s refer to the residual stress and the shrinkage stress, respectively, and σ_{fs}

represents the fracture strength of the depleted sheath, which should be significantly lower than the fracture strength of the glass fiber based on the fact that the severe strength reduction was observed on the acid-treated fibers.^{95,103}

As discussed earlier, residual stresses caused by fiber fabrication are characterized by axial stress but also has a radial portion. They are concentrated in a thin surface layer, the thickness of which is highly dependent on drawing stress as well as fiber diameter. For the fiber of 12 μm in diameter, used in this study, the surface layer loaded with residual stresses is likely to be lower than 0.6 μm if the drawing speed is higher than 21 m/s based on the research conducted by Schimann *et al.*¹²⁸ The shrinkage stresses are three-dimensional in nature. Unlike the residual stresses, these stresses are leaching-dependent; they increase as the leaching process proceeds. If the nature of the stresses is considered, the surface cracking actually is determined by three competing fracture criteria:

$$\sigma_{r,a} + \sigma_{s,a} \geq \sigma_{fs,a} , \quad (3.12)$$

$$\sigma_{s,h} \geq \sigma_{fs,h} , \quad (3.13)$$

and

$$\sigma_{r,r} + \sigma_{s,r} \geq \sigma_{fs,r} . \quad (3.14)$$

In the above three expressions, the subscripts a, h, and r stand for the axial, hoop, and radial direction in a fiber. When the ion-depletion depth is relatively small, the overall stress in the sheath is axial by nature. In this case, the surface cracking is decided by the fracture criterion in Expression 3.12. Once a crack starts at a certain point on the fiber surface, it tends to turn around the fiber with small pitch angles to attenuate the internal axial stress, the surface crack exhibiting a spiral morphology (Figures 2.59 and 2.61). When the ion-depletion depth is sufficiently larger, however, hoop stress becomes

dominant. The fracture criterion in Expression 3.13 will be favorable, and thereby axial cracks are preferentially developed on the fiber surfaces (Figure 2.57). Based on this concept, it is reasonable to assume that at a particular ion-depletion depth the fracture criteria in Expressions 3.12 and 3.13 are compatible, leading to the mixed morphology of spiral and axial cracks.⁵⁴ Obviously, this transition depth will vary with the thickness of the surface layer affected by residual stresses; the thicker the stress-loaded layer, the larger the transition depth will be. This ion-depletion-depth theory is further supported by the evidence of a much greater crack penetration depth of axial cracks when compared to spiral cracks (Figures 2.65). The formation of radial cracks can be associated with the formation of either axial (Figures 2.58 and 2.65a) or spiral cracks,^{92,119} depending on the thermal prehistory in the fiber fabrication. According to Expression 3.14, the higher the radial strain is introduced by the thermal prehistory, the less the radial shrinkage stress, i.e., the shorter the ion-depletion depth, is required to generate the radial crack.

The ion-depletion-depth theory, however, is seriously challenged by the argument that it is impossible to obtain solely axial cracks without the presence of spiral cracks given that the ion-depletion depth increases continuously during acid leaching. This dilemma can be resolved by an important experimental finding made by Bledzki *et al.*¹⁴² They confirmed that the surface crack could not form in the acid leaching process, i.e., in the wet environment, until the water in the corroded fiber was completely evaporated. This phenomenon may be caused by the reduction of the shrinkage stress in the wet environment. In acid leaching, the micro-pores produced by the ion exchange in the fiber surface will be filled with water so that the tendency toward volume shrinkage, or related shrinkage stresses, will become much smaller than it otherwise would be. As a result, overall internal stresses are not sufficiently high to promote surface cracks. During the drying process, the water in the micro-pores will be replaced by air. Since the compressibility of air is much higher than that of water, the shrinkage stress will gradually increase, finally exceeding the critical stress for fiber surface cracking.

3.3 Crack Tip Chemistry

Stress corrosion fracture of materials involves localized corrosion that is confined to the tip of a progressively propagated crack. Depending on the crack tip system, the crack tip chemistry can be significantly different from the global environment to which materials are exposed.^{161,162} In stress corrosion of GRP composites in acids, the crack tip system is extremely complex due to both the heterogeneity of composites and the interaction between selective composite components and acidic environments (Figure 3.5), leading to a less acidic, neutral, or sometimes even basic crack tip environment. GRP composites consist of three basic elements: glass fiber, resin matrix, and fiber/resin interface sizing. Glass fiber is silica based with additions of various non-siliceous oxides. Sizing generally contains both inorganic and organic groups to achieve the coupling between fiber and resin. Compared with glass fiber and sizing, resin possesses a much more complicated chemical composition. Formulated by a base polymer, a filler material, and a variety of additives, a resin actually is a mixture of assorted functional organic or inorganic compounds. Crack tip chemistry is not only dependent on the chemical compositions of each component in composites but also on global acidic environments, particularly their nature and concentration as well as environmental temperatures, and more importantly, on selective chemical attack of acidic environments on different constituents in composites.

3.3.1 Acid Leaching of Glass Fiber

In acid stress corrosion, the crack tip chemistry in a composite is dominated by acid leaching of glass fiber, which is achieved by ion-exchange reactions between non-siliceous ions in glass and hydrogen ions in acids. Because the dissolution of non-siliceous ions consumes the hydrogen ions and because depleted non-siliceous ions, mostly metal ions in E-glass, diffuse into the solution adjacent to the fiber, the pH value of the solution at the crack tip will increase, thereby causing the crack tip solution to

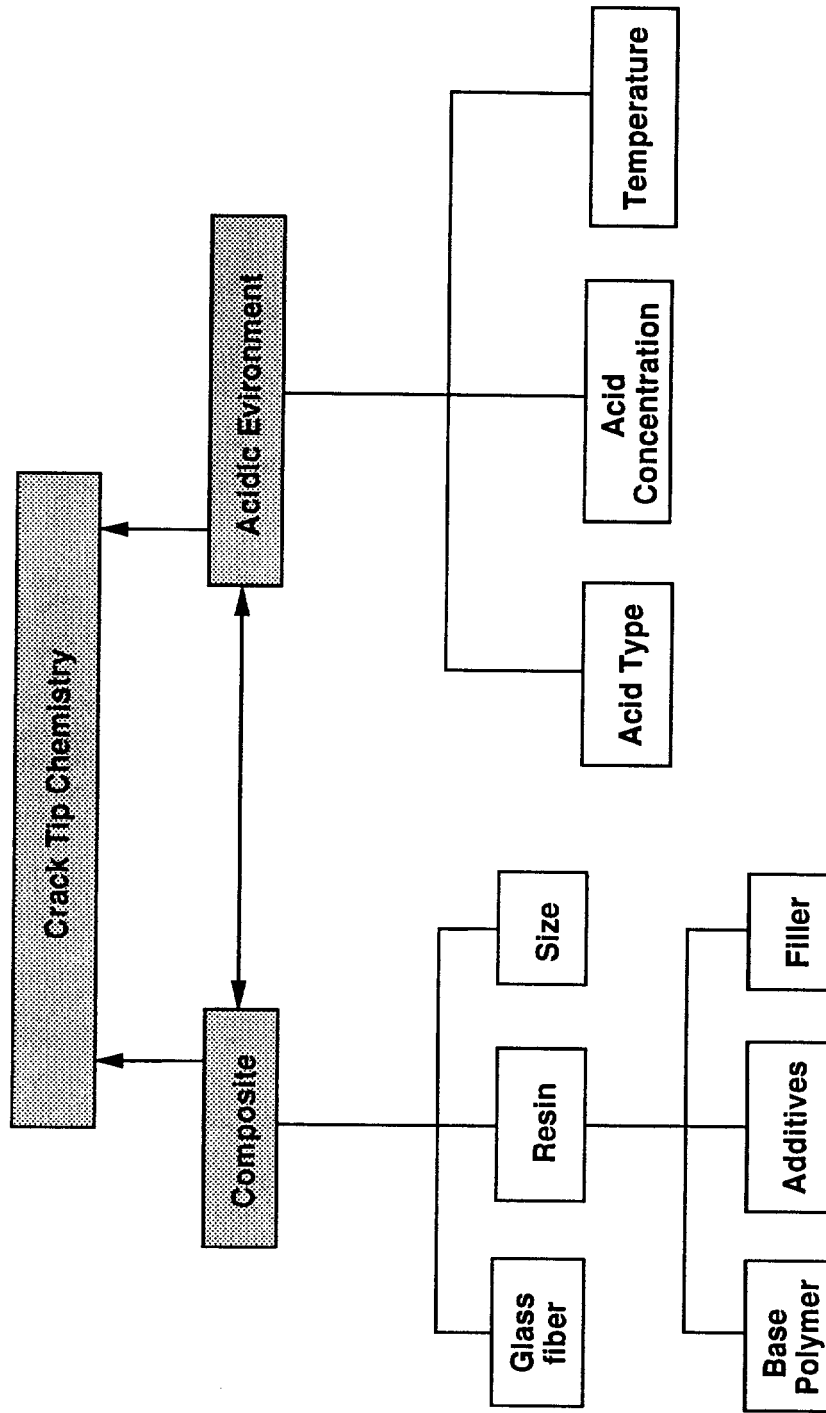


Figure 3.5 Crack tip chemistry in acid corrosion of composites.

become less acidic (Figure 3.6). A similar phenomenon was also observed by Sedriks *et al* in the study on stress corrosion cracking of aluminum alloys exposed to acidic environments.¹⁶² Their study further confirmed that crack tip chemistry would reach an equilibrium state in a short time, forming a steady pH region at the crack tip; for instance, in an aluminum alloy exposed to a bulk solution of pH 0, the crack tip solution could stabilize at approximate pH 3.5.

Based on this concept, at a certain bulk concentration, defined as a critical acid concentration, it is possible that the crack tip solution will be neutralized as a result of initial acid leaching. Under such circumstances, the crack can not propagate. This behavior was actually observed in this study during stress corrosion experiments conducted on E-glass fiber/polyester composite in both oxalic and nitric acids (Figures 3.35 and 2.38). The critical acid concentration appeared to be approximately pH 4.5 for oxalic acid and pH 3.5 for nitric acid, which is in accordance with the value proposed by Akhtar *et al* based on their stress corrosion study of E-glass/polyester and E-glass/epoxy composite rods exposed to nitric acid.¹⁷ The existence of the critical acid concentration further implies that the crack tip chemistry is not only affected by the acid concentration of the bulk solution but also by the nature of the acid itself. As discussed in Section 3.2.1, nitric acid corrosion is dominated by the acid-strength leaching mechanism, while oxalic acid corrosion is dominated by the anion-controlled leaching mechanism. Because of the involvement of oxalate anions in acid leaching, the crack tip chemistry becomes more complex, and meanwhile the capacity of the crack tip solution to neutralize the acid may be reduced, resulting in a higher critical concentration of oxalic acid. Therefore, the composite exhibited a greater susceptibility to stress corrosion cracking in oxalic acid than in nitric acid, which was consistent with the acid corrosion result obtained from this study (Figure 2.34).

The influence of anions that can form insoluble salts or complex ions on stress corrosion behavior of composites, similar to that on acid corrosion behavior of glass fibers,

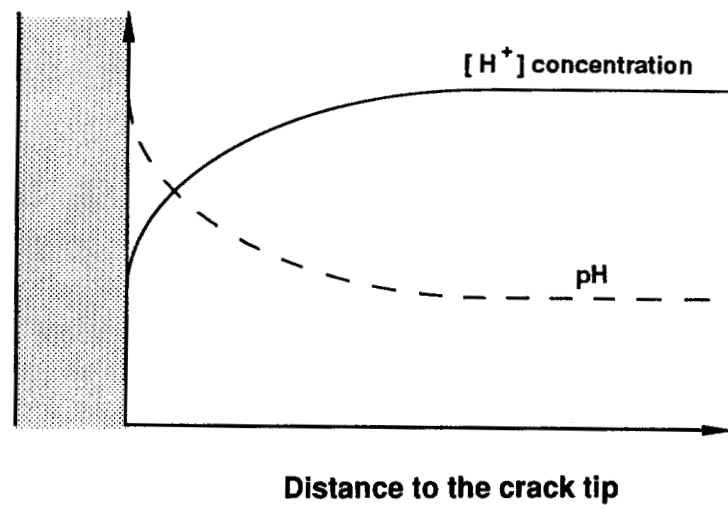
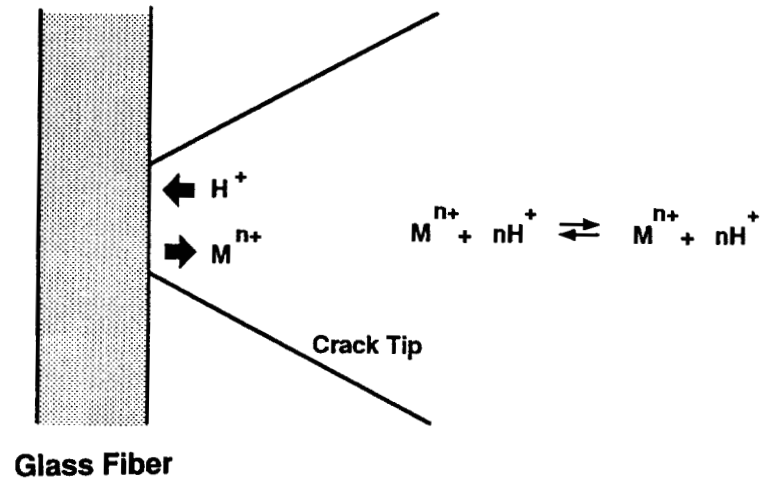


Figure 3.6 Localized environment at the crack tip.

actually is twofold: acceleration and passivation. The formation of insoluble salts or complex ions, on one hand, can also accelerate stress corrosion by increasing ion depletion rate from glass and thereby shortening the crack initiation stage but on the other hand, can inhibit stress corrosion by producing a surface film on the fiber, which functions as a barrier to ion diffusion. Whether the acceleration or passivation mechanism is dominant depends on both the nature and concentration of the acids involved. For a given acid, a lower acid concentration generally is favorable to the acceleration mechanism; however, a higher concentration is beneficial to the passivation mechanism, thus resulting in a critical acid concentration between two regions in which different mechanisms are dominated. This concept was supported by the results obtained from stress corrosion experiments in oxalic acid. The critical concentration for oxalic acid happened to be around pH 1. During the experiments, the crack growth rate accelerated with increasing the acid concentration from pH 6 to pH 2; however, the crack stopped growing when the acid concentration increased to pH 1. It was likely that the passivation mechanism was operating at this acid concentration by forming mixed precipitates of insoluble calcium oxalate and complex aluminum oxalate ions on the fiber surface at the crack tip, which acted as a barrier to further ion exchange, and thus suppressed the crack propagation.

3.3.2 Dissolution of Composites in Aqueous Solutions

Dissolution of each component in composites, particularly resins and sizing, in aqueous solutions may affect the crack tip chemistry during stress corrosion of composites in acidic environments. Relative to the influence caused by acid leaching of glass fibers, the influence of this dissolution on the crack tip chemistry is trivial at room temperature because of low solubilities of water-soluble compounds and low dissolution rates, but it becomes increasingly important with an increase in temperature. Water by nature is a good solvent for ionic compounds and can react with many oxides. When composites are exposed to water, or aqueous acid solutions, the water-soluble compounds in the

composites will be removed. The dissolution of these compounds and their further reactions with the solution may lead to a change in the solution chemistry. Depending on the nature of solutions and the constituents of composites, particularly the solubility of water-soluble compounds, the solution can become more acidic or more basic. In this study, water extraction experiments revealed that for the E-glass/polyester composite with aluminum trihydrate filler, the extract stabilized approximately at pH 5, while for the composite with calcium carbonate filler, however, the stable pH of the extract reached as high as 10. This result suggests that the E-glass/polyester composite with calcium carbonate filler may have a greater capability to neutralize diluted acid solutions at the crack tip during stress corrosion and thus less susceptibility to stress corrosion in comparison with the composite with aluminum trihydrate filler.

It should be noted that the pH value of the composite extract may not be solely attributed to the dissolution of the filler material in the resin. The water extraction experiments conducted in this study revealed that both aluminum and calcium ions were present in the extract either from the composites with aluminum trihydrate filler or from the composite with calcium carbonate filler (Figures 2.67 and 2.69), indicating that water-soluble compounds from sources other than the filler material were also involved in the extraction process. The fact that the calcium ion concentration in both of the extracts appeared to be much higher than the aluminum concentration further suggested that the filler in the resin might not be the major source of the extracted calcium and aluminum ions. The dissolution of other water-soluble compounds in the composite, likely additives in the resin, might also be responsible for calcium and aluminum concentrations in the extracts. Moreover, under solvent attack, base polymers in resins might undergo hydrolysis, which was probably acid or base catalyzed, or oxidation,¹⁰⁸ and at elevated temperatures leaching of low molecular weight compounds in resins was also possible. Given the complexity of resin formulation, other ions in addition to calcium and aluminum ions were also likely to be present in the extract, modifying the chemistry in the solution.

The chemical durability of glass fiber in water is highly dependent on the composition of glass, particularly the content of alkali oxides in glass, such as sodium and potassium oxide. The higher the content of alkali oxides in glass, the higher the susceptibility of glass to water attack. Since E-glass contains a minute amount of alkali oxides (Table 2.8), dissolution of the E-glass constituents in water is unlikely to occur. Additionally, E-glass exhibits excellent resistance to basic solutions,^{50,101} which was confirmed by the immersion test of E-glass fibers in the pH 10 extract obtained from the composite with calcium carbonate filler (Figure 2.72 and Table 2.10). Therefore, the influence of E-glass fiber on the crack tip chemistry in stress corrosion is primarily attributed to acid leaching.

3.3.3 Thermal Effects

In insulator service, localized heating caused by electrical discharges may lead to chemical degradation of composites. When exposed to elevated temperatures, a composite, particularly the resin matrix and sizing both made of organic constituents, may become unstable by losing volatile compounds (Figure 2.71 and Table 2.10). The chemical composition of decomposed compounds are likely to change with resin polymer and temperature; in the temperature range from 100 to 160°C, the thermally decomposed byproducts from E-glass fiber/polyester composite were dominated by weak organic acids. These acids, either by themselves or by reacting with other ionic species leached out from composite components, can complicate the crack-tip chemistry considerably. Furthermore, when a composite is exposed to aqueous environments, an increase in temperature generally enhances the dissolution of its water-soluble compounds by raising their solubilities and accelerates thermally activated chemical reactions involved, such as hydrolysis or leaching of polymers.

CHAPTER 4

SUMMARY

4.1 Conclusions

This systemic study leads to a comprehensive understanding of brittle fracture mechanisms of GRP insulators. The most significant conclusions obtained from the study are outlined below:

Insulator failure analysis

1. The planar fracture morphology of service-failed or -damaged insulators and the formation of large mirror sizes on the fractured fiber surfaces reveal that stress corrosion cracking is the principal failure mode for the brittle fracture of insulators.
2. Both calcium and aluminum depletion are detected in the fractured fiber ends, calcium depletion being more severe than aluminum depletion. This finding strongly suggests that acid corrosion of glass fibers in the brittle fracture process is controlled by the ion-exchange mechanism.
3. Irregular fiber and resin deformation represented by melted fibers and resin decomposition, for the first time, is identified on the insulator fracture surface. Melted fibers are located adjacent to the external surface of composite rods, while resin decomposition can either prevail over the entire fracture surface or exist in scattered local regions. High-voltage fracture experiments conducted in this study further verify that these two features are in fact the characteristics of electrical discharge-induced fracture in GRP composites.

4. All of the insulator fracture surfaces examined in this study are free from any post-failure damage; the fractured fiber surfaces retain initial fracture markings without further visible deterioration. This phenomenon indicates that service acidic environments may not be highly concentrated or only temporarily stay in contact with the fracture surface during the fracture process.
5. Zinc and iron are detected in the deposits formed on the internal fracture surfaces away from the high-voltage end. Since zinc and iron can only come from the metal casting, the identification of these elements provides direct evidence of metal casting corrosion.
6. Structural damage inside the high-voltage end, epoxy/sheath interface debonding and/or circumferential cracking in the epoxy potting material, creates the initial access for external environments to the composite rod, thereby destroying the integrity of the insulator system and promoting brittle fracture by stress corrosion cracking.
7. Estimation of the composite rod's fracture stress via the direct mirror size measurement and the rule of mixture is shown to be invalid. The stress overestimate is likely caused by extending the empirical fracture stress/mirror size relationship obtained from bare glass fibers to composite materials and by applying the rule of mixture to the strength calculation.

Stress corrosion experiments

1. Stress corrosion behavior of composites is dependent on the nature of acids. Oxalic acid is much more aggressive to E-glass fiber/polyester composite than nitric acid at the same concentration.
2. Acid concentration plays an important role in acid corrosion of composites; a higher acid concentration leads to a faster crack growth rate.
3. There likely exists a critical acid pH, above which stress corrosion fracture is inhibited. This critical acid pH, determined by crack tip chemistry, varies with

both the nature of acids and the composition of composites. For E-glass fiber/polyester composite, the critical acid pH approximates 3.5 for oxalic acid and 4.5 for nitric acid, while for different materials tested in nitric acid, the critical acid pH reduces in the sequence of E-glass fiber/polyester, /epoxy, and /vinyl ester composite.

4. Crack growth in stress corrosion accelerates with applied tensile load. The relationship between them obeys a power law.
5. The propagation behavior of stress corrosion cracks in E-glass fiber/polymer composites is highly influenced by the resin matrix. Among the three composite systems tested in nitric acid, epoxy composite exhibits better stress corrosion resistance than polyester composite, while vinyl ester composite is superior to both epoxy and polyester composites.
6. Water by itself can not initiate stress corrosion fracture in E-glass fiber/polyester composite.

Electrical discharge experiments

1. Stress corrosion fracture can be generated in GRP composites under the synergistic influence of mechanical load and electrical discharge in the presence of water.
2. The fracture morphology induced in high-voltage fracture experiments closely resembles that of service-failed insulators, particularly in the fracture initiation site.
3. Electrically discharging polyester resin and E-glass fiber/polyester composite produces various organic compounds; however, no oxalic acid is identified in the discharge byproducts.

Acid corrosion behavior of E-glass fiber

1. Acid corrosion of E-glass fiber is primarily attributed to calcium and aluminum depletion, the severity of which is determined by the nature of acids.

2. Oxalic and sulfuric acids are much more corrosive to E-glass fiber than hydrochloric and nitric acids. This behavior results from different acid leaching mechanisms; leaching is controlled by acid concentration in hydrochloric and nitric acids but dominated by the formation of insoluble salts or complex ions in oxalic and sulfuric acids.
3. Axial and spiral crack morphologies are observed in fiber acid corrosion. Based on the internal stress analysis, an ion-depletion-depth theory is established to explain fiber cracking mechanisms; the axial crack formation is likely associated with a larger ion-depletion depth relative to the spiral crack formation.
4. The susceptibility of fiber surface cracking in acids suggests that the tendency to form post-failure damage in E-glass fiber is much greater in oxalic and sulfuric acids than in hydrochloric and nitric acids.

Crack tip chemistry

1. Calcium and aluminum ions are found in the water extracts from E-glass fiber/polyester composites. Calcium ions appear to be water soluble in nature, while aluminum ions are mostly bonded with other anions, forming precipitates in the extracts.
2. The extract chemistry is not exclusively determined by the filler material used in the resin formulation but by the chemical composition of each composite component, particularly the formulation of resins as well as sizing agents.
3. The stabilized pH value of extracted composite solutions can be acidic or basic in nature, as influenced by both leached ions from composites and their further interactions.
4. E-glass fiber/polyester composite has been shown thermally unstable; the composite, particularly the resin matrix, readily decomposes at the temperature around 100°C, releasing a variety of volatile organic compounds.

From the above findings, failure mechanisms are proposed for insulator brittle fracture based on the synergistic influence of mechanical, environmental and electric stresses. In service, nitric acid induced by electrical discharges on either external surfaces of the rubber sheath and weathersheds, or on the internal fracture surfaces in the composite rod is likely to dominate insulator service environments, although other acids, such as sulfuric acid present in acid rain or oxalic acid generated by void-induced discharge in some composites, may also be involved. The failure mechanisms suggest that for the insulators with the cone end-fitting design, epoxy/sheath interface debonding and circumferential cracking in the epoxy potting material inside the high-voltage end are most likely responsible for the initiation of brittle fracture. Further interaction of acidic media with the composite components may lead to longitudinal delamination in the composite rod by fiber/resin interface debonding, thereby transferring acidic media internally to the rod section away from the high-voltage end through capillary effect. As a result of acid attack along with applied tensile loads, the composite rod will fracture in a brittle fashion by stress corrosion cracking.

4.2 Recommendations

Based on the results obtained from this study and the literature search, the following recommendations are presented in hopes of improving in-service integrity of GRP insulators under the synergistic influence of mechanical, environmental, and electric stresses, thereby minimizing the likelihood of brittle fracture:

1. The high-voltage end, a crucial component in an insulator system, usually experiences the highest mechanical, environmental, and electric stresses. Any reduction in these stresses can enhance insulator performance considerably. First, the end fitting should be designed to shield the composite rod from any environmental attack. The insulator failure analysis conducted in this study, in addition to field experience, indicates that the initiation of insulator brittle fracture

usually results from the ingress of external moisture or corrosive media into the space between the rod and the metal casting due to inadequate sealing. Second, sharp contours in the end-fitting structure should be eliminated to minimize mechanical stress concentration inside the end fitting. Additionally, mechanical properties of the end-fitting components (the composite rod, polymer sheath, and epoxy potting material) should be matched as closely as possible to ensure that the seal between one another does not break when the insulator is subjected to mechanical loading transients. Third, in high-voltage applications the end fitting should be equipped with grading rings. More importantly, the location and size of grading rings, relative to their applications, must be appropriately adjusted to achieve a maximum reduction of electric stresses near the high-voltage end and thereby to diminish electrical damage to the polymer housing materials and the tendency to form nitric acids.

2. The stress corrosion resistance of composites is highly dependent on the chemical composition of glass fibers. E-glass fiber, the commonly used reinforcement in insulator composite rods, exhibits high susceptibility to acid corrosion, given its high non-siliceous ion content. In recent years, intensive studies conducted on ECR-glass fiber and its composites have indicated an encouraging sign: ECR-glass fiber possesses superior acid resistance to E-glass fiber. Furthermore, A-glass, Cemil-glass, and R-glass are also reported to be more acid resistant than E-glass. However, electrical and mechanical properties of these glasses must be further evaluated before they can be utilized in electrical insulation applications.
3. The selection of matrix resins, in addition to glass fibers, is essential to the composite performance in stress corrosion environments. It is likely that a good combination of resin fracture toughness and chemical resistance is beneficial to stress corrosion resistance of GRP composites. The results obtained in this study suggest that for E-glass fiber reinforced composites subjected to stress corrosion in nitric acid, the vinyl ester matrix performs better than both the epoxy and polyester matrices.

4. Polymer housing materials should be formulated to optimize their hydrophobicity in polluted environments and to improve their resistance to electrical damage, particularly corona cutting and erosion.

4.3 Future Research

This study provides a deeper insight into the brittle fracture phenomenon of insulators. To obtain practical guidelines for current insulator application, further research should focus on the following critical issues:

1. One of the ultimate goals for studying insulator brittle fracture is to predict the insulator service life once brittle fracture is initiated according to crack growth rate in the stress corrosion of composites .
2. The high-voltage fracture experiments have verified that stress corrosion cracking can be generated in E-glass fiber/polyester composite subjected to the synergistic influence of mechanical and electrical stresses in the presence of water. The chemical nature of the corrosive environment induced under such a circumstance needs to be identified.
3. Further studies on stress corrosion resistance of composite systems with different combinations of glass fibers and resin matrices are essential. Since the behavior of composites under mechanical and environmental stresses may significantly differ from that when electric stresses are superimposed, stress corrosion resistance of composites should be evaluated independently in the above two situations.

REFERENCES

1. J. F. Hall, R.S. Gorur, S. Grzybowski, and T. Orbeck, "History and Bibliography of Polymeric Insulators for Outdoor Applications," Report of the IEEE Nonceramic History/Bibliography Task Force of the Transmission and Distribution Committee, 1991.
2. E.H. Abilgaard and E.A. Bauer, "Composite Longrod Insulators and Their Influence on the Design of Overhead Lines," *CIGRE 1976 Session*, Paper 22-03.
3. E.A. Cherney, "Partial Discharge - Part V: PD in Polymer-Type Line Insulators," *IEEE Electr. Insul. Mag.*, 7 (1991) 28.
4. R.N. Essig, "Polymer/Fiberglass Insulators," in *Proceedings of the 44th Annual Technical Conference & Exhibition* (The Society of Plastics Engineers, 1986) p.255.
5. E.A. Cherney and D.J. Stonkus, "Non-Ceramic Insulators for Transmission Lines," *Ontario Hydro Research Review*, 3 (1981) 25.
6. H.M. Schneider, J.F. Hall G. Karady, and J. Rendowden, "Nonceramic Insulators for Transmission Lines," *IEEE Trans. Power Delivery*, 4 (1989) 2214.
7. E.A. Cherney, "State-of-the-Art Review on Composite Insulators for Distribution," Position Paper for the Canadian Electrical Association (SD-4), 1985.
8. E.A. Cherney, "State-of-the-Art Review on Polymer Insulator Technology for Transmission," Position Report for the Canadian Electrical Association (ST-275), 1987.
9. E.A. Cherney, J. Reichman, D.J. Stonkus, and B.E. Gill, "Evaluation and Application of Dead-End Type Polymeric Insulators to Distribution," *IEEE Trans. Power Appar. Syst.*, PAS-103 (1984) 121.
10. H. Dietz, H. Karner, K.H. Muller, and H.J. Patrunky, "Latest Developments and Experience with Composite Longrod Insulators," *CIGRE 1986 Session*, Paper 15-09.
11. R.G. Houlgate, D.A. Swift, A. Cimador, F. Pourbaix, G. Marrone, and P. Nicolini, "Field Experience and Laboratory Research on Composite Insulators for Overhead Lines," *CIGRE 1986 Session*, Paper 15-12.

12. R.S. Gorier, "Surface Dielectric Behavior of Polymeric Insulation under HV Outdoor Conditions," *IEEE Trans. Electr. Insul.*, 26 (1991) 1064.
13. American National Standard for Electrical Power Insulators - Test Methods, ANSI C29.1, 1988.
14. American National Standard for Composite Suspension Insulators for Overhead Transmission Lines - Tests, ANSI C29.11, 1989.
15. K.K. Chawla, *Composite Materials Science and Engineering* (Springer-Verlag New York Inc., 1987).
16. J.C. Watson and N. Raghupathi, "Glass Fibers," in *Engineered Materials Handbook - Volume 1: Composites*, edited by ASM International Handbook Committee (ASM International, 1987) p.107.
17. A. Akhtar, J.S. Nadeau, J.Y. Wang, D.P. Romily, and C. Taggart, "Brittle Fracture of Non-Ceramic Insulators," Report for the Canadian Electrical Association (186 T 350), 1986.
18. R. Matzeg and D. Santrach, "The Contribution of ECRGLAS to the Corrosion resistance of FRP," Internal Report, Fiberglas Canada Inc., 1991.
19. J.D. Martin and J.E. Sumerak, "Pultrusion," in *Engineered Materials Handbook - Volume 1: Composites*, edited by ASM International Handbook Committee (ASM International, 1987) p.533.
20. E.L. Rodriguez, "Microdelamination due to Resin Shrinkage in Filament-Wound Fiberglass Composites," *J. Mater. Sci. Lett.*, 8 (1989) 116.
21. T.S. McQuarrie, "The Thermal, Mechanical, and Chemical Resistant Properties of Pultruded Core Rods Used in Polymeric Insulators," Presented at the NCI Workshop, High Voltage Transmission Research Center, October 1991.
22. H. Ishida and J.L. Koenig, "The Reinforcement Mechanism of Fiber-glass Reinforced Plastics under Wet Conditions: A Review," *Polym. Eng. Sci.*, 18 (1978) 128.
23. W.D. Bascom, "Fiber Sizing," in *Engineered Materials Handbook - Volume 1: Composites*, edited by ASM International Handbook Committee (ASM International, 1987) p.122.
24. W.D. Bascom, "Structure of Silane Adhesion Promoter Films on Glass and Metal Surfaces," *Macromolecules*, 5 (1972) 792.

25. W.T. Starr, "Polymeric Outdoor Insulation," *IEEE Trans. Electr. Insul.*, 25 (1990) 125.
26. R.S. Gorier, J.W. Chang, and O.G. Amburgey, "Surface Hydrophobicity of Polymers Used for Outdoor Insulation," *IEEE Trans. Power Delivery*, 5 (1990) 1923.
27. E.A. Cherney and D.J. Stonkus, "Non-Ceramic Insulators for Contaminated Environments," *IEEE Trans. Power Appar. Syst.*, PAS-100 (1981) 131.
28. T. Tanaka, K. Naito, and J. Kitagawa, "A Basic Study on Outdoor Insulators of organic Materials," *IEEE Trans. Electr. Insul.*, EI-13 (1978) 184.
29. The Ohio Brass Company, *Polymer Materials for Insulator Weathersheds*, 1991.
30. S.M. de Oliveira and C.H. de Turreil, "Aging of Distribution Composite Insulators under Environmental and Electrical Stresses," *IEEE Trans. Power Delivery*, 5 (1990) 1074.
31. American Society for Testing and Materials Standard: Zinc-Coating (Hot-Dip) on Iron and Steel, ASTM A153-82 (R1987).
32. R.A. Mitchell, M. Asce, R.M. Woolley, and N. Halsey, "High-Strength End Fitting for FRP Rod," *J. Eng. Mech. Div.*, August (1974) 687.
33. R. Mier-Maza, J. Lanteigne, and C. de Turreil, "Failure Analysis of Synthetic Insulators with Fiberglass Rod Submitted to Mechanical Loads," in *Proceedings of the IEEE/PES 1983 Winter Meeting*, 1983, Paper 133-6
34. CIGRE Working Group 10 of Study Committee 22, "Suspension and Tension Composite Insulators for Overhead Lines," *CIGRE 1980 Session*, Paper 22-80.
35. H. Chandler and J. Reynders, "Electro-Chemical Damage to Composite Insulator," *CIGRE 1984 Session*, Paper 33-08.
36. J.H. Greenwood, "The Brittle Fracture Problem in Composite Insulators," ERA Report 84-0086, 1984.
37. H. Weihe, R.E. Macey, and J.P. Reynders, "Field Experience and Testing of New Insulators in South Africa," *CIGRE 1980 Session*, Paper 22-03.
38. E. Bauer, K.H. Muller, H. Karner, and P. Verma, "Service Experience with the German Composite Long Rod Insulator with Silicone - Rubber Sheds since 1967," *CIGRE 1980 Session*, Paper 22-11.

39. F. Bianchi, G. Marrone, C. Massetti, and A. Pignini, "Recent Laboratory and Field Experiences on Composite Insulators in Italy," in *Proceedings of Italy - U.S.A. Joint UHV Program*, 1982. p.106.
40. M. Cojan, J. Perret, C. Malaguti, P. Nicolini, J.S.T. Looms, and A.W. Stannett, "Polymeric Transmission Insulators: Their Application in France, Italy, and the U.K.," *CIGRE 1980 Session*, Paper 22-10.
41. M. Ezrin and J. Gartner, "Test Method for Evaluation of the Resistance of Fiberglass Rods to Combined Mechanical and Chemical Stress," *IEEE Trans. Power Appar. Syst.*, PAS-103 (1984) 2741.
42. Bonneville Power Administration, "Field Test Insulator," Test Report, April 1992.
43. CIGRE Working Group 03 of Study Committee 22, "Guide for the Identification of Brittle Fracture of Composite Insulator FRP Rod," *Electra*, 143 (1992) 61.
44. M.J. Owen, S.J. Harris and B. Noble, "Failure of High Voltage Electrical Insulators with Pultruded Glass Fiber-Reinforced Plastic Cores," *Composites*, 17 (1986) 217.
45. S.J. Harris, B. Noble, and M.J. Owen, "Metallographic Investigation of the Damage Caused to GRP by the Combined action of Electrical, Mechanical, and Chemical Environments," *J. Mater. Sci.*, 19 (1984), 1596.
46. H.D. Chandler, R.L. Jones, and J.P. Reynders, "Stress Corrosion of Composite Long Rod Insulators," in *Proceedings of the 4th International Symposium on High Voltage Engineering*, 1983, Paper 23.09.
47. B. Noble, S.J. Harris, and M.J. Owen, "Stress Corrosion Cracking of GRP Pultruded Rods in Acid Environments," *J. Mater. Sci.*, 18 (1983) 1244.
48. C. de Turreil, "Influence of Acidic Solution on the Fracture Mode of Non-Ceramic Insulator GRP Rods," *Transactions: Engineering and Operation Division - Volume 22, Part 4* (Canadian Electrical Association, 1983) p.1.
49. A. Akhtar and J.Y. Wong, "Failure Analysis of Brittle Fracture in Nonceramic Insulators," *J. Compos. Technol. Res.*, 9 (1987) 95.
50. P.J. Hogg and D. Hull, "Corrosion and Environmental Deterioration of GRP," in *Developments in GRP Technology - Volume 1*, edited by B. Harris (Elsevier Science Publishers Ltd., 1983) p.37.

51. J.N. Price, *Stress Corrosion Cracking in Glass Reinforced Composites*, in *Fractography and Failure Mechanisms of Polymers and Composites*, edited by A.C. Roulin-Moloney (Elsevier Science Publishers Ltd., 1989) p.495.
52. H.A. Barker, I.G. Baird-Smith, and F.R. Jones, "Large Diameter GRP Pipes in Civil Engineering - The Influence of Corrosive Environments," in *Proceedings of Symposium on Reinforced Plastics in Anti-Corrosion Applications* (Great British National Engineering Laboratory, 1979) Paper 12.
53. L.S. Norwood, "GRP in Contact with Acidic Environments - A Case Study," *Composite Structure*, 2 (1984) 1.
54. H.D. Chandler, R.L. Jones, P.J. Eccleston, and J.P. Reynders, "Fractures in GRP - A Link with Corrosion," in *Proceedings of the 2nd National Conference on Fracture*, edited by R.B. Tait and G.G. Garrett (Pergamon Press, 1984) p.79.
55. P.J. Hogg, J.N. Price, and D. Hull, "Stress Corrosion of GRP," in *Proceedings of the 39th Annual Conference on Reinforced Plastics/Composites* (The Society of the Plastics Industry Inc., 1984) Session 5-C.
56. H.H. Collins, "Strain-Corrosion Cracking of GRP Laminates," *Plast. and Rubber: Mater. Appl.*, 3 (1978) 6.
57. D. Hull and P.J. Hogg, "Nucleation and propagation of Cracks during Strain Corrosion of GRP, in Advances in Composite Materials," in *Proceedings of the 3rd International Conference on Composite Materials - Volume 1*, edited by A.R. Bunsell et al (Pergamon Press, 1980) p.543.
58. B.D. Caddock, K.E. Evans, and D. Hull, "The Role of Diffusion in the Micromechanisms of Stress Corrosion Cracking of E-glass/Polyester Composites," in *Proceedings of the 2nd International Conference on Fiber Reinforced Composites* (Institution of Mechanical Engineers, 1986) p.55.
59. D. Hull, M.S. Kumosa, and P.N. Price, "Stress Corrosion of Aligned Glass Fiber-Polyester Composite Material," *Mater. Sci. Technol.*, March (1985) 177.
60. P.J. Hogg, "Factors Affecting the Stress Corrosion of GRP in Acid Environments," *Composites*, 14 (1983) 254.
61. R.C. Roberts, "Environmental Stress Cracking of GRP: Implication for Reinforced Plastics Process Equipment," *Composites*, October (1982) 299.
62. J.N. Price and D. Hull, "Propagation of Stress Corrosion Cracks in Aligned Glass Fiber Composite Materials," *J. Mater. Sci.*, 18 (1983) 2798.

63. K. Friedrich, "Stress Corrosion Crack Propagation in Glass Fiber Reinforced/ Thermoplastic PET," *J. Mater. Sci.*, 16 (1981) 3292.
64. F.R. Jones, J.W. Rock, and J.E. Bailey, "The Environmental Stress Corrosion Cracking of Glass Fiber-Reinforced Laminates and Single E-Glass Filaments," *J. Mater. Sci.*, 18 (1983)1059.
65. F.R. Jones, J.W. Rock, and A.R. Wheatley, "Stress Corrosion Cracking and its Implications for the Long-Term Durability of E-glass Fiber Composites," *Composites*, 14 (1983) 262.
66. J.N. Price, and D. Hull, "Effect of Matrix Toughness on Crack Propagation during Stress Corrosion of Glass Reinforced Composites," *Compos. Sci. Technol.*, 28 (1987) 1993.
67. P.J. Hogg, "A Model for Stress Corrosion Crack Growth in Glass Reinforced Plastics," *Compos. Sci. Technol.*, 38 (1990) 23.
68. P.J. Hogg and D. Hull, "Role of Matrix Properties on the Stress Corrosion of GRP," in *Proceedings of the 13th BPF Reinforced Plastics Congress* (British Plastics Federation, London, 1982) Paper 29.
69. H. Hojo and K. Tsuda, "Effects of Chemical Environments and Stress on Corrosion Behaviors of Glass Fiber Reinforced Plastics and Vinyl Ester Resin," in *Proceedings of the 34th Annual Technical Conference on Reinforced Plastics/ Composites* (The Society of the Plastics Industry, Inc., 1979) Section 13-B.
70. J.E. Bailey, T.M.W. Fryer, and F.R. Jones, "Environmental Stress-Corrosion Edge-Cracking of Glass Reinforced Polyesters," in *Proceedings of the 3rd International Conference on Composite Materials - Volume 1*, edited by A.R. Bunsell (Pergamon Press, Oxford, 1980) p.514.
71. F.R. Jones and J.W. Rock, "A Method for Determining Crack Velocity Stress Intensity Curves for Stress Corrosion Cracking of GRP," in *Proceedings of the 6th International Conference on Fracture - Volume 4*, edited by S.R. Valluri et al (Pergamon Press, 1984) p.3053.
72. P.J. Hogg, D. Hull, and B. Spencer, "Stress and Strain Corrosion of Glass Reinforced Plastics," *Composites*, July (1982) 166.
73. P.J. Hogg, D. Hull, and M.J. Legg, "Failure of GRP in Corrosive Environments," in *Proceedings of the 1st International Conference on Composite Structures* (Elsevier Science Publishers Ltd., 1981) p.106.

74. J.J. Mecholsky, R.W. Rice, and S.W. Freiman, "Prediction of Fracture Energy and Flaw Size in Glasses from measurements of Mirror Size," *J. Amer. Ceram. Soc.*, 57 (1974) 440.
75. J.J. Mecholsky, S.W. Freiman, and R.W. Rice, "Fracture Surface Analysis of Ceramics," *J. Mater. Sci.*, 11 (1976) 1310.
76. H.P. Kirchner and J.W. Kirchner, "Fracture Mechanics of Fracture Mirrors," *J. Amer. Ceram. Soc.*, 62 (1979) 198.
77. A.G. Metcalfe and G.K. Schmitz, "Mechanism of Stress Corrosion in E Glass Filaments," *Glass Technol.*, 13 (1972) 5.
78. C. Lhyman and J.M. Schultz, "Chemically Assisted Fracture of Thermoplastic PET Reinforced with Short E-glass Fiber," *J. Mater. Sci.*, 18 (1983) 2923.
79. J.N. Price and D. Hull, "Qualitative and Quantitative Fractography of GRP Stress Corrosion Fracture," in *Proceedings of the 6th International Conference on Composite Materials* (Elsevier Science Publishers Ltd., 1987) p.4.365.
80. P.J. Hogg and D. Hull, "Micromechanisms of Crack Growth in Composite Materials under Corrosive Environments," *Met. Sci.*, August-September (1980) 441.
81. T.J. Martin, R.M. Hunt, and G. Duff, "Evaluating the Environmental Resistance of Stress Composite Materials," *The Reinforced Plastic Congress 80* (British Plastics Federation, 1980) Paper 45.
82. E.H. Andrews, "The Short and Long Term Performance of Polymers in Different Environments," *Br. Polym. J.*, 10 (1978) 39.
83. A.C.T. Hsu and J.R. Schafner, "Surface Degradation of E-glass and S-Glass in the Presence of Water," in *Durability of Macromolecular Materials*, ACS Symposium Series 95, edited by R.K. Bey (American Chemical Society, 1978) p.411.
84. M.J. Kerper and T.G. Scuderi, "Relation of Strength of Thermally Tempered Glass to Fracture Mirror Size," *Am. Ceram. Soc. Bull.*, 44 (1965) 953.
85. H.P. Kirchner and R.M. Gruver, "Fracture Mirrors in Alumina Ceramics," *Philos. Mag.*, 27 (1973) 1433.
86. N. Shinkai and M. Hara, "Determination of the Breaking Strength of Glass from the Fracture Pattern," *Ashi Garasu Kenkyu Hokoku*, 19 (1969) 73.

87. J.J. Mecholsky and M.G. Drexhage, "Comparison of Optical and Fractographic Measurements of Residual Stress in Compressively Clad Glass Rods," *J. Amer. Ceram. Soc.*, 63 (1980) 347.
88. A.C. Jaras, B.J. Norman, and S.C. Simmen, "The Measurement of Glass Fiber Strength in Composites from Studies of their Fracture Surfaces," *J. Mater. Sci.*, 18 (1983) 2459.
89. M.F. Kanninen, E.F. Rybicki, and H.F. Brinson, "A Critical Look at Current Applications of Fracture Mechanics," *Composites*, 8 (1977) 17.
90. M.J. Owen and R.J. Cann, "Fracture Toughness and Crack Growth Measurements in GRP," *J. Mater. Sci.*, 14 (1979) 1982.
91. J. Aveston and J.M. Sillwood, "Long-Term Strength of Glass-Reinforced Plastics in Dilute Sulphuric Acid," *J. Mater. Sci.*, 17 (1982) 3491.
92. A.G. Metcalfe, M.E. Gulden, and G.K. Schmitz, "Spontaneous Cracking of Glass Filaments," *Glass Technol.*, 12 (1971) 15.
93. R.L. Jones and H.D. Chandler, "Chemical Corrosion of E-glass Fibers in Neutral Phosphate Solution," *J. Mater. Sci.*, 21 (1986) 2175.
94. B.E. Ramachandran and N. Balsubramanian, "Effect of Organic Acids on E-glass Fabric," *J. Amer. Ceram. Soc.*, 64 (1981) C-122.
95. H.D. Chandler and R.L. Jones, "Strength Loss in 'E' Glass Fibers Treated in Strong Solutions of Mineral Acids," *J. Mater. Sci.*, 19 (1984) 3849.
96. R.L. Jones and H.D. Chandler, "Strength Loss in E-glass Fibers after Exposure to Organic Acid," *J. Mater. Sci.*, 20 (1985) 3325.
97. R.L. Jones and H.D. Chandler, "Strength Loss in E-glass Fibers after Exposure to Hydrochloric, Hydrobromic, and Hydriodic Acids," *J. Mater. Sci.*, 20 (1985) 3320.
98. F.R. Jones and J.W. Rock, "On the Mechanism of Stress Corrosion of E-glass Fibers," *J. Mater. Lett.*, 2 (1983) 415.
99. S. Trop and R. Arvesen, "Influence of Glass Fiber Quality on Mechanical and Strain Corrosion Properties of FRP - Proposed Method for Quality Control," in *Proceedings of the 34th Annual Conference on Reinforced Plastics/Composites* (The Society of Plastics Industry, Inc., 1979) Section 13-D.

100. E.L. Rodriguez, "Corrosion of Glass Fibers," *J. Mater. Lett.*, 6 (1987) 718.
101. B.E. Ramachandran, B.C. Pai, and N. Balasubramanian, "Studies on the Acid Resistance of E Glass," *J. Amer. Ceram. Soc.*, 63 (1980) 1.
102. B.E. Ramachandran and N. Balasubramanian, "The Effect of Temperature on the Rate of Removal of Ions from E-glass," *J. Mater. Lett.*, 4 (1985) 688.
103. B.E. Ramachandran, G. Basavarajappa, B.C. Pai, and N. Balasubramanian, "Effects of Acid and Heat Treatment on the Tensile Properties of E-glass Fibers," *J. Mater. Lett.*, 3 (1984) 685.
104. R.F. Regester, Behavior of Fiber Reinforced Plastic Materials in Chemical Service, *Corrosion*, 25 (1969) 157.
105. J.M. Marshall, G.P. Marshall, and R.F. Pinzelli, "Diffusion of Liquids into Resin and Composites," in *Proceedings of the 37th Annual Conference on the Reinforced Plastics/Composites* (The Plastics Industry, 1982) Session 9-C.
106. R.C. Roberts, "The Effect on Chemical Environments on the Mechanical Properties of GRP," in *Proceeding of Symposium on Reinforced Plastics in Anti-Corrosion Applications*, 1979, Paper 7.
107. B.D. Caddock, K.E. Evans, and D. Hull, Diffusion of Aqueous Hydrochloric Acid into Polyester Resins, *J. Mater. Sci.*, 24 (1989) 1005.
108. R.C. Allen, "Some Corrosion Mechanisms in Attack of Resin and Resin-Glass Laminates," *Polym. Eng. Sci.*, 19 (1979) 329.
109. I. Ghorbel and D. Valentin, "Hydrothermal Effects on the Physico-Chemical Properties of Pure and Glass Fiber Reinforced Polyester and Vinylester Resins," *Polym. Compos.*, 14 (1993) 324.
110. K.H.G. Ashbee, F.C. Frank, and R.C. Wyatt, "Water Damage in Polyester Resins," *Proc. Roy. Soc.*, A300 (1969) 415.
111. K.H.G. Ashbee and R.C. Wyatt, "Water Damage in Glass Fiber-Resin Composites," *Proc. Roy. Soc.*, A312 (1969) 553.
112. O. Ishai, Environmental Effects on Deformation, "Strength, and Degradation of Unidirectional Glass-Fiber Reinforced Plastics - II. Experimental Study," *Polym. Eng. and Sci.*, 15 (1975) 491.

113. D.I. James, R.H. Norman, and M.H. Stone, "Water Attack on the Glass-Resin Bond in GRP," *Plast. & Polym.*, 36 (1968) 21.
114. G. Pritchard, R.G. Rose, and N. Taneja, "The Effect of Water on the Critical Stress Intensity Factor of Unsaturated Polymer Resin," *J. Mater. Sci.*, 11 (1976) 718.
115. D.J. Vaughan and E.L. McPherson, "The Effects of Adverse Environmental Conditions on the Resin-Glass Interface of Epoxy Composites," in *Proceedings of the 27th Annual Technical Conference on Plastics/Composites* (The Society of the Plastics Industry, Inc., 1972) Section 21-C.
116. G. Menges and H.W. Gitschner, "Sorption Behavior of Glass-Fiber Reinforced Composites and the Influence of Diffusing Media on Deformation and Failure Behavior," in *Proceedings of the 3rd International Conference on Composite Materials - Volume 1*, edited by A.R. Bunsell et al (Pergamon Press, 1980) p.25.
117. B.D. Caddock, K.E. Evans, and I.G. Masters, "Diffusion Behavior of the Core-Sheath Structure in E-glass Fibers Exposed to Aqueous HCl," *J. Mater. Sci.*, 24 (1989) 4100.
118. B. Das, B.D. Tucker, and J.C. Watson, "Acid Corrosion Analysis of Fiber Glass," *J. Mater. Sci.*, 26 (1991) 6606.
119. G. Lewis and S.W. Bedder, "Stress Corrosion of Glass Fibers in Acidic Environments," *J. Mater. Lett.*, 3 (1984) 728.
120. P.A. Sheard and F.R. Jones, "The Effect of Environment on Stress Corrosion of Single E-glass Filaments and the Nucleation of Damage in Glass Fiber Reinforced Plastics," in *Proceedings of 2nd International Conference on Fiber Reinforced Composites - Volume 3* (IMEchE Publications Ltd., London, 1986) C38/86, p.63.
121. C. Tian, W. Zhou, K. He, Z. Zhang, Z. Liu, Z.H. Zhang, X. Li, J. and Zhang, "Study of the High Purity and Ultrafine Silica Fiber," *J. Mater. Sci.*, 227 (1992) 767.
122. T.H. Elmer, "Leaching of E-glass," *J. Amer. Ceram. Soc.*, 67 (1984) 778.
123. A.H. Legge, "Sulphur and Nitrogen in the Atmosphere," *Acidic Deposition: Sulphur and Nitrogen Oxides - Chapter 2*, edited A.H. Legge and S.V. Krupa (Lewis Publishers, 1990) p.3.
124. D.V. Bubenick, *Acid Rain Information Book*, 2nd Edition (Noyes Publications, 1984).

125. Committee on Atmospheric Transport and Chemical Transformation in Acid Precipitation, *Acid Deposition - Atmospheric Processes in Eastern North America: A Review of Current Scientific Understanding* (National Academy Press, 1983).
126. T. Ishihara and L. Persson, "Fracture on FRP Rods under Long-Term Load, Laboratory Report," The Swedish State Power Board, 1985.
127. E.J. McMahon, "The Chemistry of Corona Degradation of Organic Insulating Materials in High-Voltage Fields and under Mechanical Strain," *IEEE Trans. Electr. Insul.*, EI-3 (1968) 3.
128. A. Schmiemann, M. Gehde, and G.W. Ehrenstein, Effect of Internal Stresses on Corrosion Behavior of Glass Fibers, in *Proceedings of the 44th Annual Conference on Reinforced Plastics/Composites* (The Society of the Plastics Industry, Inc., 1989) Session 2-C.
129. S.A. Boggs, "Partial Discharge: Overview and Signal Generation," *IEEE Electr. Insul. Mag.*, 6 (1990) 33.
130. S.A. Boggs, "Partial Discharge - Part III: Cavity - Induced PD in Solid Dielectrics," *IEEE Electr. Insul. Mag.*, 6 (1990) 11.
131. M.S. Kumosa, Q. Qiu, M. Ziomek-Moroz, M.V. Balakrishnan, A. Moroz, A. Bansal, and T.S. McQuarrie, "Micro-Fracture Mechanisms in Glass/Polymer Insulator Materials under Combined Effects of Electrical, Mechanical, and Environmental Stresses," Quarterly Progress Report to Bonneville Power Administration, October to December, 1993 (Contract #DE-AC79-92BP61873).
132. D. Hull, *An Introduction to Composite Materials* (Cambridge University Press, 1981).
133. M.S. Kumosa, "Failure Analysis of Composite Insulators," Internal Report, Oregon Graduate Institute of Science & Technology, July, 1994.
134. D.A. Scola, "A Study to Determine the Mechanism of S-glass/Epoxy Resin Composite Degradation due to Moist and Solvent Environments," in *Proceedings of the 30th Annual Conference on Reinforced Plastics/Composites* (The Society of the Plastics Industry, Inc., 1975) Section 22-C.
135. T.A. Collings, R.J. Harvey, and A.W. Dalziel, "The Use of Elevated Temperature in the Structural Testing of FRP Components for Simulating the Effects of Hot and Wet Environmental Exposure," *Composites*, 24 (1993) 625.

136. D.I. James, R.H. Norman, and M.H. Stone, "Water Attack on the Glass-Resin Bond in GRP," *Plast. Polym.*, February (1968) 21.
137. G. Menges and K. Lutterbeck, "Stress Corrosion in Fiber-Reinforced Plastics in Aqueous Media," in *Developments in Reinforced Plastics - Volume 3* (Elsevier Science Publishers Ltd., 1984) p.97.
138. M.S. Kumosa, Q. Qiu, J.M. Braun, M. Ziomek-Moroz, J. MaCarthy, "Micro-Fracture Mechanisms in Glass/Polymer Insulator Materials under Combined Effects of Electrical, Mechanical, and Environmental Stresses," Annual Report to Bonneville Power Administration, 1993 (Contract #DE-AC79-92BP61873).
139. M.S. Kumosa, D. Hull, and J.N. Price, "Acoustic Emission from Stress Corrosion Cracks in Aligned GRP," *J. Mater. Sci.* 22 (1987) 331.
140. M.S. Kumosa, "Acoustic Emission Monitoring of Stress Corrosion Cracks in Aligned GRP," *J. Phys., D: Appl. Phys.*, 20 (1987) 69.
141. A.C. Grag, "Technical Note: Environmental Stress Cracking Behavior of Glass Fiber Reinforced Epoxy Resins," *Eng. Fract. Mech.*, 17 (1983) 575.
142. A. Bledzki, R. Spaude, and G.W. Ehrenstein, "Corrosion Phenomenon in Glass Fibers and Glass Fiber Reinforced Thermosetting Resins," *Compos. Sci. Technol.*, 23 (1985) 263.
143. M.S. Kumosa, Q. Qiu, M. Ziomek-Moroz, A. Moroz, and J.M. Braun, "Micro-Fracture Mechanisms in Glass/Polymer Insulator Materials under Combined Effects of Electrical, Mechanical, and Environmental Stresses," Final Report to Bonneville Power Administration, 1994. (Contract #DE-AC79-92BP61873)
144. R.S. Sigmond, T. Sigmond, A. Goldman, and M. Goldman, "On the Role of Water in the Aging of Polymers in Air-insulated Electrical Systems," *IEEE Trans. Electr. Insul.*, 26 (1991) 770.
145. A. Goldman, M. Goldman, and R.S. Sigmond, Corrosion and Aging Mechanisms Investigated by Corona Discharges, in *Proceedings of the 19th International Conference on Phenomena in Ionized Gases - Invited Paper Volume*, edited by J.M. Labt (University of Belgrade, 1989) p.322.
146. A. Goldman, M. Goldman, R.S. Sigmond, and T. Sigmond, "Analysis of Corona Products by Means of Their Reactions in Water," in *Proceedings of the 9th International Symposium on Plasma Chemistry - Volume 2*, edited by R. d'Agostino (International Union of Pure and Applied Chemistry, 1989) p.1654.

147. R. Peyrous, "Numerical Simulation of the Production of Neutral Gaseous Species Created by Electrical Discharges in Moist Oxygen or Air," in *Proceedings of the 8th International Conference on Gas Discharges and Their Applications*, 1985, p.489.
148. A.F. Johnson, *Engineering Design Properties of GRP* (The British Plastic Federation, 1979).
149. B. Dewimille, J. Thoris, R. Mailfert, and A.R. Nunesell, "Hydrothermal Aging of an Unidirectional Glass-Fiber Epoxy Composite during Water Immersion," in *Proceedings of the 3rd International Conference on Composite Materials - Volume 1*, edited by A.R. Bunsell et al (Pergamon Press, 1980) p.579.
150. T.H. Elmer and M.E. Nordberg, "Solubility of Silica in Nitric Solution," *J. Amer. Ceram. Soc.*, 41 (1958) 517.
151. M.L. Huggins, K.-H. Sun, and A. Silverman, "The Vitreous State," *J. Amer. Ceram. Soc.*, 26 (1943) 393.
152. F. Helfferich, *Ion Exchange* (McGraw-Hill Book Company, Inc., 1962).
153. D.G. Holloway, *The Physical Properties of Glass* (Wykeham Publications Ltd., 1973).
154. B.M. Smets and M.G. Tholen, "Leaching of Glasses with Molar Composition $20\text{Na}_2\text{O} \cdot 10\text{RO} \cdot x\text{Al}_2\text{O}_3 \cdot (70-x)\text{SiO}_2$," *J. Amer. Ceram. Soc.*, 67 (1984) 281.
155. W.J. Eakins, "A Study of Interlaminar Shear Failure in Single Filament Wound Rings Made at the Bushing," in *Proceedings of the 17th Annual Technical Conference on Reinforced Plastics/Composites* (The Society of Plastics Industry, Inc., 1963) Section 9-C.
156. J.B. Donner, R. Battistella, and B. Chatenet, "A Study of the Surface of Glass Fibers," *Glass Technol.*, 16 (1975) 139.
157. A.E. Martell and R.M. Smith, *Critical Stability Constants - Volume 3* (Plenum Press, New York, 1977).
158. T.A. Michalske and S.W. Freiman, "A Molecular Interpretation of Stress Corrosion in Silica," *Nature*, 295 (1982) 571.
159. G.M. Bartenev, "The Structure and Strength of Glass Fibers," *J. Non-Cryst. Solids*, 1 (1968) 69.

160. H. Stockhorst and R. Bruckner, "Structure Sensitive Measurements on E-Glass Fibers," *J. Non-Cryst. Solids*, 49 (1982) 471.
161. F.P. Ford, "The Crack-Tip System and its Relevance to the Prediction of Cracking in Aqueous Environments," in *Environment-Induced Cracking of Metals*, NACE-10, edited by R.P. Gangloff (The National Association of Corrosion Engineers, 1988).
162. A.J. Sedriks, J.A.S. Green, and D.L. Novak, "Corrosion Processes and Solution Chemistry within Stress Corrosion Cracks in Aluminum Alloys," in *Localized Corrosion*, NACE-3, edited by R.W. Staehle et al (The National Association of Corrosion Engineers, 1971).

VITA

The author originally came from Beijing, China. Majoring in Materials Science and Engineering, she received her B.E. degree from Beijing Polytechnic University in 1982 and M.S. degree from Institute of Aeronautic Materials in 1985. Since 1985, she worked as a materials engineer in the Department of Physical Metallurgy at the same institute for about four years. In 1989, the author was invited as a visiting scholar by the School of Engineering at California Polytechnic State University and spent two years there doing research. In 1991, she joined the Department of Materials Science and Engineering at Oregon Graduate Institute of Science & Technology to pursue her Ph.D. degree. During the last four years, she has been conducting extensive investigation concerning the brittle fracture of GRP insulators used in electrical power transmission systems.

In her professional career, the author has developed her research interests primarily in the fields of failure analysis, surface strengthening, corrosion and stress corrosion of composites, fatigue assessment, residual stress analysis, powder metallurgy, and hot ductility evaluation of metallic materials.